



Terms and Conditions of Use of Digitised Theses from Trinity College Library Dublin

Copyright statement

All material supplied by Trinity College Library is protected by copyright (under the Copyright and Related Rights Act, 2000 as amended) and other relevant Intellectual Property Rights. By accessing and using a Digitised Thesis from Trinity College Library you acknowledge that all Intellectual Property Rights in any Works supplied are the sole and exclusive property of the copyright and/or other IPR holder. Specific copyright holders may not be explicitly identified. Use of materials from other sources within a thesis should not be construed as a claim over them.

A non-exclusive, non-transferable licence is hereby granted to those using or reproducing, in whole or in part, the material for valid purposes, providing the copyright owners are acknowledged using the normal conventions. Where specific permission to use material is required, this is identified and such permission must be sought from the copyright holder or agency cited.

Liability statement

By using a Digitised Thesis, I accept that Trinity College Dublin bears no legal responsibility for the accuracy, legality or comprehensiveness of materials contained within the thesis, and that Trinity College Dublin accepts no liability for indirect, consequential, or incidental, damages or losses arising from use of the thesis for whatever reason. Information located in a thesis may be subject to specific use constraints, details of which may not be explicitly described. It is the responsibility of potential and actual users to be aware of such constraints and to abide by them. By making use of material from a digitised thesis, you accept these copyright and disclaimer provisions. Where it is brought to the attention of Trinity College Library that there may be a breach of copyright or other restraint, it is the policy to withdraw or take down access to a thesis while the issue is being resolved.

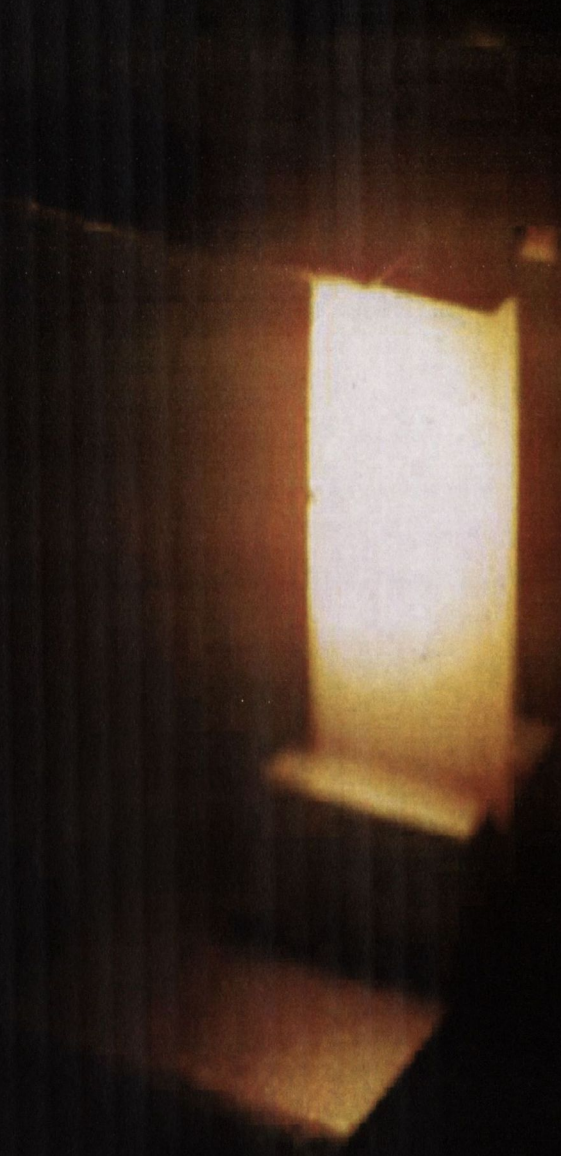
Access Agreement

By using a Digitised Thesis from Trinity College Library you are bound by the following Terms & Conditions. Please read them carefully.

I have read and I understand the following statement: All material supplied via a Digitised Thesis from Trinity College Library is protected by copyright and other intellectual property rights, and duplication or sale of all or part of any of a thesis is not permitted, except that material may be duplicated by you for your research use or for educational purposes in electronic or print form providing the copyright owners are acknowledged using the normal conventions. You must obtain permission for any other use. Electronic or print copies may not be offered, whether for sale or otherwise to anyone. This copy has been supplied on the understanding that it is copyright material and that no quotation from the thesis may be published without proper acknowledgement.

Fracture and Fatigue in High Impact Polystyrene

The Influence of Secondary Phase Morphology on Fracture and Fatigue.



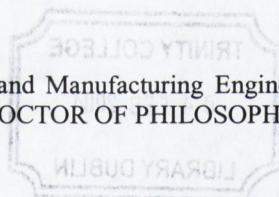
Finbar Dolan B.Sc.
May 2003

FRACTURE AND FATIGUE IN HIGH IMPACT POLYSTYRENE

THE INFLUENCE OF SECONDARY PHASE MORPHOLOGY
(*RUBBER PARTICLE SIZE AND EFFECTIVE RUBBER PHASE VOLUME*)
ON FRACTURE AND FATIGUE BEHAVIOUR IN HIPS.

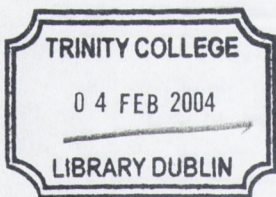
By,
Finbar Dolan.

Submitted to the Department of Mechanical and Manufacturing Engineering, The University of Dublin, Trinity College, Dublin 2. Ireland, for the Degree of DOCTOR OF PHILOSOPHY



University Of Dublin,
Trinity College.

MAY 2003



THOES
7674

Summary

The subject of the following thesis is the influence of the secondary phase morphology on fracture and fatigue behaviour in High Impact Polystyrene (HIPS). The motivation of the work was the premature failure of parts manufactured from HIPS materials whose microstructures, it was thought, were optimised for toughness and, it was assumed, for fatigue. The objective of the research was to evaluate these assumptions and establish through empirical analysis the relationship between micro-structural morphology, mechanical properties and Fracture and Fatigue behaviour to rationalise the apparent dichotomy that was observed with these HIPS in service applications.

To this end the impact, tensile, fracture, fatigue and fatigue crack propagation behaviour of seventeen HIPS materials were considered. The materials were prepared by the mechanical melt blending of three parent HIPS resins, possessing significantly different particle size (RPS) populations, to known effective rubber phase volumes (ERPV) in a polystyrene control resin whose molecular weight was equivalent to that of the matrix in the parent HIPS resins. The tests revealed that the RPS, and so the distribution in RPS, effects a primary influence on material response, determining the manner in which increases in the ERPV influences material properties. The tests established that the influence of the ERPV and RPS on impact, tensile, fracture and fatigue behaviour, is perhaps best considered in terms of the inter-particle distance, corrected and attenuated for an the efficiency (in crazing) of the secondary phase.

Five methods of characterising fracture were considered, the charpy impact test, the strain energy release rate, the J integral and the essential work of fracture. These tests established that traditional methods of characterising intrinsic toughness in HIPS, based on LEFM principles, e.g., employing impact test data on standard specimens, is unsuitable for HIPS. They also revealed that a valid and comparable J integral measurement of 'plane-tress' fracture toughness, sensitive to variations in thickness, can be determined under monotonic tensile loading on SENT specimens. It was concluded that the most efficient means of characterising intrinsic toughness in HIPS in standard wall thicknesses was to determine J_{IC} from fatigue. The results show ranking materials' toughness by impact testing does not correlate with their intrinsic or fatigue toughness.

Fatigue tests revealed that the competitive process of crazing (inhibiting crack propagation though decaying the materials strain energy absorption potential) dictates the process of fatigue crack propagation (FCP) and fatigue life. This illustrating that the mechanism responsible for impact 'toughening' HIPS detracts from the FCG resistance of the materials. The tests also showed that the secondary phase volume does not significantly contribute to the intrinsic toughness of HIPS in plane strain. They suggest that although FCP can be modeled in terms of the Paris relationship, it is, because of the nature of the micro-mechanical processes underway, perhaps more appropriate to model it in terms of an energy, damage accumulation, criterion e.g., ΔJ '. This, as such an approach accommodates the inconsistencies observed, i.e., between the supporting rationale of LEFM, associated with Paris, and the accumulation of damage observed in FCP in HIPS.

It was concluded from the results that it is possible to model the behaviour of HIPS in terms of the secondary phase morphology. Thus it is possible to prepare, by bulk polymerisation techniques, HIPS materials that are optimised for fracture and fatigue. Finally it is proposed that further research be directed at studying the influence of bimodal and polydisperse particle sizes and developing finite element methods to assist in the prescription of optimum secondary phase morphologies for HIPS that may be employed in engineering applications.

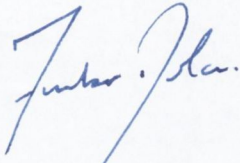
Finbar Dolan
May 2003

Declaration

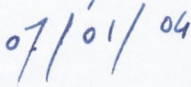
I declare that I am the sole author of this thesis and with the exception of some work by others, which is acknowledged and referenced, all of the work presented within it is my own. I also declare that this work has not been submitted as an exercise for a degree to any other University or College.

I authorise the Library of Trinity College Dublin to lend or copy this thesis on request.

Signature



Date



Dedication

To the memory, wit and wisdom of my brother Michael H. Dolan 12/10/1955 -25/1/1995, my love Elizabeth Costello and to all of my Family and Friends.

Acknowledgements

I would like to thank my Family. My parents, Tom and Evelyn, my love Elizabeth, my brothers and sisters, especially Michael, Robert and Jane and Alan.

I want to thank everyone in Trinity College Dublin, in Engineering and Chemistry especially David, for his patience and candidness, and Paul, Peter, John and Sean for their guidance, assistance and great patience.

I would like to thank everyone in the Dow Chemical Company, Terneuzen, especially, John, Martin, Ad, Nigel, Padraig, Jeff, Ronald and Regge, for their help and the good times.

I would also like to thank the Plastics Department in Athlone Institute of Technology, especially Paul and Dr. Ambi, for all their time patience and assistance.

Finally I want to thank my fellow student friends Donie, Gavin, Fergus, Paddy, Gearoid, Declan, Ronny, Jimmy, Tim, Sambo and Joe for sharing the students University of Life for all those years – it was great.

Thanks to everyone I know in Dow, Trinity, AIT, and UCD for making the research possible and contributing to it, in mind, body and spirits. To everyone; peace, prosperity, success and happiness.

“The ancients who wished to illustrate illustrious virtue throughout the kingdom, first ordered well their own states. Wishing to order well their states, they first regulated their families. Wishing to regulate their families, they first cultivated their persons. Wishing to cultivate their persons, they first rectified their hearts. Wishing to rectify their hearts, they first sought to be sincere in their thoughts. Wishing to be sincere in their thoughts, they first extended to the utmost their knowledge. Such extension of knowledge lay in the investigation of things.

Things being investigated, knowledge became complete. Their knowledge being complete, their thoughts were sincere. Their thoughts being sincere, their hearts were then rectified. Their hearts being rectified, their persons were cultivated. Their persons being cultivated, their families were regulated. Their families being regulated, their states were rightly governed. Their states being rightly governed, the whole kingdom was made tranquil and happy.”

Confucious, The Great Learning, 500 BC.

Contents

1.	<i>Chapters</i>	<i>i</i>
2.	<i>Figures</i>	<i>vi</i>
3.	<i>Tables</i>	<i>ix</i>
4.	<i>Glossary</i>	<i>x</i>

1. Chapters

Chapter 1

High Impact Polystyrene (HIPS)	1
1.1 Preview	1
1.2 The origins of High Impact Polystyrene	1
1.3 General Considerations of the Materials used in Preparing HIPS.	2
1.4 General Considerations of the Methods used in Preparing HIPS.	3
1.5 The Bulk Polymerisation of HIPS.	3
1.6 Polymerisation Reactions in the Preparation of HIPS.	4
1.6.1 Initiation	4
1.6.2 Propagation.	4
1.6.3 Termination .	5
1.6.4 Graft Reactions.	6
1.7 Phase Inversion in the Bulk polymerisation of HIPS.	8
1.8 Structural Control in the Bulk Polymerisation of HIPS.	10
1.9 Control over the Rubber Phase Volume.	10
1.10 Control over Rubber Particle size.	11
1.11 Conclusions	13
1.12 References	13

Chapter 2

EXPERIMENTAL MATERIALS	15
Materials Preparation and Characterisation.	15
2.1 Preview	15
2.2 Introduction	15
2.3 Materials Selection	18
2.4 Characterisation of Matrix materials.	18
2.5 Characterising the Secondary Phase Morphology.	18
2.6 Gel Content Studies.	19
2.6.1 Gel Content Studies; Introduction and Overview.	19
2.6.2 Procedure	19
2.6.3 Results	20
2.6.4 Discussion of Results	20
2.6.5 Conclusion from Gel content Analysis.	21
2.7 Coulter Counter Analysis	21
2.7.1 Coulter Counter Analysis; Introduction and Overview.	21
2.7.2 Procedure.	22
2.7.3 Coulter Counter Results.	22
2.7.4 Discussion of Results	24
2.7.5 Conclusions from Coulter Counter Analysis	25
2.8 TEM (Transmission Electron Microscopy) ANALYSIS	25
2.8.1 TEM Analysis; Introduction and overview.	25
2.8.2 Procedure	30
2.8.3 Results of TEM Analysis.	30
2.8.4 Discussion of TEM plates; Particle Morphology	34
2.8.5 Discussion of TEM Quantitative Image Analysis.	35
2.8.6 Conclusions from Quantitative TEM analysis	35
2.9 Preparation of Polymer blends used in the study.	36
2.10 Discussion of Conclusions from Secondary Phase Characterisation Tests	37
2.11 References	38
2.12 Appendix 2.1: Results of Coulter Counter Analysis	39
2.13 Appendix 2.2. Results of Transmission Electron Microscopy	40

Chapter 3

MICRO-STRUCTURE & MECHANICAL PROPERTIES	42
3.1 Preface	42
3.2 Contents	42
3.3 Introduction	43
3.3.1 Deformation in Plastics.	43
3.3.2 Shear Yielding.	43
3.3.3 Criteria for Shear Yielding.	44
3.3.4 Crazing.	45
3.3.5 Criteria for Crazing.	47
3.3.6 Craze nucleation and growth in HIPS; the implications for ERPV and RPS.	48
3.3.7 Rubber Toughening Theories in HIPS.	51
3.3.7.1 Thermal Influences.	54
3.3.8 Relationships between Microstructure and Mechanical Properties in HIPS.	55
3.3.8.1 Rubber Particle Structure.	56
3.3.8.2 Rubber/Matrix Adhesion.	57
3.3.9 The Influence of Particle Size and Effective Rubber Phase Volume.	58
3.3.9.1 Minimum Particle Size	58
3.3.9.2 Polydisperse and Bi-Modal size distributions and Critical Particle size.	58
3.3.9.3 Monodisperse Particle size	60
3.3.9.4 Number of Particles	60
3.3.9.5 Interparticle Distance	61
3.3.10 Secondary Phase Structure and Tensile properties	65
3.4 Impact Experimental Methods	66
3.4.1 Experimental Materials and Specimen Preparation	66
3.4.2 Impact Test Method	67
3.5 Tensile Experimental Methods	67
3.5.1 Experimental Materials and Specimen Preparation	67
3.5.2 Tensile Test Method	68
3.6 Experimental Results and Discussion	68
3.6.1 Tensile Results and Discussion	69
3.6.1.1 Secondary Phase Morphology and Strain Rate Sensitivity	69
3.6.1.2 Modelling the Secondary Phase Morphology and Tensile Properties	71
3.6.2 Impact Test Results and Discussion	74
3.6.3 Particle Size Effect	77
3.6.3.1 Modelling behaviour in terms of the Inter Particle distance (IPD).	77
3.6.3.2 Modelling behaviour in terms of a Size Corrected Inter-particle Distance RIPD	81
3.6.3.3 Rationale for Modelling HIPS in terms of the RIPD.	82
3.6.3.4 Critical particle size	87
3.7 Conclusions on micro-structure and mechanical properties of HIPS	88
3.8 Appendix 3.1. Results of Impact Tests	90
3.9 Appendix 3.2. Results of Tensile Tests	91
3.10 Appendix 3.3. Empirically modelling of the tensile properties of high impact polystyrene in terms of its secondary phase morphology.	92
3.11 References	98

Chapter 4

The Fracture Toughness of HIPS	100
4.1 Preview	100
4.2 Contents	100
4.3 Introduction	100
4.3.1 Elements of Linear elastic Fracture Mechanics.	103
4.3.2 Elements of Elasto-Plastic Fracture Mechanics.	111
4.4 Experimental	119
4.4.1 Linear Elastic Fracture Mechanics: Strain Energy Release Rate from Impact Data.	119
4.4.2 Results: strain energy release rate	121
4.4.3 Determination of J integral from Monotonic Tensile Loading	121
4.4.4 Results Monotonic Tensile J integral	126

4.4.5	Elasto-Plastic Fracture Mechanics Essential Work Studies	126
4.4.6	Determination of J' from Fatigue	127
4.4.7	Results of J_c from Fatigue	129
4.5	Discussion of HIPS Fracture Toughness	129
4.5.1	Comment on results for G_c determined from LEFM analysis of Impact test data.	130
4.5.2	Comment on the Results obtained for J from Monotonic Tests.	132
4.5.3	Comment on the Results of the Essential Work tests.	135
4.5.4	Comment on the results of J integral measurement of J' from Fatigue tests	139
4.6	Conclusions	141
4.6.1	Strain Energy Release Rate determined from analysis of impact test data	141
4.6.2	J Integral determined from analysis of Monotonic Tensile Fracture Tests.	141
4.6.3	Essential work analysis	142
4.6.4	J Integral determined from analysis of Fatigue Crack Propagation.	142
4.6.5	General Conclusions on the Characterisation of Fracture Toughness in HIPS.	142
4.7	References	144

Chapter 5

Fatigue Crack Growth in HIPS	146	
5.1	Preface	146
5.2	Contents	146
5.3	Introduction	147
5.3.1	A Brief History of Fatigue.	147
5.3.2	Fatigue as a Design Criterion in HIPS applications; The Need for Research.	148
5.3.3	The Mechanical Response of HIPS to Cyclic Loading.	149
5.3.4	Comparison of the Fatigue lives of Un-notched HIPS and PS.	151
5.3.5	Thermal effects in un-notched testing of HIPS.	152
5.3.6	The influence of mean stress on fatigue life of HIPS.	153
5.3.7	The Influence of Surface Topography on Fatigue Life in HIPS.	154
5.3.8	Influence of test frequency on the Fatigue Life of HIPS.	155
5.3.9	Characterising Fatigue Crack Growth using Fracture Mechanics.	156
5.3.10	Comparison of Fatigue Crack Propagation in Polystyrene and HIPS.	162
5.3.11	The Influence of Mean Stress on FCP in HIPS.	163
5.3.12	The Influence of Test Frequency on FCP rates in HIPS.	163
5.3.13	FCP rates in Toughened Thermoplastics.	164
5.3.14	Applications of HIPS involving Fatigue	166
5.4	Experimental	166
5.4.1	Introduction.	166
5.4.2	Experiment Materials and Equipment.	167
5.4.3	Equipment	168
5.4.4	Experimental Procedure	169
5.5	Results and discussion	170
5.5.1	Micro-Mechanism of FCP in HIPS.	170
5.5.2	Micro-deformation Processes Involved in the Micro-mechanism of FCG in HIPS.	173
5.5.3	Influence of Morphology on Fatigue Damage Accumulation in HIPS	175
5.5.4	Influence of the Secondary Phase Morphology on Fatigue Life	180
5.5.5	Evaluating the kinetics of fatigue crack growth using the Paris Law.	183
5.5.6	Modelling Fatigue Crack Propagation in terms of DJ .	191
5.6	Conclusions	197
5.6.1	Concerning Fatigue Crack initiation and propagation from Microscopy.	197
5.6.2	Concerning Fatigue Life.	197
5.6.3	Concerning Fatigue Crack Propagation.	198
5.7	Appendix 5.1: Data Acquisition and Signal Conditioning System	199
5.8	Appendix 5.2: Data Acquisition program 'CAPTURE' source code C++	200
5.9	References	211

2. Figures

Chapter 1

Figure 1.1.	Ternary phase diagram for the system styrene - polystyrene - polybutadiene rubber.	9
Figure 1.2.	Viscosity changes in HIPS prepolymer during polymerisation.	9
Figure 1.3.	Deformation behaviour of droplets at different viscosity ratios (a, b,c& d) with different levels of shear (1, 2, 3, 4 & 5) (as per [19]).	11
Figure 1.4.	Molau Particle types.	12
Figure 1.5.	Particle structures obtained by polymerisation of HIPS using SB diblock copolymers of various copolymers (solid lines without grafting dashed lines with grafting) (As per[16])	13

Chapter 2

Figure 2. 1.	Coulter Multisizer Counter™ A. Drawing of the Coulter apparatus. B. Simplified Schema of amplification circuitry and data presentation methods. .	21
Figure 2. 2.	Results plotted from the CC analysis of PSB1 Parent HIPS resin.	23
Figure 2. 3.	Results plotted from the CC analysis of PSB2 Parent HIPS resin.	23
Figure 2. 4.	Results plotted from the CC analysis of PSB3 Parent HIPS resin.	24
Figure 2. 5.	Schematics to illustrate simplified operation of the Transmission EM.	25
Figure 2. 6.	Figure schematically illustrating the manner in which the projected area in TEM image is sensitive to the section thickness of the microtomed coupe.	26
Figure 2. 7.	Illustration of the manner in which a random configuration of monodisperse particles appears to be polydisperse when viewed through a plane section.	27
Figure 2. 8.	TEM Plate of PSB1 at 30,000 x	31
Figure 2. 9.	TEM Plate of PSB2 at 10,000 x.	31
Figure 2. 10.	TEM Plate of PSB3 at 10,000x.	32
Figure 2. 11.	Results plotted from TEM analysis of PSB1 Parent HIPS resin.	32
Figure 2. 12.	Results plotted from TEM analysis of PSB2 Parent HIPS resin.	33
Figure 2. 13.	Results plotted from TEM analysis of PSB3 Parent HIPS resin.	33
Figure 2. 14.	Photograph of the Betol compounding line used to prepare materials.	36

Chapter 3

Figure 3. 1.	Diagram illustrating the formation of micro shear bands under plane strain compression in polystyrene, as would be seen under cross polarising light. The sketch illustrates how nucleation of voids occurs at intersection of craze bands[3].	44
Figure 3. 2.	Transmission electron micro-graph of HIPS illustrating structure of a craze[9].	45
Figure 3. 3.	Plots showing (a) the variation in the craze fibril extension ratio (λ) with distance from the craze centre and (b) the variation of craze fibril stress (MN/m^2) with fibril extension ratio [15].	46
Figure 3. 4.	TEM micrograph of craze fibril breakdown.	47
Figure 3. 5.	Illustration of the variation in crazing behaviour with inter-particle distance as observed by Matsuo et al [24].	49
Figure 3. 6.	Illustration of particles holding the faces of the propagating crack together as proposed by Merz et al [33].	52
Figure 3. 7.	Plot illustrating the dependence of charpy impact energy on temperature and rubber phase volume in MI type particles[32].	55
Figure 3. 8.	Schematic of the effect of some morphological parameters on selected properties in HIPS, M-Mw of matrix G(Gel Content)& Q(Swell Index)-indicative of RPV, $\dot{\phi}$ -RPS.56	
Figure 3. 9.	Stress strain curves of craze plasticity of PS with KRO -1, HIPS and CSS particles compared with PS [48].	57
Figure 3. 10.	The calculated increase in Izod impact strength (ΔJ) vs. R_w at various values of RPV $\Phi_1 < \Phi_2 < \Phi_3$; ΔJ calculated from the equation of the linear regression line of the bi-logarithmic plot [54].	59

Figure 3. 11.	Plot of the Impact energy (J/m) vs. particle size (μm) for unnotched and notched charpy specimens at 8% RPV[58].	60
Figure 3. 12.	Bilogarithmic plot of $\Delta I/N$ vs. $R_w - R_c$, where R_c has been estimated at being 0.29 μm [58].	61
Figure 3. 13.	Plot of the impact energy vs. IPD (μm)-1 for unnotched charpy specimens [57].	63
Figure 3. 14.	The 100 sec isochronous Tensile Modulus vs. rubber phase volume in two rubber particle size populations, where Δ (core shell type particles CS) < \bullet (multiple inclusion type particles, MI).	65
Figure 3. 15.	Plot of the tensile yield stress (MPa) vs. Rubber phase volume, the circular symbol represent the large MI rubber inclusions, the triangular represents the small CS type particles [63].	66
Figure 3. 16.	Ceast Fly-cutters used in notching specimens.	67
Figure 3. 17.	Loading configuration for Charpy Impact Tests.	67
Figure 3. 18.	Image of Zwick 1455 tensile test system used in tensile testing.	68
Figure 3. 19.	Tensile Modulus for PSB1-3, 5, and 25 % ERPV resins vs. strain rate (log scale) illustrating the variation in modulus with strain rate. (PSB1 \diamond , PSB2 \square , and PSB3 Δ).69	
Figure 3.20	Tensile Yield for PSB1-3 5, 15 and 25% ERPV resins vs. strain rate (log scale) illustrating variation in yield stress with strain rate. (PSB1 \diamond , PSB2 \square , and PSB3 Δ)	70
Figure 3. 21.	Normalised Tensile modulus ($T_{mm}/T_{mc} - \text{PSB0}/\text{PSB}\#$) vs. ERPV. Displaying correlation coefficients (R_2) for the individual resin series and their combined data set(red).	72
Figure 3. 22.	Comparison of the applicability of Smallwood, Guth and Ishai cohen methods for modelling tensile modulus.	72
Figure 3. 23.	Comparison of Smallwood Guth and Ishai – Cohen model predictions with tensile yield strengths obtained in testing.	73
Figure 3. 24.	Impact Strength vs. ERPV for a. PSB#1 b. PSB#2 and c. PSB#3 series of polyblends for notch depths of 0.75, 1.75, 2.75, 3.75 and 5.75.	75
Figure 3. 25.	Plot of the slope of the change in impact strength (IS) vs ERPV, i.e., $dIS/dERPV$ vs. Notch depth for the three series of parent resins.	76
Figure 3. 26.	Impact strengths vs. average RPS at notch depth of 0.75mm notch depth.	76
Figure 3. 27.	Illustration of the Cubic Lattice Model used to calculate Inter-Particle Distance.	79
Figure 3. 28.	Plot illustrating the correlation of IPD with the decay in impact strength with increasing IPD. The quotient reflects the impact strength of the matrix resin (I_{mm}) divided by that of the HIPS (I_{mc}), i.e., as impact strength falls quotient rises.	80
Figure 3. 29.	Plot illustrating the correlation of IPD with the increase in Tensile Yield strength with increasing IPD. The quotient reflects the ratio of HIPS strength (Ty_{mc}) to the matrix resin (Ty_{mm}), i.e., tensile strength increases with IPD.	80
Figure 3. 30.	Normalised Tensile Modulus versus RIPD with linear regression curves and correlation coefficients (PSB1 \diamond , PSB2 \square , and PSB3 Δ)	85
Figure 3. 31.	Normalised Tensile Yield versus RIPD with linear regression curves and correlation coefficients (PSB1 \diamond , PSB2 \square , and PSB3 Δ)	85
Figure 3. 32.	Normalised Impact Strength versus RIPD with linear regression curves and correlation coefficients (PSB1 \diamond , PSB2 \square , and PSB3 Δ)	86
Figure 3. 33.	Comparison of the craze efficiency factors obtained from tensile yield data with those obtained from charpy impact strength.	87
Figure 3. 34.	Normalised Tensile Yield Strength versus RIPD corrected for minimum particle size of 1 mm. (PSB1 \diamond , PSB2 \square , and PSB3 Δ)	88

Chapter 4.

Figure 4.1.	a. Cartesian and cylindrical coordinate systems. b. Diagram of an infinite elastic plate containing an elliptical crack of length $2a$ and thickness B .	103
Figure 4.2.	Illustration of the asymptotic rise in stress near the tip of a crack, and the plastic zone r_p .	106
Figure 4.3.	Schematic of the Dugdale model for plastic zones at the ends of a elliptical hole in an infinite elastic plate.	107
Figure 4.4.	Sketch of the plastic zone shape. As in-plane, or 'crack face' dimensions (thickness), increase the contribution of the plastic deformation zone decreases under increased constraint with the triaxial state of stress moves from plane stress to plane strain.	110
Figure 4.5.	Diagram showing the partitioning of work in load point displacement curve.	112

Figure 4.6.	Schematic plot of total specific work of fracture versus ligament length showing plane stress and plane strain region. w_e specific essential work of plane stress fracture, w_i specific essential plane strain work of fracture w_{ie} . [39]	116
Figure 4.7.	Curves for the G_c of PSB1 series resins Determination of G_c for PSB1 Series Resins.120	
Figure 4.8.	SENT fracture testing apparatus.	121
Figure 4.9.	Plot of load displacement curves for Serie 1 PSB1-5. Each curve represents a notch depth.	122
Figure 4.10.	Interpolated plot of constant crack length on Serie 1 PSB1-5.	123
Figure 4.11.	Plot of crack length vs. strain energy (Serie 1 PSB1-5)	123
Figure 4.12.	Plot of J vs. Displacement (Serie 1 PSB1-5)	124
Figure 4.13.	Plot of J vs. Δa (J-R curve for Serie1 PSB1-5)	124
Figure 4.14.	Plot of J vs. Δa (J-R curve for Serie1 PSB1-15)	125
Figure 4.15.	Plot of J vs. Δa (J-R curve for Serie1 PSB1-23.5)	125
Figure 4.16.	Plot from PSB#1-5 tests. The shaded area indicating the area used in determining the work of fracture(the area under the curve for each specimen used to determine energy).	126
Figure 4.17.	Load displacement curves from test on PSB2-15.	127
Figure 4.18.	Strain energy release G (or J integral) vs. a for PSB1-5, 15, 25 from Ω series tests.	128
Figure 4.19.	Strain energy release G (or J integral) vs. a for PSB2-5, 15, 25 from Ω series tests.	128
Figure 4.20.	Strain energy release G (or J integral) vs. a for PSB3-5, 15, 25 from Ω series tests.	129
Figure 4.21.	Plot of G_c vs. RIPD, PSB#1 - \diamond , PSB#2 - \square , PSB#3 - Δ .	130
Figure 4.22.	Plot of A_{kp} vs. ERPV, PSB#1 - \diamond , PSB#2 - \square , PSB#3 - Δ .	131
Figure 4.23.	Plot of RIPD vs. J_c determined under plane stress.	134
Figure 4.24.	Plot of Work of fracture vs. Ligament length for PSB#1.	135
Figure 4.25.	Plot of Work of fracture vs. Ligament length for PSB#2.	136
Figure 4.26.	Plot of Work of fracture vs. Ligament length for PSB#3.	136
Figure 4.27.	Plot of w_f vs L for HIPS, as per Mai et al [42]	137
Figure 4.28.	Sketches of the characteristic shapes of the damage zones for the three series	138
Figure 4.29.	Plot of J'_{1c} determined from fatigue vs. RIPD.	139

Chapter 5

Figure 5.1.	a. The cyclic Stress-Strain behaviour of a HIPS resin @21 °C illustrating the increasing hysteresis loss with successive loading due to crazing [28].	148
Figure 5.2.	Diagrams illustrating the different responses of a. ABS and b. HIPS materials observed by Bucknall and Stevens at various test intervals [30].	149
Figure 5.3.	Diagram illustrating the different hysteresis losses observed in HIPS materials cycled under the same cyclic stress amplitude at frequencies of a. 0.2 and b. 0.02 HZ [31].	150
Figure 5.4.	Plot of σ_a/σ_{ut} vs. N comparing of the fatigue lifetimes of HIPS and PS on a relative stress basis [32].	151
Figure 5.5.	Comparison of the SN curves for PS and HIPS on an absolute stress basis [33].	151
Figure 5.6.	Specimen temperature rise in HIPS (°C) vs. the number of cycles to failure (N) at various $\Delta\sigma$. [33]	152
Figure 5.7.	Figure comparing the SN curves of polished and unpolished HIPS specimens.	154
Figure 5.8.	Plots showing a. The cycles to failure vs. frequency for samples of PS and HIPS at a stress amplitude of 17.2 MPa and b. The Stress amplitude vs. the cycles to failure of HIPS specimens tested at 0.2 Hz and 21 Hz [31].	155
Figure 5.9.	Diagram illustrating a typical plot of crack length (a) against the number of cycles (N).	156
Figure 5.10.	Paris plots for some of the more common 'commodity' thermoplastics [19].	158
Figure 5.11.	Diagram illustrating the sigmoidal variation of fatigue crack growth rates ($\log da/dn$) at high and low values of ΔK .	158
Figure 5.12.	Comparison of fatigue crack propagation in HIPS and PS (Hertzberg et al, [52].	161
Figure 5.13.	Plot Illustrating the Influence of R ratio on Fatigue Crack Propagation rates in HIPS[53].	162
Figure 5.14.	Plot of $\log da/dN$ ($\mu\text{m}/\text{cycle}$) vs. $\log \Delta K$ ($\text{MPa}\sqrt{\text{m}}$), illustrating frequency effects on the FCP behaviour of HIPS [53].	163

Figure 5.15.	a. The influence of rubber content on Paris law fatigue crack propagation rate constants in toughened PSAN (ostensibly ABS materials). b. SN curves for PSAN matrix containing [25.]	164
Figure 5.16.	Plot showing the effect of Mw and rubber content on FCP.	164
Figure 5.17.	Presents the equipment used for conducting fatigue tests. The centerpiece of the system was an Instron 8501 servo-hydraulic testing frame. In order to conduct the desired testing it was necessary to develop a series of customised ancillary devices.	167
Figure 5.18.	Close-up of the arrangement of apparatus during fatigue testing.	168
Figure 5.19.	a. sketches characteristic damage or craze zones and b. illustrating the process of interrupted crack growth.	169
Figure 5.20.	4.a. Close-up of crack initiation (edge crack initiation) and the damage zone in the region about the crack/notch. 4.b. Zoom into crazed region showing orientation of individual craze bands.	170
Figure 5.21.	Fracture surface of 8mm PSB#3-45.4 material fatigues under alternating 500 N load (R=0).	171
Figure 5.22.	SEM plate of the fracture topography in PSB3-45.4 indicating the extent of damage in advance of crack front, precipitated by profuse crazing.	172
Figure 5.23.	Photo image of fatigue crack growth in PSB2-15 taken from TV screen. The image was scanned in from one produced on a video printer.	173
Figure 5.24.	High magnification image of fatigue fracture surface topology of PSB#3 45.4.	174
Figure 5.25.	Fatigue fracture surface of PSB3-5, illustrating the difference between its effectiveness in involving the matrix resin in the crazing process with PSB3-45.4	176
Figure 5.26.	SEM images of PSB3 series resins illustrating the increased disruption of the fracture surface with increased rubber phase content indicating increased levels of crazing.	177
Figure 5.27.	TEM images of PSB3 series resins sectioned beneath the plane of fracture indicating the extent of damage beneath the propagating crack front.	179
Figure 5.28.	Total fatigue life vs. ERPV for the three series.	180
Figure 5.29.	Comparison of the fatigue life consumed in crack initiation and propagation to failure vs. ERPV for the three series.	180
Figure 5.30.	Plot of ERPV vs. N_{ci}/N_{cf} for the three series. [\diamond -PSB1, \square - PSB2 and Δ - PSB3].	181
Figure 5.31.	Paris plot and linear regression curves for 5, 15 and 25 % blends of PSB#1 resin.	183
Figure 5.32.	Paris plot and linear regression curves for 5, 15 and 25 % blends of PSB#2 resin.	183
Figure 5.33.	Paris plot and linear regression curves for 5, 15 and 25 % blends of PSB#3 resin.	184
Figure 5.34.	Paris plot comparing the FCG of PSB#1- #3 with 5 % ERPV [\diamond -PSB1, \square - PSB2 and Δ - PSB3]	185
Figure 5.35.	Paris plot comparing the FCG of PSB#1- #3 with 15 % ERPV [\diamond -PSB1, \square - PSB2 and Δ - PSB3]	185
Figure 5.36.	Paris plot comparing the FCG of PSB#1- #3 with 23.5 and 25 % ERPV [\diamond -PSB1, \square - PSB2 and Δ - PSB3]	186
Figure 5.37.	Plot of RIPD vs. Paris exponent m for the three series. [\diamond -PSB1, \square - PSB2 and Δ - PSB3]	187
Figure 5.38.	Plot of da/dN vs. ΔJ for PSB1-5, 15 & 23.5	191
Figure 5.39.	Plot of da/dN vs. ΔJ for PSB2-5, 15 & 25	191
Figure 5.40.	Plot of da/dN vs. ΔJ for PSB3-5, 15 & 25	192
Figure 5.41.	The variation of N_f with ΔJ for the three series of resins.	194
Figure 5.42.	The variation of m with ERPV for the three series of resins.	195

3. *Tables*

Chapter 2

Table 2. 1.	Results of Gel Content Studies figures quoted represent % Rubber Phase Volume.	20
Table 2. 2.	Temperature profile used in compounding of polymerblends.	37
Table 2. 3.	Results of Coulter counter analysis expressed in terms of number and volume percent.	39
Table 2. 4.	Results of TEM analysis expressed in terms of number and volume percent	40
Table 2. 5.	PSB1 particle size determination	40
Table 2. 6.	PSB2 particle size determination	41
TABLE 2. 7.	PSB2 particle size determination	41

Chapter 3

Table 3. 1.	Stress enlargement factors determined for the three series from Tensile Modulus Tensile Yield and Charpy Impact Data	86
Table 3.2.	Charpy Impact Test Results (n=10)	92
Table 3. 3.	Tensile Test Results, (n = 10).	93

Chapter 4

Table 4. 1.	Results of strain energy release tests determined from impact tests for PSB#1, 2 and 3 series.	121
Table 4. 2.	Results from monotonic J_c tests for PSB#1, 2 and 3 resin series (n=3).	126
Table 4. 3.	Results of J Integral analysis (J') of fatigue tests for PSB#1, 2 and 3 resin series	129

Chapter 5

Table 5.1.	Effects of Stress Amplitude on the Cycles to Craze Initiation and specimen Fracture [31]	153
Table 5.2.	Results of Ω 8mm (500N) series Fatigue Tests.	182
Table 5.3.	Paris constants A and m obtained for PSB#1, 2 and 3 at 1Hz 500N R=0.	186
Table 5.4.	Variation in m' with ERPV	192

4. *Glossary* (OF SYMBOLS AND NOMENCLATURE)

Chapter 1

ABS	Acrylonitrile Butadiene Styrene
AZBN	Azoisobutylnitrile
EPDM	Ethylene propylene diene monomer
GPPS	General Purpose Polystyrene
HIPS	High Impact Polystyrene
PBD	Polybutadiene
POO	a polymeric oil in oil emulsion
SPE	Society of Plastics Engineers
I	initiator
R_i^*	initiated primary free radical
M	monomer (styrene)
M_i^*	activated monomer/polymer radical
$[M]$	concentration of monomer
$[M^*]$	concentration of radicals
r_i	rate of initiation
r_p	rate of propagation
r_t	rate of termination
k_d	rate constant for dissociation
k_i	rate constant for initiation
k_p	rate constant for propagation
k_t	rate constant for termination
k_{tr}	rate constant for termination through recombination
k_{tf}	rate constant for termination through disproportionation
C	constant for chain transfer
C_Q	chain transfer constant for transfer agent, Q.
P_{no}	initial degree of polymerisation
P_n	final degree of polymerisation
$[Q]$	concentration of chain transfer agent, Q.
ν	the average kinetic chain length for disproportionation (2ν for recombination)

Chapter 2

AMU	Atomic Mass Unit
CC	Coulter Counter
csa	cross sectional area
D	particle diameter
Da	mean average diameter
D_{ave}	average diameter
d_i	maximum diameter of csa's in class i ,
d_{i-1}	maximum diameter in class $i-1$ and minimum in class i
DMF	Di-methyl formamide
DMS	Dynamic Mechanical Spectroscopy
Dv	volume average diameter
$D_{z+1 CC}$	Size corrected particle diameter from Coulter counter analysis

$D_{z+1:Dow}$	Size corrected particle diameter from TEM.
EM	Electron Microscope
ERPV	Effective rubber phase volume (including PS inclusions)
GPC	Gas phase chromatography
HIPS	High Impact Polystyrene
m	number of size classifications
MI	Multiple inclusion (particle type)
Mw	Molecular weight (Number Average)
$n(d_i)$	observed distribution in particle size
$N(d_i)$	true distribution in particle size
n_i	number of spheres in class i before correction
N_i	number of spheres in class i after correction
Os	Osmium
PC	Personal Computer
PS	Polystyrene
PSB0	Experimental GPPS.
PSB1	Experimental HIPS resin 1 (possessing smallest particle size)
PSB2	Experimental HIPS resin 2 (possessing medium particle size)
PSB3	Experimental HIPS resin 3 (possessing largest particle size)
RPS	Rubber Particle Size
RPV	Rubber phase volume
S	2D (dimension) area fraction
t	section thickness
TEM	Transmission Electron Microscopy
ϕ	3D (dimensional) volume fraction
ξ	excess area fraction of Φ projected in S (under TEM)
%N	% Number of given diameter
%V	% Volume composed of particles specific diameter

Chapter 3

A	diameter of particle
ABS	acrylonitrile butadiene styrene
B	free energy for plastic deformation
C	centre to centre distance between particles
CMLT	Critical matrix ligament thickness
D	pre-exponential multiplier for determining da/dt , that is \propto surface free energy/craze flow stress.
da/dt	rate of craze advance
d_c	critical particle size (re. CMLT)
E	young's modulus
ERPV	effective Rubber Phase volume
FE	Finite Element
G_g	Shear modulus of polystyrene
h	ligament distance between discontinuities
HIPS	high Impact Polystyrene
h/R	slenderness ratio
I	(Charpy) impact strength
IPD	Interparticle distance
k	rate constant

K'	stress multiplier
K_r	bulk modulus of (the) rubber
MI	multiple inclusion
N	number of particles
PSB(0)	Polystyrene resin used to 'dilute' parent HIPS resins
PSBX	Parent HIPS resins for $X = 1, 2$ and 3
PSB#	# used to denote blends of series 1, 2 and 3
PC	polycarbonate
PMMA	poly methyl methacrylate
PS	polystyrene
R	centre to centre separation of a discontinuity
R_c	critical rubber particle radius for toughening
RIPD	size corrected interparticle distance ($IPD/C - C =$ centre to centre distance)
RPS	rubber particle size
R_w	weighted average rubber particle radius
SAN	styrene acrylonitrile
T	Temperature
T_c	Critical inter-particle distance (re. CMLT)
T_c	Tensile property of composite blend
TEM	Transmission Electron Microscopy
T_g	the α thermal transition of polystyrene
T_m	Tensile modulus
T_{mc}	Tensile modulus of HIPS polyblends
T_{mm}	Tensile modulus of matrix
T_y	Tensile yield strength
X	critical hydrostatic stress associated with crazing
x°	x degrees of angle
Y	bulk modulus for polystyrene at crazing
α	coefficient of expansion of (the) rubber
α	symbol denoting the principal glass transition temperature
α_f	exponential constant for stress field overlap or craze efficiency
α_g	coefficient of expansion of polystyrene
ϵ	strain
Φ	rubber phase volume
Φ_{ips}	Phase volume of polystyrene occlusions in rubber
τ_o	shear yield stress
τ_{oct}	octahedral yield stress
λ	(craze) fibril extension ratio ϵ_d/ϵ_0 (where ϵ is strain)
λ'_n	the rate of advance of the principle wavelength of the matrix instability
μ	micro meter
σ	mean normal stress
$^\circ C$	temperature in Celcius

Chapter 4

a	crack length
$a_{\text{effective}}$	effective crack length
a_0	nominal crack length

A_{kp}	energy lost to kinetic energy process unassociated with fracture (during impact test)
B	thickness
ds	an element of the contour, s .
DENT	specimen type - double edge notched, tension
E'	Young's modulus
EPFM	elasti-plastic fracture mechanics
G	strain energy release rate
G_c	critical strain energy release rate associated with cracking
G_{Ic}	plane strain critical strain energy release rate associated with cracking
I	impact energy
J	the J Integral
J'	the J integral determined under fatigue loading ($R=0$)
J_c	the critical J integral associated with crack growth
J_{Ic}	plane strain critical J integral associated with crack growth
J_e	elastic component of J integral
J_p	plastic component of J integral
K_I	stress intensity factor (for loading mode I)
K_{Ic}	plain strain critical stress intensity factor (for crack growth)
K_c	critical stress intensity factor (for crack growth)
L	ligament length and in reference to equation 4.40, from Williams, p. 120, the span.
LEFM	linear elastic fracture mechanics
P	load
PE	Potential Energy
PS	polystyrene
r'_p	theoretical plastic zone radius
r_p	actual plastic zone radius
S	specimen span (or height) between grips
SBR	styrent butadiene rubber
SENT	specimen type - single edge notched, tension
T	tension vector perpendicular to a contour in an outward direction
T_y	tensile yield strength
u	a component of the displacement vector, U , of a contour in the 'x' direction,
U	energy introduced to a system
U_e	component of elastic energy
U_p ,	component of plastic energy
W	width
w_{Ie}	essential work of fracture in plane strain
w_e	essential work of fracture
w_i	essential work of fracture - initiation
w_f	work of fracture
w_p	plastic work of fracture
Z	strain energy per unit volume

α	a constant for geometry
β	shape factor
Δa	change in crack length
ΔK	change in stress intensity factor
ΔJ	change in value of J (associated with crack extension)
Φ	geometrical correction factor
γ_s	surface energy
γ_p	term for plastic energy dissipation
Γ	a closed contour in a stressed solid,
η_e	factor of elastic work – for determination of J (see p. 113)
η_p	factor of plastic work – for determination of J (see p. 113)
ν	Poisson's ratio
σ	mean normal stress
σ_c	stress for crack initiation and extension
σ_y	yield stress
ω	fracture energy

Chapter 5

a	Crack length
A	Paris constant
ABS	acrylonitrile polystyrene
AN	acrylonitrile
C*	numbered Paris (paris like) constant used to set out various fatigue crack growth models
COD	crack opening displacement
da/dN	rate of crack growth
DASC	data acquisition system circuit
DCG	discontinuous growth bands
EPFM	elasti-plastic fracture mechanics
ERPv	Effective rubber phase volume
FCG	Fatigue Crack growth / fatigue crack propagation
HIPS	high impact polystyrene
Hz	Hertz
J	J integral
J	Rivlin and Thomas surface work parameter, related to $(\gamma_s + \gamma_p)$ employed to describe fatigue in Rubber
K_c	critical stress intensity factor
LEFM	linear elastic fracture mechanics
m	Paris exponent,
m'	exponent associated with description of FCG associated with ΔJ
m*	numbered Paris exponent (paris like) used to set out various fatigue crack growth models
MBS	methylene butyle strene
Mw	molecular weight

N	Number of cycles
N _{ci}	cycles to crack initiation
N _{cf}	cycles consume in propagating crack to failure total [cycles to failure - cycles to crack initiation]
N _f	total cycles to failure
PS	polystyrene
PSAN	poly styrene acrylonitrile
PVC	poly vinyl chloride
R	offset stress ratio (fluctuating load)
RIPD	size corrected interparticle distance (IPD/C - C= centre to centre distance)
SEM	Scanning electron microscopy
T _y	tensile yield strength
T _r	tensile rupture strength
TEM	Transmission electron circuitry
Δa	change in crack length
ΔJ	strain energy release range
ΔJ _{th}	threshold' value ΔJ associated with limiting crack growth
ΔK	stress intensity factor range
ΔK _{th}	alternating stress concentrating
ΔT	change in temperature
Δσ	alternating stress amplitude
λ	damage accumulation parameter
σ _a	fatigue endurance strength
σ _e	fatigue endurance strength
σ _f	ultimate tensile strength (UTS) at failure
σ _{ut}	rupture strength failure- in reference to HIPS where UTS is typically is significantly less than yield
(σ _a /σ _f)	relative stress ratio
°C	temperature - degrees celcius

N	Number of cycles
N _{ci}	cycles to crack initiation
N _{cf}	cycles consume in propagating crack to failure total [cycles to failure - cycles to crack initiation]
N _f	total cycles to failure
PS	polystyrene
PSAN	poly styrene acrylonitrile
PVC	poly vinyl chloride
R	offset stress ratio (fluctuating load)
RIPD	size corrected interparticle distance (IPD/C - C= centre to centre distance)
SEM	Scanning electron microscopy
T _y	tensile yield strength
T _r	tensile rupture strength
TEM	Transmission electron circuitry
Δa	change in crack length
ΔJ	strain energy release range
ΔJ _{th}	threshold' value ΔJ associated with limiting crack growth
ΔK	stress intensity factor range
ΔK _{th}	alternating stress concentrating
ΔT	change in temperature
Δσ	alternating stress amplitude
λ	damage accumulation parameter
σ _a	fatigue endurance strength
σ _e	fatigue endurance strength
σ _f	ultimate tensile strength (UTS) at failure
σ _{ut}	rupture strength failure- in reference to HIPS where UTS is typically is significantly less than yield
(σ _a /σ _f)	relative stress ratio
°C	temperature - degrees celcius

Chapter 1

High Impact Polystyrene (HIPS)

THE ORIGIN, COMPOSITION AND POLYMERISATION OF HIPS.

1.1 Preview

The following chapter introduces HIPS. Its focus is on reviewing the origins of the material, its preparation and the methods used to control its secondary, 'rubber', phase morphology. The central conceit of the entire work is that the materials morphology may be controlled. Although precise details of how structural control was exercised in preparing the resins used remain confidential to Dow, in order to establish the fundamental premise of the work, the principles of how polymerisation conditions do control morphology are reviewed.

High Impact Polystyrene (HIPS)	1
1.1 Preview	1
1.2 The origins of High Impact Polystyrene	1
1.3 General Considerations of the Materials used in Preparing HIPS.	2
1.4 General Considerations of the Methods used in Preparing HIPS.	3
1.5 The Bulk Polymerisation of HIPS.	3
1.6 Polymerisation Reactions in the Preparation of HIPS.	4
1.6.1 Initiation	4
1.6.2 Propagation.	4
1.6.3 Termination	5
1.6.4 Graft Reactions.	6
1.7 Phase Inversion in the Bulk polymerisation of HIPS.	8
1.8 Structural Control in the Bulk Polymerisation of HIPS.	10
1.9 Control over the Rubber Phase Volume.	10
1.10 Control over Rubber Particle size.	11
1.11 Conclusion	13
1.12 References	13

1.2 The origins of High Impact Polystyrene

High Impact Polystyrene (HIPS) is a heterogeneous polymer system that can be described as a polymer-polymer composite. It comprises of a continuous rigid polystyrene (IUPAC:-*poly(phenylethene)*) matrix and a dispersed, usually particulate, compliant rubber phase[1]. The historical engineering impetus for the preparation of the composite has been to improve the impact toughness of polystyrene.

The materials' origins date to 1927 when Ostremlinsky, an early worker on the styrene polymerisation mechanism, filed a patent for what was an intractable and ultimately unsuccessful polystyrene/rubber composite[2]. The ending of the Second World War provided the stimulus for the development of a commercial rubber toughened polystyrene material. During the war enormous amounts of energy and capital had been spent on developing and producing synthetic materials, notably, styrene butadiene rubbers for tyre production. Consequently when it ended there were abundant supplies of cheap styrene, fledgling but rapidly developing markets for synthetic materials and an established plant capacity for the production of styrene based polymers. The commercial opportunity was obvious [3].

The markets for unmodified general purpose polystyrene (GPPS-the homopolymer) material were perceived as limited because of the materials inherent brittle and rigid nature. However the market potential for tougher materials appeared enormous. The research and development efforts of a number of companies focused on seizing advantage of this. Their strategies centred on developing composite styrenic materials to take advantage of the availability of the raw materials and extend the utility of the materials and growing the market for styrene based plastics. HIPS and ABS (an acronym for acrylonitrile, butadiene & styrene) became the initial and, for a long time, only materials that took advantage of what became known as 'rubber-toughening'. Today both materials are high volume commodity resins while many more similarly modified resins have been developed, e.g., polycarbonate, epoxy, polyethylene terephthalate, poly (vinyl chloride) [4, 5, 6]. The Dow Chemical Company was first to bring HIPS to market. It began the first commercial production of HIPS in September 1948. In spite of a somewhat shaky start the material eventually achieved enormous success and a number of other companies quickly entered the market, e.g., Monsanto. An excellent review of Dow's development of HIPS and its production processes was presented at the SPE International Award Address of 1973, by J.L. Amos [3].

Research efforts, over the past fifty years have developed our knowledge of the materials', such that today it is possible for manufacturers of HIPS to prepare resins whose structures are tailored to realise rheological and monotonic mechanical property specifications desired by customers.

1.3 General Considerations of the Materials used in Preparing HIPS.

Polybutadiene (PBD) is the rubber most commonly used in the preparation of HIPS. However a wide range of other graftable elastomers have been used in order to obtain materials with 'unique' properties to suit specific applications[7]. In addition to 'neat' PBD many commercially available impact modified polystyrenes are prepared using 'secondary substrates' such as; copolymers of PBD with styrene, butyl acrylate, pentadienes, olefins and vinyl ethers; EPDMs(ethylene-propylene diene monomer); ethylene copolymers of vinyl acetate, ethylacrylate and vinyl chloride. All of whose labile hydrogen atoms offer sites for graft and crosslinking reactions. Even silicone rubbers can be employed where, for example, of the order of 10% of the methyl groups in poly(dimethyl siloxane) are replaced by vinyl groups to

allow for graft and crosslinking sites; poly-isoprenes; butyl rubbers and many more materials are also found in 'toughened' styrenic materials. In fact any elastomer possessing graftable and crosslinkable sites, a sufficient measure of compatibility with styrene monomer, incompatibility with PS and a low glass transition temperature can be entertained as a toughening agent. However use of PBD dominates and impact modified polystyrene systems based on it are synonymous with the term HIPS. As only PBD toughened materials are considered in this work only they shall be considered in the following discussion.

As expected the type and quantity of polybutadiene incorporated in the matrix resin exerts a large influence on the mechanical behaviour of the composite. However it is the morphology of the secondary phase that exerts the primary influence in any system. This determined by the chemistry of the rubber used, the manner in which it is incorporated in the (poly)styrene in the first instance and the physical and chemical conditions (blending/reaction) employed during polymerisation.

1.4 General Considerations of the Methods used in Preparing HIPS.

There are several routes to toughened polystyrene. The simplest is the mechanical melt blending of polystyrene with polybutadiene or a styrene-butadiene copolymer [8,9,10]. The process of blending can be conducted on extruders, two roll mills and batch or continuous kneaders. However in large scale production of HIPS this has long been out-moded. Polymerisation techniques offer greater cost efficiencies in production and a greater latitude in controlling morphology [11]. Blending technology is still used to make final modifications to a HIPS resins in order to achieve the optimal combination of cost, toughness, gloss and other characteristics. Solution blending of the constituent polymers is common in experimental work for preparing experimental materials [12]. However, the poor cost efficiencies associated with the method as well as difficulties in coping with solvents has prevented it being used on a commercial scale. The most common and commercially successful route is to polymerise a solution of elastomer in styrene using bulk and bulk/ suspension polymerisation methods. These are collectively termed "inter-polymerisation processes" [13].

1.5 The Bulk Polymerisation of HIPS.

Bulk polymerisation is the most common industrial technique in preparing HIPS. It involves the polymerisation of a solution of polybutadiene in styrene and can be divided into three stages;- (i) the dissolution of PBD in styrene monomer, (ii) the prepolymerisation of the system to a stage where the desired morphology is constituted and (iii) a final stage of polymerisation where the remaining styrene is reacted [14,3].

In the first stage a desired quantity of polybutadiene is dissolved in styrene monomer, sometimes in the presence of ethylbenzene. The maximum permissible addition of rubber being limited by the solubility

of the elastomer in styrene and the requirements of viscosity and concentration to allow phase inversion occur at the appropriate stage during polymerisation [15,16]. In general it is considered that the maximum addition of rubber that satisfies these requirements is of the order of $\cong 15\%$ by weight [13].

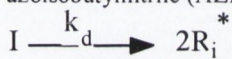
In the prepolymerisation stage the solution is polymerised at temperatures of the order of 80 to 90°C, in the presence of initiators and chain transfer agents amongst other ingredients, beyond phase inversion (see section 1.6.2.) to a level of conversion ($\cong 13\%$) where a stable polymer emulsion of desired morphology is constituted (see sections 1.6.2.&1.6.3..). Free radical polymerisation of the styrene is undergone and both polystyrene and poly(butadiene-g-styrene) are formed.

1.6 Polymerisation Reactions in the Preparation of HIPS.

The polymerisation of styrene comprises three steps, i.e., initiation, propagation and termination.

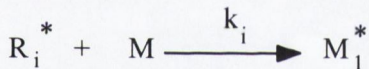
1.6.1 Initiation

Initiation involves the formation of radicals by homolytic dissociation of the initiator, e.g. azoisobutylnitrile (AZBN),



Equation 1.1.

and the addition of these primary radicals to styrene molecules,



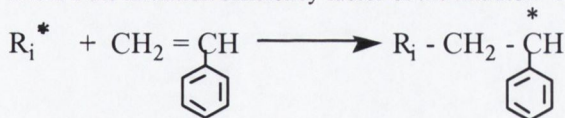
Equation 1.2.

where k_d , the rate constant for initiator dissociation and k_i the rate constant for initiation (r_i) is best described by,

$$r_i = 2fk_d[I]$$

Equation 1.3.

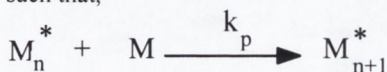
where f the initiation efficiency factor of the initiator. Thus for polystyrene,



Equation 1.4.

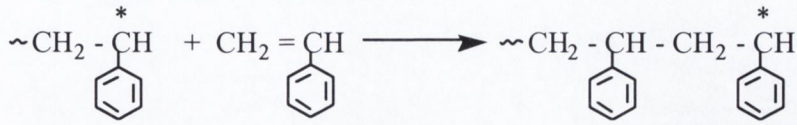
1.6.2 Propagation.

Propagation is undergone by the addition of monomer units to the active end of the propagating chain such that,



Equation 1.5.

where k_p the rate constant for propagation. The mechanism is predominantly head to tail addition. This arrangement is sterically preferred since it involves minimal interaction between bulky phenyl groups and is brought about by the greater stability of the benzylic radical over the methylene radical,



Equation 1.6.

As the rate of initiation r_i is much smaller than the rate of propagation r_p the rate of polymerisation r can be conveniently expressed in terms of the propagation rate,

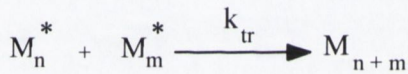
$$r_p = k_p [M^*] [M]$$

Equation 1.7.

where $[M^*]$ the concentration of radicals and $[M]$ the concentration of monomer.

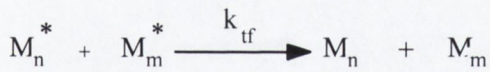
1.6.3 Termination .

Termination is almost exclusively undergone by recombination of propagating polymer radicals at temperatures up to 80°C.



Equation 1.8.

Termination by disproportionation can also occur. This is where abstraction, or transfer of a hydrogen atom from one radical chain to another results in the formation of two molecules one saturated, the other unsaturated (containing a double bond).



Equation 1.9.

Disproportionation results in a broader distribution of the degree of polymerisation. Thus where v describes the average kinetic chain length for disproportionation, then for combination the average kinetic chain length is $2v$. For constant r_p the average kinetic chain length is independent of initiation mode and characteristic of styrene. It may be expressed in the form,

$$v = \frac{r_p}{r_i} = \frac{r_p}{r_t} = \frac{k_p^2 [M]^2}{k_t r_p}$$

Equation 1.10.

However kinetic modelling has shown that the best fit for molecular weight data is obtained by considering combination rather than disproportionation as the principle mode of termination even at temperatures in excess of 80°C [17]. However at temperatures in excess of 130°C disproportionation reactions become more significant [18].

Growth of a chain may also be terminated by a chain transfer reaction. Chain transfer occurs in all radical polymerisations. The reaction of the polymer radical with an atom from another compound within the reaction system terminates growth on the propagating molecule and initiates the growth of a new molecule at the new radical site. Chain transfer must be taken into account in the kinetic scheme as it can have significant effects on the molecular weight and so the degree of polymerisation in the system. Such consideration is achieved by the inclusion of a chain transfer constant, C , i.e., C_Q where C the transfer rate constant for transfer agent Q , and defined in the expression,

$$\frac{1}{\bar{P}_n} = \frac{1}{\bar{P}_{no}} + C_Q \frac{[Q]}{[M]}$$

Equation 1.11.

Where \bar{P}_{no} and \bar{P}_n represent the initial and final degree's of polymerisation for the 'transfer' molecule, (\bar{P} - \bar{P} bar-) indicating the statistical mean averages.

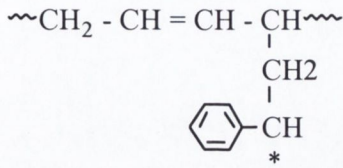
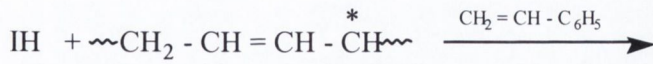
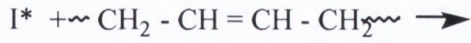
1.6.4 Graft Reactions.

During polymerisation the graft reactions to the rubber phase play a key role in the formation of the secondary phase morphology. They allow for the dispersion of the rubber particles by effecting a polymer oil in oil emulsion that inhibits the coalescence of the polybutadiene phase [20]. Consequently grafting has a large influence in determining the final structure of the materials during the polymerisation process [21, 13,14,22].

The formation of poly(butadiene-g-styrene) is also adventitious to the mechanical performance of the system, contributing to the material's toughness. In effect, anchoring the rubber particle in the matrix and allowing for the transfer of load over the particle and contributing to the stability and strength of crazes.

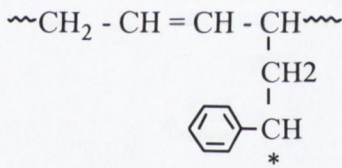
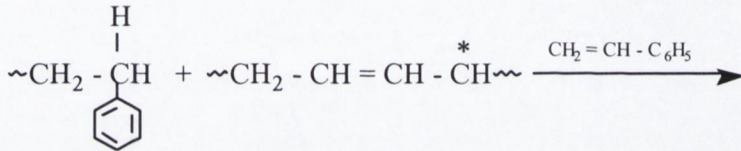
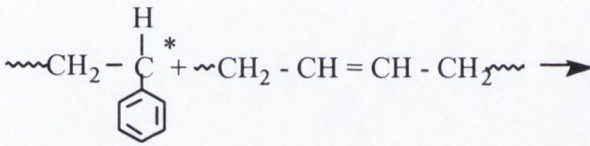
Indeed such interphase adhesion is necessary in realising a material of substantive toughness [4, 15]. The main sites for grafting in the polybutadiene repeat unit are at the double bond and the methylene hydrogen at the allylic α position relative to it. Some authors describe the reaction as hydrogen abstraction.

Such grafting through hydrogen abstraction may be effected by primary radical attack ;



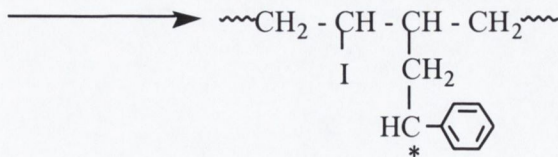
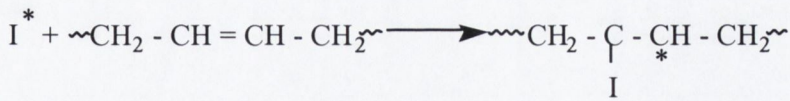
Equation 1.12.

or by attack by a polystyryl radical;



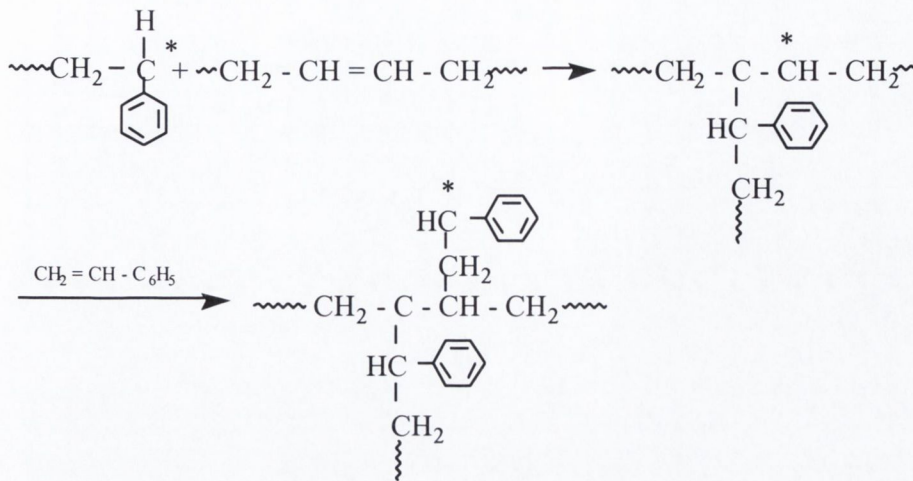
Equation 1.13.

However graft reactions would also be easily facilitated at the double bond by the reaction of a primary initiator radical at the double bond



Equation 1.14.

or by reaction at the double bond of a polystyryl radical;



Equation 1.15.

Control over grafting reactions is effected through the type of initiator system used, e.g. benzoyl peroxide initiators promote grafting while AZBNs do not, temperature and other process variables, e.g., the degree of unsaturation in the rubber, the presence of chain transfer agents[3, 4, 5].

1.7 Phase Inversion in the Bulk polymerisation of HIPS.

Agitation (stirring) always accompanies polymerisation in order for polystyrene to be the continuous phase. Without agitation the polybutadiene phase would remain continuous[23, 24], resulting in an intractable (unprocessable) material. Thus stirring of the prepolymer system is necessary in order to achieve the particulate morphology of HIPS. Molau considered agitation as a quasi catalytic function in the manufacturing process, not fundamentally responsible for the inversion of the system rather, increasing the rate at which inversion occurred. In its absence, as a consequence of the rubber phase's high viscosity (arising from the high molecular weight of the polymer), the rate of inversion, under thermal motion would be too slow and the system would solidify before inverting[20]. However the agitated system, being a dynamic system allows coalescence and re-formation of droplets occur incessantly and so bring the emulsion system come to equilibrium. Although the multiple emulsion, that normally exists after phase inversion clearly shows that equilibrium has not been wholly achieved, in a sense inversion is incomplete.

Initially as polymerisation proceeds, see **Figure 1.1.**, the polystyrene remains in solution, however, at low levels of conversion phase separation begins, **A.** As grafting concentrates at the phase boundary of the polybutadiene and polystyrene it acts as a surfactant in the system and so a polymeric oil-in-oil (POO) emulsion is seen to be established [25].

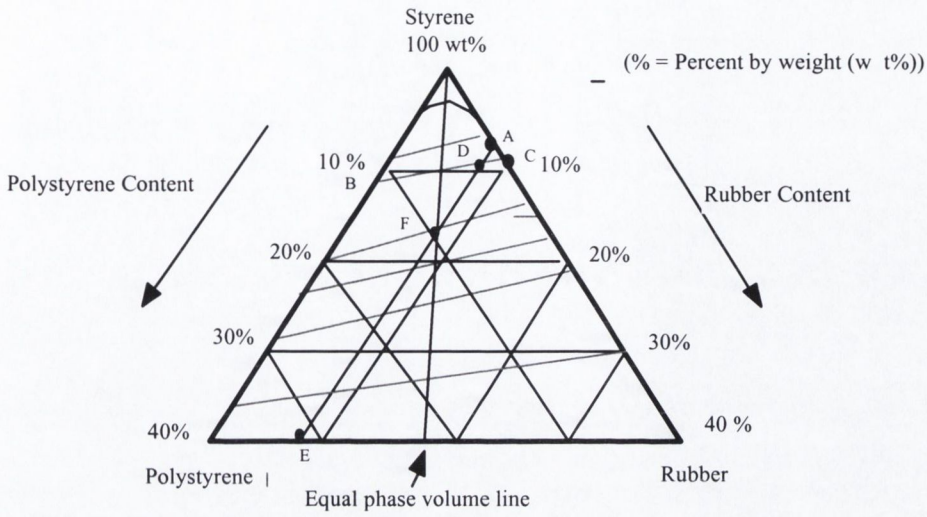


Figure 1.1. Ternary phase diagram for the system styrene - polystyrene - polybutadiene rubber.

With further conversion of the styrene the volume fraction of the polystyrene solution increases. Phase inversion takes place at a point **F**, determined by a number of inter-related factors, e.g., the viscosity of the system, the shear applied to the system, interfacial forces associated with the phases, the degree of conversion and so on [14, 11, 2, 26]. The composition of the continuous phases, at any point during polymerisation, for example **D**, may be determined from the ternary phase diagram's tie lines, i.e., for **D**, **B** and **C**. The phenomenon of phase inversion is seen to be primarily concentration dependent as it can be reversed by the addition of elastomer/styrene solution and usually occurs at a volume ratio of the order of 1 (≥ 1). Viscosity measurements (**Figure 1.2.**) show that phase inversion takes place over a relatively narrow range of conversions [13]. Typically commercial resins contain 6 - 8 % w/w polybutadiene and in such systems inversion is seen to take place at ~ 9 - 12 % styrene conversion [13].

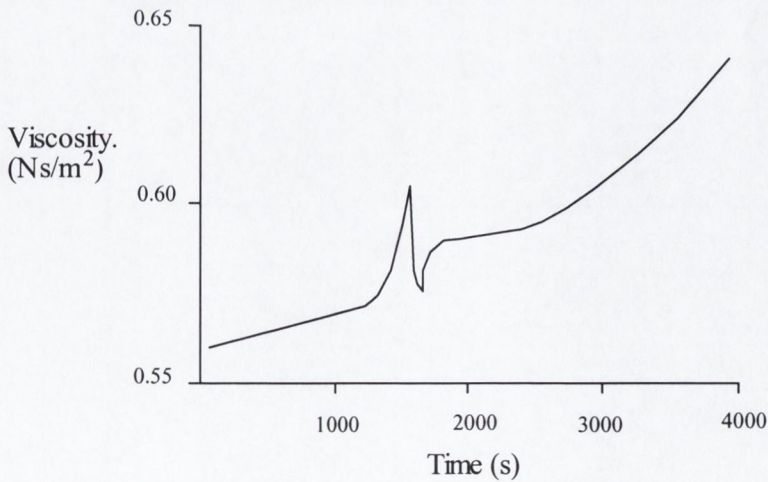


Figure 1.2. Viscosity changes in HIPS prepolymer during polymerisation.

Subsequent to inversion, polymerisation is continued to a level of conversion where viscosity is sufficiently high to prevent further changes to the basic structure and at such time prepolymerisation is seen as being complete. The prepolymer may then be stored for a time or immediately entered into the finishing cycle where polymerisation is completed in bulk or suspension at temperatures of the order of ~ 180 °C.

1.8 Structural Control in the Bulk Polymerisation of HIPS.

The basic assumption of the research is that the rubber phase morphology influences (controls) the physical properties of HIPS materials. Numerous toughening theories have been proposed to explain the general mechanism of rubber toughening and as many theories have been advanced as to how micro-structural variations effect control over the micro mechanisms of failure. And though controversy continues to date, empirical research has allowed the creation and commercialisation of HIPS whose properties have been optimised. The central conceit fuelling the research is that the morphology of materials may be tailored to realise the 'optimal' morphologies.

1.9 Control over the Rubber Phase Volume.

The phase volume of HIPS is determined by the rubber content (by weight), the number and size of particles, and the amount of PS grafted onto the rubber [23]. Investigating the mechanism of rubber particle formation by considering the morphology at various stages of monomeric conversion Molau observed that the polymerisation system, during the early stages of conversion, formed an emulsion of polystyrene solution in styrene dispersed in the polybutadiene solution [27]. In the system the polystyrene grafted on the rubber acted as an emulsifying surfactant. As polymerisation continued to low levels of conversion, first small droplets, then larger polystyrene pools, or inclusions, were formed in the coherent polybutadiene/styrene phase. With further polymerisation, and accompanying agitation, the larger pools ran together, while the smaller emulsified pools remained within the polybutadiene phase. Finally at phase inversion, discussed above, the system inverted with the emulsion of polystyrene in polybutadiene forming the dispersed second phase. The amount of polystyrene trapped, the size and abundance of polystyrene inclusions, determined by the amount of grafting, after phase inversion then determined the rubber phase volume for any given rubber content and particle size. Therefore phase volume increases when grafting increases in the very early stages of the reaction, for a given particle size.

It can be seen then that in addition to determining the onset of phase inversion agitation also influences control over the volume fraction of the rubber phase, as it effects a large control over the rubber particle size and size distribution as well as their morphological appearance. Thus the consideration of rubber phase volume is closely linked to these factors and their control during the polymerisation.

1.10 Control over Rubber Particle size.

The size and dispersion of droplets are essentially determined by the viscosity of the coherent phase, the ratio of its viscosity to the disperse phase and the interfacial tension between them, during the period between phase inversion and the high viscosity final stage. Rumscheidt and Mason evaluated the relationship between particle deformation and viscosity ratio in various shear fields [28]. Their work shows how particles are sized and how size distribution 'evolves' and may be controlled by viscosity and shear (**Figure. 1.3.**). At viscosity ratios (<0.1) deformation of the droplet is stabilised by the pushing off of small satellite droplets from the ends of the deformed particles.

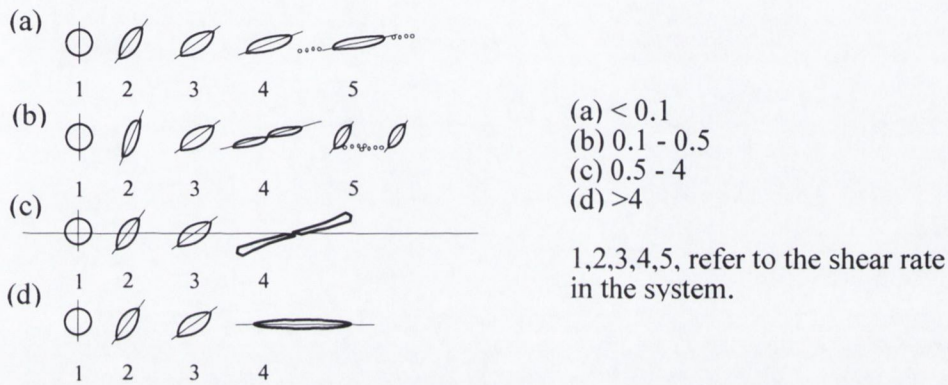


Figure 1.3. Deformation behaviour of droplets at different viscosity ratios (a, b, c & d) with different levels of shear rate (1, 2, 3, 4 & 5) (as per [19]).

At the intermediate ratio (0.1 - 1.0) the deformation and scission of the droplet into smaller droplets was observed. Higher ratios (1 - 4) led to the formation of extended droplets which disintegrated into equal sized particles.

Wagner and Robeson showed that increased agitation produced smaller rubber particles with less occluded polystyrene [29]. Echte also showed similar changes in particle size with increased stirrer rotation speeds [16].

Freegaard was of the view that immediately after inversion the rubber phase existed as clusters, or aggregates, given the shear rate was high enough that these aggregates would be disrupted into small groups so that at any time after inversion the average size of the aggregate would be a function of the shear rate and the viscosity of the system [11]. Re-formation or coalescence of the particles would be inhibited by grafted styrene on the rubber acting as a surfactant and by the increasing viscosity of the system. To some degree a similar mechanism was envisaged by Molau and Keskkula to allow the development of his smaller and morphologically distinct, Type II rubber particles at higher levels of conversion [23] (Type I particles being the large cellular (Argon [12]), Multiple Inclusion (MI) (Bucknall [15]) or 'Salami' (Cigna [30]) type of particles, in **Figure 1.4.**).

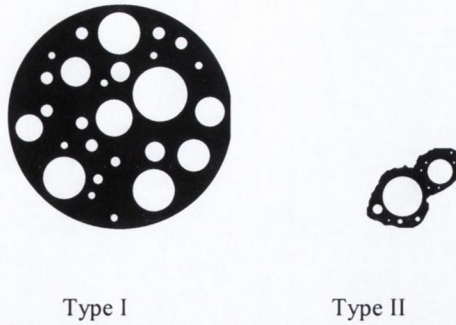


Figure 1.4. Molau Particle types.

Through alternation of the viscosity of the system using a chain transfer agent (TDM -tertiary dodecyl mercaptan) Freegaard found that larger particles could be formed[11]. The experiments by Echte considered the effect of system viscosity in manipulating rubber phase morphology and further showed that by altering the viscosity of either the rubber phase, by its molecular weight, or the polystyrene phase, through chain transfer agents, that the size of particles could be varied and controlled [16].

The interfacial tension which may be seen as being controlled by the level of grafting also was investigated by Echte and he showed that particle size could be manipulated through type, and by corollary, concentration, of initiator used [16]. Temperature and physical control of graft concentration were also seen as possible methods of controlling system viscosity and so particle size. In the latter polystyrene homopolymer may be added to the feed stock so that phase inversion takes place at lower graft levels with, as a consequence, larger particles being formed [31]. These latter methods provide industrial manufacturers of the material with the greatest opportunity of morphological control and the selection of chain transfer agents, initiators and temperature and stirrer speeds. Also the timing of their introduction/variation are critical to the preparation of structurally controlled materials [32].

Echte's classical studies were perhaps most notable for their consideration of the manner in which the structure of the rubber particles is determined, during the course of polymerisation, by grafting. Echte studied how particle structure varied in two series of HIPS prepared by solution mixing, which precluded graft reactions, and by polymerisation, where grafting occurred, using block copolymers of a variety of polystyrene contents (see **Figure 1.5.**). From the resultant particle shapes it appeared that the effect of the grafting was to cause a shift in the HIPS particle structure associated with a certain copolymer type to another associated with a higher polystyrene content (see **Figure 1.5.**). Thus for the case of the pure polybutadiene the shape of the particle structure resembled that of a HIPS, prepared using the solution technique, possessing 15% polystyrene. This was a result of grafting of polystyrene to the polybutadiene early in the polymerisation.

These observations led Echte to surmise that during the polymerisation of HIPS additional grafting onto the polybutadiene of the copolymers lead to an increase in the polystyrene content in the PS

domains of the copolymer. Consequently when the polystyrene content in the domains reached a critical limit the structure of the domains changed to that of the corresponding copolymer of the same polystyrene content. Thus Echte concluded, if such a change occurs prior to phase inversion the structural type of the particles formed is 'shifted' to correspond to those of the copolymer of higher polystyrene content. The implication of his research were that an infinite variety of particle types could be prepared by use of di-, tri, or multiblock poly(styrene-butadiene) copolymers.

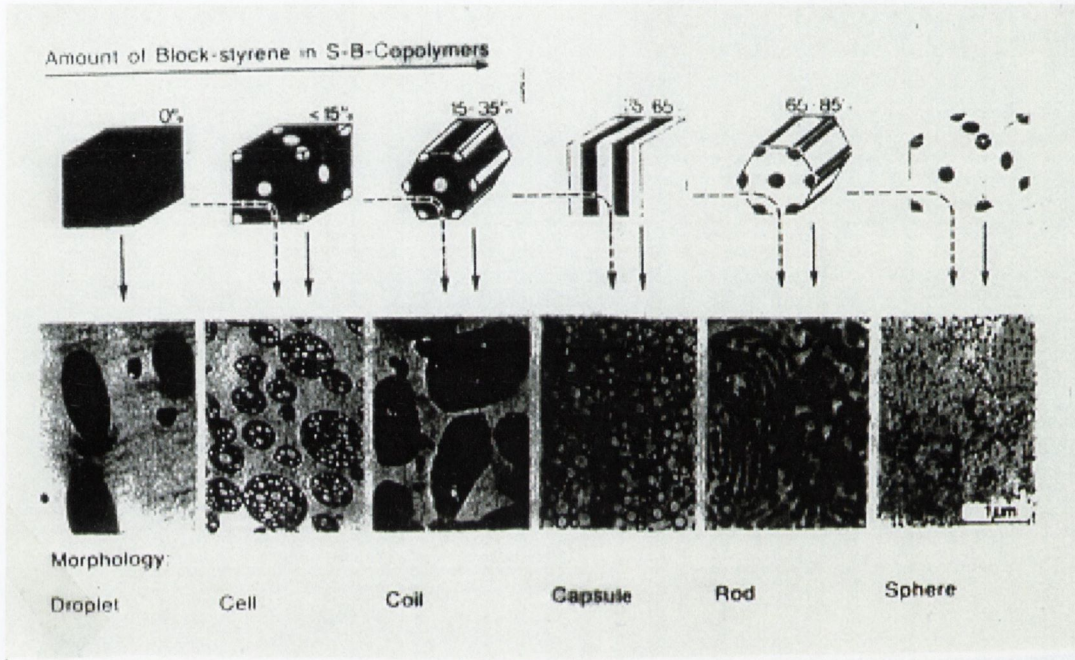


Figure 1.5. Particle structures obtained by polymerisation of HIPS using SB diblock copolymers of various copolymers (solid lines without grafting dashed lines with grafting) (As per[16])

1.11 Conclusions

- From the literature it is concluded that the morphology of the secondary phase particles may be controlled during polymerisation through both chemical, e.g., grafting, etc., and physical, e.g., shear, etc., methods.

1.12 References

- 1 ROSEN, S.L., *Polym. Eng. & Sci.*, 17, 115, 1967.

- 2 OSTROMLENSKY, I.I., US Patent, 1613673, Jan 11, 1927.
- 3 AMOS, J.L., J. Polym. Eng & Sci, 14, 1, 1, 1974.
- 4 WU, S., Polymer, 26, 1855, 1985.
- 5 GEORGE, K.E., JOSEPH, R., Polym. Eng. & Sci, 27, 15, 1130, 1987.
- 6 BUCKNALL, C.B., HEATHER, P., LAZZER, A., J. Mater. Sci, 16, 2255, 1989.
- 7 PLATZER, N., Chemtech, October, 634, 1977.
- 8 TUCHMAN, D., ROSEN, S. L., 112th meeting of Rubber Division, ACS, Cleveland, Ohio, OCT., 4-7, 1977.
- 9 PITTOLO, M., BURFORD, J., J. Mat. Sci., 21, 1769, 1986.
- 10 DURST, R.R., GRIFFITH, R.M., URBANIC, A.J., Toughness and brittleness of plastics, Chapt 19, pp. 239-246.
- 11 FREEGAURD, G.F., Br. Polym. J., 6, 205, 1974.
- 12 ARGON, A.S., COHEN, R.E., *Crazing of Polymers*, Vol. 2. *Advances in Polymer Science*, 91/92. ed., Kausch, H.H., Springer -Verlag, 1990.
- 13 MANN, J., *Rubber re-inforced Thermoplastics. The Physics of glassy Polymers. Chapter 8*, ed., Haward, R.W., Applied Science Publishers, 1973.
- 14 SILVERSTEIN, M. S., NARKIS, N., J., Appl. Polym. Sci, 40, 1583, 1990.
- 15 BUCKNALL, C.B., *Toughened Plastics*. Applied Science Publishers, 1977.
- 16 ECHE, A., *Die Angewandte Macromolekulare, Chemie*, 58/59, 846, 175, 1977.
- 17 HUI, H., J. Appl. Poly. Sci., 22, 102, 1972.
- 18 BERGER, M., 1975
- 19 VAN NUFFEL, C., Dow Benelux N.V., Internal Communication, 1990.
- 20 MOLAU, G.E., J. Polym. Sci., A3, 4235, 1965.
- 21 YENALYEV, V.D., MELNICHENKO, N.I., BOVUKUNENKO, O.P., BULATOVA, V.M., Polymer, 20, 39, 1980.
- 22 CAMERON, G. GORDON. M , & QURESHI Y. J. Polym. Sci., Polym. Chem. Ed., 18, 3149, 1980.
- 23 MOLAU, G.E., Keskkula, H.H., J. Polym. Sci., A1, 4, 1595, 1966.
- 24 WU, S., Polym. Eng. & Sci., 30, 753, 1990.
- 25 EASTMOND, G. C. "Supramolecular Structures in Mixtures of Homopolymer with Graft / Block Copolymer: Their form and Origin". *Toughening of Plastics II*, PRI, 2-4 JULY, 1985.
- 26 MOLAU, G.E., *Kolloid Zeitschrift und Zeit Band*, 238, 493, 1964.
- 27 MOLAU, G.E., J. Polym. Sci., A3, 1267, 1965.
- 28 RUMSCHEIT, F.D., MASON, S.G., J. Colloid, Sci., 16, 238, 1961.
- 29 WAGNER, E.R., ROBESON, L.M., *Rubber Chem. Tech.*, 43, 1129, 1970.
- 30 CIGNA, G., et al, J. Appl. Polym. Sci, 44, 505, 1992.
- 31 BEAR, M., J. Appl. Polym. Eng. Sci., 16, 109, 1972.
- 32 NIJHOF, B., Dow Benelux N.V., Dow Benelux N.V., Internal Communication, 1991.

Chapter 2

EXPERIMENTAL MATERIALS

Materials Preparation and Characterisation.

2.1 Preview

The following chapter presents the materials used in the research and the manner in which they were prepared and characterised. All the discussions that follow in subsequent chapters, concerning the influence of the secondary phase, take their bearing from how it was characterised, i.e., the techniques used and their findings.

Experimental Materials	15
Materials Preparation and Characterisation	15
2.1 Preview	15
2.2 Introduction	15
2.3 Materials Selection	18
2.4 Characterisation of Matrix materials	18
2.5 Characterising the Secondary Phase Morphology	18
2.6 Gel Content Studies	19
2.6.1 Gel Content Studies; Introduction and Overview	19
2.6.2 Procedure	19
2.6.3 Results	20
2.6.4 Discussion of Results	20
2.6.5 Conclusion from Gel content Analysis	21
2.7 Coulter Counter Analysis	21
2.7.1 Coulter Counter Analysis; Introduction and Overview	21
2.7.2 Procedure	22
2.7.3 Coulter Counter Results	22
2.7.4 Discussion of Results	24
2.7.5 Conclusions from Coulter Counter Analysis	25
2.8 TEM (Transmission Electron Microscopy) Analysis	25
2.8.1 TEM Analysis; Introduction and overview	25
2.8.2 Procedure	30
2.8.3 Results of TEM Analysis	30
2.8.4 Discussion of TEM plates; Particle Morphology	34
2.8.5 Discussion of TEM Quantitative Image Analysis	35
2.8.6 Conclusions from Quantitative TEM analysis	35
2.9 Preparation of Polymer blends used in the study	36
2.10 Discussion of Conclusions from Secondary Phase Characterisation Tests	37
2.11 References	38
2.12 Appendix 2.1: Results of Coulter Counter Analysis	39
2.13 Appendix 2.2. Results of Transmission Electron Microscopy	40

2.2 Introduction

Clearly, in order to determine the influence of the secondary phase morphology on mechanical properties, it needs to be well characterised. Over the years a number of strategies have been employed by researchers to prepare experimental resins whose microstructure is, or can be easily, established.

These have ranged from polymerising experimental resins of 'controlled morphology', through solution casting and melt blending known polymers in resins similar to that of their 'matrix', to dispersing pre-polymerised and sized rubber toughening particulates in a matrix resin [1,2,3,4].

To investigate the influence of RPS and ERPV[†] both must be isolated as experimental variables, and the influence of other influential structural features must be accounted for, or excluded, from the experimental system. Although studied for many years the understanding of the influence of these "other variants", is not advanced enough to allow them be excluded from test data [5,6,7]. Therefore the only means to 'exclude' them is by eliminating their variation in the experimental materials.

The ideal approach to adopt in preparing experimental material systems would be to polymerise a series of HIPS, which only varied in RPS and ERPV. Unfortunately to do so in a fashion that would realise the same materials with the same molecular weights, secondary phase particle types, levels of interphase adhesion etc., is not something that is easily achieved. Consequently an alternative strategy is required that allows the preparation of suitable materials in a reasonable time at a reasonable cost.

There are only a limited number of ways to increase the rubber phase volume during polymerisation;

1. For a given particle structure and size - increasing the rubber content (wt% fraction) and so the number of particles.
2. For a given rubber content and size - increasing the volume of PS inclusions in particles reducing the rubber content in each particle and so increasing the number of particles.
3. For a given rubber content and number of particles - increasing the volume of the PS inclusion its size and consequently the particle conformation and the effective rubber phase volume.

Altering micro-morphology while maintaining precisely the same type of particle morphology during polymerisation requires either; adding judicious amounts of rubber at an appropriate time, to increase the volume of rubber available, or, increasing the population of particle while reducing their size, by stirring or by adding other reactants that alter the polymerisation solutions viscosity. The latter is practical although inconsistencies can arise in the nature of the rubber and the uniformity of particle size populations. This then yields uneven particle size distributions that promote different micro-mechanical responses and so exhibit differences in mechanical properties.

The materials considered in this work only contained 8% rubber by weight. Increasing the rubber phase volume could only be achieved by increasing the PS content in the rubber particles. Consequently great care was necessary so that the morphology was maintained over the range of desired particle sizes. Thus sizing particles, by controlling their internal morphology and controlling their populations provided the only means of controlling size and volume.

[†] **Note.** At Polymer '94 (IMI, London, 1994) it was commented by Professors C. Bucknall & A. Pavan that it is better that the term rubber phase volume (RPV) be prefixed by the word Effective (ERPV) to underline that what is considered is the overall volume of particles and not merely the rubber phase which would be the normal connotation of the expression.

In doing this the wall thickness of rubber particle is thought to have varied somewhat that influenced the mechanical properties of the particle, e.g., the hydrostatic stress it imposed after cooling. The sensitivity of morphology to the polymerisation process is very much a mixed blessing. On one hand it offers the power to control morphology and so behaviour. Yet on the other, it constrains this freedom through the complexities of the interactions between the polymerisation process variables, i.e., reaction conditions kinetics etc., to realise specific structures.

In Chapter 1, the methods used to effect and affect rubber particle size (RPS) and effective rubber phase volume (ERPv) were reviewed. It was shown how these features could be altered, and how, by doing so, other structural characteristics that influence mechanical behaviour were also affected. For example, the introduction of catalysts and chain transfer agents, who interact implicitly with reactants, alter the rheology of the polymerisation solution. This allows manufacturer's to control RPS and ERPv easily;- simply by stirring (i.e., shear). However their addition also alters graft density levels, rates of polymerisation, and consequently particle matrix adhesion, matrix molecular weight and particle structure. Independently each of these features, can radically influence the mechanical behaviour of the subsequent material (Chapter 3). Consequently, though the motivating intent of altering a parameter, or step, during polymerisation might be to alter a specific aspect of morphology, careful thought of the broader implications of the outcome of the adjustment is necessary to insure that other features are not adversely affected [8,9,10].

A detailed consideration of the methods used to control particle size, structure and effective rubber phase volume (ERPv) during polymerisation is beyond the scope of this work. Although relevant it is not immediately pertinent, it is also confidential to the Dow Chemical Company. However from the discussions above it is clear that it is possible to polymerise materials whose micro-morphology are essentially the same. It shows that it is possible for manufacturers, albeit with some effort, to prepare 'design driven' materials.

The pragmatic approach to preparing optimised materials, and the one most commonly adopted by researchers, has been to 'solution' or 'melt' blend HIPS resins, differing in RPS, with a GPPS at different levels of concentration to realise materials of different ERPv [11,12]. The technique is also employed in industry by plastics materials compounders to prepare specialist compounds optimised or tensile, impact and gloss properties. Although the 'secondary morphological variants', e.g., rubber particle morphology, are not excluded, their influence can be minimised by minimising the differences in the structural 'character' if the HIPS used in preparing blends, and 'matching' the type of secondary morphological features. Some workers have opted to melt blend separately prepared toughening (particulate) materials, e.g., latex emulsion polymerised (n-butyl acrylate) **core-** (polystyrene) **shell** particles in polystyrene [13,14]. Although this does exclude the influence of the 'secondary morphological variants' the subsequent blends lack significant 'qualities' of a conventional HIPS resin relevant to the process of craze initiation and propagation, i.e., particle/matrix adhesion, hydrostatic stress, particle deformation, rubber phase properties, e.g., bulk modulus, tear strength, trans crystallisation of PBD during deformation, etc.

2.3 *Materials Selection*

In this work a combined approach was adopted in preparing the experimental materials. Three 'parent' experimental resins identified as PSB1, PSB2 and PSB3, possessing populations of small medium and large particle sizes, were prepared by Dow using bulk polymerisation techniques, in a fashion that yielded materials matched in matrix molecular weight, 'secondary morphological variants' and consequently varying substantially in RPS, and ERPV. These parent resins were subsequently melt blended in a polystyrene resin whose macromolecular properties were the same as the matrix of the parent HIPS resins. The precise details of preparation are not central to the work and are not disclosed.

In short the parent HIPS resins;

- were prepared using the same (polybutadiene, 8%) and under conditions that yielded the same (MI, multiple inclusion, or, 'salami') type rubber particle structure. This was done so that the physical and mechanical characteristic of the rubber phases and their interaction with matrix would be similar.
- possessed similar matrix molecular weights (M_w), of the same order, as the M_w of the base PS resin chosen for blending (PSB0) and so exclude the influence of matrix M_w variation. This also assisted dispersive and distributive mixing of the materials in the molten state, and so the uniformity of the polyblends.
- exhibited a large variation in their particle sizes so that the origin and magnitude of variations in material behaviour would be clearly exposed and identified as being a result of changes in RPS.

Thus, as the particle type and matrix resin were essentially the same, it was possible to make the assumption that the variations observed between materials arose from the variations in RPS and ERPV and not other morphological variants, and conclusions regarding their influence could be drawn.

2.4 *Characterisation of Matrix materials.*

Gas Phase Chromatography (GPC) analysis was used to reveal the molecular weights of the materials to be 180.6 , 183.4 and 178.9×10^3 AMU and that of the GPPS resin chosen (PSB0) was 202.6×10^3 AMU [15].

2.5 *Characterising the Secondary Phase Morphology.*

All of the assumptions and arguments made in the course of the thesis, concerning the secondary phase, pivot on the reliability of results obtained from the methods employed in characterising the morphology. The general composition of the resins and the assumptions made in regard to the secondary phase centred characterisation efforts on determining the RPS and ERPV. Three techniques were considered, Gel Content, Coulter Counter and Quantitative TEM. Given the relevance of the tests to all that follows they are explored at some depth. The principle of operation, protocols used and details of results from each method are presented in the following sections and the results of the analysis are presented in Appendix 2.1.

Other techniques have been used in the course of the development of the experimental resins, e.g., dynamic mechanical spectroscopy (DMS). Whilst not possessing the resolution to characterise the

microstructure, e.g., DMS can resolve, detect, anisotropic features approx. 140 μm , it can be used in a quality control fashion to fingerprint materials. Use was made of it as a quality assurance tool in verifying the morphology of melt blended resins e.g., dispersion in blends details of tests are not included.

In addition to the quantitative work on the TEM images, particle size assays, the TEM plates (images) were also studied to confirm that the structure of the secondary phase particles were indeed cellular MI (multiple inclusions).

2.6 Gel Content Studies.

2.6.1 Gel Content Studies; Introduction and Overview.

The gel content method has been used by a number of researchers to evaluate secondary phase volume in HIPS. The analysis is relatively primitive but was conducted on the materials in order to assess its utility as a low cost alternative (to TEM) in characterising RPV. The comparison was made by contrasting results of tests obtained from it with that from the more accurate, but much more time consuming and expensive TEM method.

The gel content analysis is based upon the principle of phase separation. The separation of the phases is achieved by selectively dissolving the continuous polystyrene matrix phase using an appropriate solvent, (di-methyl-formamide) DMF, and then precipitating the insoluble secondary phase out of solution usually under centrifuge. A simple comparison of the volumes of the two phases then allows for a determination of rubber phase volume.

Inaccuracies arise in the analysis from a variety of sources. Selective leaching of polystyrene from inclusions, within the particle, tend to lead to an underestimation of the RPV. Grafted polystyrene can lead to an overestimation of RPV. That measurement of the RPV is sensitive to such opposing sources of error and that the extent to which they may adversely influence or distort results is indeterminate within the analysis, undermines the veracity of the technique.

Regardless of this many investigators have used the technique in characterising RPV although no consideration appears, in the literature, to have been made as to the accuracy of the method or the influence of the potential sources of error associated with using it, in comparison to more accurate techniques.

2.6.2 Procedure

1. Eight 30g samples of the HIPS were dissolved with 100ml of DMF in centrifuge test tubes.
2. The solutions were centrifuged for ≈ 15 minutes until all of the secondary phase (gel) was judged to have precipitated from the solution.

3. The polystyrene solution (clear) was then poured off and the precipitate retained.
4. The precipitate was then washed with solvent and centrifuged for a second time before the gel content of the samples determined and average volume determined.
5. The above procedure was conducted for the PSB1, PSB2 and PSB3 HIPS resins

2.6.3 Results

The results of the Gel Content analysis are presented in the Table 2.1. below.

Material	PSB1	PSB2	PSB3
Gel Content	28.4	29.4	32.8
	28.2	29.6	33.0
	28.3	29.3	32.5

Table 2.1. Results of Gel Content Studies (% Rubber Phase Volume).

2.6.4 Discussion of Results

The test results showed that the rubber phase volume of the PSB1 was less than that of PSB2 and it less than that of PSB3. However all three parent resins were grouped at approximately 30 % volume. In so far as the results were consistent and ranked the materials correctly the tests could be considered as successful. However the findings contrast hugely with the results from TEM analysis, casting enormous doubt over the accuracy and the fundamental utility of the test data.

The results suggest there to be little difference between the rubber phase volume in the three materials. However the explicit determinations of TEM determined significant differences. It was acknowledged above that there are many potential sources of significant error in the test. Depending upon the Mw and its distribution polystyrene may be extracted from particles especially larger particles by the solvent altering the RPV determined. The most significant source of error in the case of MI particles is considered to be the grafted polystyrene, which adds significantly to mass measured in the tests and led to the three resins 'grouping' at approximately 30 % ERPV. This result does provide some corroborative insight in regard to the level of similarity between the secondary phase morphology of the resins. This is a point that will be returned to throughout the remaining chapters.

However the central conclusion drawn from the tests and their comparison with the TEM analysis is that the Gel content analysis, at best, only provides a rough estimate of the rubber phase volume. The analysis is known to be sensitive to many errors and ultimately the method should be considered advisedly or disregarded by investigators.

2.6.5 Conclusion from Gel content Analysis.

The main conclusion drawn from the tests and their comparison with the TEM analysis was that the gel content analysis, at best, only provides a rough estimate of the rubber phase volume. The method should be considered advisedly or disregarded entirely by investigators.

2.7 Coulter Counter Analysis

2.7.1 Coulter Counter Analysis; Introduction and Overview.

The principle under which the coulter counter operates and its method of operation are illustrated in Figure 2.1 below.

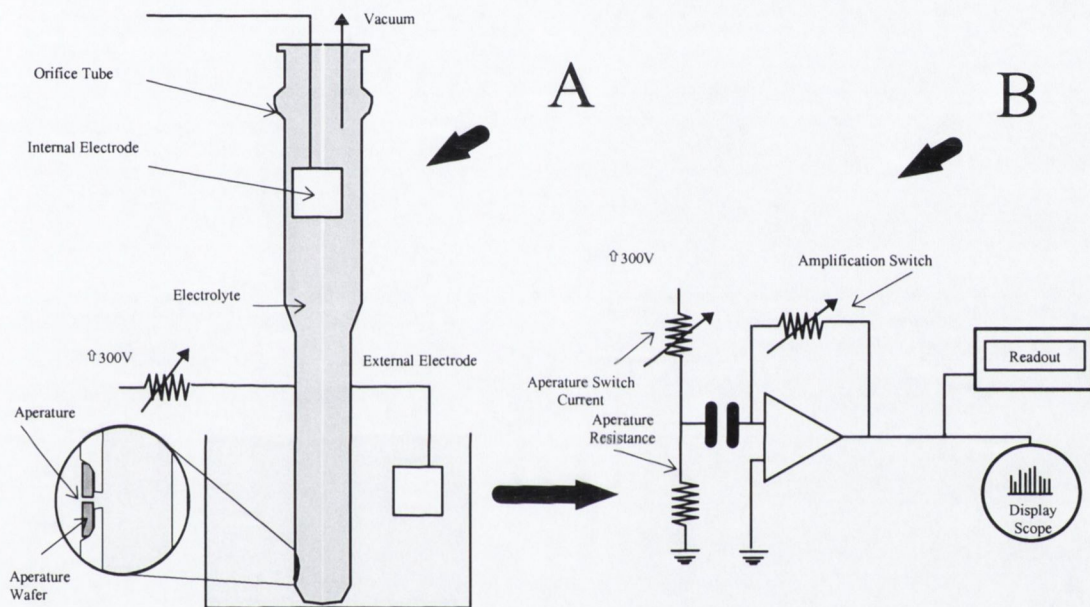


Figure 2.1. Coulter Multisizer Counter™ **A.** Drawing of the Coulter apparatus. **B.** Simplified Schema of amplification circuitry and data presentation methods. [16].

The Coulter Counter multisizer operates by monitoring changes in current between two electrodes immersed in an electrolytic dilute polymer suspension. Fluctuations in current arise as a consequence of the suspended particles moving through an aperture in the non-conductive orifice tube. The increase in the resistance between the electrodes reduces current, which modulates by amounts proportional to the volume of the particles passing through the aperture. The train of pulses obtained are then analysed by the systems software, the analysis of calibrated pulse heights producing a particle volume or an equivalent (spherical) particle diameter distribution.

The theory underlying the principle of the machines operation is precise. However certain considerations that may adversely affect the quality of the data obtained, e.g.:

1. Particle agglomerates forming within the electrolytic solution which tend to result in the true particle size being over-estimated.
2. The limited number of aperture sizes tend to skew the analysis. Large particles unable to pass through the aperture will give rise to 'clipped' pulses. Small particles provide an additional problem in that if they are less than 2 % of the aperture size they are completely lost to electric 'noise'.
3. Should a number of particles enter the sensing zone their presence will naturally give rise to an overestimate of size.
4. Rheological variations extending from the size of particles in the solutions may also impinge upon the shape of the distribution.

Thus the method is sensitive to unquantifiable errors, irrespective of the quality of the calibration. The extent of these errors can be offset by reducing the concentration of the material in solution. This may give rise to some variability in the particle size distribution curve. However the statistical significance of such variance will reduce as the average particle size increases for materials of equivalent secondary phase volume, when using a 'fixed number evaluation' or the number of samples counted is increased.

2.7.2 Procedure.

1. Approximately 30-70mg of each of the HIPS resins was dissolved in \approx 5ml of Di-methyl formamide (DMF) using an ultrasonic bath for agitation for about 15 - 20 minutes.
2. The solution was then diluted to make it suitable for rubber particle size analysis on the CC device. This done by introducing a droplet of the solution into \approx 10ml of a 2% wt/vol. solution of Ammonium-thiocyanate in DMF that had been filtered through a 0.2 μ m filter in a 20 ml beaker.
3. The contents of the beaker were then well mixed before proceeding with the analysis.
4. The analysis was conducted by first sampling 100,000 measurements using the 20 mm stand.
5. A second analysis was also conducted to ensure consistency in the results.
6. Then steps 4 and 5 were repeated using the 50 μ m stand.
7. The above procedure was conducted on all three parent resins.
8. Data obtained were then tabulated on PC and histograms of RPS developed, These are presented in Table 2.3 (Appendix 2.1, p. 39).

2.7.3 Coulter Counter Results.

The results of the Coulter Counter Analysis are presented in the Figures 2.2, 2.3 and 2.4, plotted from Table 2.3. The results were generated from 100,000 samples of particle size for each of the materials. The data has been transformed to present the data in % number (of 100,000) and % Volume (based upon an equivalent spherical diameter). The absence of an accurate quantification of the concentration of the HIPS resin present (the dilute nature of the solutions and because the volume used in determining sample set could not be determined accurately) precluded the determination of the RPV from these results.

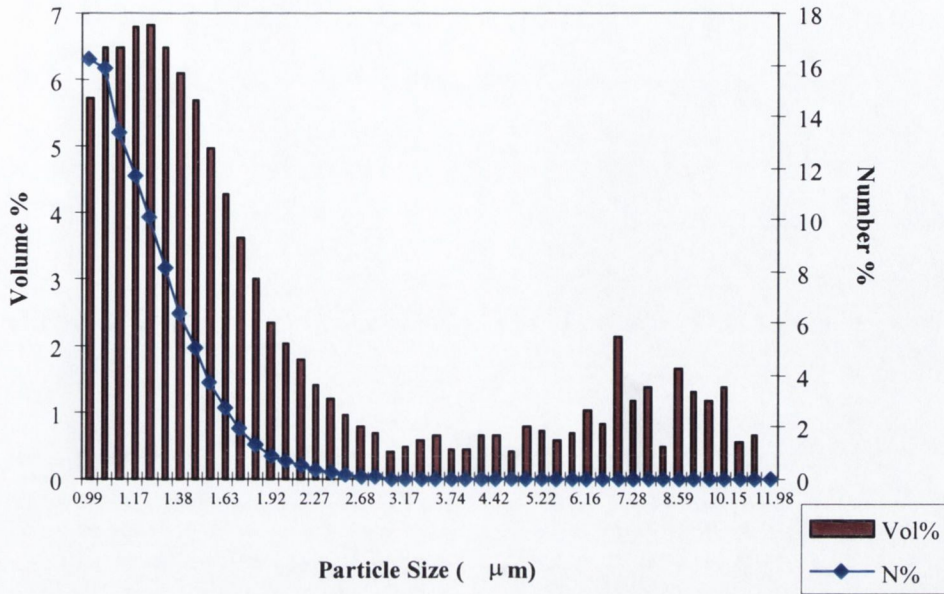


Figure 2.2. Results plotted from the CC analysis of PSB1 Parent HIPS resin.

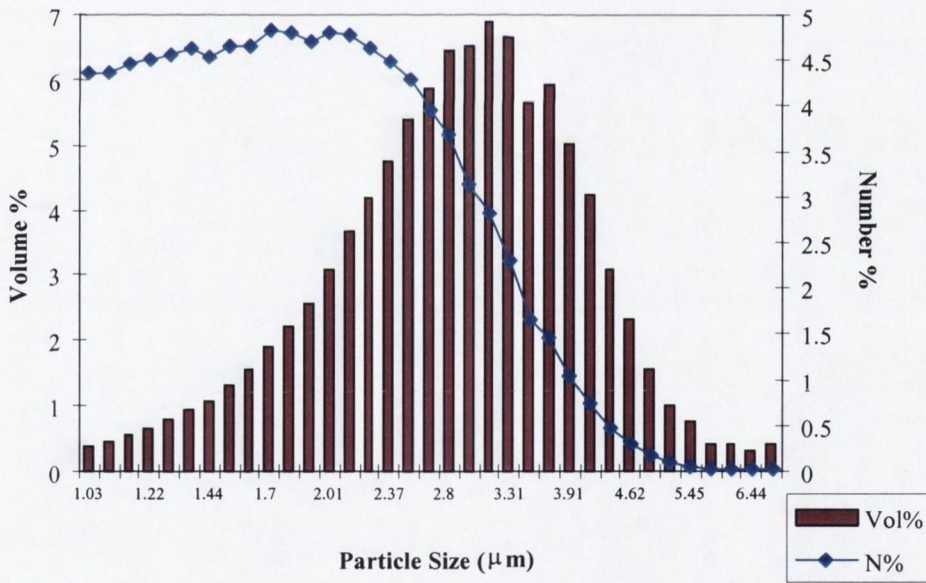


Figure 2.3. Results plotted from the CC analysis of PSB2 Parent HIPS resin.

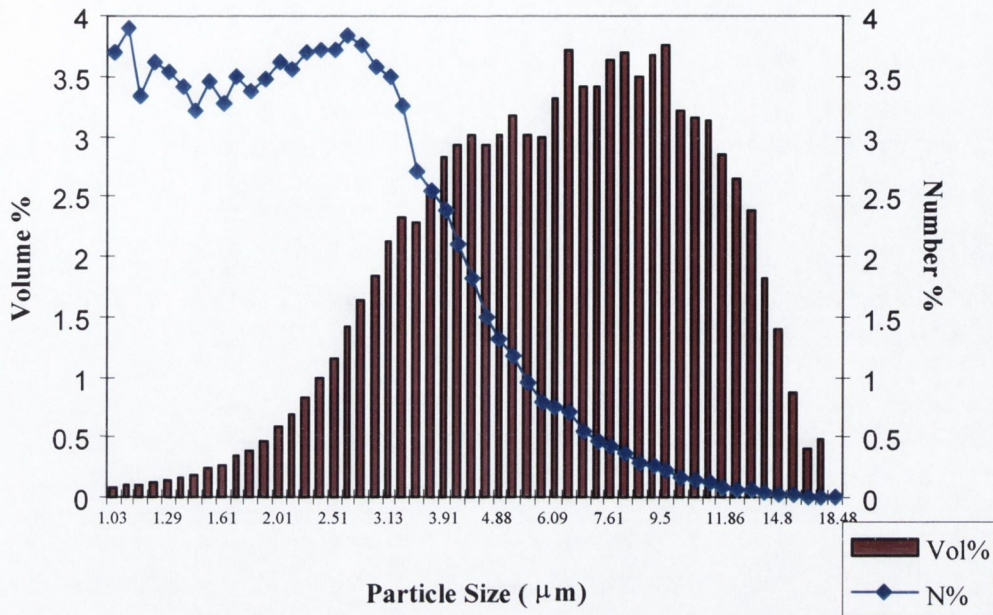


Figure 2.4. Results plotted from the CC analysis of PSB3 Parent HIPS resin.

2.7.4 Discussion of Results

The volume average particle sizes determined for the resins were 5.18, 2.66 and 3.46 μm for the PSB3, PSB2 and PSB1 respectively. The particle size distributions for both the PSB2 and PSB3 were principally monomodal, while that of the PSB1 material appeared to be bimodal. The analyser was unable to determine the presence of particles $<1 \mu\text{m}$ and this limitation prevented an accurate characterisation of the PSB1 material [16]. Though particles less than 1 μm are not considered to play a significant role in influencing mechanical behaviour, (Chapter 3), the absence of their contribution to the volume fraction, seen in TEM plates of Figures 2.8 – 2.10, undermines the utility of the technique to provide a comparative characterisation of secondary phase morphology. Although there are fewer large particles, proportionately, their contribution to the volume fraction is greater, though in the analysis it is indeterminate to an acceptable degree.

The CC analysis technique provides a very comprehensive measure of particle size. However it is a ‘solution’ state method and the use of solvents introduces the same errors as observed in the Gel content method. The absorbed solvent in the particulate rubber phase or grafted polystyrene distorting the particle size measurements made in a way that may not be corrected for within the test. Despite this the average values obtained for RPS were similar to those determined directly from TEM, especially when it is considered that particles $<1 \mu\text{m}$ were not recorded.

A number of attempts were made at measuring the ERPV using the method. The method involved determining the precise concentration of the HIPS solution and the volume of it consumed in the analysis. However the dilute concentration of the particles and the tiny volumes used in the test

undermined numerous attempts at developing a reliable procedure in the laboratory [17]. The tiny concentrations and volumes demanded an unobtainable level of accuracy. Ridiculous and extremely variable results were obtained ($>50 \pm 15\%$ ERPV) consistent with an ABS resin but not with an 8%wt rubber modified HIPS. Additional problems associated with the variable rheological character of the solution and flow rates through the aperture, that are sensitive to particle size variations present further difficulties for alternative methods of determining volume(time).

2.7.5 Conclusions from Coulter Counter Analysis

Although the technique is sensitive to analytical error, i.e., selective absorption and graft molecules giving misleading impedance measurements:

- Particle size and distribution in size were characterised comprehensively.
- Values obtained for RPS agreed reasonably well with TEM results.
- As particles $<1 \mu\text{m}$ were not considered and ERPV could not be determined the results were concluded to be insufficient to characterise the secondary phase morphology of HIPS.
- The cost, effectiveness and speed of the CC method mean future research efforts should be directed at adapting or developing the method to determine RPS and ERPV.
-

2.8 TEM (Transmission Electron Microscopy) ANALYSIS

2.8.1 TEM Analysis; Introduction and overview.

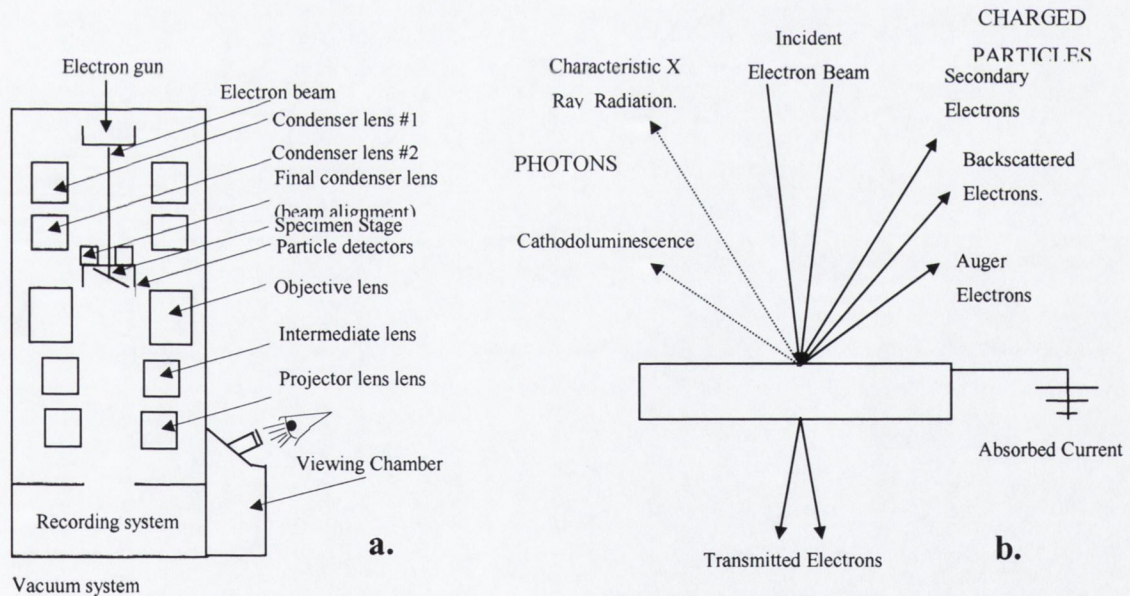


Figure 2.5. Schematics to illustrate simplified operation of the Transmission EM.

The operating principle of the transmission electron microscope mimics that of the conventional light microscope in so far as two image forming lenses are employed to magnify the object. Although the technology employed in TEM has advanced and been refined over the past 50 years the operating principle in remains the same. Figures 2.5.a&b. illustrate its fundamental construction and operation.

- A beam of electrons is accelerated under high tension from an electron emitter through a series of electromagnetic condenser (s) which direct and concentrate the beam on the specimen. A variety of photons and charged particles are emitted from the surface (Figure 2.5.b), their form and magnitude dependent upon the physical and chemical nature of the specimen.
- In transmission electron microscopy only those electrons passing through the specimen are of interest. An objective aperture filters electrons scattered through more than a certain angle and a series of objective and projector lenses (the intermediate lens functions as a first projector lens) focuses the beam forming the final image for the viewing and recording media.

Transmission Electron Microscopy (TEM) with subsequent image analysis is the most powerful experimental means of investigating the morphology of HIPS. ERPV, ϕ , is often determined directly from TEM micrographs, under the assumption that the area fraction observed, S , is the true RPV, or ϕ of the material. However this tends to overestimate the true ϕ , with the error accompanying the assumption increasing with section thickness and decreasing rubber particle size. The variation in particle size in the materials demanded this error be considered in determining particle size. The source of this inherent error arises from projected section thickness effects. Figure 2.6 illustrates this schematically. In the case of a monodisperse system that as the thickness of the microtomed coupe (section) decreases in size ($t \rightarrow 0$), the area projected under transmission microscopy will approach that of the true phase volume of the material.

Thus were the section thickness, t , to equal 0, then the value of ϕ would equal S , in a monodisperse system. However if the diameter of the particle and the thickness of the coupe approach the same order then the projected area will tend to exceed that which would be considered the 'true' secondary phase fraction. Thus in a microtomed coupe where $t > 0$ as t increases and RPS decreases, the equivalence becomes increasingly invalid.



Figure 2. 6. Figure schematically illustrating the manner in which the projected area in TEM image is sensitive to the section thickness of the microtomed coupe.

However the 2D area fraction, S , observed in TEM photographs would still be related to ϕ (the 3D volume fraction) through a function of particle size, D , (or for a polydisperse system, the distribution in sizes) and t , the section thickness through which S is viewed. Such that;

$$S(t) = \phi + \zeta(t)$$

Equation 2. 1.

where ζ denotes the excess fraction of ϕ projected in S through t .

If the number of particles present in a section of thickness t , is given by;

$$N_v \cdot t,$$

Equation 2. 2.

where N_v the particle concentration, the maximum cross-sectional area these particles may project onto the plane will be given by,

$$csa_{max} = \pi D^2/4$$

Equation 2. 3.

Thus the total maximum excess area fraction ζ is given by,

$$\zeta = N_v(\pi D^2/4) \times t$$

Equation 2. 4.

Now as $\phi = N_v \cdot \pi D^3/6$,

Equation 2. 5.

ζ may be expressed in terms of ϕ , as

$$\zeta = 3t/2D \cdot \phi$$

Equation 2. 6.

Which allows ϕ to be expressed as

$$\phi = K(t,D) \cdot S(t)$$

Equation 2. 7.

$$\text{where } K = (1 + 3t/2D)^{-1}$$

Equation 2. 8.

In the above case of a monodisperse system the particle diameter is described by a single value for D . For the case of a polydisperse system an average diameter, D_{ave} is commonly used. Unfortunately the basis, for determining the average particle size, i.e., whether it is a number, area, or volume average, is often not expressed. The more accurate correction would consider the distribution of particle sizes. The accuracy of such a method relies upon the determination of the relative particle size distribution. The Coulter Counter is very facilitating in this respect. However in the case of a sectioned TEM image it is readily appreciated, even in the case of a monodisperse system (Figure 2.7), that the observed particle distribution $n(d_i)$ does not reflect the real distribution $N(d_i)$.

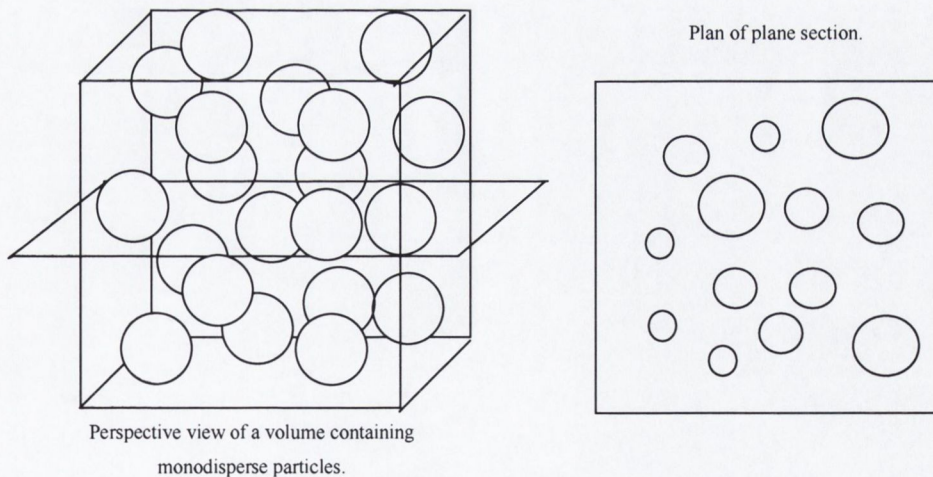


Figure 2. 7. Illustration of the manner in which a random configuration of monodisperse particles appears to be polydisperse when viewed through a plane section.

A number of methods have been proposed to correct for this thickness effect [18,19,20,21]. In this work the Schwartz particle size correction procedure was employed. This technique is based upon the assumptions that:

1. All particles are spherical.
2. The distribution of cross sections for a distribution of uniform sized spheres is known and has a definite relationship with the total number of spheres (generally through a Poisson distribution).
3. The distribution of cross sections may be divided into distinct size intervals.
4. The largest cross-sections can only originate from the largest spheres, this allowing the determination of the number of these spheres. This in turn allows for the determination of the number of cross-sections associated with the largest particle size. Thus the number of spheres of a class (e.g. m) remains unmodified while the number of spheres in the smaller classes decrease upon correction.
5. Repeating the process for the remaining sizes, the number of spheres in each size group may be computed.

The corrected number for a given class is expressed by the function,

$$N_i = n_i + \frac{\sum_{j=i+1}^m N_j \left(\sqrt{d_j^2 - d_i^2} - \sqrt{d_j^2 - d_{i-1}^2} \right)}{\sqrt{d_j^2 - d_i^2}}$$

Equation2. 9.

Where

- n_i -the number of spheres in class i before correction.
- N_i -the number of spheres in class i after correction.
- d_i -the maximum diameter in class i , with d_{i-1} , the maximum diameter in class $i-1$, the minimum diameter of spheres in class i .
- m -the total number of classes with class m containing the largest size.

Which taking section thickness into account is modified to;

$$N_i = n_i + \frac{\sum_{j=i+1}^m N_j \left(\sqrt{d_j^2 - d_i^2} - \sqrt{d_j^2 - d_{i-1}^2} \right)}{t + \sqrt{d_j^2 - d_i^2}}$$

Equation2. 10.

where t the section thickness.

Once N_i vs. d_i is obtained the number, area, volume, and $z + 1$ (a volume average diameter) the average diameter of particles can be determined according to;

$$D_n = \frac{\sum_{i=1}^m N_i \cdot \delta_i}{N}, D_a = \sqrt{\frac{\sum_{i=1}^m N_i \cdot \delta_i^2}{N}}, D_v = \sqrt[3]{\frac{\sum_{i=1}^m N_i \cdot \delta_i^3}{N}} \text{ and the } D_{Z+1} = \frac{\sum_{i=1}^m N_i \cdot \delta_i^4}{\sum_{i=1}^m N_i \cdot \delta_i^3}$$

Equation 2. 11.

where $N = \delta_i$ the mean particle diameter in a given class range of size i , and d_0 defined as 0 such that,

$$\delta_i = \frac{d_{i-1} + d_i}{2}.$$

Equation 2. 12.

Thus considering Equation 2.7 and substituting into it Equation 2.8 expressing D in terms of δ_i , S for the case of a polydisperse system can be expressed through,

$$S = \phi + (3t/2) \cdot \sum_{ii=1}^m \frac{\phi_i}{\delta_i}$$

Equation 2. 13.

Substituting for $\phi_i = N_i \cdot \pi \delta_i^3 / 6$ (from equation 2.5.)

$$S = \phi + (\pi t/4) \cdot \sum_{i=1}^m N_i \cdot \delta_i^2$$

Equation 2. 14.

Which for the case of a polydisperse system corrected using an area average RPS (D_a from Equation 2.11.b. and Equation 2.7.) may be simplified so that,

$$\phi = S - \zeta$$

Equation 2. 15.

Equation 2.15. requires N_v be known. This may be approximated through $\phi = (\pi D_v^3 \cdot N_v) / 6$. However for a polydisperse system where the relative particle size distribution is the projected average diameter provides a more precise formulation and means of determining the 'excess' volume fraction. The projected average diameter is defined by

$$D_p \equiv D_v^3 / D_a^2 = \frac{\sum_{i=1}^m N_i \cdot \delta_i^3}{\sum_{i=1}^m N_i \cdot \delta_i^2}$$

Equation 2. 16.

Thus

$$S = \phi + \pi t / 4 \cdot \left(\frac{\sum_{i=1}^m N_i \cdot \delta_i^3}{\sum_{i=1}^m N_i \cdot \delta_i^2} \right)^2$$

Equation 2. 17.

However it should be pointed out that in the final analysis the accuracy of the determination of S and the size of the rubber particles limits the accuracy of the above methods. Thus the effective rubber phase volume fraction irrespective of the methods employed is sensitive to the errors associated with the measurement. As the determination of the RPS is dependent upon these statistical fluctuations the absolute scale of the total RPV as the true value will to a degree remain uncertain.

2.8.2 Procedure

1. Strands of each of the materials considered (PSB1, PSB2 and PSB3) were prepared by extrusion through a MFR device.
2. Portions of these strands were exposed to an atmosphere of OsO₄ vapour for ≈ 8 - 10 hours. The reaction of OsO₄ with remaining double bonds in the PBD preferentially stains the rubber phase. This reaction was of additional benefit to the procedure in that it aided ultra-microtomy by hardening the rubbery phase.
3. Thin (≈ 60 μm) coupes were cryogenically ultra microtomed from the strands. Special care was taken not to introduce any artefacts from the cutting procedure that would distort determinations in the subsequent image analysis. The sections were collected on a copper grid and transferred to Specimen Stage of EM.
4. The specimens were then examined by TEM on a Phillips EM 400T and micrographs prepared at suitable magnifications.
5. The images were examined on Cambridge Instruments Quantimet 970 system.
6. The apparent rubber phase area fraction S and n_i(d_i) were determined.
7. N_i(d_i) was determined from n_i(d_i) by application of the Schwartz Correction procedure.
8. The various particle diameters were determined in accordance to *Equations 2.12.*, *Equation 2.16.* and the rubber phase volume determined from *Equation 2.17.*
9. The results were tabulated and from these histograms were generated.

2.8.3 Results of TEM Analysis.

TEM Micrographs are presented for each of the 'parent HIPS resins in Figures 2.8, 2.9 and 2.10. A visual comparison of the structure of the different materials shows them to possess the same multiple inclusion particle type. Plots of the results of the quantitative IA are presented in Figures 2.11, 2.12 and 2.13. Again as for the case of Coulter Counter analysis bi-axial plots are presented of the Number and

Volume % concentration of particles as a proportion of the overall ERPV. A full data set is presented in Appendix 2.2.

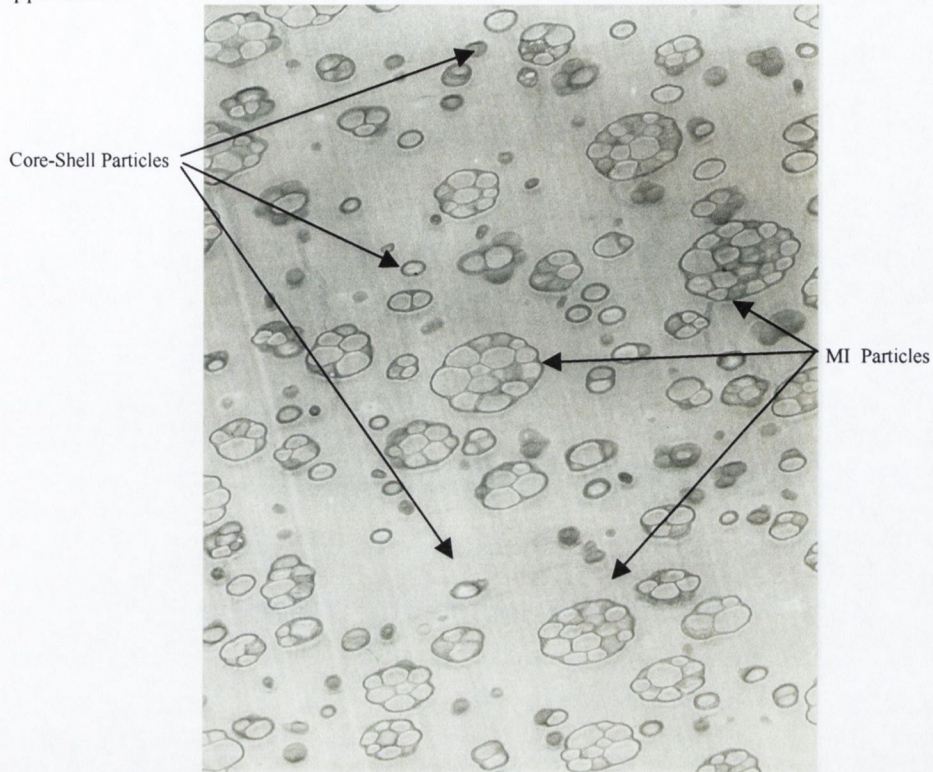


Figure 2. 8. TEM Plate of PSB1 at 30,000 x

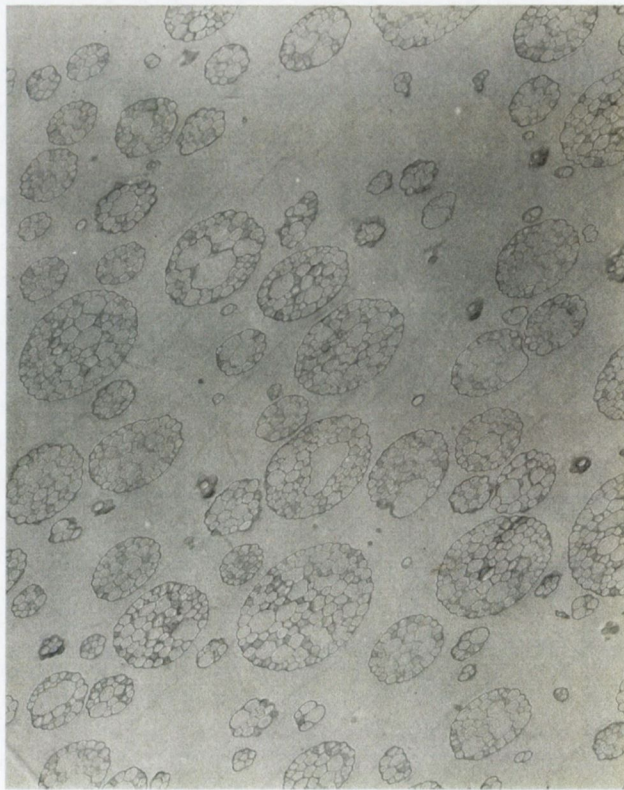


Figure 2. 9. TEM Plate of PSB2 at 10,000 x.

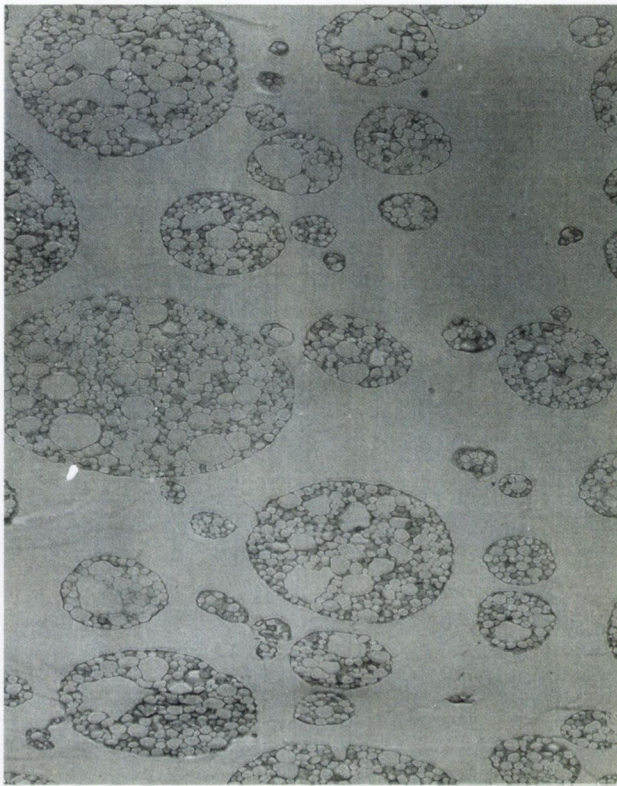


Figure 2. 10. TEM Plate of PSB3 at 10,000x.

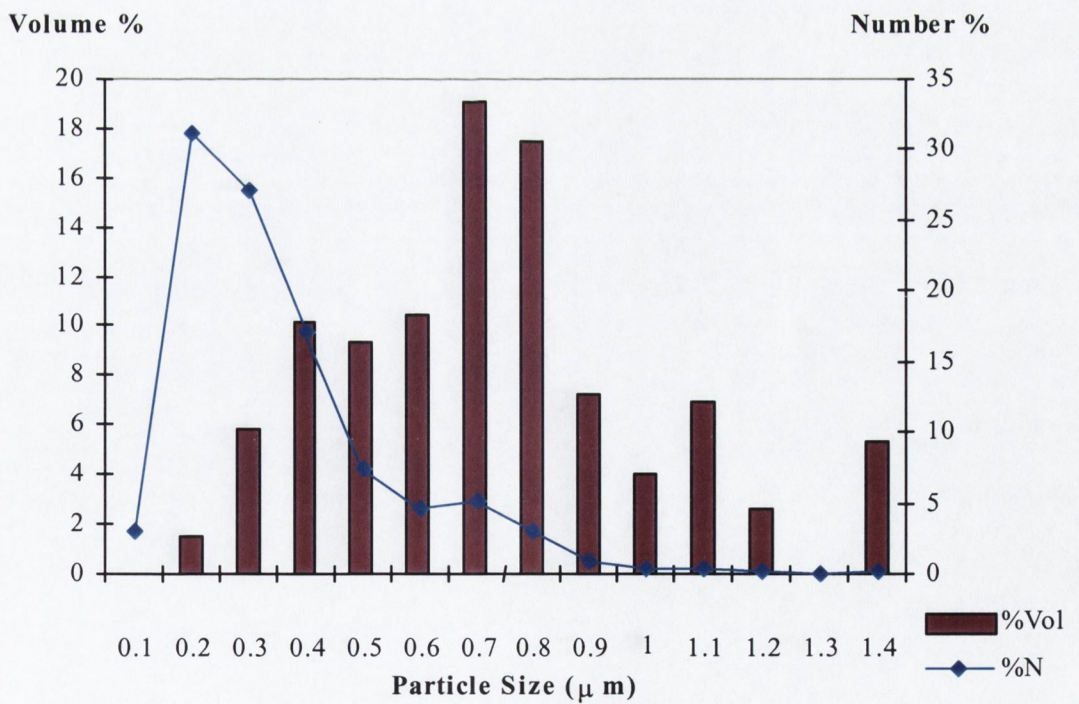


Figure 2. 11. Results plotted from TEM analysis of PSB1 Parent HIPS resin.

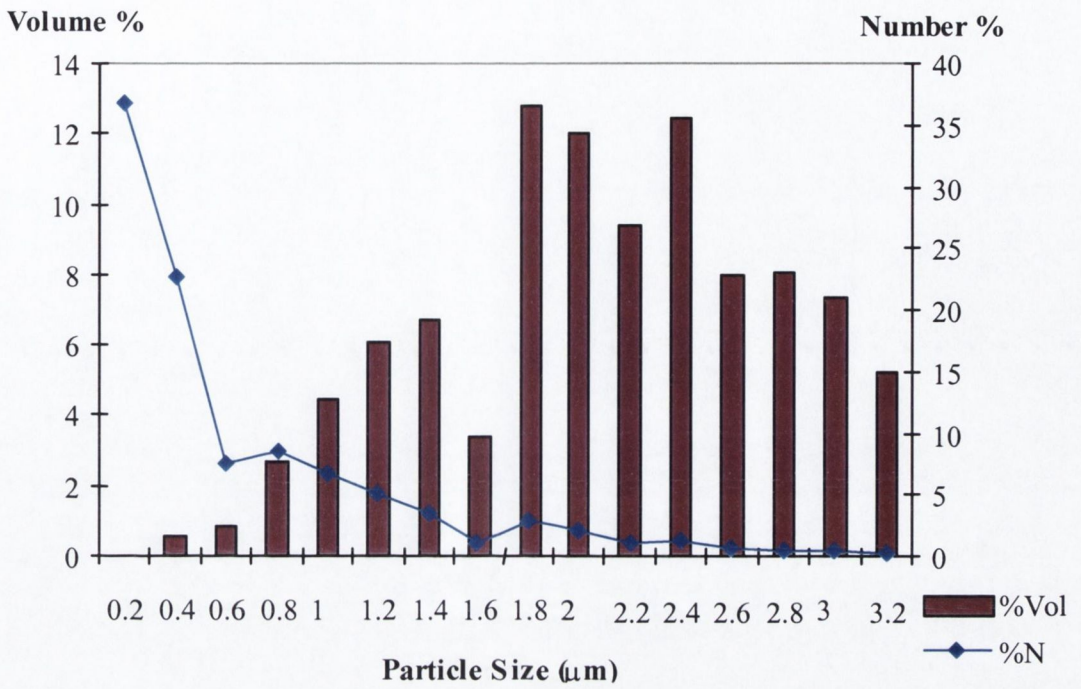


Figure 2.12. Results plotted from TEM analysis of PSB2 Parent HIPS resin.

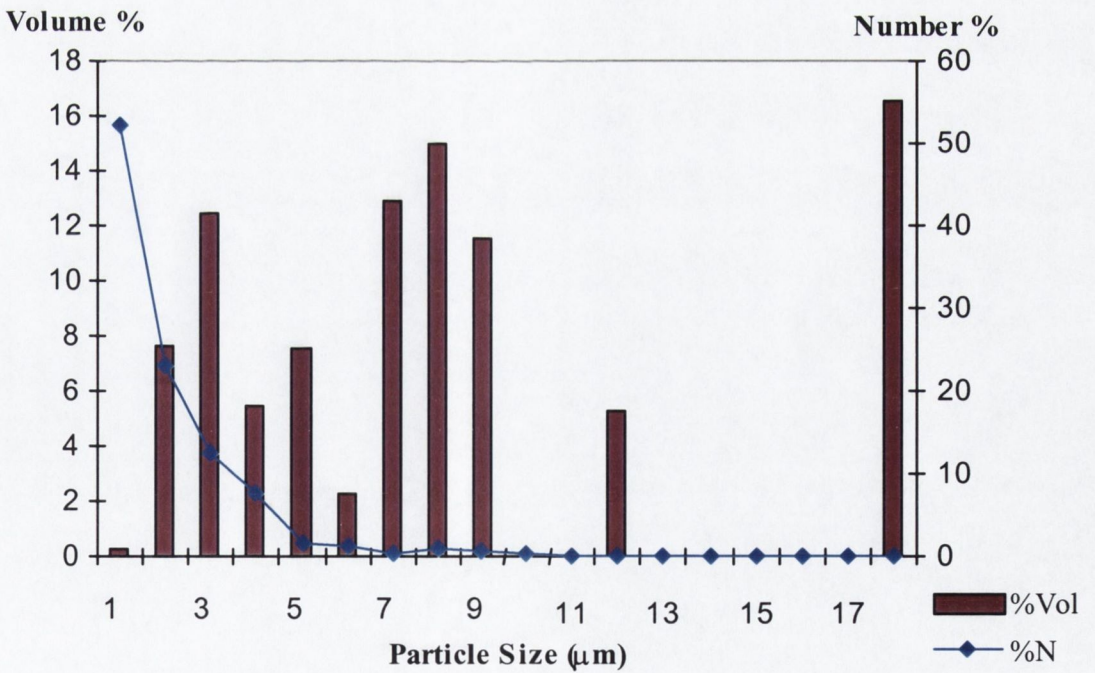


Figure 2.13. Results plotted from TEM analysis of PSB3 Parent HIPS resin.

2.8.4 Discussion of TEM plates; Particle Morphology

Transmission Electron Microscopy offered the most explicit route to assessing the secondary phase morphology. The requirement of the secondary phase was that the particles be of the same structural type. Recalling Figure 1.5 from Chapter 1 the morphology or the structural type of a particle gives a large indication of the level of PS block or graft polymer (the latter having the same effect as the former in pre-polymer systems going to phase change during conversion) and so is indicative of the level of grafting. The results of the gel content studies are considered to provide corroboration of the level of grafting and so support the observation made from TEM that the particles are the same structural type.

However this said and classifying the particles as being of the same structural type, some differences were observed to exist in the consistency of the particle structure between the three materials. Although these are not considered significant in regard to their influence on the micro-structural behaviour of the materials given the range in particle sizes achieved.

In the case of PSB1 a number of 'core-shell' particles were observed (Figure 2.8). Though some appear as they might actually be parts of other, larger, MI particles, sectioned through at bulbous points on the particle perimeter and just imaged as core-shell or type II cellular particles, the majority do appear to be core-shell particles. These core-shell particles were formed during polymerisation by breaking away from larger particles or 'pools of rubber' under shear at phase inversion. In character they have experienced much the same chemical history and the level of grafted styrene is much the same as that of the other resins, although included PS would have a lower Mw. Consequently they could be considered as highly fragmented MI particles. Both particle types are associated with the same proportion of block PS. Similar small core-shell particles are also found in PSB2 and, to a much lesser extent in PSB3. Their scarcity is due to the lower levels of shear employed than was used to achieve the PSB1 particles (at lower PS conversion).

The size of the core-shell particles are $\ll 1\mu\text{m}$, i.e., sizes at which, irrespective of structure, rubber particles are not considered to play any significant role in the micro-mechanism of deformation, i.e., the initiation and propagation of crazes, and so they have a negligible influence on mechanical behaviour [22]. The size and distribution in size of the polystyrene sub-inclusions within the rubber particles was also noted to differ in the three parent resins. The PSB2 and PSB3 particles possessed larger sub-inclusions and distributions in sub-inclusion size than PSB1. Indeed some inclusions are of the same size as the average PSB1 particle. The images show that for a given rubber loading the rubber particles do not expand uniformly, and the number of particles varies with both the rubber content and variations in particle volume and composition, or type. The observation underlines an important point in respect of TEM analysis, i.e., that both the rubber particle size and the effective rubber phase volume must be determined separately.

It is possible to determine the distributions of the size and the volume of the polystyrene sub-inclusions. However the limited value of such data compared to the time required to determine the size and size distribution of PS inclusions in a large population of rubber particles *for each* particle size range in a statistically reliable way negated the value of doing so. These structural differences between particles though detectable should be considered minimal.

It was concluded from the analysis that the particles were of the same general structural type, i.e., cellular MI type. The maintenance of particle morphology, infers the properties of the rubber were the same, reflecting the careful control exercised during polymerisation. With particles being the same structural type variations in performance between materials could then be considered to arise from variations in RPS and the ERPV alone.

Finally although it is assumed that the materials are similar in structure and that this is largely supported by the TEM plates, they are not exactly the same, in the same sense as the particles within any one of the materials is/is not the same, and the polydispersity of size between materials varies as does morphology and that these may even be interdependent.

2.8.5 Discussion of TEM Quantitative Image Analysis.

Histograms of the particle population in terms of the number and volume fractions were prepared from the TEM plates of the materials. These are presented in Figures 2.11, 2.12, 2.13 for PSB1, PSB2 and PSB3 respectively.

The plots show monomodal distributions for the case of the PSB2 and PSB3 resins although there is a notable difference in the 'resolution' in particle size of the plots. This is perhaps the greatest contrast between it and the CC analysis and arises from the sample size considered. In the TEM approach far fewer particle measurements $\approx 500 - 1000$ particles, from 20 - 100 high magnification images, are taken in comparison to the 10,000 of the CC. Although they do not present the same evidence of a bimodal distribution, for the case of the PSB1, as the CC analysis the peaks at 12 and 18 μm particle size do betray its presence. The TEM measurements were made 'directly', on particles that were 'undisturbed' in the material, which makes them more accurate than the CC determinations.

2.8.6 Conclusions from Quantitative TEM analysis

- These measurements differed greatly from the results obtained in the gel content for ERPV and the CC particle sizes, however the manner in which the results are obtained leads to the conclusion that they are indeed more accurate than the others.
- The analysis revealed volume average rubber particle sizes of 8.54, 1.99 and 0.64 μm for the PSB3, PSB2 and PSB1 resins respectively and their respective ERPV's were determined to be 45.4, 32.5 and 23.5 %.

2.9 Preparation of Polymer blends used in the study.

Having decided to use the TEM analysis because of its accuracy the materials were prepared by first hand blending the materials and then extruding them on a Betol extruder fitted with a mixing screw. See Figure 2.14.

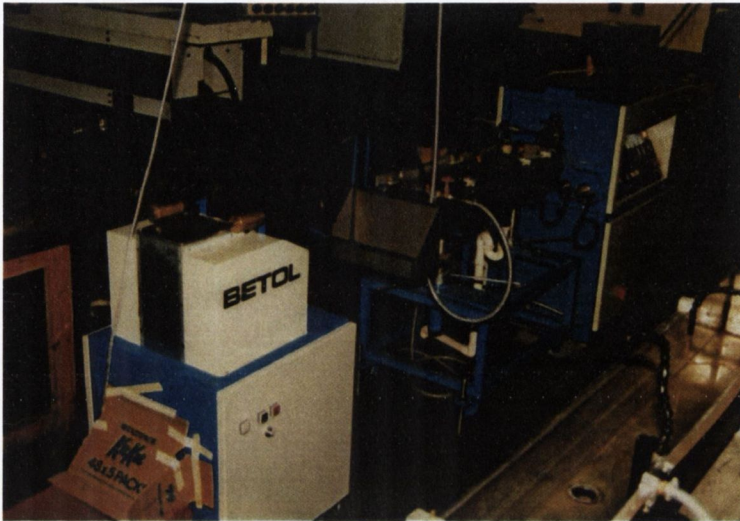


Figure 2. 14. Photograph of the Betol compounding line used in the course of material preparation.

- Based upon the TEM analysis the proportions of the HIPS and GPPS materials to be used were determined from;

$$\text{B.S.} - \left[\frac{\text{RPV}_{\text{desired}}}{\text{RPV}_{\text{Material}}} \right] \cdot \text{B.S.} = \text{Quantity of GPPS to be added to the blend}$$

where B.S. is the batch size. The quantity of HIPS to be added being the negative term on the left .Polyblends containing 5, 10, 15, 20 and 25 % ERPV were prepared for the three materials [note. In the case of the 5168 material the maximum RPV obtained was that of the unmodified HIPS, i.e., 23.5%.The appropriate quantities of material were thus determined and then weighed out in grammes to two decimal places.

- They were then 'hand mixed' in a polyethylene bag. This was done in pellet form prior to compounding to assist in the quality of distributive mixing in the blends.
- The Contents of the bag were then transferred to the hopper of the Betol extruder fitted with a mixing screw to improve dispersive mixing of the materials.
- The temperature profiles used in blending operation are presented in Table 2.2. In addition to running the blends the 'control GPPS material and the unmodified parent HIPS resins considered in the course of the work were also blended on the line. This was done to ensure that as well as could be achieved the materials would all have been exposed to similar thermal and shear histories.

ZONE	Zone 1	Zone 2	Zone 3	Zone 4	Die
Temperature °C	200	210	220	225	230

Table 2. 2. Temperature profile used in compounding of polymerblends.

- The screw speed was set to 72 rpm to provide a reasonable output without exposing the materials to an excessive shear level;- which would have tended to reduce average Mw.
- The materials were extruded through a strand die and hauled off and pelletised on Betol strand die cutters.
- The compounded blends were then bagged, sealed and stored for injection moulding of test samples at a later stage.
- Approximately 30 Kg of each of the 19 polymer blends were prepared in this way in two runs, associated with preliminary (ϕ) tests and the principal (π and Ω) test series.

2.10 Discussion of Conclusions from Secondary Phase Characterisation Tests

The TEM images of the materials provided direct means of assessing and comparing the microstructure of the HIPS particles. The observations made of the three resins revealed them to all possess the same multiple inclusion (MI) particle type. Minor differences did exist between the particle populations, e.g., surface roughness, the size of included polystyrene domains. It is recognised the interaction between the two phases is sensitive to such structural differences However they are considered to be sufficiently small to allow it be assumed that the particles of each resin possess the same micro-structure. The comparison of the gel content data also supports this conclusion (see section below)

The results obtained from the gel content tests for ERPV contrast severely with those determined by TEM methods. The gel content data combines the mass of the rubber phase with all grafted PS and overestimates the rubber phase volume due to the inclusion of surface grafted PS. At best it provides a 'rough' measure of the secondary phase volume.

However the rubber content is known (8 %wt.) for the resins, as the combined mass of the rubber phase and grafted polystyrene is $\approx 30\%$ for the three indicates they had the same level of grafted PS. The implication of this is that the primary and secondary phase materials experienced the same chemical history and so should possess the same properties, e.g., crosslink density, etc. The result corroborates the basic assumption that allows the differences between material behaviour to arise as a consequence of differences in particle size and population.

The coulter counter analysis provided the most detailed characterisation of particle size. The values determined were in reasonable agreement with the values determined using TEM especially when it is considered that particles $<1\mu\text{m}$ were not measured. However this latter limitation of the test and the material was studied after dissolution in a DMF solution, which would have 'bloomed' or shrank the particles expose sources of error. The comparison of the particle size distributions and absolute particle

sizes obtained from the CC and measured in the TEM suggest that the method overestimated particle size for PSB1 and PSB2, more a reflection of the equipments inability to measure particles less than 1 μm than a distortion of the particles. Indeed as the measure of the particle size for the PSB3 series resins were consistently undersized by the CC method the suggestion is that particles shrank in solution.

To conclude, while not as statistically attractive as the CC data the TEM results were considered more reliable than either the CC or the gel content because of the explicit manner in which the measurement was made. That is that the measurement were made directly 'in situ' on particles whilst they resided within the material and so not exposed nor distorted by the effects of solvents or other types experimental error. The only issue that does arise is in respect of section thickness, was corrected for statistically.

2.11 References

- 1 KESKKULA, H, PAUL, D.R., Mc CREEDY, K.M, Polymer, 28, 2063, 1987.
- 2 TURLEY, S. G., KESKKULA, H., Polymer, 21, 466, 1980.
- 3 PITTOLO, M., BURFORD, R.P., J. Mater. Sci., 21, 1769, 1986.
- 4 PARKER, D. S., SUE, H-J., HUANG J., et al., Polymer, 31, 2267, 1990.
- 5 HOBBS, S. Y., DEKKERS, M.E.J., WATKINS, V.H., Polymer, 29, 1598, 1988.
- 6 AMOS, J. L., J. Polym Eng & Sci., 14, 1, 1, 1974.
- 7 BUCKNALL, C.B., KARPODINIS, A., ZHNAG, Y.C., J. Mat. Sci., 29, 3377, 1988
- 8 FREEGUARD, G. F., Br. Polym. J., 6, 205, 1974.
- 9 SILVERSTEIN, M. S., NARKIS. M., J. Appl. Polym. Sci., 40, 1583, 1990.
- 10 EASTMOND, G. C., Toughening of Plastics II, PRI, 2 - 4 JULY, 1985.
- 11 BUCKNALL, C. B., Toughened plastics, Applied Science Publishers, 1977.
- 12 ARGON, A.S., COHEN, R.E., *Crazing in Polymers*, Vol. 2. *Advances in Polymer Science* 91/92, ed. Kausch, H.H., Springer Verlag, 1990.
- 13 COOK, RUDIN, PLUMBTREE, J. Mat. Sci., 48, 75, 1993.
- 14 KESKKULA, H., PAUL, D. R., Mc CREEDY, K. M., et al, Polymer, 28, 2063, 1987.
- 15 NIJHOFF, B., Confidential Communication, Dow Benelux N.V., 1992.
- 16 Coulter Counter Technical Instruction Book, Coulter Instruments.
- 17 DE WINDE, P., DE THEE, A., Dow Benelux N.V. Internal Communication, 1993.
- 18 RIGAUT, J. P., PERSON, A., J. of Microscopy, 156, 3, 371, 1989.
- 19 CRUZ-ORIVE, L. M., J. of Microscopy, 131, 3, 265, 1983.
- 20 HALL, R.A., J. Appl. Polym. Sci., 36, 1150, 1988.
- 21 SCHWARTZ, H.A., METALS & ALLOYS, 139, 1934.

2.12 Appendix 2.1: Results of Coulter Counter Analysis

PSB1			PSB2			PSB3		
RPS μm	Vol%	N%	RPS μm	Vol%	N%	RPS μm	Vol%	N%
0.99	5.73	16.24	1.03	0.38	4.36	1.03	0.08	3.7
1.04	6.49	15.86	1.09	0.45	4.36	1.09	0.1	3.9
1.1	6.5	13.43	1.15	0.54	4.46	1.15	0.1	3.32
1.17	6.8	11.67	1.22	0.65	4.49	1.22	0.13	3.63
1.23	6.82	10.08	1.29	0.78	4.56	1.29	0.15	3.54
1.3	6.49	8.12	1.36	0.93	4.64	1.36	0.17	3.42
1.38	6.09	6.37	1.44	1.08	4.54	1.44	0.19	3.23
1.46	5.7	5.04	1.52	1.3	4.65	1.52	0.24	3.46
1.54	4.98	3.75	1.61	1.55	4.66	1.61	0.27	3.27
1.63	4.26	2.7	1.7	1.89	4.83	1.7	0.34	3.5
1.72	3.61	1.95	1.8	2.23	4.8	1.8	0.39	3.38
1.82	3.01	1.37	1.9	2.57	4.7	1.9	0.47	3.47
1.92	2.34	0.91	2.01	3.1	4.79	2.01	0.58	3.61
2.03	2.04	0.67	2.13	3.67	4.77	2.13	0.68	3.56
2.15	1.81	0.5	2.25	4.21	4.64	2.25	0.83	3.69
2.27	1.41	0.33	2.37	4.74	4.47	2.37	0.98	3.72
2.4	1.19	0.24	2.51	5.39	4.28	2.51	1.16	3.71
2.54	0.96	0.16	2.65	5.86	3.95	2.65	1.41	3.83
2.68	0.81	0.12	2.8	6.44	3.68	2.8	1.63	3.76
2.83	0.7	0.08	2.96	6.51	3.15	2.96	1.83	3.57
3	0.42	0.04	3.13	6.9	2.82	3.13	2.12	3.5
3.17	0.48	0.04	3.31	6.66	2.31	3.31	2.33	3.25
3.35	0.59	0.04	3.5	5.66	1.66	3.5	2.29	2.7
3.54	0.64	0.04	3.7	5.92	1.47	3.7	2.55	2.55
3.74	0.46	0.02	3.91	5.01	1.05	3.91	2.82	2.39
3.95	0.46	0.02	4.13	4.22	0.75	4.13	2.92	2.1
4.18	0.67	0.03	4.37	3.09	0.46	4.37	3.01	1.82
4.42	0.64	0.02	4.62	2.31	0.29	4.62	2.93	1.5
4.67	0.4	0.01	4.88	1.56	0.17	4.88	3.02	1.31
4.94	0.79	0.02	5.16	0.99	0.09	5.16	3.18	1.17
5.22	0.74	0.01	5.45	0.75	0.06	5.45	3.02	0.94
5.51	0.58	0.01	5.77	0.43	0.03	5.77	3	0.79
5.83	0.69	0.01	6.09	0.42	0.02	6.09	3.31	0.74
6.16	1.02	0.01	6.44	0.3	0.01	6.44	3.71	0.7
6.51	0.84	0.01	6.81	0.41	0.02	6.81	3.42	0.55
6.88	2.13	0.02				7.2	3.42	0.46
7.28	1.18	0.01				7.61	3.63	0.42
7.69	1.39	0.02				8.04	3.7	0.36
8.13	0.47	0.01				8.5	3.5	0.29
8.59	1.66	0.05				8.98	3.68	0.26
9.08	1.31	0				9.5	3.76	0.22
9.6	1.16	0				10.04	3.22	0.16
10.15	1.37	0				10.61	3.15	0.13
10.73	0.54	0				11.22	3.14	0.11
11.34	0.64	0				11.86	2.84	0.09
11.98	0.001	0				12.53	2.64	0.07
						13.25	2.38	0.05
						14	1.81	0.03
						14.8	1.4	0.02
						15.64	0.87	0.01
						16.54	0.41	0.01
						17.48	0.49	0.01
						18.48	0	0

Table 2.3. Results of Coulter counter analysis expressed in terms of number and volume percent.

2.13 Appendix 2.2. Results of Transmission Electron Microscopy

PS1			PS2			PS3		
RPS μm	%Vol	%N	RPS μm	%Vol	%N	RPS μm	%Vol	%N
0.1	0.01	2.95	0.2	0.03	36.76	1	0.25	52.06
0.2	1.46	31.13	0.4	0.56	22.61	2	7.62	23.03
0.3	5.86	27	0.6	0.85	7.45	3	12.5	12.56
0.4	10.19	17.11	0.8	2.66	8.49	4	5.49	7.51
0.5	9.35	7.39	1	4.44	6.67	5	7.59	1.55
0.6	10.49	4.54	1.2	6.09	5.02	6	2.24	1.18
0.7	19.14	5.02	1.4	6.73	3.36	7	12.91	0.21
0.8	17.46	2.98	1.6	3.4	1.11	8	15.01	0.79
0.9	7.22	0.85	1.8	12.81	2.86	9	11.54	0.63
1	4.01	0.34	2	12.02	1.92	10	0.001	0.35
1.1	6.98	0.43	2.2	9.37	1.11	11	0.001	0.001
1.2	2.66	0.13	2.4	12.43	1.12	12	5.3	0.001
1.3	0.001	0.001	2.6	8.01	0.56	13	0.001	0.07
1.4	5.318	0.15	2.8	8.04	0.45	14	0.001	0.001
			3	7.32	0.33	15	0.001	0.001
			3.2	5.25	0.19	16	0.001	0.001
						17	0.001	0.001
						18	16.53	0.07

Table 2. 4. Results of TEM analysis expressed in terms of number and volume percent

RPS mm	PSB1					
	Da	Dv	Dz+1Dow	Dz+1Dow	Dz+1CC	DZ+1CC
0.1	3.75	0.38	0.04	0.38	0.02	0.20
0.2	129.12	25.82	5.16	25.82	2.70	13.52
0.3	214.20	64.26	19.28	64.26	10.09	33.65
0.4	406.56	162.62	65.05	162.62	34.06	85.15
0.5	62.50	31.25	15.63	31.25	8.18	16.36
0.6	163.44	98.06	58.84	98.06	30.81	51.35
0.7	245.98	172.19	120.53	172.19	63.11	90.16
0.8	139.52	111.62	89.29	111.62	46.75	58.44
0.9	28.35	25.52	22.96	25.52	12.02	13.36
1	28.00	28.00	28.00	28.00	14.66	14.66
1.1	15.73	17.30	19.03	17.30	9.97	9.06
1.2	15.12	18.14	21.77	18.14	11.40	9.50
1.3	0.08	0.11	0.14	0.11	0.07	0.06
1.4	20.19	28.26	39.57	28.26	20.72	14.80
Sum	1472.54	783.53	505.29	783.53	264.57	410.26
Values	0.38	0.53		0.64		0.64

Table 2. 5. PSB1 particle size determination

PSB2						
RPS mm	Da	Dv	Dz+1Dow	Dz+1Dow	Dz+1CC	DZ+1CC
0.2	147.04	29.41	5.88	29.41	3.08	15.40
0.4	361.76	144.70	57.88	144.70	30.31	75.77
0.6	268.20	160.92	96.55	160.92	50.55	84.26
0.8	543.36	434.69	347.75	434.69	182.08	227.60
1	667.00	667.00	667.00	667.00	349.24	349.24
1.2	722.88	867.46	1040.95	867.46	545.04	454.20
1.4	658.56	921.98	1290.78	921.98	675.85	482.75
1.6	284.16	454.66	727.45	454.66	380.89	238.06
1.8	926.64	1667.95	3002.31	1667.95	1572.01	873.34
2	768.00	1536.00	3072.00	1536.00	1608.50	804.25
2.2	537.24	1181.93	2600.24	1181.93	1361.48	618.86
2.4	645.12	1548.29	3715.89	1548.29	1945.64	810.68
2.6	310.96	808.50	2102.09	808.50	1100.65	423.33
2.8	352.80	987.84	2765.95	987.84	1448.25	517.23
3	252.00	756.00	2268.00	756.00	1187.52	395.84
3.2	102.40	327.68	1048.58	327.68	549.03	171.57
Sum	7548.12	12495.00	24809.30	12495.00	12990.12	6542.37
Values	0.87	0.91		1.99		1.99

Table 2. 6. PSB2 particle size determination

PSB3						
RPS mm	Da	Dv	Dz+1Dow	Dz+1Dow	Dz+1CC	DZ+1CC
1	5200.00	5200.00	5200.00	5200.00	2722.71	2722.71
2	9200.00	18400.00	36800.00	18400.00	19268.43	9634.22
3	11304.00	33912.00	101736.00	33912.00	53268.85	17756.28
4	12016.00	48064.00	192256.00	48064.00	100665.01	25166.25
5	3875.00	19375.00	96875.00	19375.00	50723.63	10144.73
6	4248.00	25488.00	152928.00	25488.00	80072.91	13345.49
7	1029.00	7203.00	50421.00	7203.00	26400.37	3771.48
8	4160.00	33280.00	266240.00	33280.00	139402.94	17425.37
9	5427.00	48843.00	439587.00	48843.00	230167.21	25574.13
10	5600.00	56000.00	560000.00	56000.00	293215.31	29321.53
11	5445.00	59895.00	658845.00	59895.00	344970.44	31360.95
12	28.80	345.60	4147.20	345.60	2171.47	180.96
13	1352.00	17576.00	228488.00	17576.00	119636.04	9202.77
14	19.60	274.40	3841.60	274.40	2011.46	143.68
15	22.50	337.50	5062.50	337.50	2650.72	176.71
16	25.60	409.60	6553.60	409.60	3431.46	214.47
17	28.90	491.30	8352.10	491.30	4373.15	257.24
18	2268.00	40824.00	734832.00	40824.00	384757.14	21375.40
Sum	71249.40	415918.40	3552165.00	415918.40	1859909.24	217774.36
Values	2.67	1.92		8.54		8.54

Table 2. 7. PSB2 particle size determination

Chapter 3

MICRO-STRUCTURE & MECHANICAL PROPERTIES

MODELLING MONOTONIC TENSILE AND IMPACT PROPERTIES IN HIPS.

3.1 Preface

The following chapter reviews the literature published on structure property relationships in HIPS. This has traditionally considered the materials behaviour in terms of its impact and tensile properties and modelled it in terms of rubber phase volume. These properties of the experimental resins are evaluated and discussed in terms of the previous findings and the behaviour of the resins is considered in terms of a 'Corrected' Inter-Particle Distance. Finally the latter's suitability as a parameter for interpreting behaviour is compared with others.

3.2 Contents

<i>Micro-Structure & Mechanical Properties</i>	42
3.1 Preface	42
3.2 Contents.....	42
3.3 Introduction.....	43
3.3.1 Deformation in Plastics.	43
3.3.2 Shear Yielding.....	43
3.3.3 Criteria for Shear Yielding.	44
3.3.4 Crazeing.	45
3.3.5 Criteria for Crazeing.	47
3.3.6 Craze nucleation and growth in HIPS; the implications for ERPV and RPS.	48
3.3.7 Rubber Toughening Theories in HIPS.....	51
3.3.8 Relationships between Microstructure and Mechanical Properties in HIPS.	55
3.3.9 The Influence of Particle Size and Effective Rubber Phase Volume.	58
3.3.10 Secondary Phase Structure and Tensile properties	65
3.4 Impact Experimental Methods.....	66
3.4.1 Experimental Materials and Specimen Preparation.....	66
3.4.2 Impact Test Method	67
3.5 Tensile Experimental Methods	67
3.5.1 Experimental Materials and Specimen Preparation.....	67
3.5.2 Tensile Test Method.....	68
3.6 Experimental Results and Discussion	68
3.6.1 Tensile Results and Discussion.....	69
3.6.2 Impact Test Results and Discussion.....	74
3.6.3 Particle Size Effect.....	77
3.7 Conclusions on micro-structure and mechanical properties of HIPS.....	88
3.8 Appendix 3.1. Results of Impact Tests	90
3.9 Appendix 3.2. Results of Tensile Tests.....	91
3.10 Appendix 3.3. Empirically Modelling the Tensile Properties of High Impact Polystyrene in Terms of its Secondary Phase Morphology.....	92
3.11 References	98

3.3 Introduction

The following literature review reveals that the structure property relationships in HIPS have, almost exclusively, been considered in terms of the effect of microstructure on impact and tensile behaviour. They also show that the morphological features of rubber particle size (RPS) and effective rubber phase volume (ERP_V) have dominated the analysis, interpretation and modelling of these properties. The motivation for the present research meant evaluating the impact behaviour of the experimental resins was necessary, and tensile tests were required before proceeding with fracture and fatigue tests. These tests provided an opportunity to, 1) compare the behaviour of the experimental materials with that already observed in the literature and 2) construct an alternative paradigm for modelling behaviour.

3.3.1 Deformation in Plastics.

Deformation mechanisms in polymers may be classified as being either shear or cavitation processes [1]. Shear processes include diffuse homogeneous and localised heterogeneous shear yielding, which occur without loss of material cohesion or a change in volume. Shear processes are only observed in PS and HIPS under compression [2]. Since in this work only tensile, or dilatational behaviour, is considered shear processes are only considered briefly. Cavitation processes include crazing and microvoiding, which involve the loss of inter molecular cohesion resulting in a decrease in density. These dominate plastic deformation in HIPS under tension and will be examined in some detail.

Both mechanisms are precursors to crack formation and, eventually, ultimate failure and both have their origins in the localisation of strain. Strain localisation may arise as a consequence of a geometrical instability, typically provided for by variations in cross sectional areas, surface defects, or, from internal heterogeneities within a material. Conceptually however, what is more fundamentally responsible for strain localisation and the inhomogeneous deformation associated with yielding is strain softening. The term strain softening is used to describe the decrease in true stress accompanying increases in the extension ratio (λ) beyond yield, i.e., what is required to produce further deformation and/or allow local deformation to occur about a stress raiser. The tendency or propensity to strain softening is dependent upon the chemistry of a polymer, its thermal history and the conditions of ambient temperature and strain rate.

These concepts control deformation at a micro-scale level and as macroscopic behaviour is defined by micro-scale response, in turn they also control it. In such light the basis of this work, that the micro-particulate secondary phase morphology determines the macroscopic mechanical behaviour of HIPS, seems self evident given the dominant direct influence it exerts over the stress field patterns in the material at a micro-scale level.

3.3.2 Shear Yielding.

Beyond yield, accentuated strain softening in a polymer permits the relative motion of shear bands under the action of a localised shear strain, as internal heterogeneities give rise to localised strain and lower the resistance to shear and encourage local slip. The chemistry, thermal history, conditions of ambient temperature and straining rate determine its propensity toward shear deformation. Studies on PS in compression have examined the influence of the latter (temperature and straining rate) on strain

softening and shear processes [3]. The studies found that upon reducing the test temperature from 80°C to 75°C that the magnitude of yield stress and the drop in stress following yield, for all deformation rates, increased significantly. At 65°C shear yielding in the material was found to change from diffuse shear banding to localised or micro shear banding. Shear strain values in the polystyrene determined from birefringence techniques were unusually high, approximately 2, while the thickness of the shear bands was found to be of the order of $\approx 0.1\mu\text{m}$ [3].

Although plasticity theory predicts that micro shear bands should lie at 45° to the loading axis, in plastics it is usually found that the angle between the shear micro band and the loading axis is less than 45° in compression and greater than 45° in tension. For PS, shear microbands form at 38° to the axis of loading upon subjecting a notched specimen to compressive loading [3,4]. In tension crazing dominates at service temperatures and shear banding does not occur. However, micro shear banding is often a precursor to crack formation in PS in compression with cracks commonly being initiated at the intersection of two shear bands (see **Figure 3.1**).

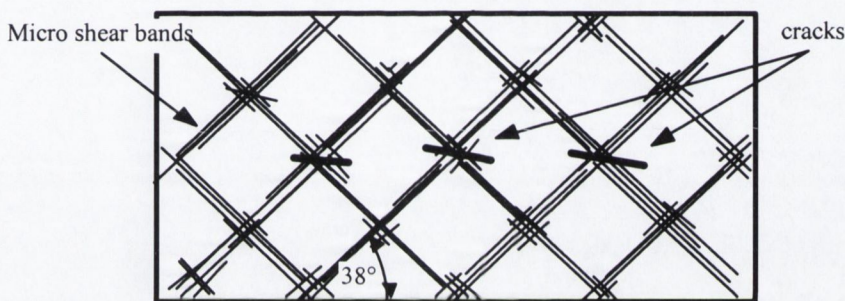


Figure 3.1. Diagram illustrating the formation of micro shear bands under plane strain compression in polystyrene, as would be seen under cross polarising light. The sketch illustrates how nucleation of voids occurs at intersection of craze bands[3].

3.3.3 Criteria for Shear Yielding.

A number of criteria have been proposed for shear yielding in plastics and many are modifications of the Von Mises yield criterion [5]. One commonly referred to, in regard to plastics, was proposed by Sternstein and Ongchin [6]. It may be expressed as,

$$\tau_{\text{oct}} = \tau_0 - \mu\sigma_m$$

Equation 3.1.

Where, τ_{oct} is the octahedral yield stress, i.e. that stress acting on a plane whose normal makes the same angle to the three directions of principal stress (where $\sigma_1 = \sigma_2 = \sigma_3$) τ_0 and μ are material constants and σ_m is the mean normal stress.

3.3.4 Crazeing.

Contemporary theories of toughening recognize crazing as the crucial process responsible for toughening in HIPS [7]. The process is unique to polymers and it dominates during tensile deformation in HIPS, below the T_g of polystyrene [8].



Figure 3. 2. Transmission electron micro-graph of HIPS illustrating structure of a craze[9].

Crazing typifies the mechanical response of amorphous polymers to tensile loading at temperatures below their T_g [8]. Crazes were defined by Kausch as - *“the well confined straightly bounded zones formed in glassy and semicrystalline polymers, perpendicular to the largest principal tensile stress, which contain considerably stretched and voided material”*[9]. It is perhaps easier to visualise them as planar crack like defects in which the separated surfaces of the continuous void are abridged by load bearing fibrils (see **Figure 3.2.**). The size of these fibrils in polystyrene ranges typically from $\approx 5\text{nm}$ to 50nm in diameter [10, 11]. They are composed of highly oriented polymer molecules that lie parallel to the main principal stress direction [10, 11, 12].

It was first speculated that crazes advanced by nucleating individual voids ahead of their tip that then coalesced to form a continuous void. However, it is now accepted that craze advance is achieved by the finger like growth produced by the Taylor meniscus instability mechanism. In this it is envisioned that the crazes advance by 'finger' like growth and the fibrils are formed at the polymer webs between the fingers [7, 13].

The resulting rate of craze advance (da/dt) in a homogeneous polymer has been expressed as,

$$\frac{da}{dt} = D \exp \left[-\frac{B}{kT} \left(1 - \left(\frac{\sigma_{\infty} \lambda'_n}{Y} \right)^{\frac{5}{6}} \right) \right]$$

Equation 3. 2.

where D , is a pre-exponential factor directly proportional to the ratio of the surface free energy to the craze flow stress (σ_∞), B is an effective activation free energy for plastic flow, k is a constant, T is temperature, λ_n a function of the principal wavelength of the advancing instability and Y is the athermal equivalent tensile plastic resistance of the polymer [7].

As a craze advances it thickens by drawing more material in from its surface. As the region just behind the advancing tip is so narrow, of the order of 10nm, most of the crazes' fibrillar structure is formed by drawing material in from the 'ceiling' and 'floor' interfaces with the matrix [14].

The process of fibril creation at the craze tip and fibril drawing from the craze surfaces have been theoretically modelled by Kramer using a treatment first used by Fields and Ashby for modelling diffusion controlled crack growth in grain boundaries by meniscus instability [10].

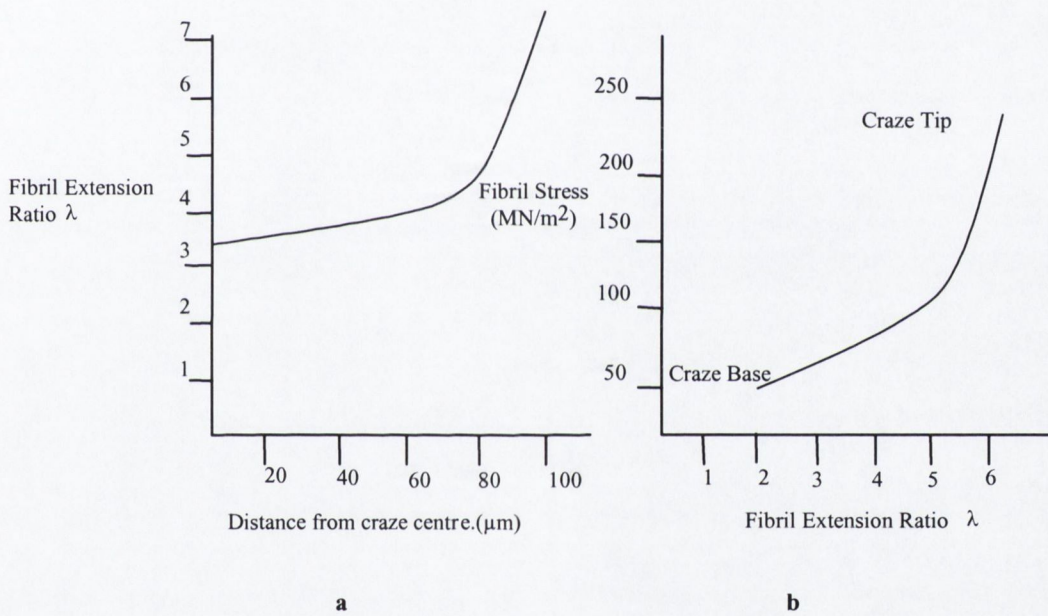


Figure 3.3. Plots showing (a) the variation in the craze fibril extension ratio (λ) with distance from the craze centre and (b) the variation of craze fibril stress (MN/m^2) with fibril extension ratio [15].

Lautausser and Kramer using transmission electron microscopy techniques experimentally measured fibril extension ratios (λ) over the length of a craze [15]. They found that although λ was constant over much of the craze that it increased sharply behind the craze tip and again at the craze centre, see **Figure 3.3**.

Crazes then may be distinguished from cracks in that they are load bearing. However, cracks may form within or from crazes by the breakdown of craze fibrils. **Figure 3.4.** is a TEM micrograph of fibril breakdown in a polystyrene craze, typical of the pattern of fibril breakdown.

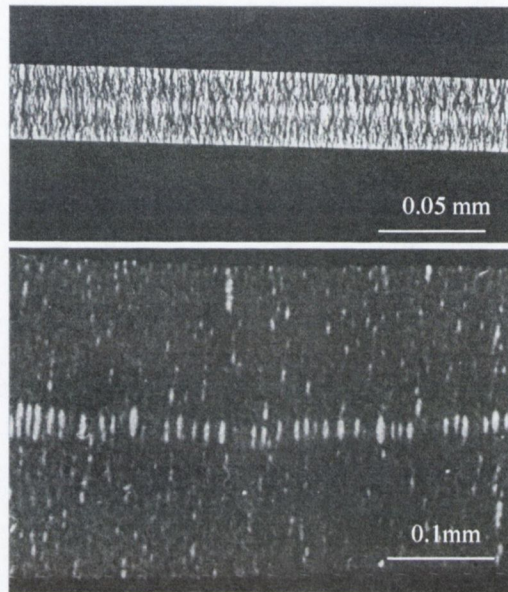


Figure 3.4. TEM micrograph illustrating craze fibril breakdown [16].

In tension the voids, generated by the breakdown of fibrils, expand slowly as fibrils are drawn apart until eventually rupturing. Eventually these voids reach a size where they may be termed microcracks. Under sustained loading, either by growing itself, or by coalescing with other crazes and/or microcracks, these cracks ultimately propagate to failure. Micrographic studies suggest the process of fibril failure may involve both viscous unentangling of molecules and actual chain scission. Although the craze stress of a polymer increases with M_w , inferring that viscous unentangling dominates the failure process, the relative contribution of the processes to craze breakdown remains unknown [17,18].

3.3.5 Criteria for Crazing.

A number of criteria for craze nucleation have been proposed. That of Oxborough and Bowden is commonly cited in reviews [19,20]. Oxborough and Bowden proposed that crazes form when the maximum principal strain (ϵ_1), given by,

$$\epsilon_1 = \frac{[\sigma_1 - \nu(\sigma_2 + \sigma_3)]}{E}$$

Equation 3.3.

(where, E is Young's modulus and ν is Poissons ratio) reaches a critical value ϵ_c , which is dependent upon the first stress invariant i.e. $(\sigma_1 + \sigma_2 + \sigma_3)$. Thus the criterion takes the form

$$\sigma_1 - \nu(\sigma_2 + \sigma_3) = \left[\frac{X}{\sigma_1 + \sigma_2 + \sigma_3} \right] \div Y$$

Equation 3.4.

where X and Y are empirically derived material constants, for critical hydro static stress and bulk modulus, for the case of polystyrene, $X \approx 100 \text{ MPa}$ and $Y \approx 10 \text{ GPa}$.

3.3.6 Craze nucleation and growth in HIPS; the implications for ERPV and RPS.

Bucknall and Smith first proposed that crazes were nucleated at the equatorial plane of the rubber particles, coinciding with the plane of maximum principal strain [21]. From this point of initiation they showed that they propagated outward, under the action of the applied load before terminating when either, 1) the craze tip stress fell below a critical value for propagation, or, 2) they encountered another particle. Bucknall and Smith explained 'stress whitening' associated with plastic deformation of HIPS as zones of crazing. This accounted for the absence of macroscopic lateral contraction accompanying the large strains to yield and fracture in the material, and the increased energy absorbed in fracture.

Microscopic studies clearly show that rubber particles do act as sites of craze nucleation in HIPS [22]. However, characterising the stress concentrating effect of the rubber particles by theoretical stress analysis is complicated by the complex composite structure of the particles and the high volume densities in which they are present in a typical HIPS resin.

At very low concentrations the problem can be approached using Goodier's analysis of an isolated spherical particle, bound perfectly to an isotropic body, in a state of uniaxial tension at all points remote from the particle [23]. The equations developed by Goodier show that a maximum stress concentration of ≈ 2.50 occurs at the particle equator and that it falls sharply with distance from the particle surface. Thus at the surface of an isolated particle, $\sigma_1 \approx 2.50 \sigma_\infty$, $\sigma_2 \approx 0$ and $\sigma_3 \approx 0$.

However, Goodier's solutions only apply to materials containing tiny particle concentrations. At larger concentrations the close proximity of particles leads to stress field overlap which renders Goodier's solutions ineffective in describing stress fields in HIPS. The experimental work of Matsuo et al considered stress field overlap in a model PS system [24]. The work employed an improvised simplified experimental model of HIPS that consisted of two large rubber particles $\approx 3 \text{ mm}$ in radius (R), that were grafted to the polystyrene matrix. The effect of stress field overlap on craze formation was then observed by reducing the distances between the particles, **Figure 3.5**. The authors noted that as they reduced the distance from $3R$ to $0.3R$ that the tensile stress required to effect crazing in the system fell quickly and that crazing became increasingly more concentrated over the distance separating the two particles.

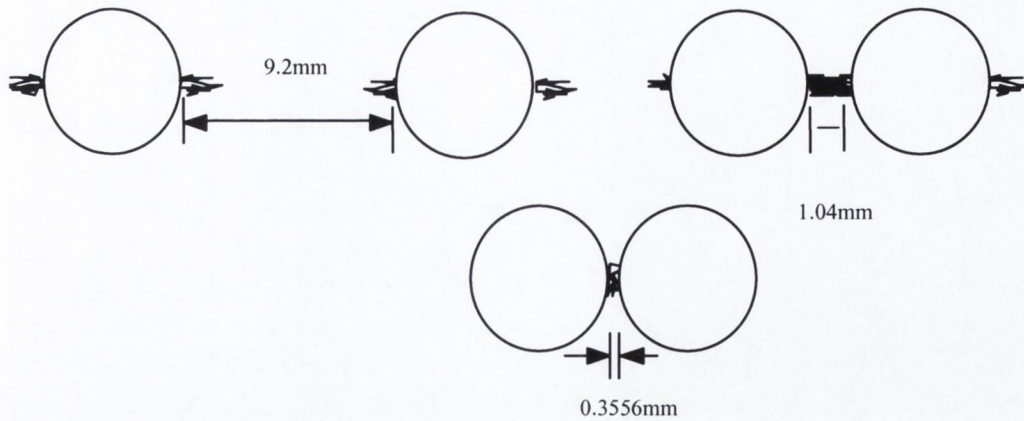


Figure 3.5. Sketch illustrating the variation in crazing behaviour with inter-particle distance as observed by Matsuo et al, under equivalent stress of 9.0Mpa. [24].

As far back as the early 1970's Broughtman and Panizza and Agarwal and Broughtman broached the matter of determining the stress concentrations about the particles at high particle volume densities using finite element analysis [25,26]. The approach was effective in describing the stress fields in the idealised structural models considered, and at low volume loadings the results were in agreement with Goodier's solutions. However, in real HIPS, possessing a distribution of particle sizes, where particles are randomly arranged in the matrix, the maximum stress concentration at the surface of the particles would be significantly higher than they projected, e.g., where a particle elevates stress within the stress field of another particle. Continuing research in applying FE techniques to modelling cavitation and large-scale deformation about particles in rubber toughened materials is on-going [27,28,29,30]. However even with today's processing power the number of particles present in a material would prohibit applying FE to model stress field relationships in a part design with the materials.

Stresses in the material not only arise from external loads. Different thermal expansion properties, lead to internal stresses being created between the phases. These hydrostatic stresses (σ_r°) set up by the different thermal expansion coefficients of the rubber and the PS phases, are at a maximum at the surface of the rubber particle and are purely deviatoric in character [1]. The radial stress set up by the thermal mismatch is tensile and the two tangential stresses, compressive and equal to $1/2 \sigma_r^\circ$, thus according to Bucknall the radial stress in an isotropic rubber particle [1],

$$\sigma_r^\circ = \frac{4(\alpha_r - \alpha_g)(T_g - T)}{(3G_g^{-1} + 4K_r^{-1})}$$

Equation 3.5.

where α_r is the expansion coefficient of the rubber and α_g is the expansion coefficient of polystyrene, T_g is the α thermal transition of polystyrene, T is the ambient temperature, G_g is the shear modulus of polystyrene and K_r is the bulk modulus of the rubber.

However, as seen in Chapter 2 particles are generally anisotropic, comprising of polystyrene sub inclusions within a rubber phase. These inclusions substantially affect the thermal contraction stress, reducing it by a factor equivalent to the phase volume of polystyrene (Φ_{IPS}) of the occlusions in the particle [31]. Thus, in the case of a low volume density of particles, Ricco et al, using Goodier's analysis, expressed the combined principal stress at the rubber particle equator as ,

$$\sigma_z \approx 2\sigma_\infty - \frac{1}{2}\sigma_r^\circ\Phi_{IPS}$$

Equation 3. 6.

$$\sigma_r \approx \sigma_r^\circ\Phi_{IPS}$$

Equation 3. 7.

$$\sigma_y \approx \frac{1}{2}\sigma_r^\circ\Phi_{IPS}$$

Equation 3. 8.

which when they combined with Oxborough and Bowden's solution (Equation 3.4.) set out a criterion for craze nucleation at a rubber particle interface, i.e.,

$$2\sigma_\infty \approx \left[\frac{\frac{1}{2}X}{\sigma_\infty} \div Y \right] \div \left[\frac{1}{2}(1-\nu)\sigma_r^\circ\Phi_{IPS} \right]$$

Equation 3. 9.

The model yields values for crazing stress that are far greater than those experienced in regular HIPS materials but illustrates the effect that particle structure may have on the process of crazing and thence toughening.

A further complication to the experimental and theoretical approaches to modelling crazing is the observation that small particles tend to be poorer at craze nucleation. For a homogeneous particle classical continuum mechanics suggests that the magnitude of its stress concentrating effect is independent of its size; however this is not borne out in experiments [11,32]. The evidence suggests that there is a critical particle size below which particles become less efficient in nucleating crazes. Merz et al referred to this size as the domain size of the matrix [33]. Rosen postulated that in order to be effective the size of a rubber particle should be large enough to exhibit typical rubbery properties and suggested a minimum particle size of the order of $0.01\mu\text{m}$ [34]. Ricco et al, considered the effect of the polystyrene sub inclusions on the shear modulus of heterogeneous rubber particles in an effort to relate it to stress field concentrations but found that although it did affect the shape of the fields that there was little change to the applied stress concentration factor at the particle equator [35].

Argon had suggested that the size effect was a consequence of the rippled surface of the rubber particle [36]. The concept being that ripples would give rise to additional stress concentrations at the surface of the particle that increase with particle size and so realise preferential nucleation of crazes in the larger particles.

Bucknall et al and Donald and Kramer suggested that a possible explanation might be the inability of a small particles to concentrate stress over a sufficiently large area to satisfy the spatial requirements of the meniscus instability mechanism of craze growth, i.e., that the stress concentration would be maintained over a sufficient distance from the particle interface to allow a craze to develop [32, 11]. This requires a small volume of shear yielded matter to form at the tip of the advancing craze tip. There is some evidence to support this hypothesis. Donald and Kramer calculated the fall in stress concentration at a distance of 75nm, a distance equivalent to approximately three fibril spacings [11]. It was seen that for particles less than 1 μm in diameter that the stress enhancement at this distance fell sharply with the stress concentration being halved only $\approx 10\text{nm}$ from the surface of 0.1 μm particles. Therefore, if 75 nm were accepted as the critical stress concentration distance, it would follow that particles smaller than 1 μm in diameter should be poor at initiating crazes. This was observed in the experiments reported on HIPS herein (Section 3.6.6 p. 89 and Figure 5.37 Chapter 5) .

The intricate interactions between the variables and the variability in their magnitude highlights the intrinsic complexity in developing a numerical approach to the problem of modelling crazing and macroscopic behaviour in HIPS. The theoretical relationships that have been proposed and the experimental analysis that has been conducted provides the basis for attempts to numerically model aspects of the material's behaviour [e.g., 27,29,30]. The processing times required are not the only reason for implementing of FE techniques in designing for specific applications; a more detailed understanding of the various other relationships between the materials is also required to create models that can model behaviour precisely. However there is no doubt that in the future numerical methods will provide solutions to meet the requirements of the materials designers, manufacturers and engineers considering macroscopic behaviour of HIPS.

3.3.7 Rubber Toughening Theories in HIPS.

Thus far the discussion has centred on the processes of deformation in HIPS and considered the effect of the secondary phase inclusions on these. This section takes one step back to elaborate on the theories that have been proposed for toughening in HIPS. HIPS should perhaps be considered an alloy, a composite blend of materials of such contrasting characteristics that combined, create a synergistic hybrid. Its development, motivated by the economic forces of supply and demand has been more the product of commercial opportunism, intuitive innovation, trial and error, than the application of any well understood theory (Chapter 1). However combining materials to provide either more cost effective or functional composite materials has been a regular, frequently misinterpreted, but largely successful practise in the history of engineering materials. The motivation of HIPS meant that for many years even the manufacturers did not fully understand how the improved toughness was achieved.

Indeed, although it was recognised early in the materials development that agitation was necessary during its polymerisation, the precise function and the implications of agitation as a means of

controlling material structure and performance was not understood [37]. Even after over half a century of research there is still much to learn and understand in terms of controlling this aspect of preparation.

The earliest theory on toughening in HIPS was published by Merz et al [33]. It proposed that the increase in impact strength was a result of the rubber particles holding the faces of a propagating crack together, **Figure 3.6**. The proposition was that the energy required to advance a crack was the sum of the energies to fracture of the glassy PS matrix and the compliant PBD secondary phase. To explain the phenomena of stress whitening and increased ductility, they proposed that upon loading a large number of microcracks formed within the matrix, each one abridged by a rubber particle. The microcracks were perceived as being separated by layers of PS that deformed, or buckled, under load allowing the microcracks to open. Microcrack theory also explained the other phenomena observed under tensile loading, e.g., decrease in density and large strains to failure.

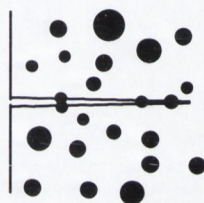


Figure 3. 6. Illustration of particles holding the faces of the propagating crack together as proposed by Merz et al [33].

Schmitt and Keskkula's proposal was similar to Merz et al [38]. The qualitative difference was that they suggested that the concentration of stress about particles generated a large number of small microcracks about the particle surface. The abundance of these microcracks meant more strain energy could be absorbed which caused the increased material ductility and toughness.

However these microcrack theories of Merz, Schmitt and Keskkula could not wholly explain the magnitude of the increase in toughness but were adapted and further developed by Bucknall and Smith [21]. Their consideration of the mechanism followed the work of Sauer et al and Kambour on the phenomenon of crazing in glassy polymers (Section 3.6)[39,40].

Bucknall and Smith utilised the concept of crazing in preference to the previous notion of microcracking. Instead of accrediting the deformation and fracture of rubber particles with the increased fracture energy and elongation to failure as others had done before, they contended that the rubber particles controlled both the initiation and growth of crazes within the matrix. The formation of crazes, realising a higher strain energy density in the PS phase, was responsible for the increased ductility and energy of fracture. This emphasis, on the energy contribution of the PS phase rather than the rubber

phase, in increasing ductility and toughness, cast a different perspective on the role of the secondary phase. Today the process of plastic deformation manifest in HIPS is accepted as being dominated by crazing and it is often termed 'pseudo-plastic' deformation to reflect the distinction between it and the dilatational shear processes normally associated with deformation beyond yield.

Kunz-Douglass, Beaumont and Ashby in modelling the increased toughness in rubber toughened epoxy reverted to the fundamental hypothesis of Merz, i.e., that the increased toughness arose from the additional energy required to rupture the rubber particle. This they did as they felt that ascribing the increased toughness to an increased energy contribution of the matrix was implausible where "only isolated and largely speculative observations of crazes and shear bands *had* been reported". Subsequent work by Yee and Pearson and Hwang et al contradicted their approach and showed that the stress concentrating particles did in fact enhance shear deformation within the rubber toughened epoxy and that it was this which was responsible for the increase in toughness [41,42,43]. However as will be pointed out at a later stage there remains some merit in this notion when discussing purely brittle fracture in the materials.

Another contemporary opinion would see the main role of rubber particles in stabilising or retarding craze growth by bearing load, and so deintensifying craze tip stress and slowing growth rates. A greater knowledge of crazes and the process of crazing in rubber toughened materials over the past thirty years has contributed much to the understanding of the problem, however many questions still remain and a fully satisfactory and complete theory continues to elude researchers [44].

Current ideas on the micro mechanisms of rubber toughening then retain much of the essential thrust of Bucknall and Smith's hypothesis[21]. Rubber particles are seen as craze nucleation sites and many still adhere to the notion of the particles acting as craze stoppers, interrupting and slowing the growth of crazes to catastrophic sizes.

Nevertheless it would seem logical to presume there must be an energy contribution arising from the tearing of the rubber particle. However the magnitude and importance of this seems to be an unresolved issue. For HIPS the work of Castellani and Maestrini on the rubber like tensile behaviour of yielded HIPS obliquely touched on the matter [45]. They suggested that it was possible that deformation of both the rubber particles and craze fibrils contributed to the mechanical response. However they were unable to separate their contribution.

In HIPS even under conditions of fracture that might be considered as plane strain, crack propagation will, at best, follow a quasi-brittle/ductile mechanism. Thus it follows that the rubber phase contributes directly post yield, in the region about a propagating crack tip, and thence at fracture. However the magnitude of its contribution remains an enigma though naturally it will be dependent upon the mechanical characteristics of the rubber.

The literature portrays crazing as dictating the level of increased toughness, yet the precise manner of how it does and the contribution it and other processes make is not resolved. It is accepted that the perturbation of stress field by the dispersed phase, precipitates the initiation of craze and/or micro shear entities in the matrix continuum at lower nominal stress levels. By doing so it involves a greater volume of material in strain deformation, possibly by changing the effective state of local stress at a microscopic level, and increasing the strain energy absorbing potential of the materials.

The by-line for rubber toughened materials then is that the secondary phase particles instigate, contribute to and control the processes of micro-deformation and by so doing enhance the material's facility for absorbing energy, its properties of toughness and its ductility. Their efficacy in affecting toughness is not simply a consequence of their providing a geometric instability.

3.3.7.1 *Thermal Influences.*

The behavioural dependency of the rubber phase in HIPS on temperature was also considered by Bucknall and co-workers [32]. They considered the variation in impact strength over a temperature range of -80 to 80°C. The tests revealed the presence of two 'ductile/brittle' transition temperatures (where an increase in temperature lead to a sharp increase in the material's impact strength) at -40°C and 0°C, (Figure 3.7.).

The impact strength was also found to increase at different rates depending upon the rubber phase volume, rising more rapidly in materials possessing higher rubber phase volumes. Additionally it was noted that levels of stress whitening fell with temperature, such that at -40°C stress whitening was completely absent.

These observations and similar experiences encountered in izod impact tests on ABS led Bucknall et al to believe that the toughness transitions observed might be explained in terms of conformational motions in the polybutadiene phase associated with its glass transition temperature (≈ -70 and -80°C). Thus in rapid impact loading a shift of -30 to -40°C occurred in the effective T_g of polybutadiene, which inhibited the formation of crazes and resulted in little or no toughening of the matrix at lower temperatures.

The greater rate of increase in the impact strength associated with higher volume loadings they considered to be a consequence of the lower stress levels required to initiate crazes in materials with high RPV as temperature increased.

From this can be concluded that it is not enough that structural anisotropy be present to provide local stress concentrations but that the rubber particle be capable of providing a mismatch in the transfer of load and the matrix be capable of transmitting strain through the system.

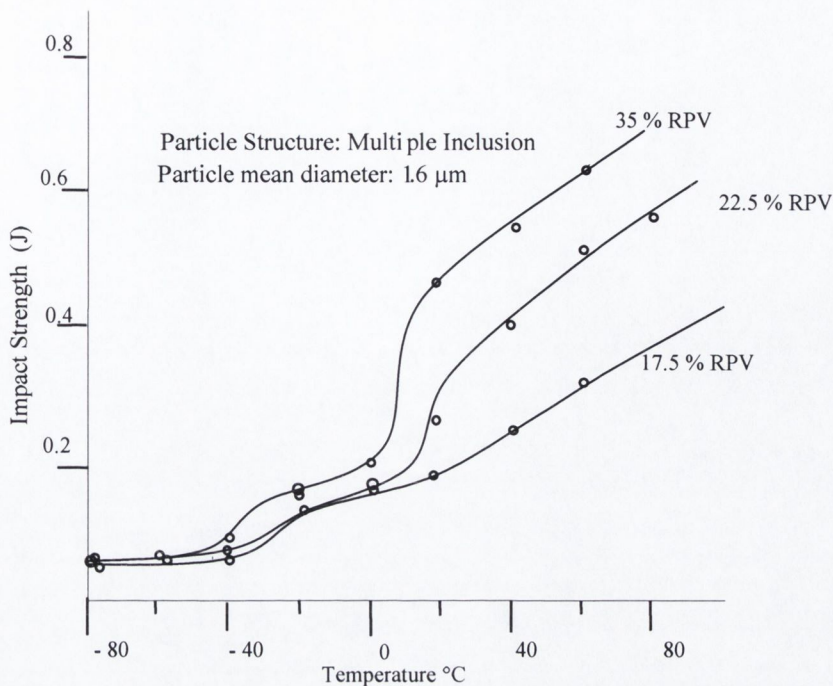


Figure 3. 7. Plot illustrating the dependence of Charpy impact energy on temperature and rubber phase volume in MI type particles[32].

Theories proposed for the micro-mechanism of rubber toughening in HIPS have ranged from the plausible to the fantastic. A mechanism proposed by Bragaw contended that the dispersed phase effected an increase in the energy absorbing volume of the material by dynamic branching of cracks and/or crazes by the Yoffe mechanism [46]. The proposition was that when a growing craze encountered a particle its energy expended in the creation of new crazes. However such a proposition does not only appear to be unlikely but untenable, as the growth rate at which branching becomes possible ($\approx 0.6 \times c$; where c the speed of sound in the material) is many orders of magnitude greater than the speed of craze growth encountered in normal tests (Izod & Charpy tests) and so cannot be seen as essential let alone dominant in toughening [47].

3.3.8 Relationships between Microstructure and Mechanical Properties in HIPS.

The discussions above make obvious the importance of the fundamental role played by the secondary phase in determining the micro-mechanical response of HIPS. The type of the rubber, the structure of the particle, the mechanical characteristics of the dispersed rubber, e.g., molecular weight, degree of crosslinking, amount of included PS, etc., the nature of the interfacial adhesion, etc., etc. are all factors that influence behaviour significantly. Their number and the complex relationships between them makes dealing with them individually, in detail, impossible within the scope of this work.

Figure 3.8. presents a schematic that attempts to present some general trends in mechanical properties associated with changes in the rubber phase morphology. In keeping with the imperatives of this research, which is focused on bulk polymerised HIPS resins, the discussion of structure/property relationships only briefly alludes to the influence of the type of rubber, the level of matrix adhesion and the rubber particle structure, on mechanical properties. The dominant morphological variants that can be effectively controlled during such polymerisations, i.e., the rubber particle size and the phase volume, are considered in more detail.

	Molecular Weight M	Lubricant Content	Gel Content	Swell Index	Particle Size
Stiffness					
Impact Toughness					
Heat Distort. Temp					
Gloss					
Viscosity					

Figure 3. 8. Schematic table illustrating the trends in material properties (rows) associated with changes in the morphology (columns). Dow Communication on HIPS.

3.3.8.1 Rubber Particle Structure.

Sections 3.3.6 and 3.3.7 introduced how variations to the structure and the composition of rubber particles, influence the magnitude and state of stress about them and consequently throughout the continuum of the material. That their structure influences their efficacy in nucleating crazes presents it as a means of manipulating behaviour. In effect, controlling craze initiation provides control over macro-mechanical properties. Chapter 1 introduced and reviewed how HIPS is prepared and also the means by which an almost infinite number of variations in secondary phase structure can be achieved. The research focus for some has been to investigate this aspect of morphology and how it might be optimised for mechanical performance.

The work of Donald and Kramer considered the influence of the internal morphology of rubber particles on craze formation, growth and breakdown [22]. They found that occluded particles were slightly better at nucleating crazes than solid particles of the same size. This finding was anticipated from the different level of hydrostatic stress imposed by the particles. But surprisingly they found the growth of crazes from occluded particles to be more stable than in 'whole' particles.

The influence of particle structure was also considered, in detail, by Argon et al in a series of papers in the late 1980's [48,49]. In their work, Argon et al, compared the mechanical performance of a variety of compliant (polybutadiene) morphologies in high molecular weight polystyrene matrices.

They found that changing the structural morphology of particles, e.g., from rod shaped laminate particles (KRO-1 resin structures) to typical cellular, i.e., multiple inclusion (MI) morphologies, and spherical 'shell in shell' (CSS resins), or 'onion type' morphologies, resulted in significant changes in the properties of the HIPS formed.

Figure 3.9. illustrates this in terms of the response of these materials to tensile loading. It was concluded, that the differences in behaviour could be explained in terms of the different micro-mechanical processes of crazing and fracture that were attendant to the variations in structure.

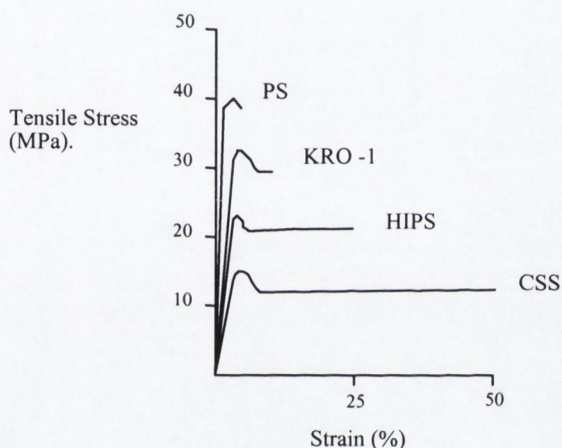


Figure 3.9. Stress strain curves illustrating craze plasticity of PS toughened with KRO -1, HIPS and CSS particles compared with PS [48].

3.3.8.2 Rubber/Matrix Adhesion.

One of the prerequisites for obtaining improved toughness in rubber toughened polymers is that good adhesion be achieved between the matrix and the rubber phase [1]. This is obvious as were it not the case then voids or glass beads would act equally well in toughening as they provide for strain localisation and consequently sites for craze nucleation. Poor adhesion to the matrix limits their ability to bear load and playing a role in the kinetics of craze growth and breakdown, at least in tension. Consequently without some adhesion the presence of the particles would contribute little to improving toughness.

Experimental work by Nicholais and Narkis considered the use of glass beads as tougheners [67]. Although some improvement was observed in impact strength, it represented only a fraction of that obtained using rubber particles. More poignantly illustrative of the importance of good adhesion and interaction between phases was the work of Durst and Griffith [50]. It considered the variation of

impact strength in a series of blends prepared by blending polystyrene with polybutadiene copolymers of various PS graft lengths. The difference between the mechanical properties of materials possessing high graft densities and molecular weights and those with low was dramatic. The work confirms the importance of interfacial adhesion, grafting, in improving toughness.

3.3.9 The Influence of Particle Size and Effective Rubber Phase Volume.

Particle size and effective rubber phase volume are generally considered separately. In the main structure property relationships in HIPS resins are considered solely in terms of the influence of ERPV. In the context of continuum mechanics this is not unusual. Changes in behaviour would not be anticipated from RPS alone. Were such to exist, the assessment of size dependence would need to exclude the potential bias that might arise from variations in rubber phase volume, particle type (structure) and composition (e.g. type of rubber, degree of crosslinking, etc.). Similarly to appreciate the influence of ERPV, these other aspects of morphology should also have been excluded.

Although a large body of research has considered the influence of these and other features on impact and tensile behaviour numerical models that exclude any of them as variables have not been developed. Certain trends have been identified, e.g., increasing the R PV increases toughness (Figure 3.7). This trend appears insensitive to changes in other aspects of morphology, e.g., particle structure, size, etc., and impact test methods employed [51,52]. This is generally explained in terms of the reduced cross sectional area and improved stress concentrating efficiencies that accompany the increase in the rubber particle population, (required to increase ERPV), which fuels the generation of more profuse and expansive energy absorbing crazing.

3.3.9.1 *Minimum Particle Size*

The scope of a relationship between particle size and crazing was introduced earlier. The vital point being that it is considered that a minimum particle size is necessary to instigate crazing, and below it the improvement in impact toughness is minimal. Rosen suggested particles needed to be $> 0.1 \mu\text{m}$ [34]. Donald and Kramer found particles $< 1 \mu\text{m}$ ineffective [22]. Silberberg and Han suggested the threshold was $\approx 1 \mu\text{m}$ [53]. Bucknall proposed that $0.8 \mu\text{m}$ was the critical RPS but once the critical size is exceeded that particle size does not exert influence [1]. There appears to be some general agreement.

3.3.9.2 *Polydisperse and Bi-Modal size distributions and Critical Particle size.*

The literature also shows that polydisperse systems, of equivalent ERPV, are more effective in improving toughness than monodisperse systems [54]. The explanation for this is best exemplified by work by Lavengood of Monsanto who found mixing two HIPS with significantly different particle sizes realised a HIPS polyblend with improved impact strength and gloss (an aesthetic characteristic).

Hobbs first considered this phenomenon of bimodal particle size distribution and found that better impact toughness can be achieved in an optimal bimodal HIPS than a monomodal one of the same rubber content. He subsequently proposed a mechanism based on the assumption that all particles operated as craze initiators with the inclusion of large particles effecting improved toughness by inhibiting the growth of crazes. Wrotecki et al, studying rubber toughened PMMA using FEM analysis, took a similar view and suggested that crazes were initiated from small particles, that were in the vicinity of the larger particles where the interaction of the stress fields provided the necessary concentration of stress [55]. They argued that the larger particles subsequently arrested the growth of crazes initiated from the smaller particles and so effected the increased apparent toughness.

Okamoto et al proposed that all particles act as initiators, but that larger particles contribute more to toughness by initiating crazes that grew in a more stable fashion, as opposed to terminating craze growth [56]. Amid the distinctions between each hypothesis regarding the role of the larger particles there is agreement that the stress field interactions in polydisperse systems tend to promote initiation in smaller particles, reducing the minimum effective RPS and increasing the amount of the rubber phase that is effective in toughening.

The existence of an optimum rubber particle size, beyond which toughness falls with increasing RPS, is another feature of rubber-toughened systems. **Figure 3.11.** presents the results from Cigna et al of izod impact energy plotted against R_w (weight average particle diameter) for HIPS at various rubber phase volumes illustrating that a maximum toughness was achieved at $R_w = 1.15 \mu\text{m}$ (diameter $2.3\mu\text{m}$).

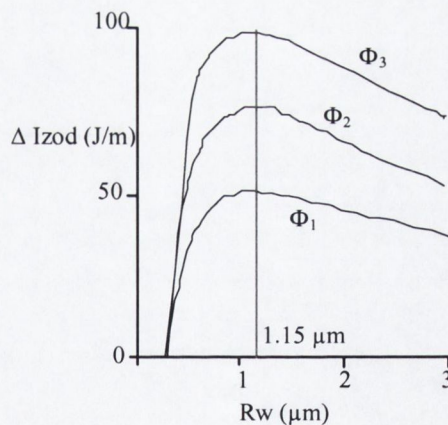


Figure 3. 10. The calculated increase in Izod impact strength (ΔI) vs. R_w at various values of RPV $\Phi_1 < \Phi_2 < \Phi_3$; ΔI calculated from the equation of the linear regression line of the bi-logarithmic plot [54].

This was evident in the early work of Merz et al which presented data that showed the impact strength to fall off beyond a certain 'degree of working' (agitation) which would have been proportional to particle size [33]. The optimum particle size is seen to be characteristic of, and to vary with, the type of matrix material. Cigna et al also considered the optimum particle size (radius) in HIPS and rubber

toughened SAN systems, finding the optimum RPS radius for SAN to be $\approx 0.5 \mu\text{m}$ compared with $\approx 1.15 \mu\text{m}$ in HIPS [54].

Although the reported figures for an optimum RPS for HIPS suggest little agreement on a value, most see it lying in a 1-6 μm range. The fact that particle size in HIPS is polydisperse, and that RPS distributions vary between materials and that the techniques used to determine RPS are susceptible to inaccuracies, introduces a cushion of error that could accommodate the spread in values.

3.3.9.3 Monodisperse Particle size

In their investigations Cook, Rudin and Plumbtree created a monodisperse HIPS by incorporating monodisperse poly(n-butyl acrylate) particles (with a polydispersity factor of $\cong 1.00$) in various volume fractions in PS [57]. Their work suggested the optimum particle size existed in the range of 2 - 3 μm . This is in general agreement with the values quoted by others however as it is based on the behaviour of a monodisperse system it should perhaps be considered as being a more reliable evaluation of an optimum RPS.

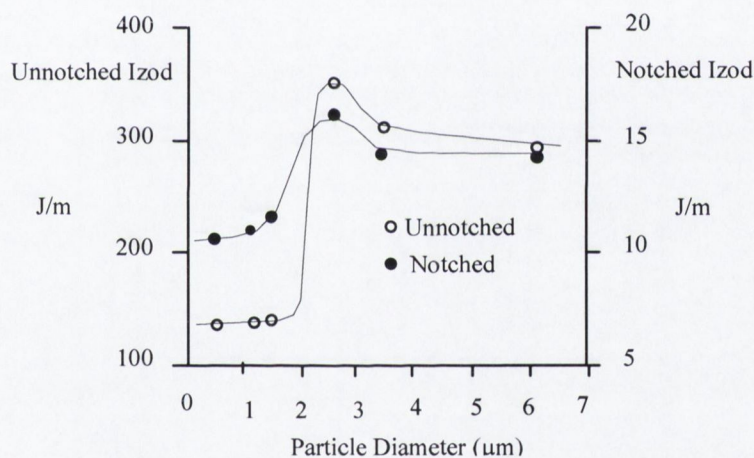


Figure 3.11. Plot of the Impact energy (J/m) vs. particle size (μm) for unnotched and notched Charpy specimens at 8% RPV[57].

3.3.9.4 Number of Particles

Implicit in the discussions above is the notion that it is not just the size of the particle or the effective phase volume that are fundamental to the toughening mechanism but the way and extent to which the matrix responds to their combined effect on the stress fields within the continuum.

However, intuitively, the influence of the two morphological features should be linked. In such an approach, linking the contribution of size and volume, Cigna et al modelled their data in terms of the incremental increase in impact strength ΔI with the number of particles (N) per unit volume where,

$$N = \frac{\Phi}{\frac{4}{3}\pi R^3}$$

Equation 3.10.

where Φ is the rubber phase volume and R is the particle radius[58]. By introducing a critical rubber particle radius (R_c), below which no toughening effect was observed and plotting $\Delta I/N$ against $(R_w - R_c)$ (where R_w is the weight average particle radius) they obtained a linear fit for their data over the particle sizes considered, see **Figure 3.12**.

Cigna et al felt that the meaning of the correlation, "required further research", its empirical utility was validated by similar correlations with impact data from tests on toughened SAN (polystyrene-acrylonitrile) and rubber toughened Nylon.

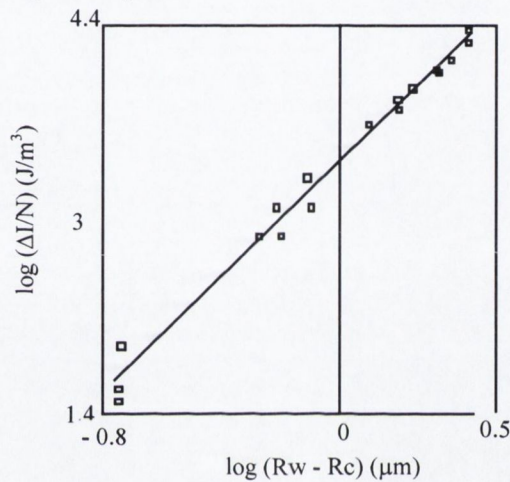


Figure 3.12. Bilogarithmic plot of $\Delta I/N$ vs. $R_w - R_c$, where R_c has been estimated at being $0.29 \mu\text{m}$ [58].

Although the minimum, or, critical particle size radius they determined for HIPS ($0.29 \mu\text{m}$) was greater than that predicted by Rosen ($0.1 \mu\text{m}$ -diameter) it was less than half the conventionally accepted value of $1 \mu\text{m}$ (diameter). A simple explanation for the lack of correlation might be the origin of the values. They were extrapolated from experimental data while evidence suggesting Rosen's $0.1 \mu\text{m}$ critical RPS was based on microscopy work. That the value was generated from impact tests on materials with polydisperse size distributions points to another vulnerability, i.e., that most systems contain polydisperse distributions of particles and in these overlapping stress fields can promote the incipience of crazes from smaller particles and so serve to lower the apparent limiting particle size. This point does not appear to have been explored.

3.3.9.5 Interparticle Distance

The notion of the interparticle distance was embodied in a criterion for rubber toughening proposed by Wu [59]. In considering ductile brittle transition in rubber toughened nylon Wu found the transition could be best modelled in terms of a critical interparticle distance. This Wu termed the critical matrix ligament thickness (CMLT) and interpreted its value as a material property independent of the particle

size and effective phase volume. Wu considered the origin of the brittle tough transition to be due to stress field overlap. He envisaged the centre to centre particle distance to be the critical parameter and that more effective toughening would accompany increased particle size, which is not the general case, i.e., volume density alters the stress field greatly. This led Wu to propose a generalised criterion for rubber toughening that perceived the transition from brittle to ductile behaviour to result from enhanced matrix yielding [60]. Thus the CMLT was the minimum ligament length that provided sufficient connectivity between ligaments to support ligament yielding. Treating this as a matrix property extended its utility beyond materials which yielded by shearing mechanisms, e.g., Nylon, and brittle matrices, e.g., HIPS and Rubber Toughened PMMA to materials that exhibited mixed modes such as ABS and PC, as well other types and shapes of particulate networks, e.g., platelets, rods etc.

There are some limitations to Wu's treatment of the CMLT. The basis of the criterion is that the matrix ligament thickness should be smaller than a critical value in order to effect substantial toughening. In the toughened resin the perturbed stress field then must extend over the critical ligament thickness and allow it to yield. However, as has been discussed above, the ability of different secondary phases to promote enhanced micro deformation mechanisms is dependent upon their mechanical properties and conformational alignment. Thus values for the CMLT determined from the physical distance separating discontinuous entities will vary with the mechanical, geometric and conformational arrangement of the secondary phase. This undermines the concept of the CMLT as a matrix material property as it is dependent upon the efficacy of the secondary phase entities to influence the stress field, and basing its determination on the physical distance separating them.

Also in his work Wu only considered the implications of the interparticle distance in terms of the ductile brittle transition a transmutation in the micro-mechanical process of deformation. This transition he saw as occurring at a critical particle size, d_c , at constant effective rubber volume fraction, Φ_r , and matrix adhesion, when the interparticle distance between two nearest neighbouring particles is at a critical value, T_c , with,

$$d_c = T_c \left[\left(\frac{\pi}{6\Phi_r} \right)^{\frac{1}{3}} - 1 \right]^{-1}$$

Equation 3.11.

In the treatment he considered the critical ligament thickness to be linked to a critical volume fraction of particles, or particles of a critical size, at a given volume fraction. This suited the nature of the system he was considering. For nylon, and also the epoxy systems, it is necessary that the size of the particles be sufficiently small to promote the micro-shear mechanisms. In such systems both the requirements of ligament size and connectivity are necessary and are not met by larger particles which limit their ability to transform the mechanism of matrix deformation. Replicating the macroscopic mechanical response at a microscopic level transforms the state of stress at microscopic level by setting up a triaxial stress field.

However in systems such as HIPS or other brittle amorphous thermoplastics such as PMMA where the micro process of crazing is the general mechanism of deformation in the material, it would seem that no great transformation in the mechanism of micro-mechanical response is required. In these materials the particles are required to be either sufficiently large or resident in the stress field of other particles so that they impose an adequate perturbation in the local stress field to initiate crazes. From this perspective the implications of the interparticle distance (IPD) are different, i.e., not determining whether a system will be capable of promoting crazing or improving toughness, but determining the effectiveness with which it does so.

The relationship between the IPD and toughness was explored by Cook Rudin and Plumbtree [57]. They modelled their data by plotting the Izod impact data against the inverse of a cubic lattice particle arrangement IPD. The plots were linear, and allowed for a qualitative prediction of the results, with the best fit being offered by the unnotched specimens (Figure 3.13.).

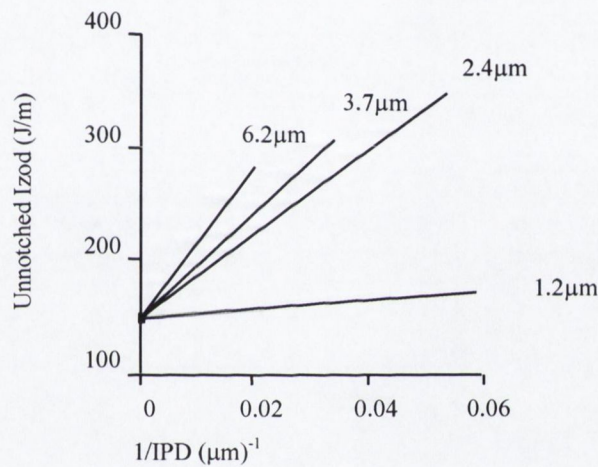


Figure 3.13. Plot of the impact energy vs. IPD (μm^{-1}) for unnotched Izod HIPS specimens possessing various particle diameters [57].

Cook et al postulated the correlation could be interpreted in terms of the breakdown of crazes between particles. The essential proposition was that microcracks grew by the breakdown of crazes extending from the surface of neighbouring particles, of a separating craze, and coalescing at its centre.

The work of Lautausser and Kramer, showing that the maximum fibril extension ratio occurs at the centres and tips of crazes and the later work of Kramer and Berger showing craze breakdown to generally occur at the centre of the craze, support such a mechanism of craze breakdown [15,61]. Indeed Donald and Kramer did note fibril breakdown occurring at the particle/craze interface [22]. Cook et al did not include any of these references in corroborating their assumptions. But their proposition rationalises a basis for a relationship between the impact energy and the distance between two particles and the effective phase volume inspiring and supporting plotting impact energy vs. the

inverse IPD. The interpretation seems logical, as there must be some relationship between craze breakdown and the distance separating particles.

Gilbert and Donald, in a series of microscopy studies on crazing in HIPS systems, showed that ductile matrix yielding occurred in PS ligaments after crazing. The studies showed that the extent of ductile behaviour was dependent upon the size of the ligaments separating the crazes [62].

In systems with high volume loadings of particles, greater densities of crazing were observed. The average ligament width between crazes was reduced to such an extent that the critical thickness for the brittle ductile transition of PS was approached. This critical thickness the authors found to be of the order of $3\mu\text{m}$. The work unveiled and underlined the importance of ductile matrix yielding in permitting a larger volume of material to craze and facilitate and contribute to the improvement in toughness. Ductile deformation of the matrix screened the stress concentrating effects of particles and craze tips and slowed craze growth and the onset of fibril breakdown. This provided better stress transfer through the continuum under loading and allowed other particles, including those which might have initially been ineffective ($<1\mu\text{m}$), to nucleate crazes. Consequently the volume of material involved in crazing increases and further crazing remote from the initial crazed volume becomes possible leading to an increase in the strain energy absorbed under loading. Finally as the PS ligaments are narrow and capable of ductile deformation they tend to fail in a ductile manner that adds further to the energy absorbed in deformation and fracture.

Gilbert and Donald noted that systems with low volume loadings only provided a marginal improvement in toughness. When crazes formed they grew quite rapidly until growth slowed as their stress fields overlapped. Craze thickening ensued until fibril breakdown left only a bridging ligament separating the crazes. This then deformed and secondary crazes formed at the ligament root leading to the eventual coalescence of, what by this time were essentially microcrack entities. These experimental observations vindicate Cook et al's hypothesis.

The conclusion drawn was that only when the distance separating particles is small will a blend exhibit a significant increase in its apparent toughness. Wu in reviewing his perspective of the critical particle distance drew on Gilberts and Donald's work. The CMLT was a parameter that explained their observations. If the matrix ligament distance was less than the CMLT the material would be toughened, if it was greater then no substantial toughness would accrue from the incorporation of a rubber phase. Some of the observations of Gilbert and Donald were apparent in the fracture process zones of some materials considered in this work (Chapters 4 & 5).

Gilbert and Donald suggest that some improvement in toughness should be achieved even if crazes are not nucleated purely by the transmutation of the deformation mechanism. However the contribution of multiple crazing followed by ductility of ligaments would be far larger and overshadow such contributions, i.e., transmutation achieves much greater levels of toughening.

3.3.10 Secondary Phase Structure and Tensile properties

Studies of the relationship between the rubber phase volume and tensile behaviour in HIPS have shown that material behaviour is influenced by the secondary phase throughout its entire loading history [63]. The tensile modulus, a material property determined in the elastic range, varies linearly with increasing rubber phase volume (Figure 3.14). The results suggested to Bucknall et al that the effect of rubber particle size was redundant and the rubber phase volume was pre-eminent of in influencing tensile moduli in HIPS resins.

Although the data for materials possessing smaller particles did appear to lie on a separate line the divergence observed in behaviour was concluded to be due to the lower shear moduli associated with a greater rubber (polybutadiene) content in the smaller particles.

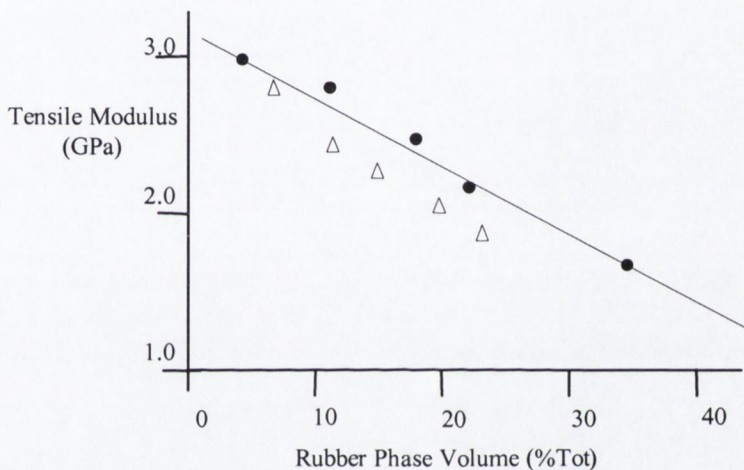


Figure 3.14. The 100 sec isochronous Tensile Modulus vs. rubber phase volume in two rubber particle size populations, where core shell type particles (Δ) were smaller than the MI-multiple inclusion particles (\bullet) [63].

The linear correlation between modulus and rubber phase volume appears to be accepted in the literature. For example, in their rubber toughened SAN, Cigna et al found a better linear correlation between the tensile modulus data with the sum of the rubber and graft SAN (as a weight percent), indicative of the effective rubber phase volume than with the rubber content alone [58].

The tensile yield strength of HIPS materials also appears to be dominated by the rubber phase volume [63]. Bucknall et al showed reasonable agreement between the experimental data for tensile yield using the Ishai-Cohen effective area model [64]. Whilst Ishai and Cohen had developed their model to describe the tensile modulus and found a linear relation between it and the modulus for the case of a porous ceramic Bucknall et al found it provided a good model for tensile yield. The method is based on a simplified model for stress concentrations produced by holes in a continuous matrix. The model predicts that stress will vary with Φ , the relative volume of holes, so that at yield it may be described by,

$$\sigma_y(\Phi) = \sigma_y(0) \left(\left[1 - \pi \left(\frac{3}{4\pi} \right)^{\frac{2}{3}} \Phi^{\frac{2}{3}} \right]^{-1} \right)$$

Equation 3.12.

where $\sigma_y(\Phi)$ is the tensile yield of the composite material and $\sigma_y(0)$ is the yield strength of the unreinforced matrix material. Buchnall et al again found some variation between species containing small and large particles. They noted that while the larger particle appeared to give a good fit to the model the small particles tended to have yield stresses above the expectations of Ishai-Cohen (see Figure 3.15). The poorer compliance of the small particles to the model was excused as being the result of batch to batch variation arising from the methods used in sample preparation. However the fact that the variations with the particle size were observed might better be considered as corroborative of the combined influence of particle size and phase volume.

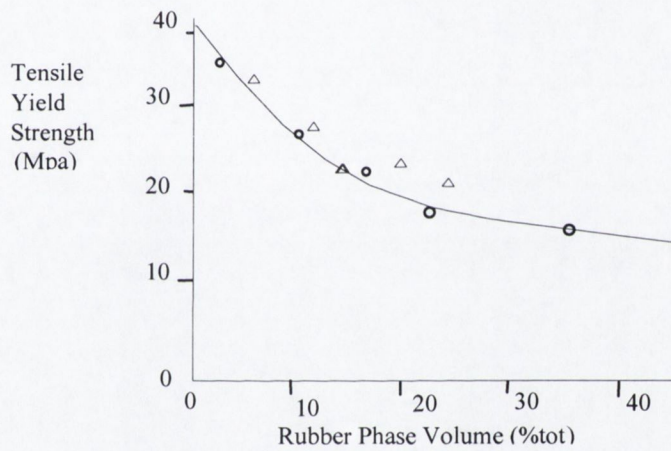


Figure 3.15. Plot of the tensile yield stress (MPa) vs. Rubber phase volume, the circular symbol represent the large MI rubber inclusions, the triangular represents the small CS type particles [63].

3.4 Impact Experimental Methods

3.4.1 Experimental Materials and Specimen Preparation

- In the experiments conducted for the present investigation, ASTM 256-88 Charpy impact specimens were prepared by injection moulding on a Krausse Maffei 60 ton injection moulding machine according to standard moulding conditions.
- Specimens of the polystyrene (PSB0), and 5, 10, 15, 0, 25 % ERPV blends of PSB1, PSB2, PSB3 materials in PSB0, identified henceforth as PSB#1 PSB#2 and PSB#3 were manufactured and residual thermal stresses eliminated by annealing at 60°C for 2 hours on silicone oil/talc mixture. All of the resins moulded well, including the control polystyrene resin, and only very minor alterations were made in the course of the entire moulding run.

- The specimens were notched to depths of 0.75, 0.75, 1.75, 2.75, 3.75 and 5.75 mm using a Ceast fly cutters fitted with a 45° notching blade with a 0.25 mm notch root radius (Figure 3.16.).

3.4.2 Impact Test Method

- The samples were fractured in 3 pt bending (Charpy) on a Ceast pendulum impacter using a 1J hammer. Samples were loaded on the impact test rig with the pendulum aligned with the specimen's notch (see Figure 3.17).
- Seven specimens of each material were tested using an L/D ratio of 4 (Figure 3.17). Results for each test were recorded and are presented in Table 3.2 in appendix 3.1.

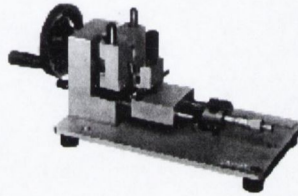


Figure 3.16. Ceast Fly-cutters used in notching specimens.

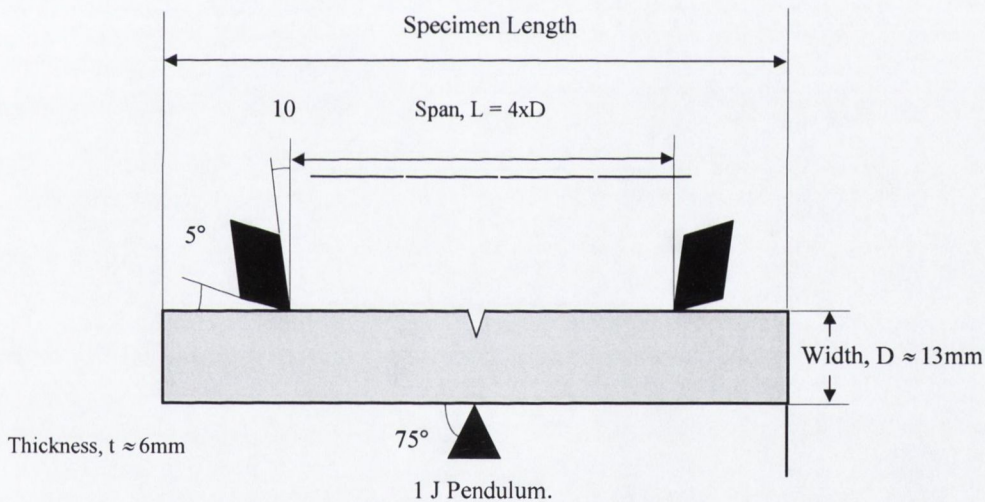


Figure 3.17. Loading configuration for Charpy Impact Tests.

3.5 Tensile Experimental Methods

3.5.1 Experimental Materials and Specimen Preparation

ASTM 256 Type 1 tensile specimens were moulded under standard moulding conditions on a Krausse Maffei 60 ton Injection Moulding machine.

3.5.2 Tensile Test Method

- The thickness and width of each specimen were recorded and entered into the control PC before testing. Specimens were tested at 2, 20 and 200 mm/min on a Zwick tensile tester.
- The mean value was determined from 10 tests of each specimen at each test speed.
- Tensile Modulus (T_m) was determined from the slope of the rising load per unit area vs. displacement curve. Tensile Yield (T_y) at the peak inflection of the curve and ultimate tensile strength (T_r) at rupture. The strain to yield and the strain to failure were also recorded.
- Results from all tests were recorded and are tabulated in Table 3.3 of the appendix 3.2.

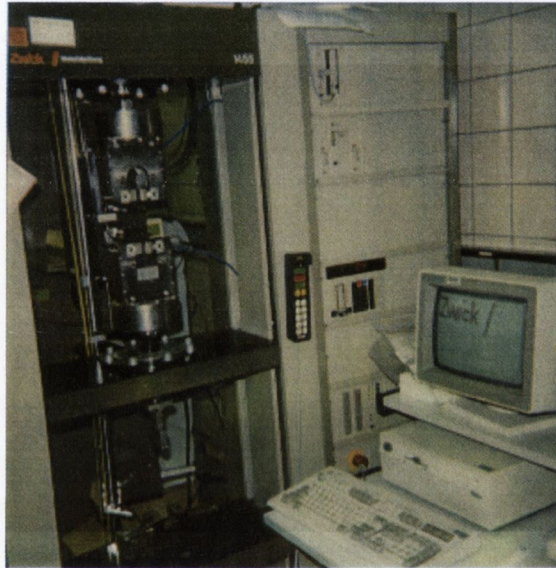


Figure 3. 18. Image of Zwick 1455 tensile test system used in tensile testing.

3.6 Experimental Results and Discussion

The results of the impact and tensile tests are presented in Table 3.2 and Table 3.3 (Appendix 3). To discuss the effect of changes in the secondary phase morphology on mechanical behaviour some assumptions regarding morphology are required, these are corroborated in Chapter 2, i.e.,

1. That the particles are of the same type, i.e., multiple inclusion (MI). This was concluded to be the case, though the size of the PSB1 materials meant that they possessed fewer inclusions, see TEM studies in Chapter 2.
2. That the Mw of the GPPS (PSB0) used to 'dilute' the experimental HIPS resins to the desired RPVs matched that of the HIPS matrices (i.e., that it, in itself, would not be seen as being responsible for the observed changes). Again this is an acceptable assumption as the molecular weight of PS matrix in the HIPS used closely matched that of the PSB0.

3.6.1 Tensile Results and Discussion

3.6.1.1 Secondary Phase Morphology and Strain Rate Sensitivity

The results of the tensile tests are tabulated in TableA.3.2 of the appendix. The tensile properties considered were the tensile modulus (T_m) and tensile yield (T_y). These measurements provide details of the mechanical response of the material over its elastic and plastic loading history.

Tests were conducted over three decades of applied loading rates, i.e., 2, 20 and 200 mm/min, to determine how sensitive the resins were to loading rate over the range that they would experience during fatigue testing.

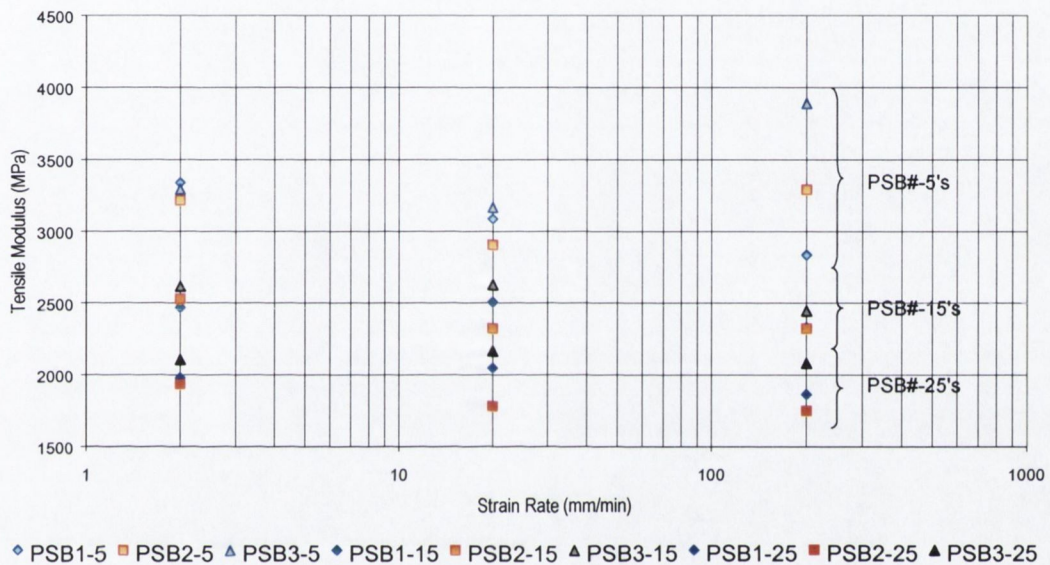


Figure 3.19. Tensile Modulus results for 5, 15 and 25 % ERPV polyblends for PSB#2 and PSB#3 and 5, 15 and 23.5 for PSB#1 series, plotted against log strain rate. (PSB1 \diamond , PSB2 \square , and PSB3 Δ). See Appendix 3.2.

The measurements of tensile modulus, presented in Figure 3.19, show that increasing strain rate did not effect a significant change in modulus. However an increase in the scatter accompanied higher strain rates in the case of the low ERPV. The change in slope is different and equations of regression curves show not only inconsistent slopes but also poor correlation coefficients(Appendix 3.2 - Table 3.4.). It would have been anticipated that increasing strain rate would have increased T_m . However no consistent trend was observed between the measurements, strain rate and the material's morphology over their elastic range of deformation; largely dictated by the matrix PS. The variations that were observed were inconsistent and its thought arose from experimental error. The source of such error may have been small variations in dimensions or the manner in which the on-board (the tensile tester) data acquisition system calculates modulus. The latter can arise, in the case of automated data processing systems, where only a limited number of points along the elastic range are acquired to calculate modulus. This was thought to account for the increased scatter obtained at the highest loading rate. In conclusion as variations could not be assigned to changes in straining rate, the materials were concluded to be insensitive to it over their elastic range of deformation.

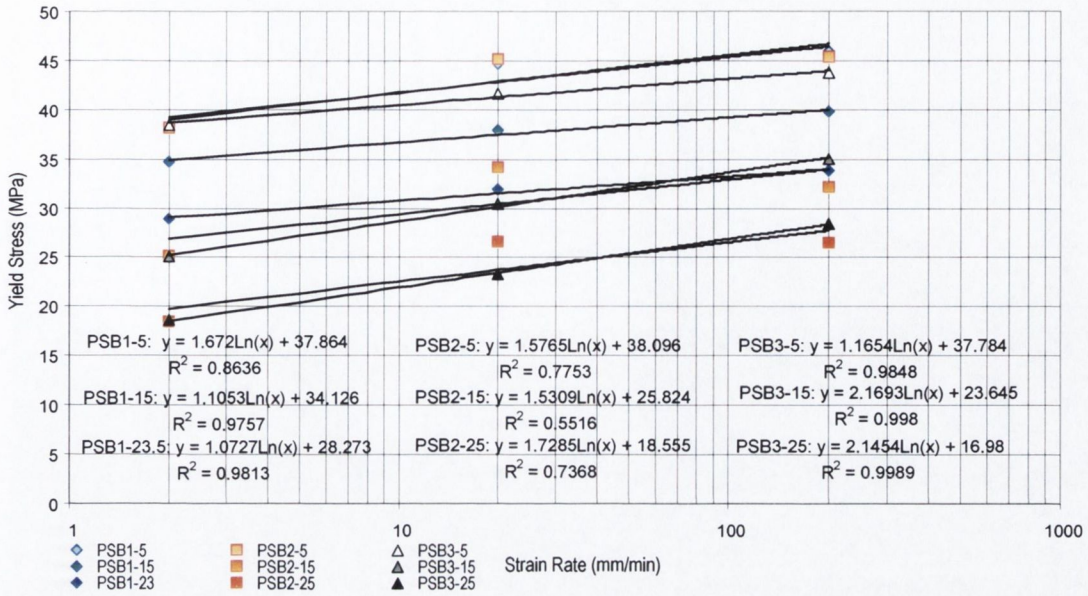


Figure 3.20. Tensile Yield for PSB1-3 5, 15, 23.5 (for PSB1) and 25% ERPV resins vs. strain rate (log scale) illustrating variation in yield stress with strain rate. (PSB1 \diamond , PSB2 \square , and PSB3 \triangle)

The tensile yield data revealed interesting information concerning the sensitivity of the materials to crazing under as applied loading rates were increased, as yield in HIPS coincides with the onset of crazing. Tensile yield strength was expected to be a more sensitive to straining rate than the modulus, as the process of crazing, in materials with an equivalent PS matrix, was highly dependent upon changes in micro-structural morphology.

The yield strength fell as the ERPV was increased in each of the series. The effect of increasing strain rate was to increase the tensile yield stress. The extent to which it did so appeared to be consistent in each polyblend series. The slopes of the curves, presented in Figure 3.20, provided a relative indication of the sensitivity of the tensile yield to straining rate.

The extent to which the strain rate influenced values, with increasing ERPV in the tree series, varied little. The observation illustrated the consistency with which successive additions of secondary phase had on mechanical response in each series. However the variation in the magnitude of the slope between each family of resins was more intriguing. Though only three strain rates were considered, it was clear from the results that the difference in the slopes associated with each family, i.e., PSB#1, 2 and 3, was greater than the difference observed with varying ERPV, especially for higher volume loading, >10%. This suggested that the differences between the particle populations, i.e., size, or distribution in sizes, in each of series exercised more influence on straining rate sensitivity. The rationale extending from this was that the influence of particle size was more fundamental, than ERPV, in determining the materials mechanical response, i.e., the relative sensitivity of a materials mechanical

response to increasing ERPV was dictated by its particle size population. This ranking of influence appeared to be corroborated by other observations made of the tensile and impact test data.

3.6.1.2 Modelling the Secondary Phase Morphology and Tensile Properties

Modelling the influence of a suspension of particles on the tensile properties of a composite can be considered and treated in a similar fashion to modelling their influence on the rheological properties of a fluid. Thus Smallwood, to model the relationship between particulate phase volume and tensile modulus, derived the equation,

$$T_{mc} = T_{mm} (1 - 2.5\Phi_c)$$

Equation 3.13.

Where, T_{mc} is the modulus of the composite blend, T_{mm} the modulus of the matrix, 2.5 is the Einstein coefficient for spherical particles and Φ_c the volume fraction of the secondary phase. In Smallwood's treatment the distance between particles is considered to be large and this is not the case in materials with high volume loadings of particles [65]. Guth modified the equation to account for higher concentrations of secondary phase particles and included an additional term to accommodate the stress field overlap associated with the higher concentrations[66],

$$T_{mc} = T_{mm} (1 - 2.5\Phi_c + 1.4\Phi_c^2)$$

Equation 3.14.

Ishai and Cohen modelled the variation in the tensile modulus in terms of the change in the load bearing area [64]. They originally developed their model for a porous ceramic, rationalising that the reduction in modulus would be proportional to the reduction in the cross section, or load bearing area, see equation 3.12. Their effective area model has been employed by many to model tensile yield as well as tensile modulus of polymer composites. Nicolais et al adopted the technique in studying effects of filler in polymers [67]. Bucknall et al used the method to model the tensile yield behaviour of HIPS [63].

In the present work the influence of the secondary phase on the tensile moduli (T_{mc}) of the polyblends was examined by first normalising the modulus data for the three series of polyblends with respect to that of the matrix resin. Thus the tensile modulus obtained for the unmodified polystyrene resin (T_{mm}) was divided by that obtained for each polyblend.

This value [T_{mm}/T_{mc}] was subsequently plotted against the ERPV(Figure 3.21). The plots appeared to 'present' the data for the three series of resins on a single regression curve. However when individual regression curves were fitted to each data series it was noted that the correlation coefficients were higher for each series than for the combined data set. The implication was that the secondary phase, of each resin series, exerted a 'unique', or characteristic, influence on behaviour. When rationalised in terms of the unique, size, or polydispersity, of the particle population in each of the three series the observation supported the comments made above regarding the sensitivity to straining rate.

The approach challenges the basis of the previous models, in terms of volume fraction and reduced cross sectional area. Modelling modulus in terms of ERPV alone is not sufficient. However Figure

3.21 shows that the moduli predicted using these do provide good agreement with the experimental data.

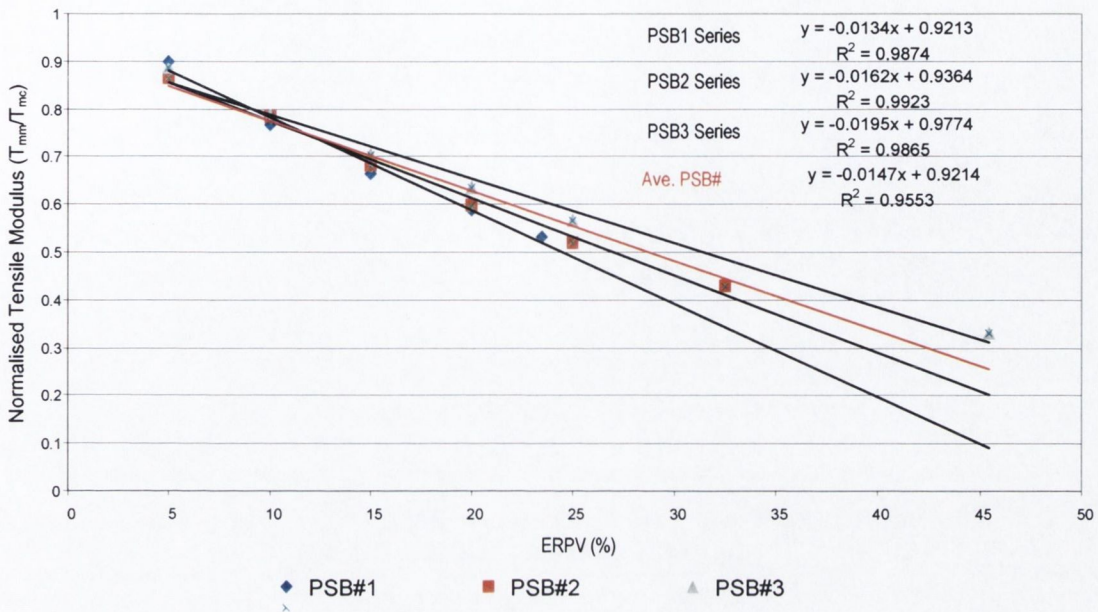


Figure 3. 21. Tensile modulus (T_{mm}/T_{mc} -PSB0/PSB#'s) (Normalised, with respect to PSB0) vs. ERPV. Displaying correlation coefficients (R^2) for the individual resin series and their combined data set (blue x).

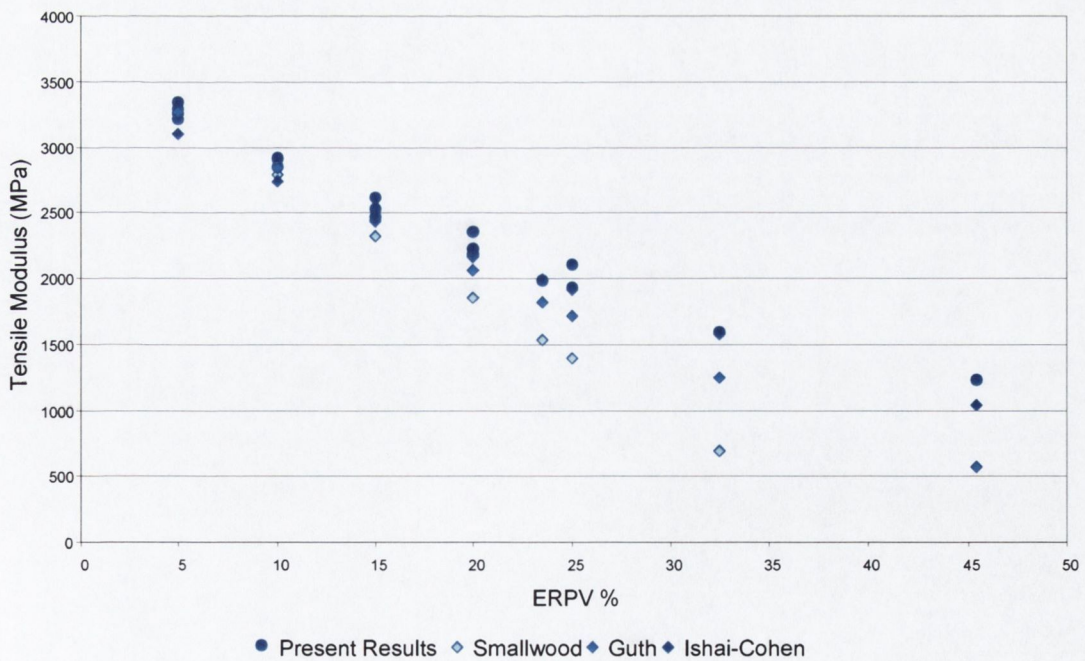


Figure 3. 22. A comparison between experimental results for tensile modulus with the predictions of the Smallwood, Guth and Ishai-Cohen methods.

Though they are not absolutely accurate, the methods employing the ERPV do provide effective means of modelling the elastic behaviour of the material. The relative suitability of Smallwood's, Guth's and Ishai and Cohen's methods are presented in Figure 3.22. Each predicts tensile modulus quite well with the Ishai Cohens effective area model appearing to best fit the data series whilst Smallwood's is worst.

Ishai-Cohen's effective area model also provided the best fit to the tensile yield data. The model's predictions were in excellent agreement with the data for the PSB#2 and PSB#3 series, especially for ERPV > 10 %. However neither it, nor the other models, predicted the values for the PSB#1 series very well. The experimental values were offset significantly from those predicted which perhaps undermines the reliability of basing predictions of structure property relationships on ERPV alone, Figure 3.23.

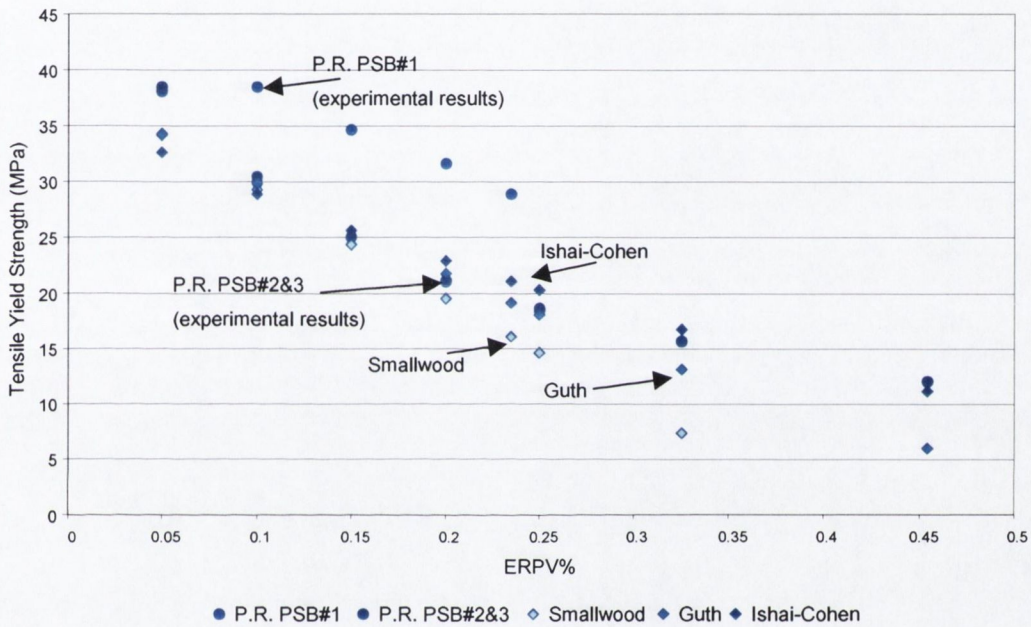


Figure 3.23. Comparison between the present results (P.R.) results for the three series (identifying PSB#1 separately) and the predictions of Smallwood, Guth and Ishai – Cohen model for tensile yield strength.

The results, and the predictions of the models, show that the ERPV was very influential in determining the mechanical response of the composite materials. However the distinctive behaviour observed for each of the series suggested that it was not the sole, nor even the primary, micro-structural factor determining behaviour. The plots in Figures 3.21 and 3.23 also suggested that the particle size, and/or particle size population, exert a more basic influence dictating how changes in the ERPV, which are greater in magnitude, will express their influence on the mechanical response of the material.

The suggestion appears to be substantiated by published results. Referring back to Bucknall's work, Figure 3.15, it's clear that the curves plotted for the two parent resins are distinct. Though this was not commented upon, the graph shows there was a difference in the response of the two materials as the volume fraction of secondary phase particles was increased.

3.6.2 Impact Test Results and Discussion

The observations made in the tensile tests, concerning the influence of particle size, were supported by the data obtained from the series of impact tests, for the different polyblends. The results were also in keeping with the observations of previous investigators who had studied the effect of rubber phase volume on Izod and Charpy impact behaviour in HIPS and other rubber toughened systems, see Section 3.3.9.

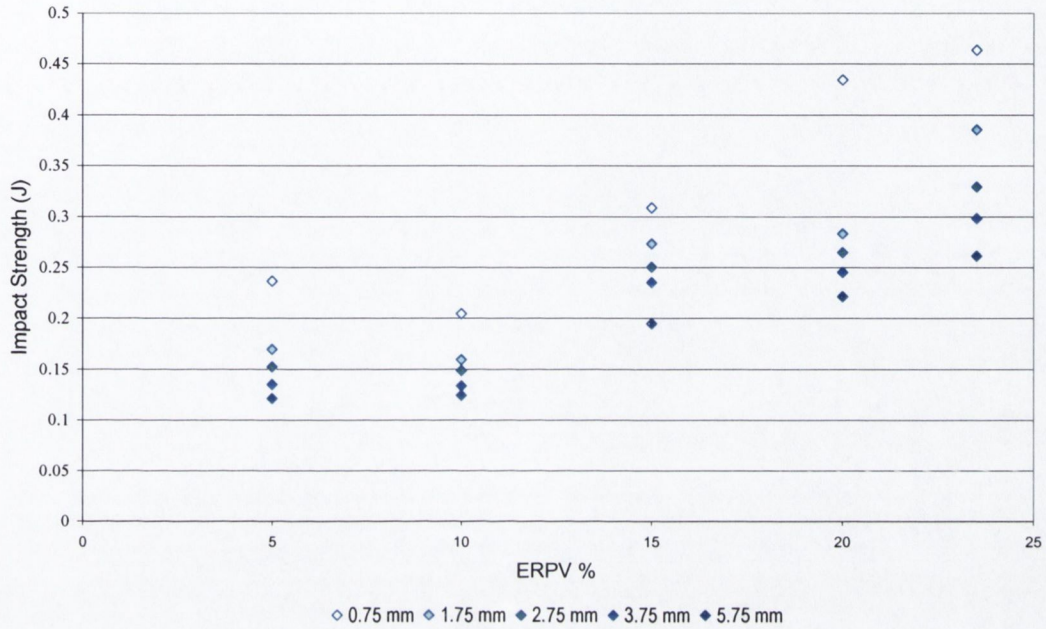


Figure 3.24 a. Charpy Impact Strength: ERPV vs. notch depth for PSB#1 series blends.

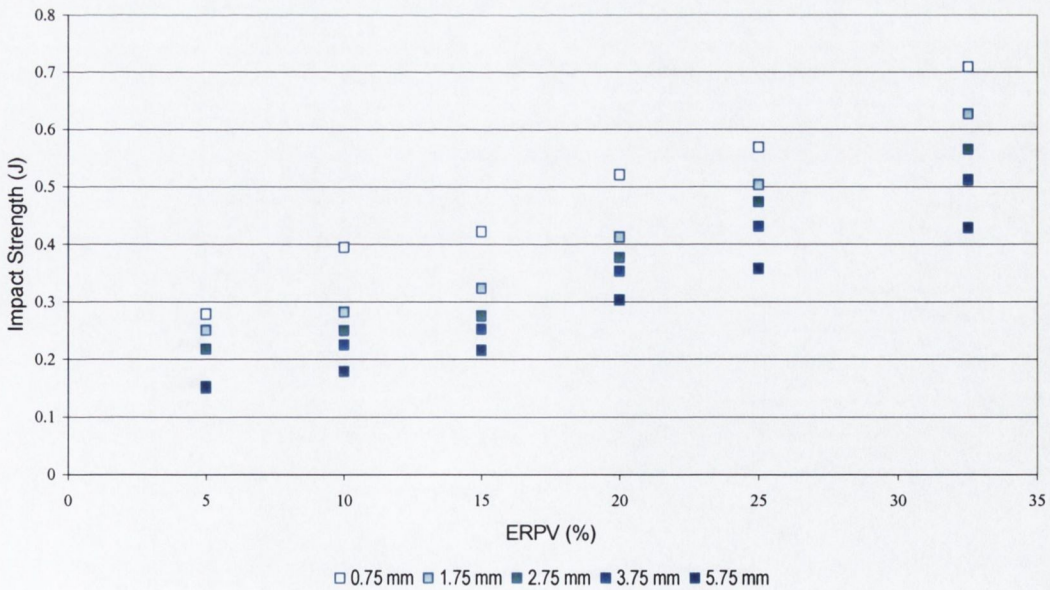


Figure 3.24 b. Charpy Impact Strength: ERPV vs. notch depth for PSB#2 series blends.

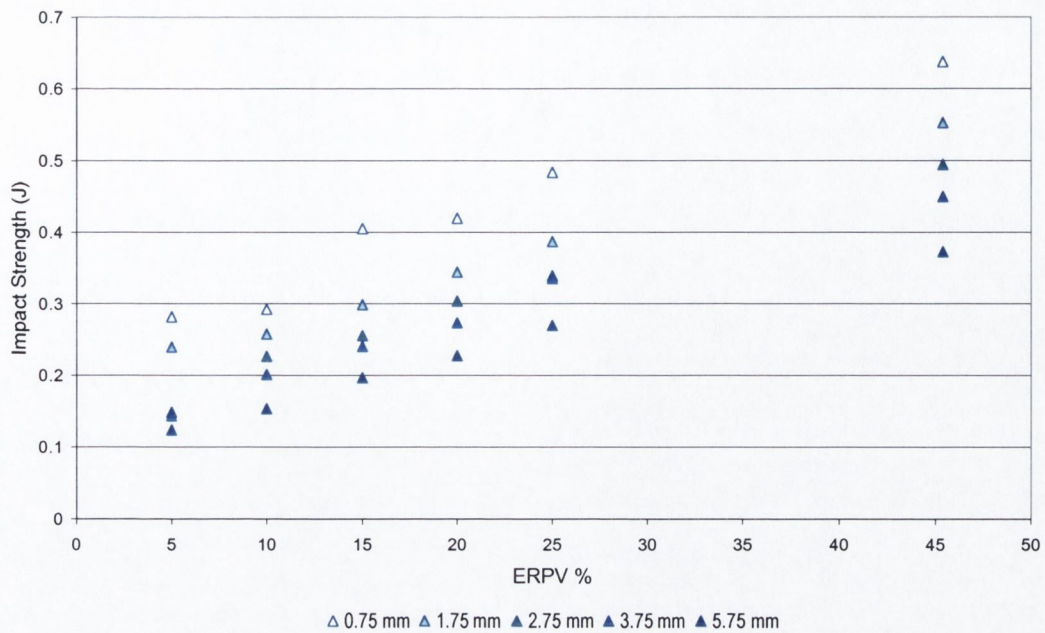


Figure 3.24 c. Charpy Impact Strength: ERPV vs. notch depth for PSB#3 series blends.

Figure 3.24. Charpy Impact Strength vs. ERPV for a. PSB#1 b. PSB#2 and c. PSB#3 series of polyblends for notch depths of 0.75, 1.75, 2.75, 3.75 and 5.75.

Increasing the ERPV in each series of polyblends, increased the impact strength, see Figure 3.24. As expected impact strength fell as the notch depth was increased, and it appeared to do so almost uniformly in each series. The slope of linear regression curves fitted to the three series of data provided an indication of the effectiveness, of the increasing ERPV, at improving the impact toughness in the three parent particle size populations (presented in Figure 3.25). The difference between the slopes of the curves obtained at different notch depths was noted to be slightly less than that between the three series for any particular notch depth. The observation echoed that made with regard to the tensile results above, and again implied that the different particle sizes, or the distribution of particle sizes in each series, exercised a defining influence on the micro-deformation of the materials.

The values for slope, in effect representing a 'craze efficiency factor', obtained for each ERPV from plots in Figure 3.24, were plotted against the notch depth in Figure 3.25, in order to determine the influence of increasing geometrical constraint on the impact toughness measurements. It was noted that the magnitude of the change in impact strength associated with increasing rubber phase volume fell as the notch depth was increased. The increasing level of constraint associated with the increase in notch depth explained this trend. It served to reduce the volume of matrix resin involved in fracture and so the ability of the particle size population in each of the parent resins to exert their own distinct influence over crazing. The observation illustrates the limitation of standard sized specimens in imposing uniform stress states and the danger in inferring intrinsic toughness from impact test data.

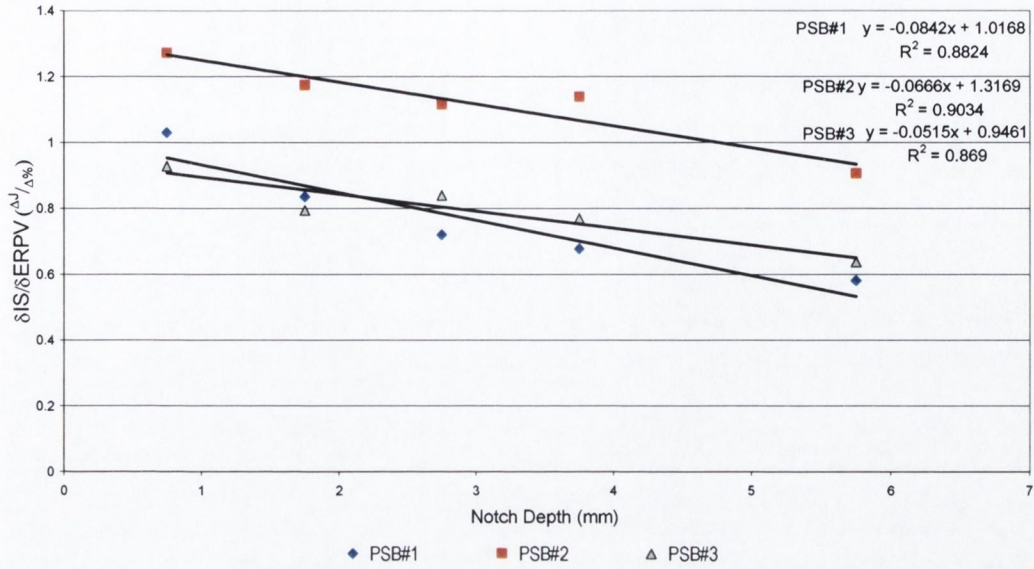


Figure 3. 25. Plot of the slope of the change in Charpy impact strength (IS) vs ERPV, i.e., dIS/dERPV vs. Notch depth for the three series of parent resins.

The slope of the three subsequent plots (in Figure 3.25) showed there to be relatively little difference between the sensitivity of each series to increasing notch depth, indicating that the effect of geometrical constraint, was consistent, or relatively so, for each of series of polyblends. However the plots graphically emphasised the difference between the magnitude of slopes obtained in Figure 3.24 for the PSB#2 compared with those of either the PSB#1 or PSB#3 series.

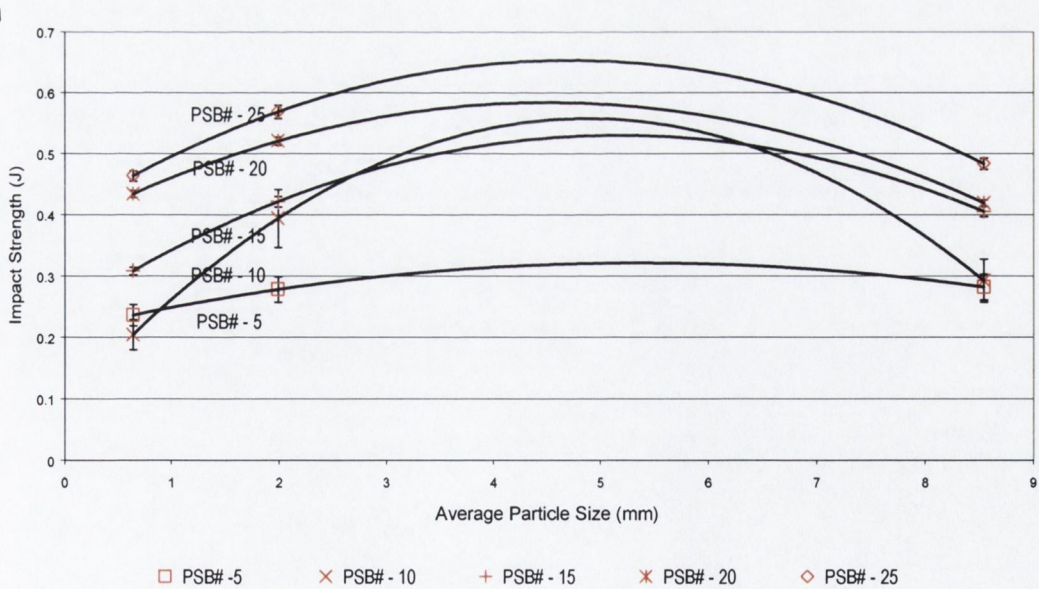


Figure 3. 26. Impact strengths vs. average RPS at notch depth of 0.75mm notch depth.

The, apparently, more craze efficient particle size distribution of the PSB#2 series polyblends exhibited far greater impact strengths at equivalent ERPV loadings. Their values for impact strengths were consistently greater than either the PSB#1 or PSB#3 materials. This allowed the conclusion be made that the particle size population does exert an influence on behaviour that is independent of the ERPV.

A very speculative plot of impact strength against particle size for 0.75 mm notch depth samples is made in Figure 3.26. The curves fitted to the data, suggests that an optimum particle size exists, between $\approx 4 - 5 \mu\text{m}$. The error bars on the graph are indicate the mean % difference of the standard deviations for the three series of materials at each ERPV. In the case of the 5 and 10% ERPV the scatter is greater, biased by the greater scatter obtained in the PSB#1 series. For higher ERPV the typical scatter is 2%. Thus, though speculative, the consistency between the curves for the 0.75mm notch depth, and those for the other notch depths, lends credence to the conclusion. The results also indicate how easily the hypothesis of optimum particle sizes, or range of sizes, could be evaluated with a greater number of particle sizes. The main challenge would be preparing systems with suitable particle size distributions.

3.6.3 Particle Size Effect

This observation, of particle size exerting an influence on behaviour independent of the ERPV, casts further light upon how the micro-structural morphology in HIPS influences toughening. The rationale it presents, outlined below, highlights a dichotomy that exists in the way in which structure property relationships in HIPS are dealt with. On one hand it is accepted that there is a particle size effect, this is not accommodated within the conventional continuum approaches to modelling behaviour.

Also though the spatial dimensions of the secondary phase morphology are assumed to determine behaviour, it is important to recognise they are not the only factors. Others, such as the type and properties of the rubber, the ambient temperature, the process/thermal history, the levels of interphase adhesion and grafted polystyrene, the molecular entanglement density, the hydrostatic stress exerted by the secondary phase, etc, all influence behaviour. Combined they can have a significant influence and all are aspects of morphology determined during polymerisation and subsequent processing. Consequently it is understood that changes to the polymerisation process, even slight ones, can alter these properties. Though it is possible some of these other factors may have played some role in distinguishing the response of the three series, it should also be borne in mind that the experimental resins were prepared using very similar methods; and the three series were chosen to limit the extent to which such variations and allow conclusions be made regarding the influence of the particle size and effective rubber phase volume. Nevertheless some differences were likely and the three particle size distributions obtained, which restrict the interpretation of particle size effects, illustrate the limitations of control that were possible.

Returning to the factors of particle size and volume and their influence on mechanical behaviour. Section 3.3 introduced how 'toughening' is achieved in HIPS, i.e., by the secondary phase serving to increase the amount of matrix that crazes in the process of crack initiation and propagation and so increase the amount of energy required to fracture the material. Increasing the volume of particles, by

increasing their size, or number, reduces the distance between them and increases the interaction of their stress fields and contributes to the level of crazing and so the apparent strength of the materials. For a given ERPV, larger particles will concentrate stress more efficiently, through a greater volume, than small particles in the matrix material surrounding them, and by doing so, they will tend to promote crazing more efficiently. Smaller particles, at a given ERPV, are more numerous and provide more sites for crazing. The abundance of the smaller particles compensates for their individual inability to raise stress through as large a volume, or over as great a distance, as larger particles.

The effective area model presumes an 'equilibrium' in the balance between both rationales. Thus the Ishai Cohen model appears to model one size as effectively as a distribution of sizes, by considering the ERPV alone. However the results show that although it predicts behaviour reasonably well it does not do so precisely. The data implies that there is a trade off between the number and the size of particles, one that appears to be mitigated by the respective populations' effectiveness in raising stress. The proposition arising from this being that altering the number of particles, of a given type and size, or changing the particle size, for a given portion of the particle population, can achieve an optimum toughening effect.

3.6.3.1 Modelling behaviour in terms of the Inter Particle Distance (IPD).

Figure's 3.23 and 3.25 again show that the response of the materials' tensile and impact strength to changes in the ERPV is biased by the sizes of particles or the distribution in their sizes within the population. It seems neglectful to model behaviour in terms of the micro-structural properties without considering this aspect of morphology or building it into parameters that can accommodate the effects of size. Consequently models that do not consider them are incomplete while those that do can be considered as somewhat more complete.

It was noted above how some have sought to correlate behaviour with particle size attributes, section 3.3. These they have represented by parameters that reflect the spatial distances between particles and their number. Interest in modelling behaviour using interparticle distances emerged at the end of the 1980's and through the early 1990's. Wu first correlated the change in impact strength ΔI with particle size and inter-particle distance (IPD). His concept was that key distances, associated with critical domain sizes, were responsible for 'transforming' the dominant internal deformation processes, i.e., from cavitation to shear, which then radically affected behaviour.

The critical IPD was seen as a matrix material property that, for composites of equivalent ERPV, was dependent on particle size. Wu's studies were based mostly on experiments with rubber toughened epoxy resins, where extensive shear deformation of the matrix was possible. However it is possible to translate the concept to HIPS in the critical/minimum particle size necessary for crazing, envisaged by Rosen, Silberberg and Han, Donald and Kramer, Cook et al, etc. Especially the latter who correlated HIPS impact strength with the inter-particle distance, i.e., $1/IPD$. They rationalised the correlation in terms of the shorter distances between particles associated with the breakdown of crazes.

The correlation identified by Cigna et al, also in HIPS, between the rate of change in the impact strength with the number of particles ($\log(\Delta I/N)$), with the particle size difference between the average particle size (R_w) and a critical particle size (R_c), i.e., $\log(\Delta I/N)$ vs. $(R_w - R_c)$, was similar. Though Cigna et al, felt further exploration of the relationship was required in order to understand its implications their observations can be linked to the IPD, through N (equation 3.10) and $(R_w - R_c)$ both proportional to IPD, i.e., $IPD = (1/N)^{1/3} - 2R$, where $R = RPS/2$. In essence each had modelled the same elements of morphology. Different parameters were used and different rationales offered to explain the correlations obtained. However each was successful due to their modelling behaviour in terms of distances and critical domain sizes. These distances dictate stress field interactions within the matrix continuum that in turn determined the process of deformation and so toughness.

The inter-particle distance then can be successfully used to model size effects for different material properties and for mono and polydisperse particle size populations. In the following plots, Figures 3.28 and 3.29, the tensile and impact (from 3.75mm notch depth) data for the three series of materials are modelled in terms of a cubic lattice inter-particle distance.

The IPD used in Figures 3.28 and 3.29 was determined using the volume average particle sizes of each parent population. Particle volume was modelled as a cube*, i.e., A^3 in Figure 3.27. The number of 'cubic' particles (N) accommodated within the ERPV fraction of unit volume was divided into unit volume to determine the volume available to accommodate each one, C^3 . Subtracting A from C yielded the cubic lattice IPD similar to Wu and Cook, and proportional to the parameters used by Cigna.

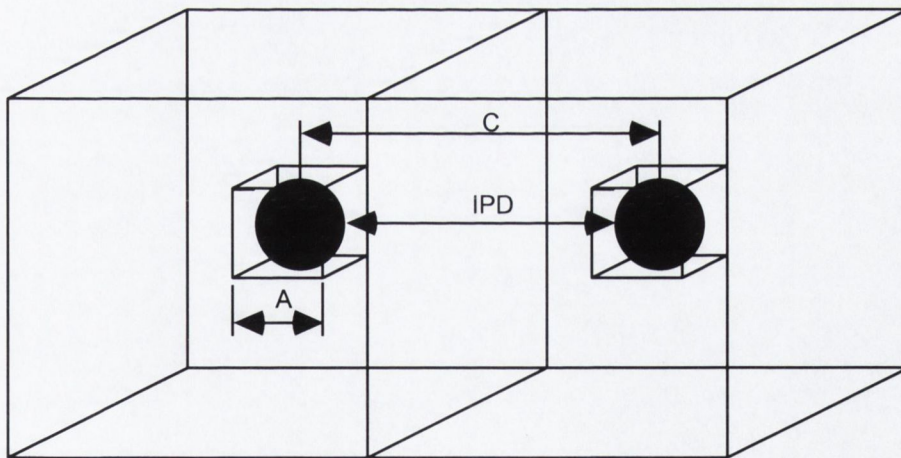


Figure 3. 27. Illustration of the Cubic Lattice Model used to calculate Inter-Particle Distance.

$$IPD = \sqrt[3]{1/N} - A$$

Equation 3. 15.

* **Note.** In the evaluation of the $Dz+1$ the volume occupied by a particle is approximated to the particle diameter cubed – see Tables in the Appendix of Chapter 2.

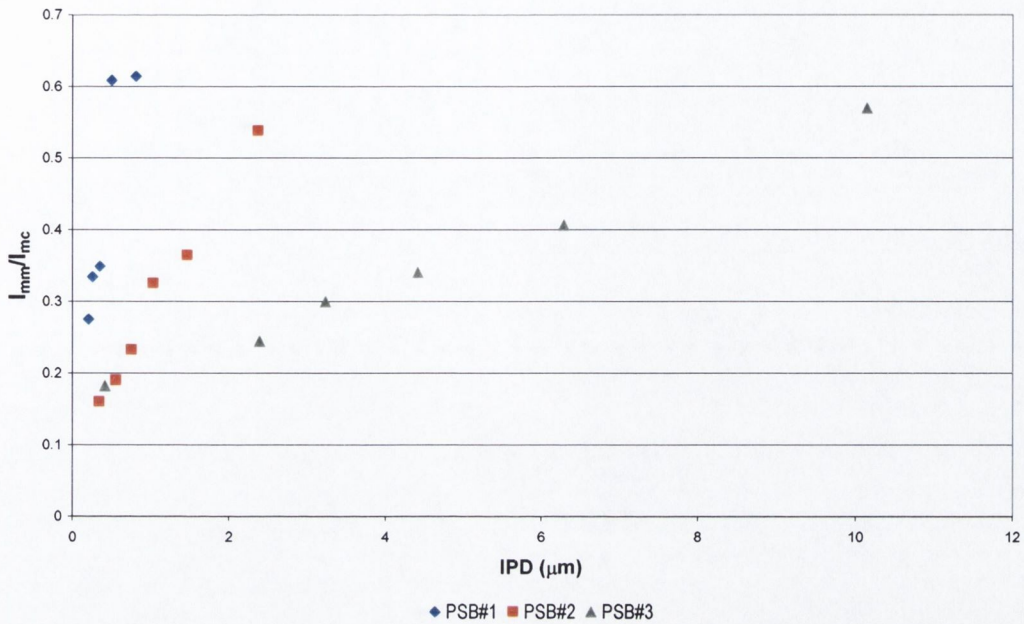


Figure 3. 28. Plot illustrating the correlation of IPD with the decay in impact strength with increasing IPD. The quotient reflects the impact strength of the matrix resin (I_{mm}) divided by that of the HIPS (I_{mc}), i.e., as impact strength falls quotient rises.

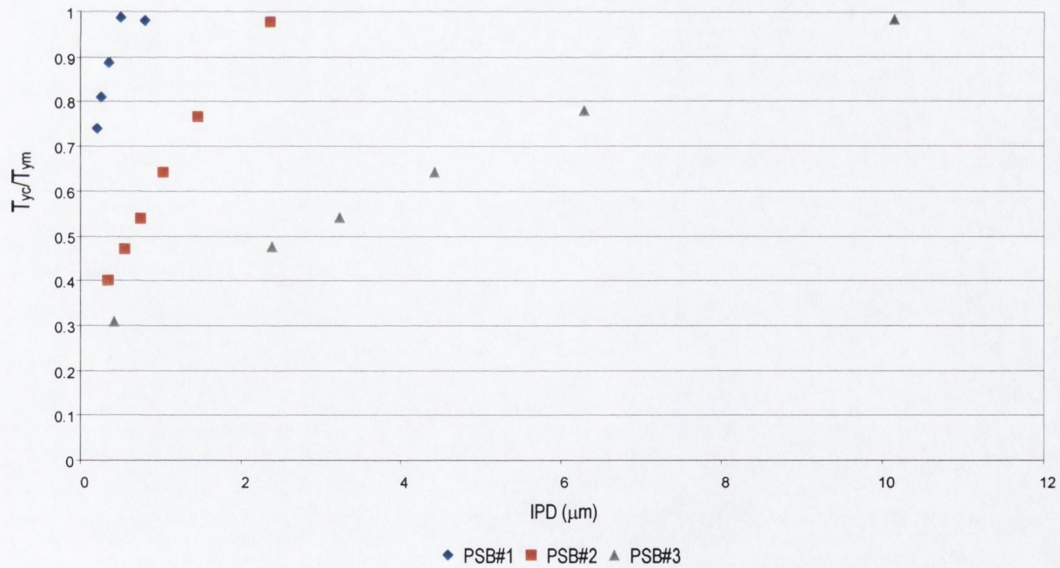


Figure 3. 29. Plot illustrating the correlation of IPD with the increase in Tensile Yield strength with increasing IPD. The quotient reflects the ratio of HIPS strength (T_{ye}) to the matrix resin (T_{ym}), i.e., tensile strength increases with IPD.

The units were expressed in meters. Both the increase in impact strength and the decrease in tensile strength correlated with increasing IPD. Figure 3.28 illustrates this increase for impact strength with IPD, over that of the matrix resin, using the 3.75mm notched charpy impact strength data as an

example. The shape and slope of the plots was preserved at the other notch depths considered. Figure 3.29, models the decrease in tensile yield strength with IPD.

The plots serve to highlight the distinction between the sensitivities of the different series of blends. They emphasise the influence of particle size and inter-particle distance in promoting crazing. In both the tensile and the impact strength plots, the contrast between the sensitivity of the three series of materials to micro-structural changes was evident. The PSB#1 series exhibited greatest sensitivity to change in the IPD whilst the PSB#3 the least.

The complexities encountered in particulate composites curtail the applicability of generalised models to describe mechanical behaviour. Many investigators have introduced semi-empirical parameters to accommodate the variability arising from factors such as interfacial effects particulate geometry and packing fraction. Turcsanyi et al proposed a semi-empirical relationship of the form

$$\sigma_c = \sigma_m \frac{1 - \Phi_f}{1 + 2.5\Phi_f} e^{B\Phi_f}$$

Equation 3. 16.

Where is B a constant related to the composite system, accommodating the other factors influencing the micro-structural response of the material [68].

A similar quotient was employed to model the tensile properties of the HIPS resins studied in this work. The response of the materials being predicted by,

$$T_c = T_m \left(1 - e^{-\frac{\alpha_f}{RPS} IPD} \right)$$

Equation 3. 17.

Where T_c is the composite tensile property (T_{mc} for modulus or T_{yc} for yield) T_m the complementary subscript associated with the strengths of the matrix polystyrene (T_{mm} and T_{ym}) and α_f a material constant for the system under load. The value of α_f varied with differences in the particle size population and the tensile property being considered. The parameter (α_f) was considered to be a stress field 'overlap' function, reflecting the particulate populations' efficiency in nucleating crazes [69], Appendix 3.3.

Empirically derived correction factors, are convenient and can accommodate the diverse range of possible interactions between particles and matrix affecting mechanical response; active reinforcement of the matrix, localised strain softening and cavitation, to transforming the micro-mechanism of response. They provide solutions and can contribute to understanding but emphasise the need for continuing research and better understanding.

3.6.3.2 *Modelling behaviour in terms of a Size Corrected Inter-particle Distance RIPD*

Herein modelling behaviour in terms of the inter-particle distance is fostered by the interpretation of the micro-structural sensitivity of the materials as something that originates from the efficiency of the secondary phase in modifying stress field interactions to promote crazing. The relative influence that each has on the stress field intensity.

As has been seen, larger particles, being less dependent upon neighbouring particles to elevate stress over sufficient area to initiate crazing, responded more slowly to change in IPD or ERPV. Smaller particles, heavily dependent upon neighbouring particles, were the most sensitive to change. Their relative dependence was a function of the different stress fields experienced in the particle size populations.

The approach adopted then focuses on the stress field interactions of the secondary phase as the influential factor. Rather than simply visiting the correlations observed between the spatial distances associated with micro-structural morphology and the materials behaviour in terms of the specific physical events; - though these are used to determine the relative crazing efficiency of the systems. The relevance of the approach, of modelling behaviour in terms of a size corrected inter-particle distance, is in exposing the efficiency of the system in redistributing relieving stress. It provides a more coherent means for modelling behaviour, one that could be used to consider micro-scale stress concentration and extended to interpret relationships between microstructure and other physical and mechanical properties. The parameter is also thought to facilitate the use of micro-structural data in FEM and meso-scale modelling approaches.

3.6.3.3 *Rationale for Modelling HIPS in terms of the RIPD.*

The complex interactions between stress fields surrounding particles of different sizes arranged randomly in the matrix would make the calculation of the true stresses in the composite very laborious and extremely time consuming. Instead for the time being it is considered wiser to model these and their influence in terms of a parameter on which both, particle size and true stress, are dependent. Consequently in linking the IPD to indeterminate but relative levels of stress concentration a quotient IPD/C (C : see Fig. 3.27), the RIPD, was used.

It is possible to use analytical techniques (FESEM- field emission scanning electron microscopy, μ TAC- thermal probe calorimetry) to construct three-dimensional models of real materials and finite element methods to calculate stresses in these models. Such approaches are the direction for modelling behaviour in the future and so the future in designing, polymerising and processing of optimised materials. However for the present they are impractical, e.g., constructing FE models and generating solutions for even moderate populations of particles would require hundreds of processor hours. Developments in analytical techniques, image and computer processing and materials science, will undoubtedly make these approaches practical options for materials designers over the coming decades. However in the interim meso-scale modelling techniques offer a practical means of bridging the capabilities and requirements of technology and theory. The rationale used to model HIPS structure

property behaviour in terms of the RIPD, contributes to this approach, by providing a parametric framework to bridge micro and macro scale response.

The quotient, RIPD, is equivalent to h/R , the ratio between the 'centre to centre' separation of a discontinuity (R) and the attending ligament distance between it and another, or an edge (h). This quotient is referred to by many names in the literature, e.g., the slenderness ratio, the ligament efficiency and the relative material density ratio [70,71,72]. It has been used in modelling stress concentrations in 'perforated' plates since the late '50's.

Its relationship with the applied nominal stress and the average maximum stress around the stress raiser (hole/sphere/inclusion) simplifies the presentation of data in tables and plots for design engineers interested in using stress concentration data. It can also be used here to simplify the relationship between the stress and inter-particle distance.

Horvay expressed the maximum average ligament stress in a perforated plate using the relationship,

$$\sigma_m = K' \frac{\sigma_p}{h/R} = K' \sigma_0$$

Equation 3.18.

Where σ_m is the maximum average stress experienced about the ligament (separating distance), σ_p the larger principal stress attending the ligament, σ_0 the nominal stress and K' the stress multiplier. The stress multiplier, K' , is not a true stress concentration factor in the conventional sense of the term, but the product of the stress concentration factor and a 'stress enlargement factor'. The latter term is the ratio of the average maximum stress in a separating 'ligament' to the nominal stress, σ_0 . In the case of small particles and large ligaments, or inter-particle distances, the value of K' reverts to that of the stress concentration factor. However for small inter-particle distances, or high particle concentrations, the stress enlargement factor dominates [69].

In considering the behaviour of a HIPS material it is not the stress in individual ligaments, nor the average stress about specific particles that is of interest, but the average about a number of particles that exercise a consistent influence over another volume of incorporated particles that characterise the response of the entire system. These are considered to be additive with the potential to amplify nominal stress levels above those conventionally associated with stress concentration.

Horvay, using conventional continuum mechanics theory, derived expressions to describe the stress enlargement factor and predict micro-scale stress levels in perforated plates. It would be possible to employ FE to predict the levels of stress enlargement associated with various particle size distributions. Consequently it may be speculated, with some certainty, that, in time, it will become possible to predict macro-scale stress fields in three dimensions with a micro-scale level of resolution. However, for the present, in translating the concept of modelling the macro-mechanical response in terms of the stress concentrating effect of complex micro stress field perturbations, it is possible to consider the holistic

response in terms of its relationship with the microstructure at specific occasions that regard comparable levels of stress in the modified and unmodified resins. Examples where the micro-scale stress is equivalent and response the same, are in the linear elastic response of the material, i.e., elastic modulus, or, in the case of HIPS at yield, where cavitation is promoted in the matrix at a critical level of stress. Impact strength, which is dependent upon the level of crazing, can be considered to be similarly sensitive to critical stress levels.

In these instances the response of the modified compared to that of the unmodified resin is dictated by the stress multiplying effect of the incorporated phase. This evident in the relative difference in stress required to effect similar responses in the matrix. The response observed is the product of the entire population under consideration, i.e., the behaviour of a population necessary to effect the characteristic response, summed and averaged over the number of such sub populations activated in the response measured. In itself the quotient, h/R , is independent of the level of stress and the actual concentration of stress. However the magnitude of the principal stress invariant at any specific point varies with the quotient. When summed and averaged about a particle, or a population of particles, the average maximum stress level in volumes of matrix separating particles will vary with the quotient. Similarly the relative tensile yield stress or tensile modulus will vary with the quotient.

For systems containing similar particle types, in similar volume densities and particle size distributions the mechanical response will be the same. Where the volume density varies, h/R will vary proportionately so will the mechanical response. For other populations of similar particle types, present in similar volume densities, but different particle size distributions, differences in particle packing will perturb the interaction of stress fields and so the volume of particles required to effect a characteristic response from the matrix will vary. This in turn will vary with the ERPV.

Modelling behaviour in terms of h/R , i.e., the RIPD, preserves the proportionality of ERPV and the effective area response, in the stress multiplier, and accommodates the variation in the average maximum stress arising from the different stress concentrating efficiencies, or different stress field interactions achieved with different particle size distributions and packing ratios. That is can be predicted at a micro-scale level and measured at a macro-scale level presents the RIPD as a parameter that bridges the micro/macro mechanical response. For these reasons it is considered a better parameter to use in modelling the behaviour of the materials.

The RIPD then whilst a parameter whose magnitude is equivalent to h/R actually represents the interpretation of the relationship between the interaction of stress fields associated with the particle size distribution and the particle configuration whose average is used to determine RIPD.

In the three series of polyblends the increase in the ERPV can be considered as a change in h/R , or RIPD. The variation in the relative tensile and impact strength with RIPD can be considered in terms of the stress multiplying effect of the secondary phase. The stress multiplier while different in each case is

proportional to the RIPD for each particle size population. HIPS, consisting of a high modulus brittle PS phase and compliant spherical secondary phase can be represented by the idealised case of isotropic tensile loading the variation in the relative stress vs. the RIPD, or h/R in equation 3.18, is 1.

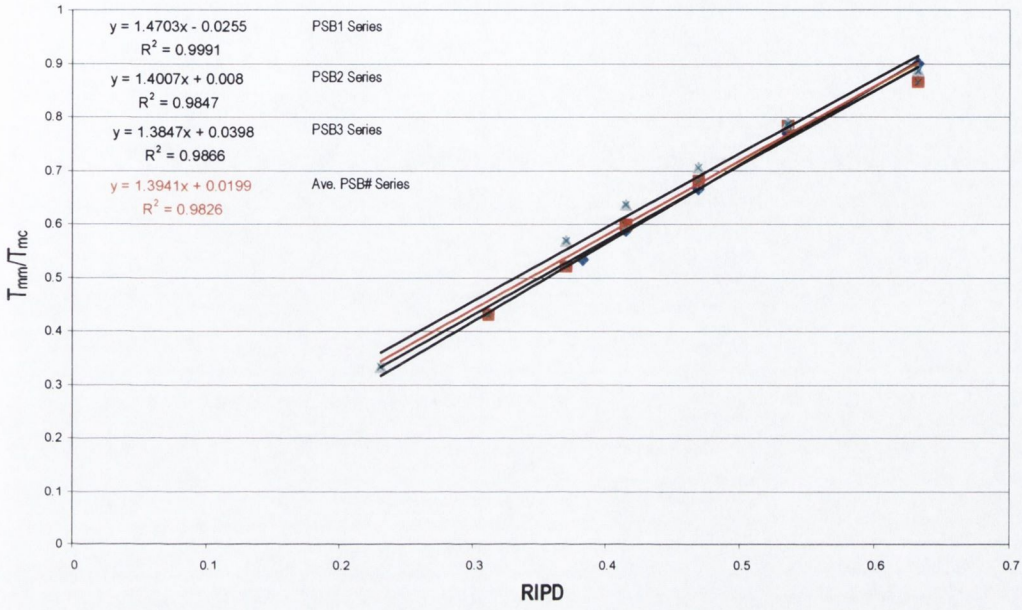


Figure 3.30. The Inverse Normalised Tensile Modulus versus RIPD with linear regression curves and correlation coefficients (PSB1 \diamond , PSB2 \square , and PSB3 \triangle)

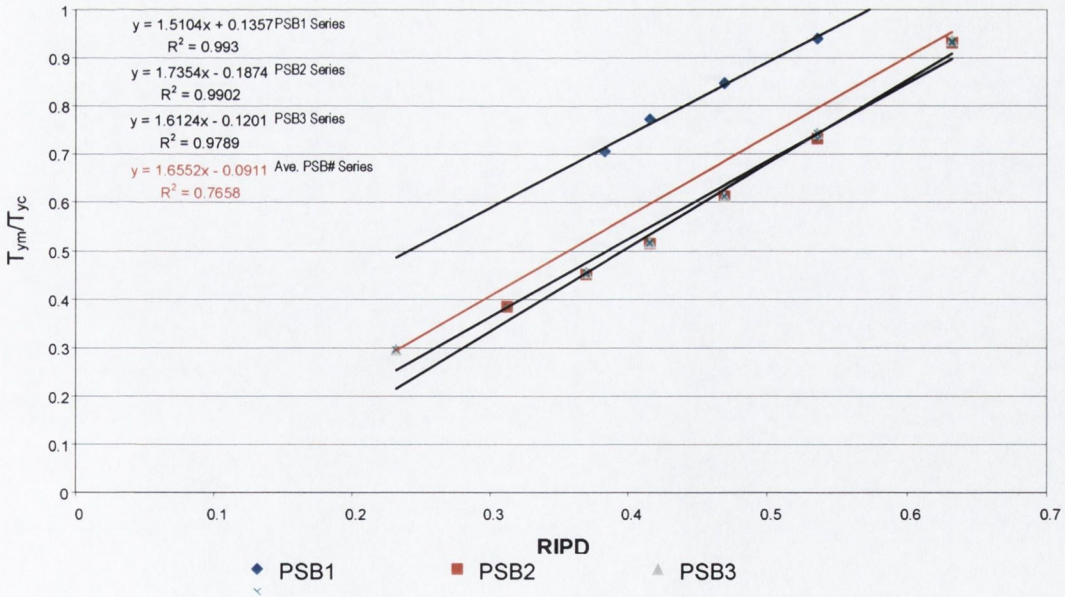


Figure 3.31. The Inverse Normalised Tensile Yield versus RIPD with linear regression curves and correlation coefficients (PSB1 \diamond , PSB2 \square , and PSB3 \triangle)

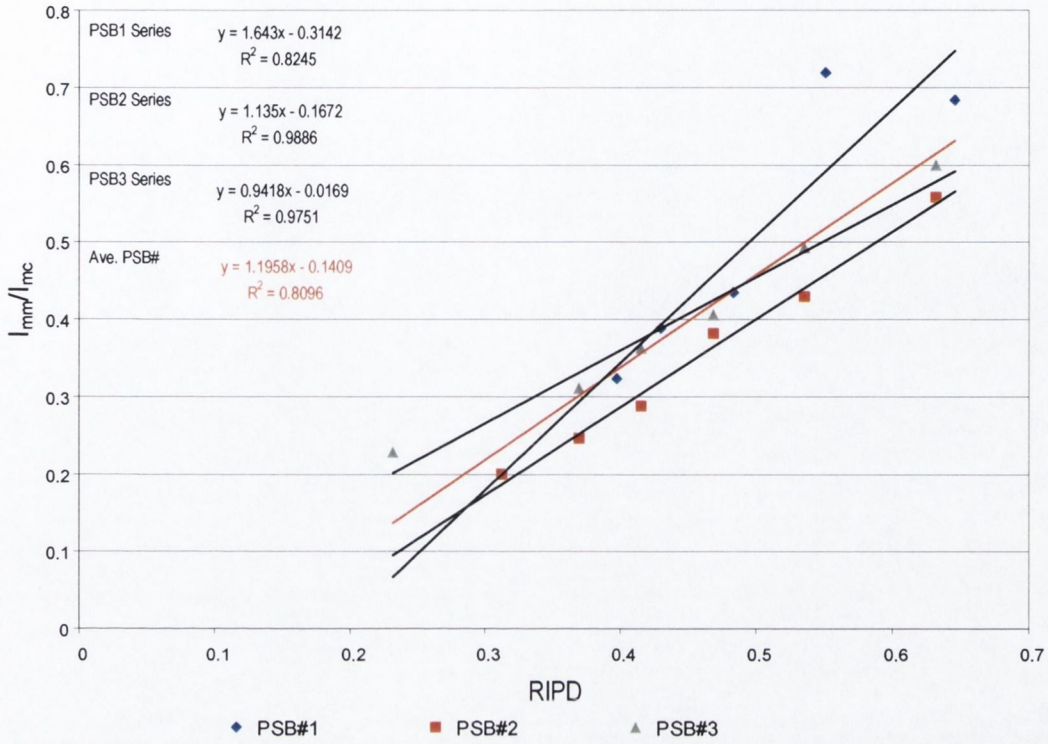


Figure 3. 32. The Inverse Normalised Impact Strength versus RIPD with linear regression curves and correlation coefficients (PSB1 \diamond , PSB2 \square , and PSB3 Δ)

The tensile modulus tensile yield and impact strength were all found to correlate with the RIPD in Figures 3.30, 3.31 3.32. All of the materials possess values of K' close to 1 indicating the dominance of the stress enlargement factor in determining the stress state and the close agreement of the effective area models. The values of the stress multiplier, or stress enhancement factor, reflecting the craze efficiency of the three series of resins, are presented in Table 3. 1.

Craze Efficiency (Stress Enlargement Factor)			
Material	Tm	Ty	K'
PSB#1	1.4703	1.5104	1.643
PSB#2	1.4007	1.7354	1.135
PSB#3	1.3847	1.6124	0.9418
AVE	1.3941	1.6552	1.1958

Table 3. 1. Stress enlargement factors determined for the three series of HIPS, from Tensile modulus tensile yield and Impact strength data.

The high correlation coefficients obtained for each of the three series validate the approach though some weaknesses are identified. The difference between the values obtained for the stress enlargement factors vary somewhat but not greatly. In the case of the tensile modulus data the difference in the

values for K' are imperceptible. In the case of the impact data the results of the low volume additions of PSB#1 distorts the value of the concept and indicates the limitations of the approach and possibly alludes to the difficulties associated with comparable stress state in impact tests.

However the tensile yield plots, based upon the best data series (most consistent), show the PSB#2 series to exhibit a greater stress enhancement value than the other two series. The result echoes the results obtained for the increased impact toughness achieved with addition of secondary phase in each of the three series. Comparing the craze efficiency factors of the three series obtained from tensile yield and impact (from Figure 3.25) is very striking.

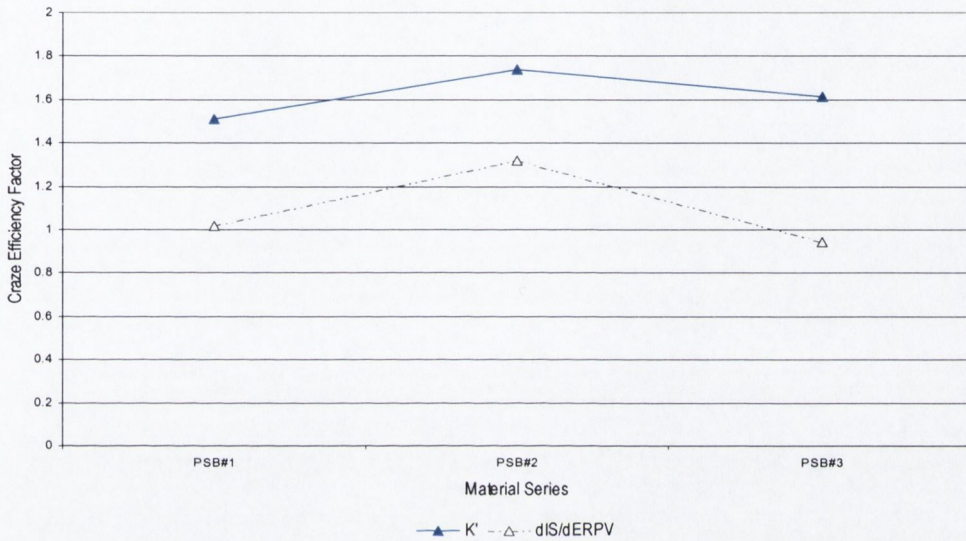


Figure 3.33. Comparison of the craze efficiency factors obtained from tensile yield data with those obtained from Charpy impact strength.

The result confirmed the difference in the effectiveness of the different secondary phases in nucleating crazes and effecting change in the response of the materials. The correlation with the impact data its considered validates the concept of a craze efficiency factor and the modelling of behaviour in terms of the RIPD.

3.6.3.4 Critical particle size

The results of the tensile yield data presented in Figures 3.23 and 3.31 show the PSB#1 series to be offset from the values of the other two series. A number of investigators have commented on the existence of a minimum particle size necessary to effect crazing. Estimates of for the critical particle size have ranged from 0.1 – 2 μm , though the Bucknall and Donald and Kramer envisaged a value closer to 1 μm [1, 22, 34, 53].

In considering the data from the TEM analysis of particle size particle sizes less than 1 μm and their effective phase volume was eliminated from PSB#1 and PSB#2 TEM data. Correcting for this

minimum particle size recalculating RIPD and plotting the data aligned the PSB#1 and PSB#2 series with the PSB#3.

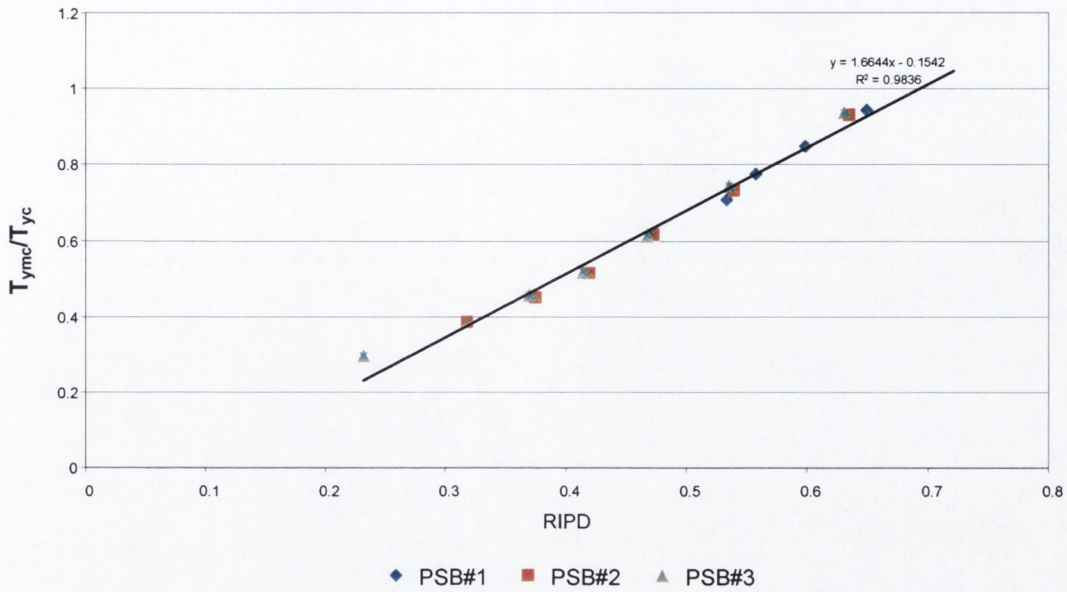


Figure 3.34. Normalised Tensile Yield Strength versus RIPD corrected for minimum particle size of 1 μm . (PSB1 \diamond , PSB2 \square , and PSB3 \triangle)

The agreement of the data suggests that indeed there is a critical particle size, and that particles less than 1 μm play no role in toughening. This is considered that this is as much a factor of inter-particle distance and the ability of the stress fields associated with the secondary phase to effect a change in the response in the matrix than a specific limitation of the particles in concentrating stress. It is considered that were the IPD of the order of the particle size that the effect on the behaviour of Polystyrene would be dramatic. In effect this is the case of styrene-co-butadiene block copolymers. In these systems the stress field interactions effect a transmutation in the micro-mechanical deformation of the material transforming it from cavitation to shear. The potential power of these observations are reminded in the results of work by Berlotti and Fulrath on micro porous glass, which showed that pore diameters in the range of 5-10 μm effected an increase in the toughness of glass [73].

By referring to these final points it is hoped to point to facility the RIPD parameter provides a means of modelling problems within both the micro and macro world of materials and provide tools for FE methods to interface modelling both.

3.7 Conclusions on micro-structure and mechanical properties of HIPS

The main purposes of the chapter were to investigate:

1. The strain rate sensitivity of the resins.
2. If the properties of the polyblends were the same as those of previous workers.
3. If particle size and/or particle size distribution influenced the mechanical properties of HIPS.

To this end it is possible to conclude from the results of the tests that

1. On strain rate sensitivity

- Changes to micro-morphology did not result in significant change in strain rate sensitivity.
- There was no detectable change in the tensile modulus with increasing strain rate
- The slight increase in the tensile yield strength with strain rate was in line with expectations

2. On the quality of results and materials

- The tensile and impact behaviour of the polyblends concurred with the previous findings
- The agreement of results with previous work validated the methods used to prepare materials.
- Tensile modulus and tensile yield strength fell with increasing addition of secondary phase.
- The impact strength of the materials increased with increasing ERPV.
- The impact strength fell with increasing notch depth.
- The Ishai Cohen effective area model provided good agreement with the tensile properties.

3. On particle size effects

The particle size and/or distribution in size were found to exert a primary influence on behaviour

- Particle size and population effects can be rationalised in terms of craze nucleating efficiency.
- RIPD provides a coherent means of appreciating the influence of RPS and ERPV.
- Influence of ERPV and RPS are modelled more accurately using RIPD.
- The concept of craze efficiency factor rationalises particle size effects in HIPS.
- Particles <1micron in size appear to play no role in crazing – and hence toughening.
- Straining rate sensitivity was greater between each series of blends than between ERPV.
- Correlation of T_m data with ERPV were higher for each series than for the combined data set.
- Differences between series in T_y data undermined modelling behaviour on ERPV.
- The variation in impact strength between series was greater than with series.
- The increase in toughness associated with increased ERPV was distinct in each series.
- The impact data suggests that an optimum particle size, or range of sizes and ERPV, does exist for polystyrenes.

3.8 Appendix 3.1. Results of Impact Tests

0.25mm			0.25mm			0.25mm		
	mean	Std. Dev.		mean	Std. Dev.		mean	Std. Dev.
PSB1-5	0.299	0.021817	PSB2-5	0.288	0.0148772	PSB3-5	0.419	0.0093095
PSB1-10	0.298	0.065385	PSB2-10	0.4376	0.0104307	PSB3-10	0.3915	0.005972
PSB1-15	0.4616	0.00726	PSB2-15	0.47	0.008	PSB3-15	0.4612	0.0060992
PSB1-20	0.4984	0.046203	PSB2-20	0.6012	0.0083555	PSB3-20	0.4744	0.0071274
PSB-23.5	0.56	0.011832	PSB2-25	0.6268	0.0076942	PSB3-25	0.5664	0.0175157
			PSB2	0.8176	0.0112605	PSB3	0.7	0.0110954
0.75mm			0.75mm			0.75mm		
	mean	Std. Dev.		mean	Std. Dev.		mean	Std. Dev.
PSB1-5	0.2364	0.0472101	PSB2-5	0.2784	0.0043358	PSB3-5	0.2828	0.0022803
PSB1-10	0.2044	0.0672814	PSB2-10	0.394	0.007814	PSB3-10	0.2924	0.003847
PSB1-15	0.3084	0.0093166	PSB2-15	0.4215	0.006608	PSB3-15	0.4052	0.0036331
PSB1-20	0.434	0.0037416	PSB2-20	0.5208	0.0057619	PSB3-20	0.4192	0.0091214
PSB-23.5	0.4635	0.0118181	PSB2-25	0.5688	0.0112783	PSB3-25	0.4836	0.0065421
			PSB2	0.7092	0.006099	PSB3	0.6372	0.0054037
1.75mm			1.75mm			1.75mm		
	mean	Std. Dev.		mean	Std. Dev.		mean	Std. Dev.
PSB1-5	0.1485	0.0064631	PSB2-5	0.2505	0.0179907	PSB3-5	0.2396	0.0079246
PSB1-10	0.1592	0.005932	PSB2-10	0.282	0.0046904	PSB3-10	0.258	0.0028284
PSB1-15	0.2728	0.0041473	PSB2-15	0.3228	0.0100598	PSB3-15	0.2988	0.0113666
PSB1-20	0.283	0.002	PSB2-20	0.412	0.0014142	PSB3-20	0.327333	0.0080829
PSB-23.5	0.3852	0.0065726	PSB2-25	0.5036	0.0026076	PSB3-25	0.387	0.0088694
			PSB2	0.6272	0.0076941	PSB3	0.5524	0.003847
2.75mm			2.75mm			2.75mm		
	mean	Std. Dev.		mean	Std. Dev.		mean	Std. Dev.
PSB1-5			PSB2-5	0.2176	0.0032863	PSB3-5	0.1492	0.0010954
PSB1-10	0.1484	0.002607	PSB2-10	0.25	0.0014142	PSB3-10	0.2268	0.0075631
PSB1-15	0.25	0.0024494	PSB2-15	0.2748	0.0003315	PSB3-15	0.2556	0.0016733
PSB1-20	0.2645	0.006608	PSB2-20	0.3764	0.0119499	PSB3-20	0.304	0.008124
PSB-23.5	0.3292	0.0064187	PSB2-25	0.4736	0.0076681	PSB3-25	0.3392	0.0114543
			PSB2	0.5652	0.0054037	PSB3	0.494	0.0024495
3.75mm			3.75mm			3.75mm		
	mean	Std. Dev.		mean	Std. Dev.		mean	Std. Dev.
PSB1-5	0.1348	0.0041472	PSB2-5	0.1524	0.0245519	PSB3-5	0.144	0.002
PSB1-10	0.1336	0.0076681	PSB2-10	0.2248	0.0036332	PSB3-10	0.2016	0.0094234
PSB1-15	0.235	0.0011547	PSB2-15	0.252	0.005164	PSB3-15	0.2408	0.0033466
PSB1-20	0.2452	0.0086718	PSB2-20	0.3542	0.0038471	PSB3-20	0.2736	0.0026077
PSB-23.5	0.298	0.0076157	PSB2-25	0.4308	0.0026833	PSB3-25	0.3352	0.0217532
			PSB2	0.512	0.0132665	PSB3	0.4496	0.0008944
5.75mm			5.75mm			5.75mm		
	mean	Std. Dev.		mean	Std. Dev.		mean	Std. Dev.
PSB1-5	0.121	0.0011547	PSB2-5	0.15	0.0023094	PSB3-5	0.124	0.0023094
PSB1-10	0.12	0.0081649	PSB2-10	0.1788	0.0086179	PSB3-10	0.154	0.0024495
PSB1-15	0.1945	0.007188	PSB2-15	0.2156	0.0105262	PSB3-15	0.1968	0.0026833
PSB1-20	0.2212	0.002683	PSB2-20	0.3028	0.0030332	PSB3-20	0.2276	0.0035777
PSB-23.5	0.2608	0.046208	PSB2-25	0.3572	0.0036332	PSB3-25	0.2853333	0.0098658
			PSB2	0.4284	0.0157098	PSB3	0.3728	0.0054037

Table 3. 2. Charpy Impact Test Results (n=10)

3.9 Appendix 3.2. Results of Tensile Tests

2mm/min						
ERPv	Tm	Std. Dev.	Ty	Std. Dev.	Tr	Std. Dev.
0	3713.60	132.67	38.20	3.30	38.20	3.30
5	3338.50	136.61	38.14	2.37	38.14	2.37
10	2852.60	128.14	38.48	0.88	38.48	0.82
15	2468.75	20.73	34.66	0.25	31.20	0.53
20	2180.60	9.38	31.60	0.31	27.54	0.79
23.5	1978.60	21.12	28.82	0.15	26.66	0.62
5	3213.60	40.91	38.06	0.17	37.38	0.17
10	2911.20	119.28	29.90	0.29	28.92	0.25
15	2526.00	48.38	25.05	0.87	25.63	0.18
20	2224.30	26.75	21.00	0.17	22.06	0.12
25	1932.20	36.53	18.38	0.10	19.54	0.52
32.5	1592.00	0.00	15.66	0.05	17.10	0.09
5	3292.60	107.74	38.40	0.16	2.20	0.06
10	2922.00	88.17	30.38	0.15	31.78	0.32
15	2616.00	57.12	25.02	0.19	28.44	0.67
20	2358.20	31.40	21.14	0.05	24.66	0.10
25	2107.00	18.08	18.56	0.10	22.18	0.15
45.4	1232.20	32.21	12.08	0.07	16.20	0.09
20mm/min						
ERPv	Tm	Std. Dev.	Ty	Std. Dev.	Tr	Std. Dev.
0	3488.67	45.73	43.46	1.51	43.17	1.55
5	3086.80	48.08	44.64	0.25	44.56	0.22
10	2861.00	60.72	42.60	0.24	40.58	0.41
15	2506.00	53.49	37.90	0.33	35.20	1.77
20	2222.00	30.00	35.05	0.27	30.40	0.31
23.5	2046.00	28.60	31.88	0.10	28.62	0.74
5	2904.25	34.66	45.08	0.26	44.50	0.52
10	2611.20	55.85	38.46	0.22	35.82	0.58
15	2321.00	42.84	34.08	0.15	30.76	0.34
20	2011.20	14.05	30.02	0.19	27.90	0.29
25	1778.80	19.09	26.48	0.07	25.30	0.23
32.5	1476.40	15.49	22.16	0.10	22.82	0.34
5	3167.80	109.01	41.66	0.29	41.46	0.36
10	2931.00	70.57	36.10	0.25	35.25	0.29
15	2628.00	76.28	30.40	0.29	30.18	0.44
20	2355.20	66.44	26.14	0.26	27.82	0.12
25	2166.60	33.52	23.22	0.37	25.62	0.38
45.4	1261.00	16.09	13.74	0.19	17.90	0.22
200mm/min						
ERPv	Tm	Std. Dev.	Ty	Std. Dev.	Tr	Std. Dev.
0	3626.60	72.34	46.00	0.77	45.70	1.99
5	2836.67	72.45	45.84	0.15	45.52	0.38
10	2655.60	412.14	42.94	0.25	41.82	0.47
15	2331.00	63.67	39.75	0.32	36.98	0.51
20	2101.60	30.67	37.70	0.00	33.56	0.19
23.5	1864.00	45.04	33.76	0.71	31.06	0.96
5	3287.50	227.19	45.32	0.13	44.34	0.20
10	2372.00	17.25	37.23	0.16	35.63	1.10
15	2321.00	42.84	32.10	0.30	28.84	0.32
20	2032.00	34.77	29.95	0.15	27.70	0.16
25	1747.40	27.45	26.34	0.17	25.30	0.37
32.5	1560.00	40.40	22.36	0.05	22.46	0.69
5	3889.33	342.49	43.77	0.33	43.57	0.33
10	3076.00	75.49	49.06	0.37	38.64	0.15
15	2447.75	138.12	35.01	0.87	33.76	0.85
20	2251.80	82.63	31.52	0.32	30.64	0.32
25	2083.60	74.67	28.44	0.46	28.26	0.88
45.4	1382.00	24.76	17.38	0.32	21.60	0.38

2mm/min	
PSB1-5	$y = -2.0704x + 3240.5$ [R2 = 0.8162]
PSB2-5	$y = 1.0851x + 3054.8$ [R2 = 0.3414]
PSB3-5	$y = 3.4171x + 3197$ [R2 = 0.9413]
20mm/min	
PSB1-15	$y = -0.8078x + 2495$ [R2 = 0.9206]
PSB2-25	$y = -0.6156x + 2434.9$ [R2 = 0.3243]
PSB3-25	$y = -0.9112x + 2631.3$ [R2 = 0.98]
200mm/min	
PSB1-23.5	$y = -0.7541x + 2018.7$ [R2 = 0.8051]
PSB2-25	$y = -0.6257x + 1865.8$ [R2 = 0.4799]
PSB3-25	$y = -0.2572x + 2138.1$ [R2 = 0.433]

Table 3.4.
Linear Regression Curves
for Tensile Modulus
(MPa vs. Strain Rate
(mm/min))

Table 3.3. Tensile Test Results, (n = 10).

3.10 Appendix 3.3. Empirically modelling of the tensile properties of high impact polystyrene in terms of its secondary phase morphology.

Key Engineering Materials Vols. 99-100 (1995) pp. 79-84
 © 1995 Trans Tech Publications, Switzerland

Empirical modelling of the tensile properties of high impact polystyrene in terms of its secondary phase morphology

F. Dolan¹, D. Taylor¹ and P.A. Blackie²

¹ Department of Mechanical and Manufacturing Engineering, Trinity College Dublin, Dublin 2, Ireland

² Department of Plastics Engineering, Regional Technical College Athlone, County Westmeath, Ireland

Keywords: Polymer composite high impact polystyrene, rubber particle size & phase volume tensile props

ABSTRACT.

The effects of Rubber Phase Volume (RPV) and Particle Size (RPS) on the tensile properties of High Impact Polystyrene (HIPS) have been studied. Three series of materials possessing similar matrix M.w. and particle sizes less than (0.68 μm), equal to (1.99 μm) and greater than (8.54 μm) that associated with optimum impact and tensile toughening were considered. Polyblends possessing a range of rubber phase volumes (0-20%) were prepared by melt blending the parent resins with a general purpose polystyrene resin of M.w. similar to that of the matrix in the HIPS.

An empirical method of modelling the tensile behaviour of HIPS, based upon a cubic lattice interparticle distance (IPD) is presented based on the findings of these tests. The IPD value used in the method being calculated as a function of the volume average rubber particle size and the effective rubber phase volume offers a means of modelling tensile behaviour in terms of these two dominant parameters and comparing their relative influence on tensile behaviour.

INTRODUCTION.

Of the many features of the rubber phase morphology that have been identified as being of importance in determining the mechanical response of HIPS the rubber particle size and the rubber phase volume are often seen as being dominant [1]. Their influence has been considered in detail by a number of researchers [2,3,4,5,6]. In general it has been found that the properties of tensile yield and modulus can be reasonably described within the bounds of continuum mechanics, in terms of the HIPS rubber phase volume.

Since the mid 1980's an increasingly popular approach to characterising the behaviour of HIPS has been in terms of an interparticle distance (IPD). Wu in studying particle size effects in rubber toughened nylon, first suggested the existence of a critical interparticle spacing for optimum toughness [7]. Hobbs made use of an interaction distance in his 'craze pinning' numerical model of craze termination in HIPS [8]. Wu proposed that the critical IPD was purely a property of the matrix and independent of the rubber particle size and rubber phase volume [9]. The notion of there being optimum and critical particle sizes continues to thrive and much experimental work would seem to confirm their existence. These 'critical' and 'optimum' sizes are often associated with thresholds in mechanical performance or changes in mechanisms of deformation. Their effects are seen as being independent of phase volume effects. For the case of HIPS the work of Donald & Kramer which showed that crazes were rarely nucleated from particles of < 1 μm in diameter is commonly quoted in the literature as evidence of the existence of a critical particle size [10]. Donald and Kramer rationalised the critical particle size effect to be the result of a drop in the stress concentration in the region about a particle (at a distance less than 3 fibril spacings from the particle surface) below a critical level required to nucleate a craze.

Critical particle sizes have been used by other authors as a basis for modelling material behaviour. Cigna et al [11] found a linear relationship between the normalised impact strength, $\Delta\text{IS}/N$, [where $\Delta\text{IS}/N$ the change in Impact Strength (IS) associated with change in the number of particles (N)] and the difference between the average particle size and a critical particle size, in bilogarithmic plots of the two. The approach adopted by Cigna et al is not far removed from modelling behaviour in terms of the IPD since, for a cubic lattice arrangement, $\text{IPD} \propto \sqrt[3]{1/N \cdot \text{RPS}}$.

In addition to HIPS, Cigna and co-workers also considered the behaviour of SAN matrix materials which, in addition to crazing, may also undergo plastic deformation under tension by shear. Their work suggested that in these materials there existed a threshold particle size associated with a change in the dominant mechanism of deformation from localised shear yielding to crazing. The belief that such a change over in the mechanism of plastic deformation can be effected by changing the particle size would concur with the work of Wu on ductile matrix rubber toughened nylons. Thus the IPD is a parameter which may allow a means of modelling material behaviour across the broad range of rubber toughened materials irrespective of their mechanism of [matrix] plastic deformation, be it shear or craze based once particle size effects are taken into consideration. Most recently Cook, Rudin and Plumbtree [12] made use of an IPD in modelling the behaviour of HIPS, finding the impact strength to be proportional to $1/IPD$.

It may be concluded, from the interest shown by a large number of workers and its successes to date, that the IPD does provide for a useful means of characterising the mechanical behaviour of rubber toughened materials on an empirical basis, as well as offering a basis for a mechanistic approach.

EXPERIMENTAL MATERIALS AND METHODS.

In order to investigate the influence of the RPV and RPS on tensile behaviour it is first necessary to isolate them as material variables. Rubber Phase volume and particle size were isolated as morphological variants by melt blending three HIPS materials of differing volume average particle size (0.64, 1.99 & 8.54 microns) but similar rubber particle structure (multiple inclusion or salami type) and matrix molecular weight with a general purpose polystyrene of similar M.w. Thus three series of polyblends possessing 5, 10 and 20% RPV were prepared from the parent materials Mat1, Mat2 and Mat3. These materials were supplied by Bert Nijhof of Dow Benelux N.V. After preferential staining of the rubber phase using OsO_4 , characterisation of the rubber phase in each of the materials was conducted by transmission electron microscopy (TEM) on a Philips 400T EM and subsequent image analysis (IA) using Quantimet's 970 IA system. The effective rubber phase volume [4] of the materials and the volume average particle diameter were determined ASTM 638 standard tensile specimens were prepared by injection moulding on a Krause Maffei 60Tonne MC3.

Tensile tests were conducted on an Instron 6022 tensile testing machine fitted with a 10kN load cell calibrated for 1000N full scale, under a constant straining rate of 20mm/min over a specimen gauge length of 100mm. At least five samples were tested for each material. Results were obtained from a flat bed trace recording of stress versus. strain in each test. The values recorded for tensile modulus, tensile yield and ultimate tensile strength were recorded and are presented in Table 1.

Table 1. IPD values and Tensile Results.

Material	IPD (μm)	Tensile Modulus (MPa)	Tensile Yield Strength (MPa)	Ultimate Tensile Strength (MPa)
GPPS	NA	2062	51.383*	51.383*
5-Mat.1	1.165	1918	48.257	49.940
10-Mat.1	0.782	1796	43.913	46.703
20-Mat.1	0.482	1400	34.709	39.459
Mat.1	0.422	1280	32.842	36.311
5-Mat.2	3.411	1921	46.072	43.226
10-Mat.2	2.297	1706	38.958	35.631
20-Mat.2	1.412	1432	29.815	28.892
Mat.2	0.904	1110	21.157	23.524
5-Mat.3	14.641	1914	47.365	45.881
10-Mat.3	9.858	1743	42.024	40.220
20-Mat.3	6.063	1441	31.559	33.049
Mat.3	2.563	844	16.967	24.738

Where in x-Mat_y; x:-the rubber phase volume(%) y:- the material number.

DISCUSSION OF RESULTS.

When considering the results of these tests in terms of the variation in the rubber phase it is necessary to make a number of assumptions. Firstly that crazing is the only process by which plastic deformation is undergone [1]. That the particles are of a similar type, i.e., the Multiple Inclusion (MI) type used in this work[3]. That the Mw of the GPPS is not responsible for any observed changes in material behaviour. These assumptions are made so that from the outset it may be assumed that differences in the rubber phase morphology are solely responsible for the changes in the material behaviour.

In Figure 1 the Tensile Modulus is plotted against the rubber phase volume. Continuum mechanics would predict that no difference in behaviour should arise as a consequence of changes in the rubber particle size. The linear relationship offered in Figure 1.A. is in line with these expectations. To date there has been a general acceptance of this linear relationship between the RPV and the tensile modulus [4, 11]. However, it was noted that the correlation coefficients of the linear regression fits to each individual series in Figure 1.B were higher than that in Figure 1.A. This suggests that the magnitude of the tensile modulus is somehow dependent upon the rubber particle size.

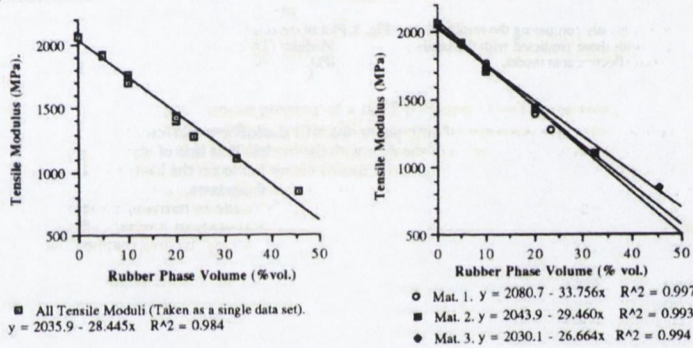


Figure 1. Graphs illustrating the variation in the Tensile modulus with Rubber Phase Volume. A. the case where regression curve is fitted to results for all of the materials. B. The regression fits for each material. (R^2 the correlation coefficient).

The Ishai-Cohen [13] effective area model was used with some success by Bucknall et al [5] to describe the changes in the yield strength of HIPS to changes in the rubber phase volume. It predicts that the tensile yield strength (σ_{TY}) of a material possessing a RPV(θ) of inclusions or particles, i.e., $\sigma_{TY}(\theta)$, is given by the expression,

$$\sigma_{TY}(\theta) = \sigma_{TY}(0) (1 - 1.21 (\theta)^{2/3})$$

Equation 1.

where $\sigma_{TY}(0)$ the yield strength of the matrix material. It is based on a simplified model for stress concentrations produced by a spherical inclusion or particle in a continuous matrix, the average stress concentration factor, γ , given by,

$$\gamma = (1 - 1.21(\theta)^{2/3})^{-1}$$

Equation 2.

In Figure 2 values of σ_{TY} for Mat.1., Mat. 2. and Mat. 3. Polyblends are presented within a plot of Ishai-Cohen predicted values of σ_{TY} versus RPV. They are offset from values predicted by the Ishai-Cohen relationship yet perhaps within bounds of error. The apparent lack of compliance with the relationship could be perceived as scatter in the results arising from experimental error.

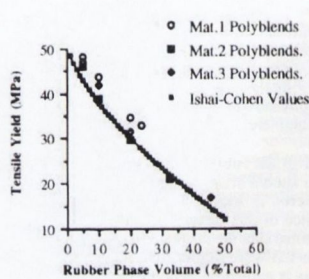


Fig. 2. Plot graphically comparing the results of tests with those predicted with the Ishai-Cohen effective area model.

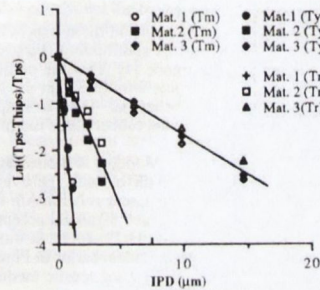


Fig. 3. Plot of the relative fall in Tensile properties Modulus (Tm), Yield (Ty) and failure (Tr) versus IPD.

However for the purposes of this paper we will discount experimental error as being responsible for the lack of correlation of the data with the model. This line of argument is pursued, not to dispute the integrity of the continuum mechanics theory but to set the basis for what follows, which with further work it is hoped will be incorporated within those laws.

It is our belief that a more likely explanation might be made in terms of a rubber particle size effect. Although the theoretical values of stress concentrations about a spherical particle are seen to be independent of its size, size does play a role in determining the area mapped out by the stress field about the particle.

In the case of conventional HIPS materials where high volume loadings of particles are present the stress fields of individual particles over-lap and contribute to the formation of denser crazing at lower stresses in a greater volume of the material. As the typical stress concentration about a particle falls from ~ 1.92 to 1.80 over 0.02 units of particle radius [1] it can be seen that the distance over which the stress concentration remains effective for crazing reduces with particle size. Thus, at a constant volume fraction of rubber phase, reducing the particle size reduces the crazing efficiency of the rubber phase while increasing particle size increases the sensitivity and efficiency of the material to crazing [11].

There is therefore an experimental and theoretical foundation for modelling the tensile behaviour in terms of particle size. Thus the IPD should offer a convenient means of evaluating and describing the influence of both rubber phase volume and particle size.

In the following model the particle size, obtained from TEM image analysis is used in determining the cubic lattice average IPD (CLIPD). It is a weighted average of the particle size distribution. However no consideration of variation in the dispersion or size of distribution is considered directly in the IPD. Thus it is necessary to further assume that the range in distribution is the same or a function of the average size in each of the materials.

The volume occupied by a particle is modelled as a cube. Thus the volume occupied by a particle with a RPS of A, is A^3 . The number of these 'cubic' particles accommodated within a fraction of unit volume equivalent to the rubber phase volume is determined and then divided into unit volume to determine the volume available to accommodate each particle, C^3 . Subtracting A from C gives the Cubic Lattice IPD.

Calculation of Inter-Particle Distance may be easily made using the expression;

$$IPD = 3\sqrt[3]{N} - A \tag{Equation 3.}$$

where the units of A and IPD are expressed in metres and $N = RPV/RPS^3$.

From the assumptions set out at the start of this discussion it is also assumed that the magnitude of the tensile properties in the limit of $IPD \rightarrow \infty$ approach those of unmodified PS. Thus

an exponential relationship between the relative change in tensile property with increasing IPD would seem likely. In Figure 3 all of the tensile data is plotted on this basis.

On initial inspection a single regression line might seem to satisfy the various tensile properties for each series of materials possessing different particle sizes. However such speculation is an over simplification of the problem. The influence of the rubber phase morphology would be anticipated to extend to failure, either by stabilising the growth of existing crazes or nucleating new crazes. However it would not be expected that it should exert the same magnitude of influence over the entire loading history. Also it would not seem plausible to expect the influence of the different particle sizes to effect the same relative influence in stabilising craze growth or nucleating more crazes post nucleation. For example, it has been experimentally shown that the crazes nucleated from large particles are more numerous and stable than those nucleated from small particles[8,10].

Better fits for each data set were obtained by treating each tensile property individually. The curves for each of the data sets were found to be concurrent intersecting at 0 which corresponds with the tensile property of the matrix polystyrene resin.

The form of the plots, i.e., the linear relationship between $\ln((T_{ps}-T_{hips})/T_{ps})$ and IPD and the large influence of the rubber particle size suggest that the changes in tensile properties can be described by an expression of the form,

$$T_{hips} = T_{ps} (1 - e^{-\frac{\alpha_x}{IPD}}) \tag{Equation 4}$$

where T_{hips} is the tensile property of a HIPS polyblend and T_{ps} the tensile yield strength of the matrix polystyrene, with α_x a material constant which varies with conditions of testing mechanical property and is also dependent on morphological variants. Because of the small size of the data set available from current work the precise description of α_x or the power to which the exponential is raised is not readily available. Current work on the model is attempting to develop a more succinct expression and express it in terms of engineering variables.

In the present hypothesis α_x is construed as an 'overlap' function dependent upon the interparticle distance required for craze nucleation in the matrix considered, as such it may also be considered as a particle efficiency (in craze nucleation) function.

The plots in Figure 4 compare the values measured in tests with those predicted from the model. The predictions of the Ishai-Cohen effective area model, the Cubic Lattice IPD model and the measured values of Tensile Yield are made in Figure 5. The CLIPD model by considering the effect of particle size appears to offer a more accurate prediction of tensile yield properties.

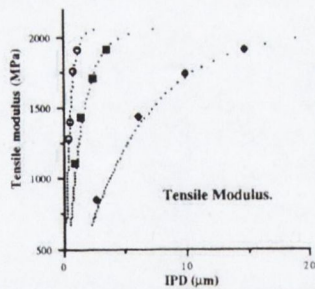


Fig. 4.a. Plot comparing values predicted by the CLIPD for Tensile Modulus with those obtained in tests.

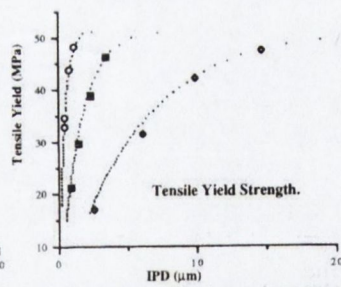


Fig. 4.b. Plot comparing values predicted by the CLIPD for Tensile Yield with those obtained in tests.

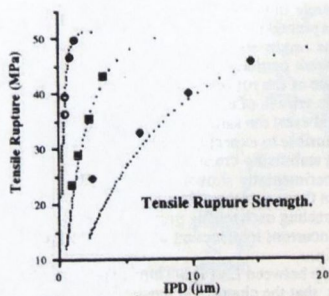


Fig. 4.c.. Plot comparing values predicted by the CLIPD for Tensile rupture with those obtained in tests.

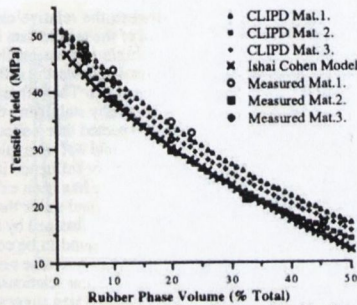


Fig. 5. Plots comparing values predicted by the Ishai-Cohen effective area model and the CLIPD model with values obtained in tests.

Concluding Remarks.

It may be concluded that the influence of the secondary phase morphological variants of RPS and RPV on tensile behaviour are interdependent. Their influence on tensile behaviour can be empirically modelled using the IPD. The basis for the correlation is purely phenomenological, the theoretical basis is only loosely understood. From a physical viewpoint the premise upon which it is based, is logical, i.e., that there should be a direct relationship between the magnitude of the distance separating particles and their proficiency in nucleating crazes and controlling craze growth. Further investigation is necessary to develop the model and express it in more satisfactory terms.

Acknowledgements.

The Authors would like to thank Dow Benelux N.V. for its financial and material assistance in this project. A special thanks is extended to John Royston, Martin Guest, Rony Van Daele, Ad de Kok and Bert Nijhof for their advice, assistance and encouragement

References

- [1] Bucknall, C.B. Toughened Plastics, Applied Science Publishers, 1977.
- [2] Argon, A.S., Sources of Toughness in Polymers. X. Fracture in Non-Metallic Materials, Vol. 4., Proc. 7th Int. Conf. Fract., Ed. K. Salama, Houston, Texas, USA, 20-24 March, 1989.
- [3] Argon, A.S., Cohen, R.E., Crazing and Toughness of Block Copolymer Blends., Crazing in Polymers, Vol. 2., Advances in Polymer Science, 91/92, ed. Kausch, H.H., Springer Verlag, 1990.
- [4] Bucknall, C.B., Cote, F.F.P., Partridge, I.K., J. Mat. Sci., 21, 1986, 301.
- [5] Bucknall, C.B., Davis, P., Partridge, I.K., J. Mat. Sci., 21, 1986, 307.
- [6] Bucknall, C.B., Partridge, I.K., Toughening of Plastics II, 2-4 July, 1985, Paper 28.
- [7] Wu, S., Polymer, 26, Nov. 1985, 1855.
- [8] Hobbs, S.Y., Polym. Eng. Sci., 26, 1986, 74.
- [9] Wu, S., J. App. Polym. Sci., 35, 1988, 549.
- [10] Donald, A.M., Kramer, E.J., J. Mat. Sci., 17, 1982, 235.
- [11] Cigna, G., Lomellini, P., Merlotti, M., J. App., Sci., 37, 1989, 1527.
- [12] Cook, D.G., Rudin, A., Plumbtree, A., J. Appl. Polym. Sci., 48, 1993, 75.
- [13] Ishai, O., Cohen, L.J., J. Compos. Mater., 2, 1968, 302.

3.11 References

- 1 BUCKNALL, C. B., *Toughened Plastics*, Applied Science Publishers, London, 1977.
- 2 BUCKNALL, C. B., *Rubber Chemistry and Technology*, 60, 35, 1987.
- 3 BOWDEN, P.B., RAHA, S., *Philos. Mag. Ser. 8.*, 22, 436, 1971.
- 4 SULTAN, J.N., MCGARRY, F.J. *Polym. Eng. Sci.*, 14, 4, 282, 1974.
- 5 HERTZBERG, R.W., *Deformation and Fracture Mechanics of Materials*, Wiley, 1989.
- 6 STERNSTEIN, S.S., ONGCHIN, L., *ACS, Polym. Preprints*, 10, 2, 117, 1969.
- 7 SPIELBERG, S. H., ARGON, A.S., COHEN, R.E., *J. App. Polym. Sci.*, 48, 85, 1993.
- 8 DONALD, A. M., *J. Appl. Mat. Sci.*, 20, 2630, 1985.
- 9 KAUSCH, H.H., *Ad. Polym. Sci.*, 91/92, (preface), Springer Verlag, 1990.
- 10 KRAMER, E. J., *Polym. Eng. & Sci.*, 24, 10, 761, 1984.
- 11 DONALD, A. M., KRAMER, E.J., *J. Mat. Sci.* 17, 2351, 1982.
- 12 FARRAR, N.R., KRAMER, E. J., *Polymer*, 22, 691, 1981.
- 13 PLUMMER, C. J. G., DONALD, A.M., *J. Mat. Sci.*, 24, 1399, 1989.
- 14 WARREN, W. E., *J. Polym. Eng. & Sci.*, 24, 10, 814, 1984.
- 15 LAUTAUSSE, B.D., KRAMER, E.J., *Phil. Mag.*, A-39, 469, 1979.
- 16 KRAMER, E.J., *Ad. Polym. Sci.*, 52/53, Springer Verlag, 1983.
- 17 VERHEULPEN-HEYMANS, N., *Polym. Eng. Sci.*, 24, 10, 809, 1984.
- 18 HENKEE, C. S., KRAMER, E.J., *J. Mater. Sci.*, 21, 1398, 1986.
- 19 JUSKA, T., HARRISON, I.R., *Polym. Eng. & Sci.*, 22, 12, 766, 1982.
- 20 OXBOROUGH, R.J., BOWDEN, P.B., *Philos. Mag. Ser. 8*, 28, 547, 1973.
- 21 BUCKNALL, C.B., SMITH, R.R., *Polymer*, 6, 437, 1965.
- 22 DONALD, A.M., KRAMER, E.J., *J. Mat. Sci.*, 17, 2351, 1982.
- 23 GOODIER, J.N., *Appl. Mech.*, 55, 39, 1933.
- 24 MATSOU, M., TSUEY, T., *J. Polym. Sci.*, A-2, 10, 1085, 1972.
- 25 BROUGHTMAN, L.J., PANIZZA, G., *Int. J. Polym. Mat.*, 1, 95, 1972.
- 26 AGARWAL, B. D., BROUGHTMAN, L.J., *Fibre Sci. Tech.*, 7, 6, 1974
- 27 BUCKNALL, C.B., KARPODINIS, A., et al, *J. Mat. Sci.*, 29, 3377, 1994.
- 28 LEE, B. J., PARKS D. M., AHZI S., *J. Mech. Phys. Solids*, 41, 10, 1651, 1993
- 29 XIAO, Z. M., PAE, K.D., *Polym. Eng. & Sci.*, 33, 18, 1188, 1993.
- 30 FUKAHORI, Y., W. SEKI, W., *J. Mater. Sci*, 28, 4471, 1993.
- 31 RICCO, T., RINK, M., et al, *Proc. Toughening of Plastics 2*, PRI, 2-4 July 1985.
- 32 BUCKNALL, C.B., DAVIS S. P. et al, *J. Mat.Sci.*, 21, 307, 1987.
- 33 MERZ, E.A., CLAVER, G.C., et al, *J. Polym. Sci.*, 22, 325, 1956.
- 34 ROSEN, S.L, *Polym. Eng. & Sci.*, 17, 115, 1967.
- 35 RICCO, T., PAVAN, A., et al, *Polym. Eng. Sci.* 18, 744, 1978.
- 36 ARGON, A.S., *Pure and App. Chem.*, 43, 247, 1975.
- 37 AMOS, J.L., *Polym. Eng. Sci.*, 14, 1, 1970.

- 38 SCHMIDT, A.X., KESKKULA, H.H., Principles of High Polymer Theory and Practise, McGraw Hill, NY, p.48, 1958.
- 39 SAUER, J. A., MARIN, J., J. App. Phys., 21, 1071, 1959.
- 40 KAMBOUR, R.P., Nature, 195, 1299, 1962.
- 41 YEE, A.F., PEARSON, R.A., J. Mat. Sci. 21, 2462, 1986.
- 42 PEARSON, R.A., YEE, A.F., J. Mat. Sci. 24, 2571, 1989.
- 43 HWANG, J.F., MANSON, J.A., et al, Polym. Eng. Sci., 29, 1466, 1989.
- 44 LIN, C.S., AYRE, D.S., BUCKNALL, C.B., J. Mat. Sci. (Lett.), 17, 669, 1998.
- 45 MAESTRINI, C., CASTELLINI, L., et al, Polymer, 33,7, 1556, 1992.
- 46 BRAGAW, P.B., Adv. Chem. Ser., 99, 86, 1971.
- 47 YENALYEV, V.D., NOSKOVA, N.A., et al, Donstk University, 1988.
- 48 ARGON, A.S., COHEN, R.E., et al, Toughening of Plastics II, PRI, 2 - 4 JULY, 1985.
- 49 GEBIZLIOGLU, O.S., ARGON, A.S., Polymer, 26, 519, 1985.
- 50 DURST, R.R., GRIFFITH, R.F., et al, Paper 19, Proc. Toughness and Brittleness of Plastics, SPE, 239, 1973.
- 51 BUCKNALL, C.B., COTE, F.F.P., et al, J. Mat. Sci., 21, 301, 1986.
- 52 TURLEY, S. G., KESKKULA, H., Polymer, Vol. 21, 466, 1980
- 53 SILBERBERG, J., HAN, C.D., J. App. Polym. Sci., 22, 599, 1978.
- 54 HOBBS, S. Y., DEKKERS, M.E.J., WATKINS, V.H., Polymer, 29, 1598, 1988.
- 55 WROTECKI, C., HEIM, P., GAILLARD, P., Polym Eng. Sci., 31,4, 213, 1991.
- 56 OKAMOTO, Y., MIYAGI, M., TAKAHASHI, K., et al, Macromolecules, 24, 5639, 1991.
- 57 COOK, RUDIN, PLUMBTREE, J. Mat. Sci. 28,1993.
- 58 CIGNA, G., J. Appl. Polym. Sci, 44, 505, 1992.
- 59 WU, S., Polymer, 26, 1855, 1985.
- 60 MARGOLINA, A., WU, S., Polymer, 29, 2171, 1988.
- 61 KRAMER, E.J., BERGER, L.L. Vol. 2, Adv. Polym. Sci., 91/92, Springer Verlag, 1990.
- 62 GILBERT, D. G., DONALD, A.M., J. Mater Sci., 21, 1819,1986.
- 63 BUCKNALL, C.B., DAVIES, P., PARTRIDGE, I.K., J. Mat. Sci.,21,307,1986.
- 64 ISHAI, ORI, COHEN, L.J., J. Composite Materials, 2, 3, 302. 1968.
- 65 SMALLWOOD, H., J. Appl. Phys., 15, 758, 1944.
- 66 GUTH, E., J. Appl. Phys., 16, 20, 1945.
- 67 NICOLAIS, L., NARKIS, M., Polym. Eng. Sci., 11, 3, 194, 1971.
- 68 TURCSANYI, B., PUKANSKY, B., TUDOS, F., J. Mat. Sci., Letters, 7, 2, 160, 1988.
- 69 DOLAN, F., TAYLOR, D., BLACKIE, P.A., Key engineering materials, 99-100, 79, 1995.
- 70 HORVAY, G., Trans. ASME, Vol. 74, SERIES E, Applied Mechanics Section, 1952.
- 71 O' DONNELL, W. J., Bulletin / Welding Research Council, New York, 1, 1961.
- 72 HULBERT, L E. NIEDENFUHR, F.W., ASME Trans. J. Eng. Ind., 87B, 331, 1965.
- 73 BERTOLOTTI, R.L., FULRATH, R.M., J. of the Amer. Ceramics Soc., Nov., 558, 1967

Chapter 4

THE FRACTURE TOUGHNESS OF HIPS

CHARACTERISING FRACTURE TOUGHNESS IN HIPS.

4.1 Preview

The following chapter considers the relationship between impact strength, intrinsic toughness and the influence of the secondary phase morphology in HIPS. It also examines the suitability of various theoretical and experimental approaches to characterising and analysing fracture in HIPS. Monotonic linear elastic, elasto-plastic and essential work methods as well as a cyclic loading technique are considered in measuring intrinsic toughness. The discussion pivots on the characterisation of HIPS intrinsic toughness and its interpretation at a microstructural level. The purpose is to evaluate the toughness of the experimental resins and the implications of the process of crazing on the characterisation of toughness in HIPS.

4.2 Contents

The Fracture Toughness of HIPS.....	100
4.1 Preview	100
4.2 Contents	100
4.3 Introduction	100
4.3.1 Elements of Linear elastic Fracture Mechanics.	103
4.3.2 Elements of Elasto-Plastic Fracture Mechanics.	111
4.4 Experimental	119
4.4.1 Linear Elastic Fracture Mechanics: Strain Energy Release Rate from Impact Data.	119
4.4.2 Results: strain energy release rate	121
4.4.3 Determination of J integral from Monotonic Tensile Loading	121
4.4.4 Results Monotonic Tensile J integral	126
4.4.5 Elasto -Plastic Fracture Mechanics Essential Work Studies	126
4.4.6 Determination of J' from Fatigue	127
4.4.7 Results of J _c from Fatigue	129
4.5 Discussion of HIPS Fracture Toughness	129
4.5.1 Comment on results for G _c determined from LEFM analysis of Impact test data.	130
4.5.2 Comment on the Results obtained for J from Monotonic Tests.	132
4.5.3 Comment on the Results of the Essential Work tests.	135
4.5.4 Comment on the results of J integral measurement of J' from Fatigue tests	139
4.6 Conclusions	141
4.6.1 Strain Energy Release Rate determined from analysis of impact test data	141
4.6.2 J Integral determined from analysis of Monotonic Tensile Fracture Tests.	141
4.6.3 Essential work analysis	142
4.6.4 J Integral determined from analysis of Fatigue Crack Propagation.	142
4.6.5 General Conclusions on the Characterisation of Fracture Toughness in HIPS.	142
4.7 References	144

4.3 Introduction

The previous chapter considered the influence of changes to the secondary phase micro-structure on the mechanical behaviour of the experimental resins and modelled it in terms of the ERPV and the RIPD. Conventional engineering parameters were used to describe toughness and tensile strength. However the impact strength, used to describe toughness, is not an intrinsic material property. Its value, and its ranking of material toughness varies with the conditions of testing. It does not represent, the inherent, or intrinsic, toughness of a material and so can't be used in designing against fracture [1].

The notion of an intrinsic toughness is that it represents a limiting value of toughness for a material, i.e., where the mechanical energy introduced to a system to fracture a material is dissipated solely in the creation of two new fracture surfaces. Achieving conditions where this is purely the case is not easy. Thus parameters that describe the property are not easily defined, nor determined. Nevertheless to appreciate a material's toughness and to design against its fracture they are necessary.

Engineering design against fracture lies within the remit of fracture mechanics. Theories were developed during the last century to identify intrinsic toughness parameters for design purposes. These were defined within the context of continuum mechanics theory, allowing designers to integrate 'toughness' in design calculations easily [2,3,4,5]. Indeed it is surprising that it was not until the last century that a coherent quantitative theoretical framework to describe the mechanics of fracture was developed. The contribution it has made to society through improved engineering design, especially in regard to safety, has been enormous. It has facilitated advances in architecture and design, allowing the creation of larger, lighter and, most importantly, safer buildings, ships, planes, etc., and the development of advanced engineering materials for ever more challenging applications [9].

Fracture mechanics treatments have found applicability not only in describing monotonic fracture toughness but also in describing fatigue fracture. Consequently, in testing the primary hypothesis that a HIPS resin optimised for impact toughness should provide an optimum resistance to fatigue fracture, they provide a convenient means to investigate; 1) the underlying premise that such HIPS materials do in fact possess a greater intrinsic toughness, and; 2) whether this effects a greater resistance to fatigue crack propagation. Intuitively, it would be expected that the ranking of materials offered in impact studies would be preserved in ranking their intrinsic toughness [1,9]. Though true for many instances it will be seen that it is not necessarily so for all.

Fracture mechanics was founded upon the engineering community's experience with ceramic and metal fractures [2, 6, 21]. Its adaptation and application to plastics materials followed the acceptance of plastic in engineering design. This had not been immediate. When they first appeared plastics were considered as 'cheap' substitute materials and their true physical properties often undermined the use of conventional characterisation methods and design techniques. However as their value became more apparent, during the latter half of the century, interest grew in using them in more demanding engineering applications and with this a requirement for practical techniques to characterise their toughness and design against their fracture emerged. About the same time, the 1960's, interest in fracture mechanics grew [9,10,11,23]. Advances in the field included the conception of new approaches that accommodated the foibles of designing against the fracture of 'real' materials. There were some difficulties in applying the fracture theories developed for metals and ceramics to plastics. Most difficulties stemmed from the difference in their mechanical response [1]. Plastics are visco-elastic, and their non-linear time and temperature dependent behaviour to loading challenges and complicates the use of the conventional methods, especially in regard to dynamic fracture [1]. Though facets of their behaviour undermined many assumptions of the conventional approaches, adjustments to these methods, explored throughout the 1970's and 80's, could be used to accommodate for the differences in response. Many of these modified techniques were considered to be successful. However many of the problems posed by plastics persist [1].

In the case of HIPS, viscoelastic behaviour is not the primary challenge to the conventional fracture mechanics approaches. Instead it is its pseudoplastic behaviour. The discussion in the previous chapter rationalised the influence of the secondary phase on the mechanical behaviour of HIPS in terms of crazing, the micro-mechanical process responsible for the material's pseudoplastic deformation. Diffuse crazing of the brittle polystyrene matrix explained both the increase in impact toughness and the decrease of nominal elastic modulus and yield stress. The 'stress amplifying' effect of the secondary phase was observed in chapter 3 to be characteristic for each particle size (particle size distribution); it was rationalised to elevate local stress levels and initiate crazing which lowered yield strength and increased the energy consumed in the initiation and propagation of a crack. The difference in behaviour arising from the changes in morphology was concluded to be independent of the matrix's intrinsic response, it remained the same, but the cumulative effect of the secondary phase was concluded to be sensitive to the modification of stress fields within the bulk of the matrix.

In so far as the matrix material is understood to be unaffected by incorporating the secondary phase its intrinsic toughness remains the same, i.e., the energy required to instigate and 'grow' individual crazes is the same and so independent of stress field distribution and geometry. However the energy made available for crazing, and so the amount of crazing, is dependent upon both, i.e. the number and size of particles determines the volume in which stress is elevated. This though confuses the perception and measurement of toughness in HIPS. When toughness is measured in bulk, as in the impact test, it is not the matrix's intrinsic resistance to fracture that is measured but the amount of the matrix that has crazed. This masks the appreciation of what is intrinsic to limiting the lower bound energy required for fracture and raises the issue of resolution or scale and the role of geometry in distributing load.

So the extent to which the bulk of material can craze, varies not only with the secondary phase morphology but also the level of constraint imposed on the material by its geometry and the manner and rate of loading. For any given level of constraint it may be characteristic for the resin. When constraint is high the full potential of the gross yielding mechanism cannot be realised and a minimum level of toughness is observed (See Chapter 3). When constraint is lowered the energy required to propagate a crack increases as the volume of material that is exposed to higher levels of stress increases depending upon the efficiency of the secondary phase to craze under the imposed conditions of loading and constraint.

Thus a HIPS optimised for impact strength may, or may not, exhibit a greater level of toughness than another depending upon how its raised potential resistance to fracture can be expressed under the conditions of loading. However, in order to make comparisons between resins it is necessary to make measurements under conditions of equivalent constraint. The easiest means of doing so is to impose the maximum level of constraint, i.e., plane strain. The variable sensitivity of the materials to imposed levels of constraint makes this difficult, as the relative thickness required for achieving maximum constraint will vary for each resin. This challenge can be resolved using fracture mechanics principles. In the following sections the principles of various fracture mechanics approaches are briefly introduced before the results of tests that employ them are considered in regard to the series of HIPS considered in this study.

4.3.1 Elements of Linear elastic Fracture Mechanics.

All contemporary theories of fracture originate from the work of Griffith [2,3]. However it was not until the nineteen forties and fifties, with the failure of wartime shipping and the ascent of aerospace and nuclear industries, that fracture mechanics found extensive application in engineering. Since then the precepts developed by Griffith have been advanced to describe and model fracture phenomenon in numerous materials under a variety of conditions [9].

Griffith proposed that 'for unit crack extension to occur under the influence of an applied stress the decrease in potential energy in the system by virtue of the displacement of the outer boundaries and the change in the stored elastic energy, must equal the increase in surface energy due to crack extension'. Using the stress analysis of Inglis, for an elliptical hole in an infinite elastic plate (Figure 4.1.b)[4],

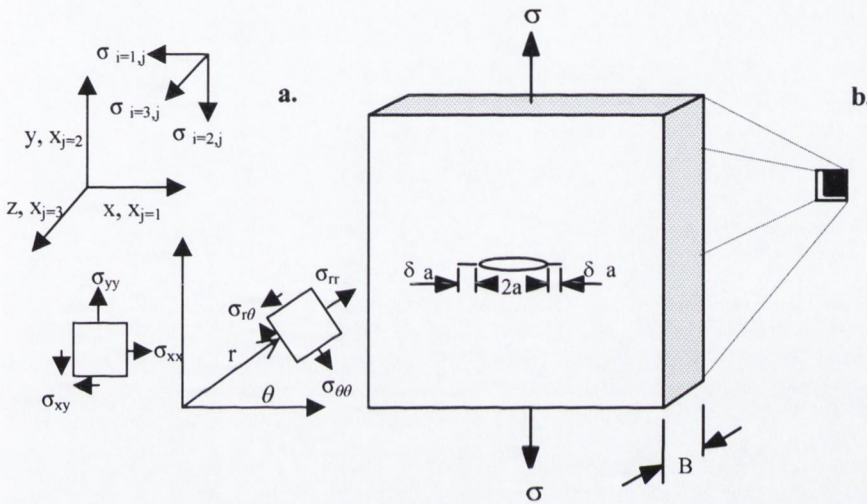


Figure 4.1. a. Cartesian and cylindrical coordinate systems. b. Diagram of an infinite elastic plate containing an elliptical crack of length 2a and thickness B.

Griffith showed that the critical stress for crack initiation (and unstable propagation) is related to the surface energy, γ_s , according to,

$$\sigma = \left(\frac{2E' \gamma_s}{\pi a} \right)^{\frac{1}{2}}$$

Equation 4.1.

where, the modulus $E' = \frac{E}{1 - \nu^2}$ and $E' = E$ for conditions of plane strain and plane stress respectively

and ν is Poisson's ratio. Fracture experiments performed by Griffith on hollow cracked rods and spheres of glass provided somewhat reasonable agreement with an extrapolated value of surface energy based on surface tension results. However Griffith's idealised model for brittle fracture, where the near tip stresses in a sharp notch exceed the cohesive energy of the material, could not be applied to most conventional engineering solids directly. This because the non-linear deformation processes induced near the crack tip allows more energy to be dissipated in propagating the tip than the cohesive strength of the material.

In the late 40's though, Orowan extended Griffith's energy absorbing concept to metals by including a term for plastic energy dissipation, γ_p , such that the fracture initiation stress should be expressed as [5],

$$\sigma = \left(\frac{2E'(\gamma_s + \gamma_p)}{\pi a} \right)^{\frac{1}{2}}$$

Equation 4.2.

The plastic energy term accommodated the balance of energy associated with fracture that exceeded $2\gamma_s$. Typically, the plastic component of the total fracture energy is orders of magnitude greater than the surface energy component. This fact is very pronounced in plastics materials. For example in a typical glassy polymer, such as polystyrene, bond rupture is seen to contribute only about 0.1 J/m^2 to fracture energies that are of the order of $10^2 - 10^3 \text{ J/m}^2$ [1]. Even in the case of semi crystalline polymers the contribution is still not greater than 10% of the fracture energy [1].

Around the same time as Orowan incorporated the contribution from plastic work, Irwin, using Griffith's energy balance approach, reconsidered the case of the cracked plate of unit thickness B , (Figure 4.1.) [6]. He termed the rate of decrease of the potential energy of the system due to crack advance, δa , the strain energy release rate G (in respect to Griffith), i.e.;

$$G = - \frac{\delta(PE)}{\delta a}$$

Equation 4.3.

where PE , the potential energy of the system. The stress for crack initiation and extension (σ_c) is then given by;

$$\sigma_c = \left(\frac{EG_c}{\pi a} \right)^{\frac{1}{2}}$$

Equation 4.4.

The magnitude of G_c , in the case of an ideal solid then is;

$$G_c = 2\gamma_s$$

Equation 4.5.

And, for the case of conventional materials, the contribution from associated plastic deformation;

$$G_c = 2(\gamma_s + \gamma_p)$$

Equation 4.6.

Irwin formulated the critical conditions for the growth of flaws using Westergaard's solution to quantify the near tip fields for a linear elastic crack in terms of the stress intensity factor, K [6,7].

The stress at any point about the crack tip could be expressed in cylindrical co-ordinates which for Mode I deformation, could be expressed as;

$$\sigma_{ij} = \frac{K_I}{(2\pi r)^{1/2}} (\sigma_{ij}[\theta])_I$$

Equation 4.7.

Where σ_{ij} is the ' i^{th} ' component of force per unit area normal to the a plane of the positive direction, j , of the force, see Figure 4.1., yielding, as $r \rightarrow 0$ the Mode I the stress intensity factor K_I ;

$$K_I = \lim_{r \rightarrow 0} \left\{ (2\pi r \sigma_{yy})^{1/2} \Big|_{\theta=0} \right\}$$

Equation 4.8.

Similar expressions can be developed for loading Modes II and III and these may be found in Tada, Paris and Irwin [8]. Irwin's stress intensity factor approach could be related to the energy release rate approach. The critical stress intensity factor K required for crack propagation K_c can then be expressed in terms of the critical strain energy release rate;

$$K_c = (EG_c)^{1/2}$$

Equation 4.9.

Irwin's critical stress intensity factor provides engineering with a convenient and accessible fracture parameter. However in order to apply the treatment to any given geometry, correction must be made for edge effects. These edge effects arise due to edges restricting the loading distribution around a crack and creating greater stress concentrations in comparison to an 'infinite plate'. Correction factors for single edge notched tension, SENT, (Equation 4.10) and 3 pt bending, (Equation 4.11.) are presented below, solutions for other geometry's may be found in other references [e.g., 9].

$$K_I = \sigma \sqrt{a} \left[1.99 - 0.41 \frac{a}{W} + 18.7 \left(\frac{a}{W} \right)^2 - 38.48 \left(\frac{a}{W} \right)^3 + 53.85 \left(\frac{a}{W} \right)^4 \right]$$

Equation 4.10.

$$K_I = \frac{PS}{BW^{3/2}} \left[2.9 \left(\frac{a}{W} \right)^{1/2} - 4.6 \left(\frac{a}{W} \right)^{3/2} + 21.8 \left(\frac{a}{W} \right)^{5/2} - 37.6 \left(\frac{a}{W} \right)^{7/2} + 38.7 \left(\frac{a}{W} \right)^{9/2} \right]$$

Equation 4.11.

In comparing the toughness of real materials it is important to keep these numerical treatments in perspective as the extent to which the idealised state of constraint is achieved in practise is relative. Theoretically the process zone is confined within a characteristic volume, K 's value is determined by an actual volume. In the case of plane strain the difference between theory and practise might be small and edge effects very limited in comparison to the size of the crack and corrections for there is effective. In practise though the success of the correction methods are relative to the actual states of stress achieved.

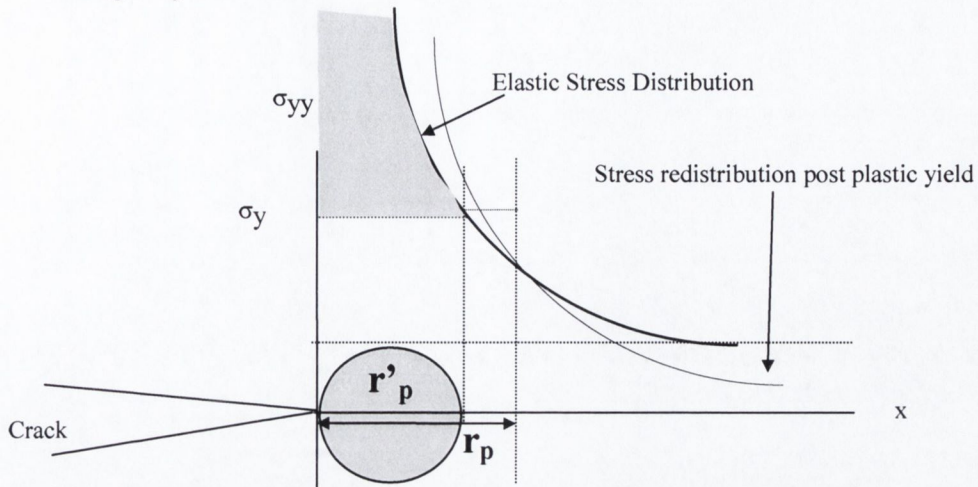
4.3.1.1 The region of K dominance.

Figure 4.2. Illustration of the asymptotic rise in stress (σ) near the tip of a crack (σ_{yy}), and the theoretical plastic zone r'_p with the actual r_p for a material with a specific yield stress (σ_{ys})

The notion of a 'region of K dominance' is part and parcel of what is required in both Orowan and Irwin approaches to fracture. The essential concept is also required in applying or comparing elasto-plastic approaches to fracture such as the J integral (section 4.3.2.). In LEFM approaches it is necessary to allow, or assume, that the continuum solutions (of Inglis and Irwin-Westergaard) describe the state and magnitude of stress in the crack tip region. Paradoxically it is in this region, where the process of fracture occurs, that the Inglis and Irwin solutions do not hold. In the region about the crack tip their treatments, describing stress at the crack tip, predict that the effective levels of stress rise asymptotically to infinity as the crack tip is approached. Obviously this cannot be the case. Instead the intrinsic properties of materials provide an upper bound, prescribing conditions for valid application of the LEFM solutions. Irwins' stress intensity factor then is best considered as a measure of the 'near tip' stress intensity, with its magnitude varying with the radial and angular components of force about the crack tip, i.e., with $\sqrt{2\pi r}$ and (θ) respectively, in the region where K dominates.

From Equations 4.7. and 4.8 then, the local stress at the crack tip is predicted to rise asymptotically as r approaches 0 (see Figures 4.2.) However the onset of plastic deformation, when the local stress approaches the yield stress of the material, prevents stress in the material rising above this value. A 'plastic zone' forms ahead of the crack tip. It is in this region of plastic deformation the elastic solution Equation 4.7, does not hold. However outside this the stress intensity may be extended to describe, or identify with, the propagation of a crack, despite the material in the region local to the crack tip having undergone inelastic deformation, provided its size conforms to the condition of 'small scale yielding'. This requirement is that the crack tip plastic zone, undergoing plastic deformation, is confined well within the region of K dominance. Thus the relationship provides a reasonable approximation to the full solution for stress intensity. In other words the outer radius of this zone is considered to be at a distance at which the approximate singular solution deviates from the fully elastic solution.

4.3.1.2 Plastic Zone Size Approximations.

Where the requirements of small scale yielding are not met contingencies can be introduced to circumvent the problem. A common approach is to introduce an apparent plastic zone size. Irwin, using Equation 4.12, approximated the plastic zone size by determining the crack tip zone within which the Von Mises equivalent stress exceeds that of the materials yield strength [10]. The proposition being that the plastic zone amounts, in effect, to an increased apparent, or effective, crack length, i.e., (see Figure 4.2.above);

$$a_{\text{effective}} = a_0 + r_p.$$

Equation 4.12.

Such that for $\theta=0$ ahead of the crack tip, the plastic zone, r_p , is proportional to K_I^2 and;

$$r_p = \frac{1}{3\pi} \left(\frac{K}{\sigma_y} \right)^2$$

Equation 4.13.

for the case of plane strain. While for plane stress;

$$r_p = \frac{1}{\pi} \left(\frac{K}{\sigma_y} \right)^2$$

Equation 4.14.

Alternative models that have been proposed for plastic zone size approximations. Dugdale’s model is perhaps the most popular of these and has been employed by a number of researchers to characterise fracture behaviour in plastics [1,2,11,12]. In this approach the crack is considered as a sharp slot of length $2(a + r_p)$ in an infinite plate under a remote tensile load (σ^∞), normal to the major axis of the ellipse.

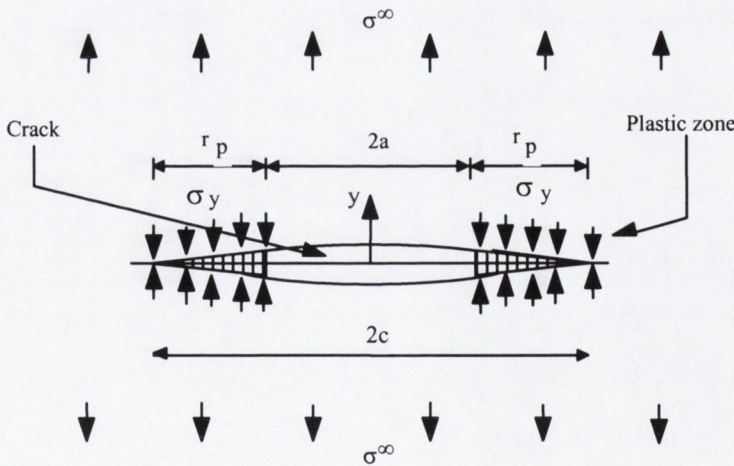


Figure 4.3. Schematic of the Dugdale model for plastic zones at the ends of an elliptical hole in an infinite elastic plate.

The plastic zone is then considered to extend a distance $2r_p$ ahead of the crack tip, while its boundary with the rest of the continuum is assumed to be under uniform internal stress, Figure 4.3. Static equilibrium is achieved by imposing equal and opposite compressive stresses, σ_y . Dugdale applied an elastic solution developed by Muskhelishvili [13] to describe the plastic zone size, that, for the case of 'small scale' yielding, where $\sigma^\infty \ll \sigma_y$ and $r_p \ll a$, i.e.;

$$r_p = \frac{\pi}{8} \left(\frac{K}{\sigma_y} \right)^2$$

Equation 4.15.

Dugdale also used an analytical expression derived by Goodier and Field to describe the opening displacements of these elastic-perfectly plastic boundaries in front and behind the crack tip (δ) [14];

$$\delta = \frac{8a\sigma_y}{\pi E} \ln \sec \left(\frac{\pi\sigma^\infty}{2\sigma_y} \right)$$

Equation 4.16.

which he then reduced in the limit of plane strain (small scale yielding) to;

$$\delta = \frac{K_I^2}{\sigma_y E}$$

Equation 4.17.

These evaluations of the plastic zone size are only theoretical projections and, more often than not, when measurements of actual fracture process zones are made they are found to be either greater or less than predicted. This makes the assumptions upon which the concept is based seem misleading, if not inappropriate. For example measurements by Doll et al contradicted Dugdales' assumptions regarding the distribution of stress in the plastic zone, though some earlier findings appeared to have validated them [e.g.,15], [16]. However from even an intuitive level it is difficult to accept assumptions of the model made in relation to stress concentration, e.g., it is hard to imagine a fracture in which the stress at the tip of a crack is not greater than that along its trailing plane.

Kramer and Hart pointed out these and other theoretical objections to Dugdales model in considering crack advancement and conducted a series of experiments to validate their reservations [17]. They showed there were many instances where craze face tractions along propagating cracks are not constant, but rise sharply, and significantly, as the crack tip is approached along the craze/crack plane. This is important as it shows that as a crack advances there is only partial shielding of stress intensity at its tip. This significant finite level of stress that exists at the crack tip is neglected in the absence of a stress intensity factor in Dugdale's model. The debates surrounding the assumptions and the validity of the rationales used to justify correcting crack size using plastic zone size approximations, in what should be a linear elastic fracture analysis, adds some reservation to the widespread use of LEFM. The approximations can vary greatly and are, in many instances, found to be inconsistent with experimental findings, or irrelevant in many materials and geometries.

It is acknowledged that the purpose of the technique is to 'improve' the comparison of results obtained from tests with theory and so improve the practical utility of experimental data. How accurately the theoretical stress distribution reflects upon the actual micro-processes of deformation in the region about the crack tip and its encompassing r_p , dictating its size, is another matter when comparing the toughness of materials. However incorporating a correction factor, such as r_p creates agreement between experimental and theoretical results in a fashion that is compliant with the rationale of LEFM. The plausibility of an effective crack length, the agreement that can be often achieved between results and its simplicity make the approach attractive for design. However the utility of r_p is questionable where the intention is to make comparisons between the toughness of materials based upon values determined for K_{Ic} or G_c . This is especially true for the case of rubber toughened materials where the apparent crack lengths become very large and the microstructure disperses load.

The fundamental assumption of LEFM contends that fracture processes are controlled by the crack tip stresses and strains and nothing else. The validity of any comparisons made between values of K_{Ic} or G_c depend upon the amount of plastic work that has occurred in the region about the crack tip and the state of stress in the region of the tip. Their comparison depends upon how accurately these are described by the theory. In using r_p the failure of a material to adhere to LEFM conditions is acknowledged, which immediately cautions the comparison. The magnitude of r_p , the state of triaxial stress and the magnitude of stress are greatly influenced by loading rate, geometry. Consequently the true values of K_{Ic} and G_c will vary with these and in turn with the secondary phase morphology. In that it is sensitive to these variations compounds the variability associated with measurements such factors and so it is thought undermines the utility of the approach in generating parameters for comparing the fracture properties of materials, and especially between the rubber toughened materials used in this study.

4.3.1.3 *Size effects and Comparisons of Fracture Toughness.*

Ultimately in order to provide valid, consistent and comparable results it's necessary to characterise fracture parameters under a single comparable stress state. The condition that causes the maximum concentrated stress and minimum deformation about the crack tip is maximum constraint. To achieve it a state of plane strain must exist. This returns attention to the points made above regarding small scale yielding and the requirements of maximum constraint. In a fracture test specimen the principal requirement is that the in-plane dimension exceeds some multiple of the plastic zone at the tip of the crack. A low depth to width ratio minimises the size of the plastic deformation zone (*see Figure 4.4 below*), and imposes a higher degree of constraint on the material allowing the material at the crack tip move, as it increases, toward a dominant triaxial state of plane strain. The extent to which it does so being progressive but relative.

The limitation on size forms the basis of the minimum test piece size requirements of the ASTM E-399 standard for valid determination of K_{Ic} (K_{Ic}) which is given by;

$$a, B, W - a \geq 2.5 \left(\frac{K_C}{\sigma_Y} \right)^2$$

Equation 4.18.

where B is thickness and W is width.

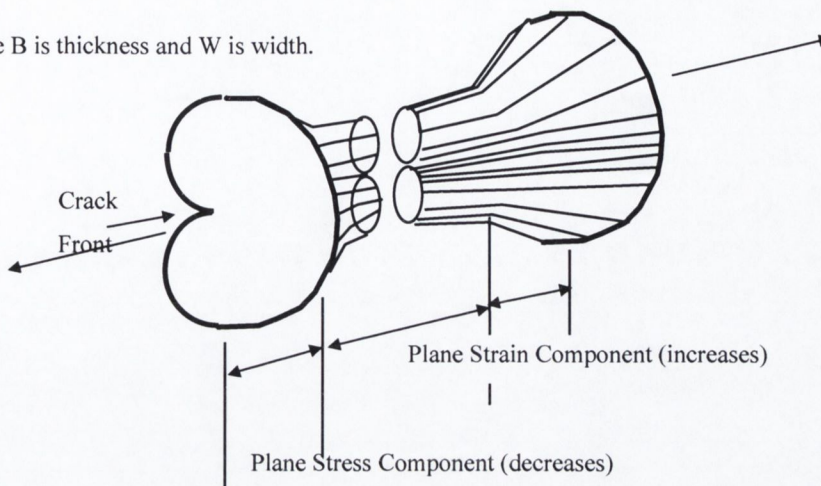


Figure 4.4. Sketch of the plastic zone shape. As in-plane, or ‘crack face’ dimensions (thickness), increase the contribution of the plastic deformation zone decreases under increased constraint and the triaxial state of stress moves from plane stress to plane strain.

In spite of the discussions above and the concerns regarding viscoelastic behaviour which have only been alluded to, linear elastic fracture mechanics can be successfully applied to characterise the fracture properties for many polymers. K_{Ic} and G_{Ic} values have been obtained that provide, in so far as it is possible, true material constants for many glassy polymers once the size criteria to achieve conditions approaching plane strain are met. For many glassy materials such as PMMA, PS and some semi-crystalline resins, e.g., HDPE these requirements are reasonably easy to achieve at dimensions that are often used in ‘real-life’ designs [1].

However in toughened polymers (containing secondary phases), and especially in HIPS, low yield stresses and high toughness values often mean that the specimen sizes required to determine acceptable, or valid, K_{Ic} or G_{Ic} are impractical to manufacture. Nevertheless, if fracture occurs within a contained zone around the crack, then modified LEFM analysis (e.g. using r_p') can give useful values for toughness. However the values are not the unique geometry independent lower bound value associated with plane strain and their magnitude will change with different geometries and compositions. Thus as the extent of plastic deformation increases the utility of modifying LEFM reduces until it eventually becomes meaningless.

In HIPS, a change in the plastic zone size accompanies changes in morphology, and accordingly, the magnitude of the apparent fracture toughness. In turn the relative compliance of the system with the requirements of LEFM varies and so the comparability of measurements between materials. Comparisons that are made must be qualified, e.g., in terms of the ratio of stress intensity factor to modulus, yield strength etc. However this would require the effect of other factors and their inter-relationships to be understood, e.g., the effects of varying thickness and morphology. As the effect of the micro-morphology on intrinsic toughness does not appear to have been considered before, this is not possible.

To determine valid plane strain toughness values for HIPS huge sample thickness are required. Yap, Mai and Cotterell considered this fundamental difficulty of constraint in HIPS [18]. Their work showed that the thickness required to achieve conditions approaching plane strain was in the region of ≈ 22 mm, far greater (by 4-10 times) than section thickness' typically used (2-5mm). The critical elastic stress intensity factor determined, by Yap et al, for the material under plane strain was $1.45 \text{ MPa m}^{1/2}$, little more than that obtained for polystyrene $1.0 \text{ MPa m}^{1/2}$, explaining why parts of such thickness are seldom fabricated. However it also questions the interpretation of HIPS being a 'tough' material. This highlights the importance of understanding its intrinsic toughness as brittle behaviour can occur in the thin parts used in applications where, for example, a part may have a scratch introduced along its surface, or where it is subjected to cyclic (fatigue) loading. Mai et al only considered one secondary phase volume in studying the effect of sample thickness. In view of the previous discussion then it would be considered that as the secondary phase volume would be reduced that the thickness required for establishing plane strain would also fall. The results of Chapter 3 suggest a similar fall would accompany a drop in the particle size below $1 \mu\text{m}$.

An important observation to make from these comments, regarding the achievement of valid and comparable measurements, is that most tough or 'ductile' polymers are used in parts that rarely exceed 5mm in thickness. Thus it is the case in most applications that the utility of LEFM is limited. As a consequence alternative theoretical paradigms are necessary to describe the process of fracture involving non-linear behaviour. Elasto-plastic fracture mechanics methods have been developed to describe fracture in such systems.

4.3.2 Elements of Elasto-Plastic Fracture Mechanics.

4.3.2.1 The J-Integral.

The J integral has become the most popular method for characterising fracture in ductile materials. For investigators considering toughened resins it is attractive because it accommodates non-linear behaviour, and thus may be extended to consider plastic deformation. Another attraction is that it is far less stringent in regard to sample size than LEFM but it, i.e., J_{1c} , can be equated to G_{1c} in the limit of maximum constraint. Consequently resins ranging from highly extensible nylon to ABS, where the pseudo-plastic processes of crazing compete with shear, and HIPS where crazing dominates have all been successfully characterised in terms of the J integral [19].

Conceptually the J integral is a path independent, line integral. The parameter has its origins in a two-dimensional form of a contour integral defined by Eshelby (1956) for use in an energy based continuum approach to lattice defects [20]. In the sixties, Sanders (1960), Rice (1968) and Cherepanov (1969) independently applied Eshelby's line contour integrals to fracture mechanics problems [21,22,23]. The form proposed by them of the line integral provides a unifying theoretical basis for non-linear fracture mechanics, the J integral, defined as;

$$J = \int_{\Gamma} \left\{ Z \delta y - T \frac{\partial U}{\partial x} ds \right\}$$

Equation 4.19.

Where,

Γ is a closed contour in a stressed solid, T is the tension vector perpendicular to the contour in an outward direction, u is the component of the displacement vector, U , of the contour in the 'x' direction, 'ds' is an element of the contour and Z is the strain energy per unit volume.

In essence, the J integral represents a non-linear strain energy release rate. What Rice and the others showed was that the J integral was the rate of change of potential energy with crack extension for a non-linear elastic solid, equivalent to G in the case of a linear elastic material, i.e.;

$$J = G = -\frac{\partial(PE)}{\partial a} \text{ and so} \tag{Equation 4.20.}$$

$$\Rightarrow J = \frac{K^2}{E} \tag{Equation 4.21.}$$

This is illustrated graphically in Figure 4.5 where, in the case of a brittle crack, the potential (elastic) energy, is the shaded area. An experimental procedure to determine the critical J integral, J_c , was later suggested by Begley and Landes [24]. J_c was determined by constructing a crack growth resistance curve (J - R curve), by plotting the area beneath the load displacement curve, the absorbed energy, against stable ductile crack extension, Δa . The point of intersection between the J - R curve with a crack blunting line, defined as $2\sigma_y\Delta a$, yielded J_c . The procedure was later standardised in ASTM protocol E813 [25].

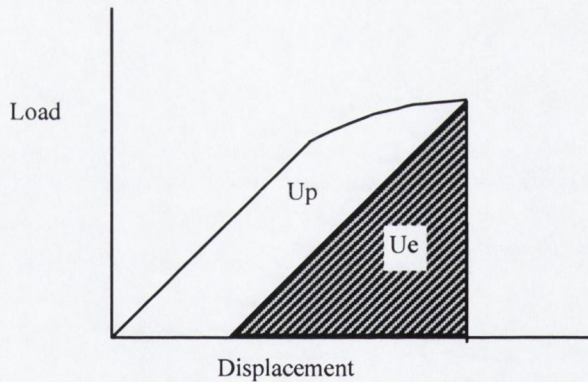


Figure 4.5. Diagram showing the partitioning of work in a load point displacement curve.

The method is based upon the definition of J comprised of elastic and plastic components, i.e.,

$$J = J_e + J_p \tag{Equation 4.22.}$$

where

$$J_e = \frac{\eta_e U_e}{B(W - a)} \text{ and } J_p = \frac{\eta_p U_p}{B(W - a)} \tag{Equation 4.23.}$$

where U_e and U_p are the elastic and plastic energy component see Figure 4.5. η_e and η_p are the elastic and plastic work factors. Thus J can be expressed as;

$$J = \frac{1}{B(W-a)} (\eta_e U_e + \eta_p U_p)$$

Equation 4.24.

The elastic work factor η_e can be evaluated for a given specimen geometry experimentally from the compliance curve, or from the shape factor Y and η_p from the limit load analysis such that, from [26];

$$\eta_e = \frac{(W-a)Y^2 a}{\int Y^2 a da + (SW/2)} \quad \text{and} \quad \eta_p = \frac{W-a}{W\alpha \left\{ \frac{(W-a)}{[W(\alpha - a/W)] + 1} \right\}^{-1}}$$

Equation 4.25.

$$\text{where } \alpha = [1 - 2a/W + 2(a/W)^2]^{1/2}$$

Equation 4.26.

$$\text{and (for SENT) } Y = 1.99 - 0.41(a/W) + 18.7(a/W)^2 - 38.48(a/W)^3 + 53.85(a/W)^4$$

Equation 4.27.

Where S is the span/height between grips. Thus for specimens of known dimensions, where η_e and η_p have been solved for, in X , J may then be determined from, [26];

$$J = \frac{XU_{Total}}{B(W-a)}$$

Equation 4.28.

In the procedure specimens are loaded at a constant cross-head speed to various displacements producing cracks of different lengths (Δa). They are then unloaded and broken under rapid fracture, for example on an impact testing device, in order to determine the crack growth length, a . J is then determined by the integrating the area under the load vs. displacement curve (U_{total}) and substituting in the above equation. Finally J_c is determined by plotting J for various crack lengths (J-R curve) and extrapolating to zero crack extension.

Three versions exist of the standard ASTM method, E813-81, E813-87 and E813-89, the primary difference between them being the manner in which the J-R curve is constructed (similar to G-R) and how J_{1c} is defined on the curve [25]. With three versions it is unsurprising that some ambiguity surrounds the evaluation of J . In E813 81, acceptable points for constructing the J-R curve are chosen between two exclusion lines, parallel to the blunting line, at $0.006 \Delta a$ and $0.06 \Delta a$. A line is then interpolated through the acceptable data using linear regression, to generate the J-R curve. The intersection of the J-R curve with the blunting line gives the J_{1c} . E813-87 and E813-89 proffer different exclusion lines, between $\Delta a = 0.15$ and 1.5 and use a power law regression line to fit the J-R curve, and J_c is defined in the intersection between the J-R curve with an 0.2 mm offset line, to correct for crack tip blunting.

The multi specimen methods are very time consuming and in the past decade a number of alternatives have been proposed, e.g., the single specimen and the hysteresis method [27,28]. These techniques are less complicated and are gaining popularity amongst researchers.

Some controversy remains about the usefulness of the J-Integral. At the heart of the concerns is the fact that many of its assumptions are invalid or difficult to achieve. The fundamental assumption, that the load deflection curve, i.e., the integral defining J, is path independent, a supposition arising from the law of energy conservation is most often, in reality, invalid. Crack growth stability, another important assumption in evaluating the J integral, necessary in applying the J integral analysis to non-elastic systems, is a difficult condition to impose and maintain, but required in order to construct a valid J-R curve. The debate about the methods used to determine J add to concerns about applying it in design. Though the experience with toughened polymers tends to have been more positive their compliance is sometimes viewed with suspicion. Hashemi and Williams showed linearity in J-R plots for toughened polymers extended over greater ranges of ligament length than would have been anticipated [30]. Huang and Williams found no dynamic effects at high loading rates though these should have existed. Work by Narisawa and Takamori showed the crack blunting line to be superfluous to J_{1c} determination in toughened polymers. The latter was an unexpected finding as such a correction would seem most necessary in the case of these materials that blunt significantly in advance of crack initiation [29].

In spite of some reservations the J-Integral has been employed, in accordance with a variety of experimental methods, to characterise fracture in a wide range of polymers from ductile polyolefins, e.g., PE, PP, Nylon, and to craze sensitive amorphous materials such as PC. It is accepted as the most appropriate fracture analysis for ductile materials, partly because of its success in characterising the toughness of ductile polymers [30,31,32]. However amidst the success in describing toughness in such diverse materials questions exist regarding the consistency and reproducibility of the results that have been obtained. In the case of plastics materials the values obtained for J_{1c} in different laboratories have differed enormously. Values for ABS resins have been obtained that range from 2.9 to 6kJm^{-2} while values ranging from 4.8 to 30.0kJm^{-2} have been quoted for the same rubber toughened nylon [33]. This is 'J's' weakness. The conditions of loading under which it is determined determines its magnitude. As these may vary, even where they continue to meet the requirements for determining a valid measure of J, the values obtained for it may not be directly comparable. In addition to the debates regarding the crack blunting line this, often large, variability in the values quoted in the literature for many materials undermines its integrity and utility as a parameter for characterising intrinsic toughness.

The J integral of HIPS has been characterised by a number of investigators, Lee et al's 1993 work provides a comprehensive comparison of values determined under the various ASTM methods [34]. Their research, conducted on a BC Chemicals grade of HIPS (Maxiflex 301-similar to the parent resins considered in this work) also considered a hysteresis method. Using the standard techniques they determined values of J_c , which varied from 3.0 to 4.9kJm^{-2} .

The lack of consistency they observed between the values obtained for the same materials its thought has roots in the level of constraint arising from factors already mentioned above in relation to linear elastic fracture. As with K , in order to meet the requirements for J controlled growth, specimen dimensions must exceed some multiple of J_c/σ_y . To generate plane strain along the crack front, the ASTM guidelines are that, the plane strain value of J_c (J_{Ic}) may be determined whenever [9],

$$a, B, W - a \geq 25 \left(\frac{J_c}{\sigma_y} \right)^2$$

Equation 4.29.

However what is crack tip specific, or process zone related, remains somewhat arbitrary, and as the results quoted in the literature show, irrespective of investigator's opinions, it is ultimately determined by the often wide-ranging interpretation of material deformation mechanisms.

Ironically Lee et al showed that an alternative hysteresis method, that ignores geometry issues, offered a simpler means of achieving, what were considered as being more accurate results. This method, based on a physical event of an inflection in the hysteresis loss, associated with crack advance, provides a simple means of determining J directly from a single test [35].

Thus in many respects whilst J is a useful parameter for describing the process of fracture in ductile materials, it is, from many respects, sensitive to the same frailties in respect to the validity of comparisons based upon it as those based upon the findings of the linear elastic approaches.

4.3.2.2 The Essential Work of Fracture

An increasingly popular alternative to the J Integral is the essential work of fracture. The concept originates from work by Broberg and Gurney and it has been championed by Mai and Cotterell and their coworkers, over the past 20 years [1,36,37,38].

In many respects the physical meaning of the concept is similar to the J integral. Broberg proposed that the non elastic region at a crack could be divided into two regions [36]: one where fracture occurs at the crack tip, the 'end' region, and the second, the 'outer' region, where plastic deformation takes place to accommodate the large strains of the end region. He proposed it would be possible to partition the total work of fracture W_f into these regions. The two portions can be termed the essential (W_e) and the inessential, or plastic (W_p), works of fracture. Thus;

$$W_f = W_e + W_p$$

Equation 4.30.

With the essential work of fracture being proportional to the ligament length ($W-a$) and the non-essential work proportional to $(W-a)^2$, the total work of fracture can be expressed as[39];

$$W_f = w_e B(W-a) + \beta w_p B(W-a)^2$$

Equation 4.31.

Where w_e is the specific essential work of fracture and w_p is the specific non essential component for unit thickness B and ligament length $(W-a)$ and β is a shape factor depending upon the geometry of the plastic zone. Dividing across by $B(W-a)$ gives,

$$w_f = w_e + \beta w_p(W-a)$$

Equation 4.32.

where w_f is the total specific work of fracture.

The intercept of the line at 0 length gives the specific essential work of fracture w_e while the slope of the line provides a measure of βw_p the non-essential specific work term as shown in Fig.4.6.

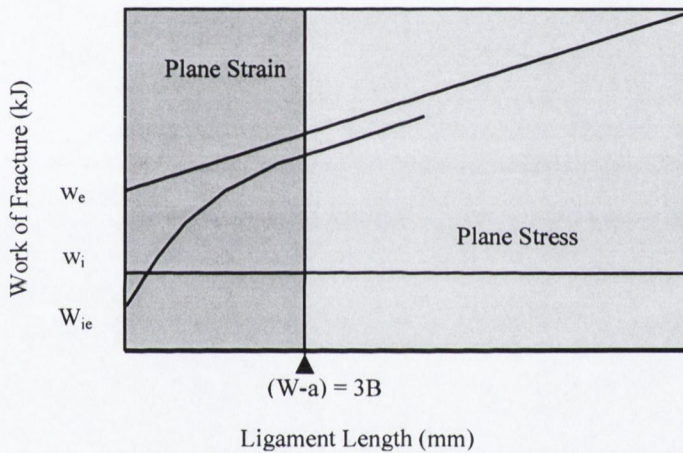


Figure 4.6. Schematic plot of total specific work of fracture versus ligament length showing plane stress and plane strain region. w_e = specific essential work of plane stress fracture, w_i = the work of initiation and w_{1e} = the specific essential plane strain work of fracture. [39]

For equation 4.31 to yield a straight-line relationship such that w_e , w_p and β are all independent of the ligament length, the dimensions of the specimen must be such that a state of pure plane stress exists in the specimen, as only then will w_e , w_p , and β be constant (Figure 4.6).

To generate pure plane-stress, the ligament length must be greater than the specimen thickness (B). Consequently fracture experiments must be conducted on specimens with $(W-a)/B$ ratio's greater than 3 - 5. For specimens smaller than $3B$ a plane stress/strain fracture transition occurs and solutions for Equation 4.32 become non-linear. The increased plastic flow constraint that accompanies the decrease in ligament length reduces both the work to initiation (w_i) and the work of fracture (w_f) gradually as in Figure 4.6. to a

point of convergence in w_{1e} at $B = 0$. This provides a plane strain specific intrinsic essential work of fracture, provided that the sheet thickness meets the conditions specified for J_{1c} measurement e.g., $B > 25 (w_{1e}/\sigma_y)$. If the requirements for plane strain are not satisfied, then a 'near' plane strain w_{1e} is determined.

The specific essential work of fracture can be identified with the J integral, i.e., the value of the specific fracture work w_f and the J-Integral are equivalent provided J controlled crack growth conditions are satisfied, i.e.;

$$w_f = J = J_c + \frac{dJ_R}{da} \Delta a$$

Equation 4.33.

thus from equation 4.32 and equation 4. 33

$$w_e \equiv J_c$$

$$\beta w_p \equiv \alpha \frac{dJ_R}{da}$$

Equation 4.34.

where α is a constant depending on the specimen geometry(Equation 4.26). These relationships have been confirmed for a range of ductile materials and several different specimen geometries[28,40,41]. Thus the specific fracture work technique, which is easier to perform, provides an alternative to the J-Integral analysis.

The simplicity of its experimental method and the fact that material behaviour does not undermine essential assumptions of the theory, suggest that the approach is more appropriate for characterising the fracture properties of ductile materials.

The method has been applied to HIPS by Mai et al to evaluate the toughness of two HIPS materials, one a conventional bulk polymerised material the second a SBR/PS solution cast blend [42]. Values of 1.1 and 3.0 kJm^{-2} were obtained for the two materials respectively. There is a significant difference between the materials though this should be expected given the difference in the morphology associated with both. The value obtained for the bulk polymerised resin was significantly less than the J integral values obtained for similarly prepared HIPS by Lee et al [34]. However that the value tends to that associated with the fracture toughness of polystyrene, supports its assessment of the plane stress fracture toughness[18]. There were some issues identified by Mai et al in characterising HIPS, and interpreting the results that shall be returned to in the discussion of the experimental results.

4.3.2.3 Characterisation of intrinsic fracture toughness from fatigue

From the previous discussions it is seen that the preoccupation of the methods used in characterising fracture mechanics parameters revolves around creating appropriate conditions of stress state in order to allow the determination of valid and comparable measures of intrinsic toughness. It was noted in relation to the LEFM that imposing maximum constraint proved the most reliable means of doing so. Concern was

also raised in regard to evaluating J , in that quasi-stable crack growth conditions should exist during tests, so that valid and comparable measurements of J were yielded from tests. The last section, concerning the essential work, the importance of prescribing, and applying, conditions of either plane stress or plane strain, in order to discriminate, and understand, the meaning of results that obtained from tests was highlighted.

The high level of constraint experienced in materials undergoing fatigue fracture, that occurs under low levels of imposed load, creates an interesting opportunity to characterise intrinsic toughness of relatively tough or extensible materials in relatively thin cross sections. The most useful, and often most meaningful, measure of intrinsic toughness is that obtained under conditions of maximum constraint or plane strain. Under this condition fracture parameters may be related through LEFM to each other, i.e., $G_c = J_c = w_e$, and to other mechanical properties, e.g., E , T_y etc., to obtain K and ν . By imposing conditions close to maximum constraint, especially in the early stages of fatigue crack growth, its thought that a low cycle fatigue test can facilitate the measurement of plane strain intrinsic toughness. As observed above, high levels of constraint counteract the propensity of HIPS to craze and as it is increased the size of plastic zones associated with crack propagation is reduced.

Strebel and Moet first proposed the determination of the J integral directly from fatigue tests on low density polyethylene [43]. The concept of the technique is simple and it provides for the determination of the J integral directly from first principles. Fluctuating loads, with $R=0$, allows J to be measured directly from first principles, through monitoring the strain energy released during crack advance. The extrapolation of ΔJ to 0 crack length gives J . Provided the volume in which yielding occurs is 'contained', the intrinsic toughness, J_{1c} , of the material is measured. Though time dependence is not included in G , it may be considered in the J integral analysis. It is obviously a factor in determining the toughness of a polymer in long term tests. However it is considered that in low load and low cycle fatigue tests under a fluctuating load with $R=0$ that the measurement of strain energy release in propagating a fatigue crack unit distance provides a valid measure of toughness. This is because it reflects the overall balance of mechanical energy within the system and accommodates changes in compliance which are most likely to be small especially where only small scale yielding is associated with deformation at the crack tip. In fatigue then, the reconciliation between plastic zone size and measured toughness is offered by limiting the extent to which the material can express its ability to react to an applied load. It so contributes to comparing the effect of the secondary phase morphology on intrinsic toughness by characterising it from fractures where the process zones are of comparable size.

However basic assumptions concerning J 's definition are violated, most notably that fully reversed loads are applied and that crack closure, pseudo-plastic and hysteretic material responses impede the full recovery of the material between cycles. This comment should be balanced by noting that assumptions associated with its definition are not adhered to by the other test regimes used to determine it in plastics [9,44]. Be this as it may as Strebel and Moet point out, in spite of the technical reservations, the extrapolation of J to 0 crack length does yield valid measures of J_c and J_{1c} , and thus G_c and G_{1c} and w_{1c} . Nevertheless, in recognition of this and to distinguish the parameter obtained from fatigue tests J' is used to denote the parameter obtained in fatigue.

The parameter, J' , is defined by, the change in the potential energy (U), with respect to crack length (a), per unit thickness (B), in the same way as LEFMs' G , and its non-linear equivalent J determined from monotonic tests. In the load displacement curve, the area to the left of the load displacement curve, represents the negative potential energy ($-U$) of the system. Its change with respect to crack length is proportional to J , i.e.;

$$J = J' = -\frac{1}{B} \left(\frac{dU}{da} \right)$$

Equation 4.35.

Thus J' can be calculated directly from the loading curve in fatigue tests by determining the energy under the loading curve and so the resistance to crack extension, or by applying the energy definition of the J integral, Eqn. 4.20. The measure of the potential energy and its changes reflect the potential energy released, J' (or J), as a crack advances. When extrapolated to 0 crack length it provides a measure of the minimum energy required to advance the crack. Where the measurement is made under maximum constraint the measure J'_{1c} is equivalent to J_{1c} and W_{1c} and the measurement is normalised for the minimum fracture process volume required to allow a crack to propagate.

The attraction of the method in considering HIPS is that it allows the intrinsic fracture toughness of materials to be determined from specimens whose dimensions are of the order of those used in conventional designs. In this study it provides a basis for determining whether the incorporation of increased secondary phase volumes does actually effect an increase in the intrinsic toughness of the materials. It also allows comparisons to be drawn between the results obtained from other test methods. Measurements made under the high levels of constraint in fatigue would be considered to offer more realistic evaluations of intrinsic toughness.

4.4 Experimental

4.4.1 Linear Elastic Fracture Mechanics: Strain Energy Release Rate from Impact Data.

As a first step in considering the material's intrinsic fracture toughness, linear elastic fracture mechanics was applied to the results of Charpy impact tests according to the concept of a critical strain energy release rate. The strain energy release rate (G) for a specimen of uniform thickness B can be expressed as,

$$G = \frac{1}{B} \left(\frac{d\omega}{da} \right)$$

Equation 4.36.

where ω is the energy associated with fracture and a is the crack length. As presented in the introduction the critical level of G , G_c , associated with linear elastic fracture, may also be expressed in terms of the critical stress intensity factor, i.e.,

$$K_c^2 = EG_c$$

Equation 4.37.

Where K_c^2 , the critical stress intensity factor, may be expressed in terms of load and geometry according by;

$$K_c^2 = Y^2 \sigma^2 a$$

Equation 4.38.

Where σ is the applied stress and Y is a correction factor for geometry and edge effects which is a function of 'crack length to specimen width' ratio. In the case of the Charpy 3 pt. bend specimen geometry it may be expressed in the form,

$$Y = \left[2.9(a/D)^{1/2} - 4.6(a/D)^{3/2} + 21.8(a/D)^{5/2} - 37.6(a/D)^{7/2} + 38.7(a/WD)^{9/2} \right]$$

Equation 4.39.

Where energy and not load is measured then another expression, Φ , may be used to correct for these effects. Φ may then be used to evaluate G [1]. In the case of 3 pt bend Φ can be expressed in terms of Y according to the relationship, where L the span of the specimen to be loaded; and D is specimen width.

$$\Phi = \frac{\int Y^2(a/D)d(a/D)}{Y^2(a/D)} + \left[\frac{L}{18D} \right] \times \frac{1}{Y^2(a/D)}$$

Equation 4.40.

Thus G_c may now be determined from the expression [1];

$$G_c = \frac{\omega}{BD\Phi}$$

Equation 4.41.

Consequently the entire impact data set of results were plotted against $BD\Phi$ and G determined from the slope. As illustrated in Figure 4.7.

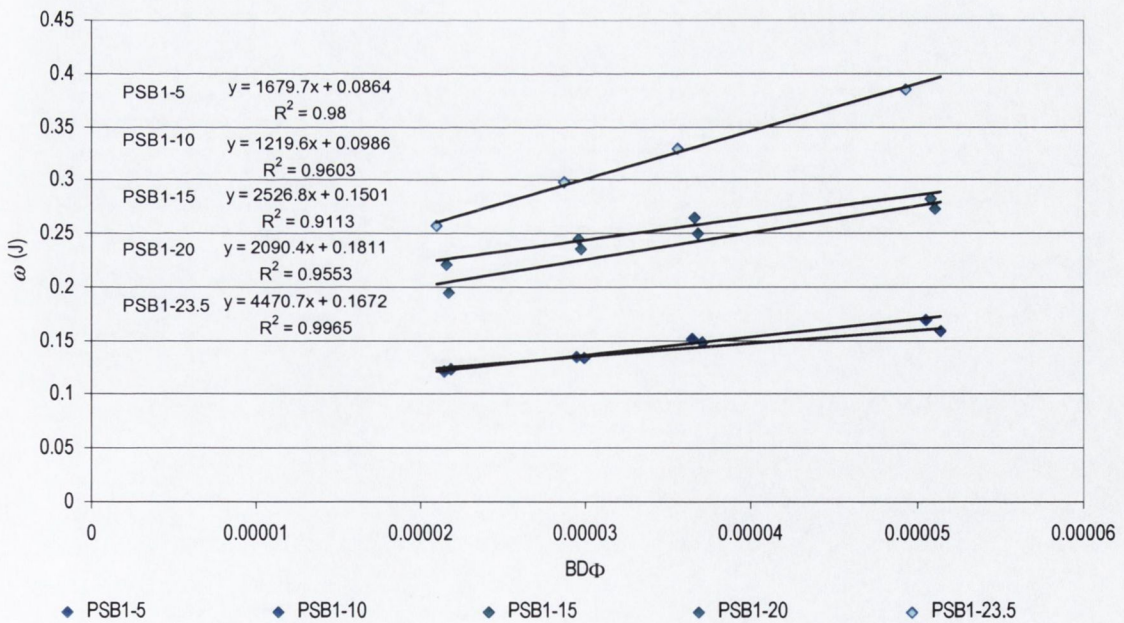


Figure 4.7. Curves for the G_c of PSB1 series resins Determination of G_c for PSB1 Series Resins.

4.4.2 Results: strain energy release rate

The results of tests on all of the materials are presented in the table 4.1. below.

LEFM Materials	G _c (kJm ⁻²)		
	PSB#1	PSB#2	PSB#3
PSB#-5	0.84	1.97	1.87
PSB#-10	0.61	1.72	1.69
PSB#-15	1.26	1.67	1.79
PSB#-20	1.34	1.96	1.79
PSB1-23.5	2.19		
PSB#-25		1.85	2.42
PSB2-32.5		3.05	
PSB3-45.4			3.34

Table 4.1. Results of strain energy release tests determined from impact tests for PSB#1, 2 and 3 series.

4.4.3 Determination of J integral from Monotonic Tensile Loading

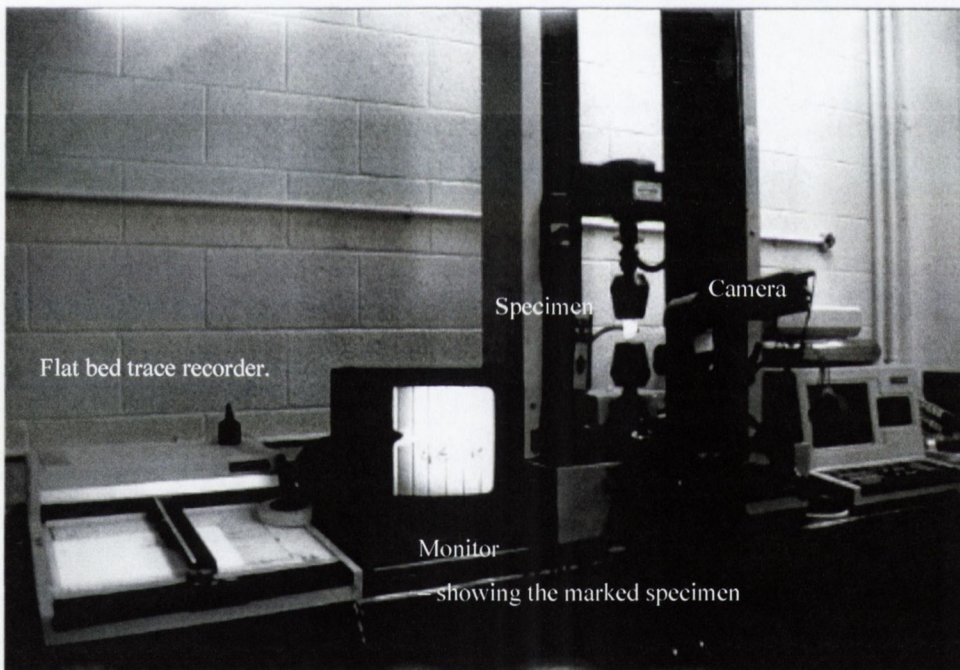


Figure 4.8. SENT fracture testing apparatus.

The 4 x 25 x 100 mm specimens were used to determine the J integral values for the materials. The following steps outline the method used to determine J_c for each resin.

- Three 4 x 25 x 100 mm specimens of each material were notched to 2, 4, 8, 12, 16 and 18 mm.
- Lines were drawn perpendicular to the notch at 2mm intervals across the specimen width.
 - The monitor in Figure 4.8 is imaging such a specimen.
- The sample was then loaded in vice grips and a monotonic load applied at 0.5 mm/min.

- A load - displacement curve and video of crack growth were recorded for the test.
- When completed the video record of crack growth was used to mark out the occasions of unit crack extension on the load displacement curve.
 - Figure 4.9 is presents such a modified plot from one series of tests on PSB1-5.
- Curves for fixed crack length were then drawn on the original load-displacement curves by interpolating between the marks for fixed crack lengths.
 - Figure 4.10 present the interpolated plot for the PSB1-5 test series.
- These curves were then photocopied and graphically integrated up to fixed crack length to determine the energy associated with the extension to fixed crack length.
 - Figure 4.11 presents crack length vs. strain energy for PSB1-5.
- J -fixed crack length, was then plotted against displacement yielding a characteristic curve for J.
 - Figure 4.12 showing J vs. displacement.
- The characteristic curve was then use to determine the measure of J for each point of crack extension on the original load displacement curve.
 - Figure 4.13-4.15 shows the J vs. Δa curves generated for PSB#1- 5, 15 and 25 and J_c determined from the intercept of the linear regression line of best fit through the data set at $a = 0$.
- The results for all of the materials are presented in Table 4.2.

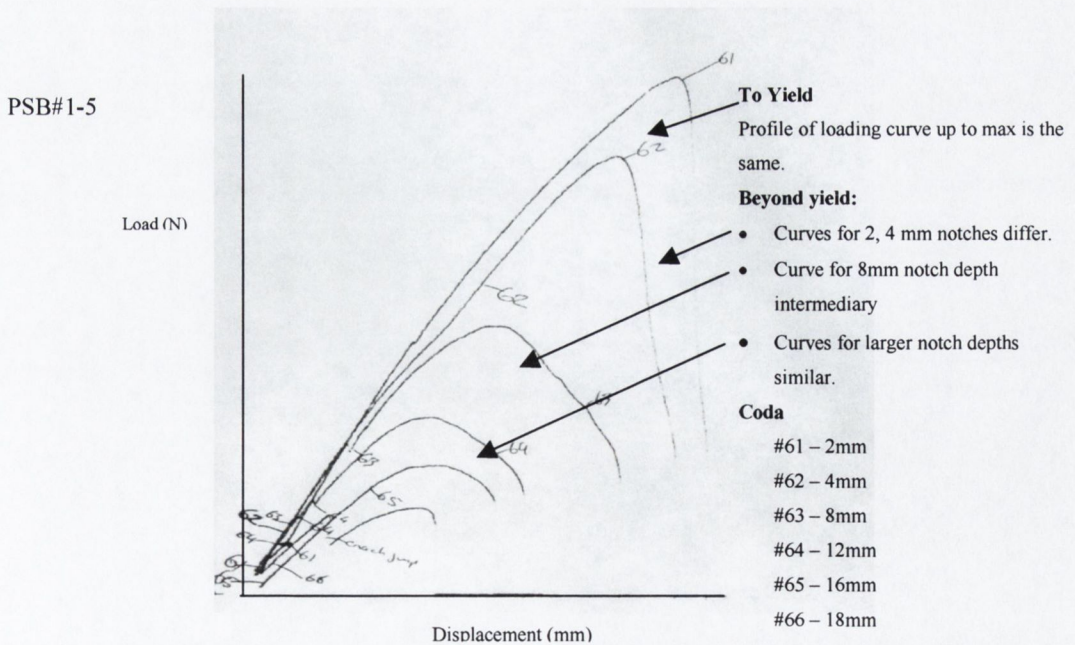
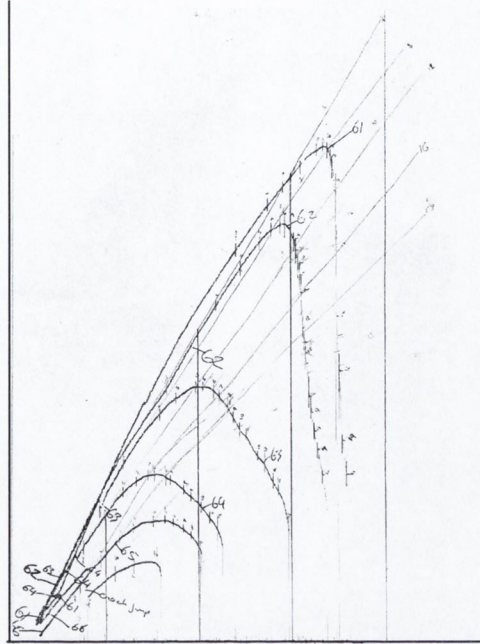


Figure 4.9. Plot of load displacement curves for Serie 1 PSB1-5. Each curve represents a notch depth.

Material: PSB#1-5

Load (N)



Displacement (mm)

Interpolated Curve

- Points on curves mark progress of crack extension.
- Interpolated curve created by joining points for constant crack length.
- Plot used to determine the energy absorbed to fixed displacement (each vertical line = 0.25mm)

Coda

- #61 – 2mm
- #62 – 4mm
- #63 – 8mm
- #64 – 12mm
- #65 – 14mm
- #66 – 18mm

Figure 4.10. Interpolated plot of constant crack length on Serie 1 PSB1-5.

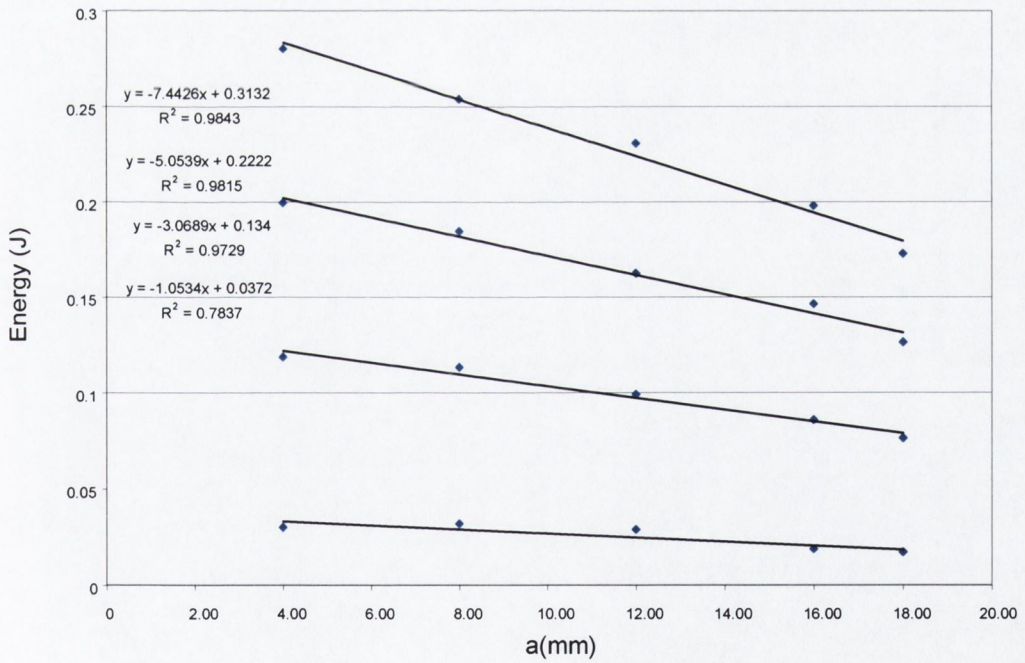


Figure 4.11. Plot of crack length vs. strain energy consumed in the propagation of crack to fixed length, from interpolated plots (Series 1 PSB1-5)

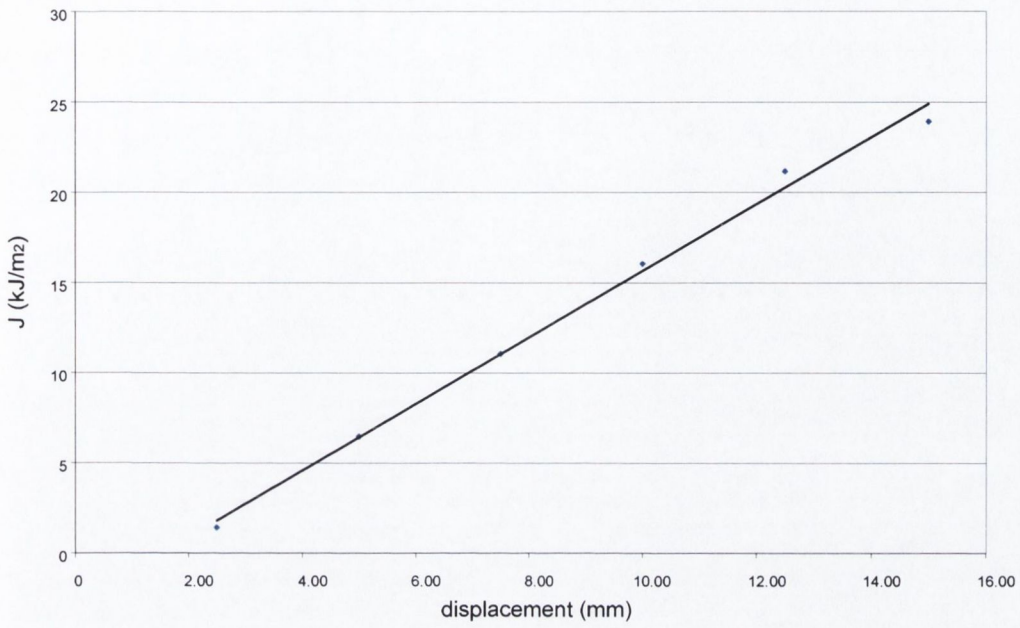


Figure 4.12. Plot of J vs. Displacement (Series 1 PSB1-5)

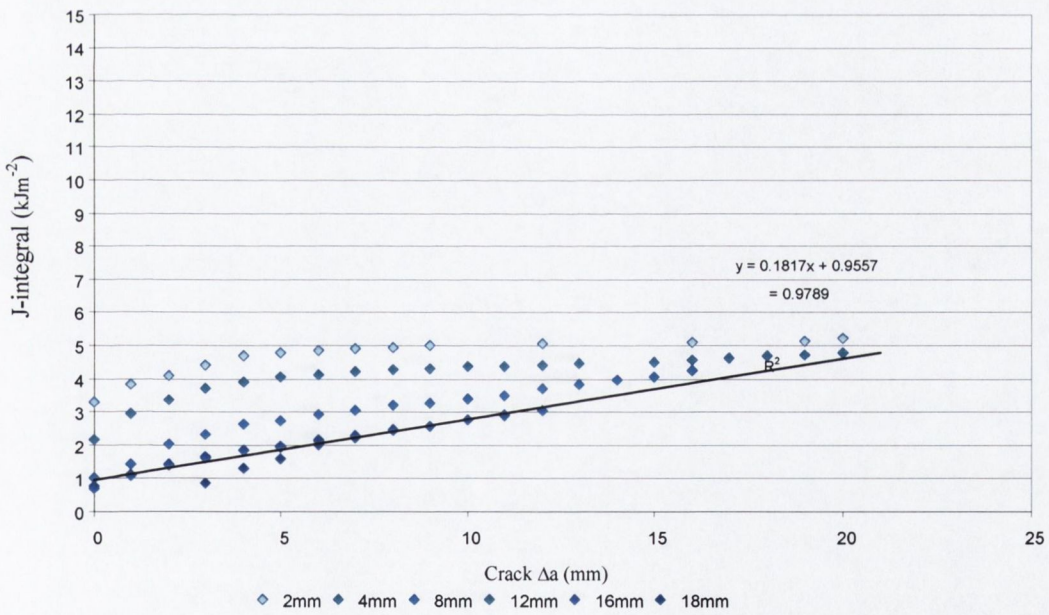


Figure 4.13. Plot of J vs. Δa (J-R curve for Series 1 PSB1-5)

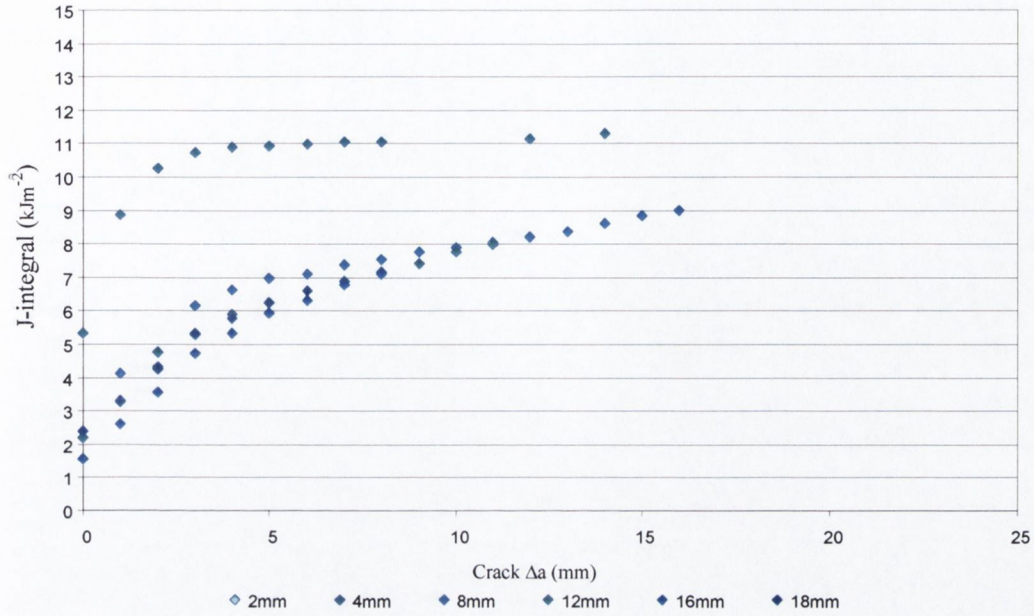


Figure 4.14. Plot of J vs. Δa (J-R curve for Serie1 PSB1-15)

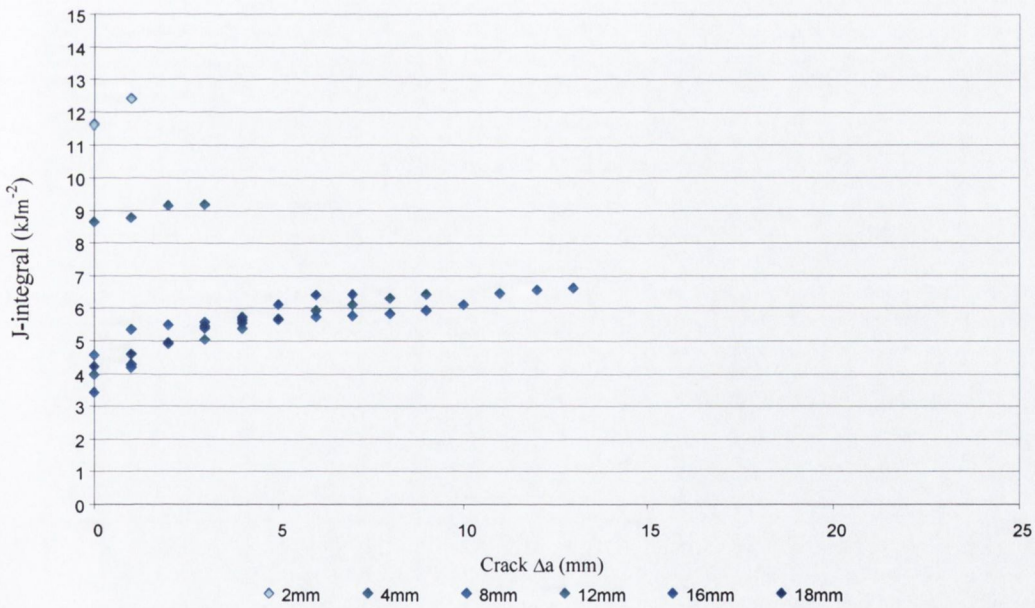


Figure 4.15. Plot of J vs. Δa (J-R curve for Serie1 PSB1-23.5)

Figures 4.13-4.15 illustrate the range of results that could be obtained at different notch depths. It is clear that the values that would be obtained in extrapolating the curves to zero crack length tend to decrease as the constraint was raised (notch depth increased). The J_c was determined from these notch depths where constraint was greater and most comparable.

4.4.4 Results Monotonic Tensile J integral

J Integral	Jc (kJm ⁻²)		
	PSB#1	PSB#2	PSB#3
PSB#-5	0.96	0.81	1.67
PSB#-10	1.12	1.48	1.36
PSB#-15	2.10	1.89	1.67
PSB#-20	3.24	3.66	2.93
PSB1-23.5	4.30		
PSB#-25		8.57	4.06
PSB2-32.5		7.32	
PSB3-45.4			5.44

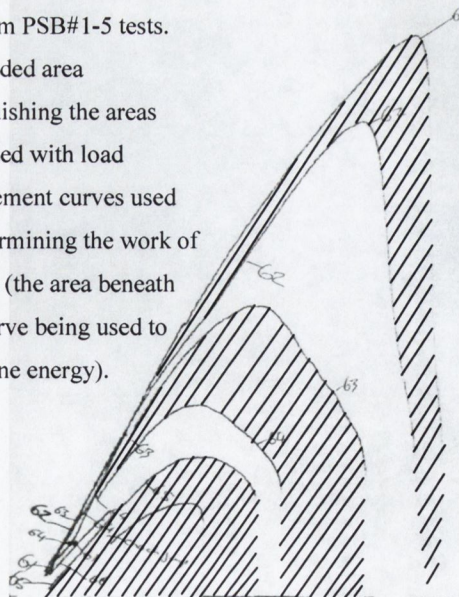
Table 4. 2. Results from monotonic J_c tests for PSB#1, 2 and 3 resin series (n=3).

4.4.5 Elasto –Plastic Fracture Mechanics Essential Work Studies

The essential work tests were conducted using the same samples as were used in the determining the resins J integral values. The concept of the essential work and its relationship with the previous methods was discussed in the introduction. Its simplicity and the ease with which it may be applied to testing any material is its greatest attraction.

1. The method used to characterise the materials involved the graphical integration of the areas under each of the curves associated with each notch depth.
 - a. The shaded area in Figure 4.16 illustrates the area for the case of the PSB1-5 series.
2. These measures of the work of fracture were then plotted against the ligament length.
 - a. Figure 4.24-4.26 illustrates the measure for the case of the PSB1 series of resins
3. The intersection of the curve with the ordinate is characteristic of the essential work of fracture whilst the slope of the line, indicative of the magnitude of the inessential component of fracture the plastic work and/or the size and shape of the damaged zone.

Figure 4.16 Plot from PSB#1-5 tests.
The shaded area distinguishing the areas associated with load displacement curves used for determining the work of fracture (the area beneath each curve being used to determine energy).



1

4.4.6 Determination of J' from Fatigue

The J integral was determined during the fatigue tests. The experimental apparatus recorded load displacement and crack extension data from which the J' (J_c) was determined.

- 2mm notches were introduced into 8 x 25 x 100mm specimens.
- The samples were cyclically loaded at 500 N and $R \approx 0$.
- Load, displacement and crack extension were recorded over the course of the tests
- The potential energy associated with the 'loading half' of the cycle was determined at crack each length.
 - Figure 4.17 presents a plot of the load vs. displacement curve for the PSB2-15 resin. The energy associated with the area to the right of the curves was integrated to determine the (potential) strain energy.
- The strain energy was plotted against crack extension.
 - Figure 4.18-4.20 illustrate the curves for the 5, 15 and 25 % ERPV polyblends for the PSB#1 – 3.
- The critical J_c was determined by fitting a linear regression curve to points associated with crack growth (up to 6.0 mm) and extrapolating to zero crack length.

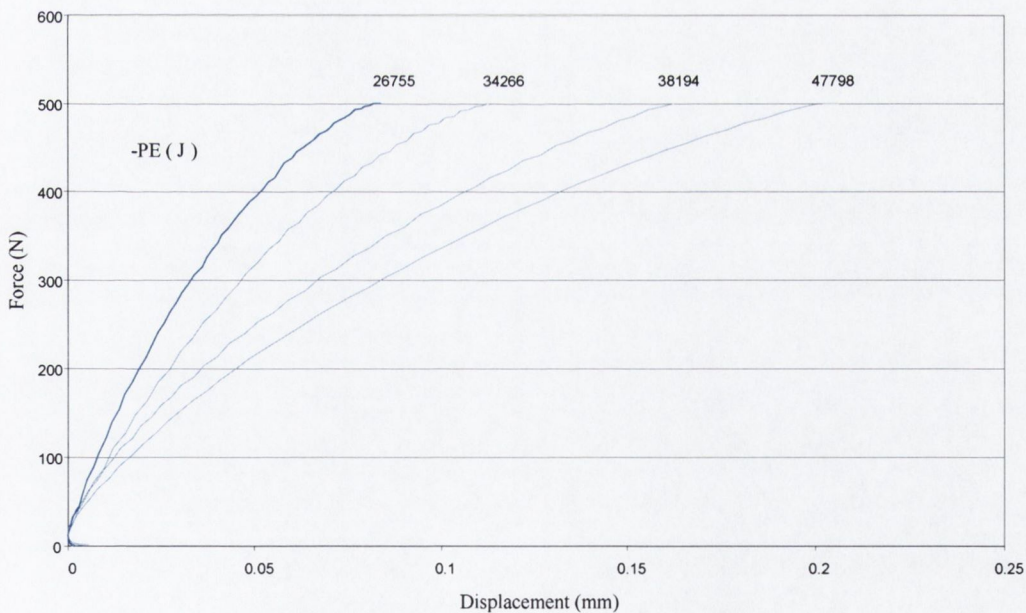


Figure 4.17. Load displacement curves from test on PSB2-15.

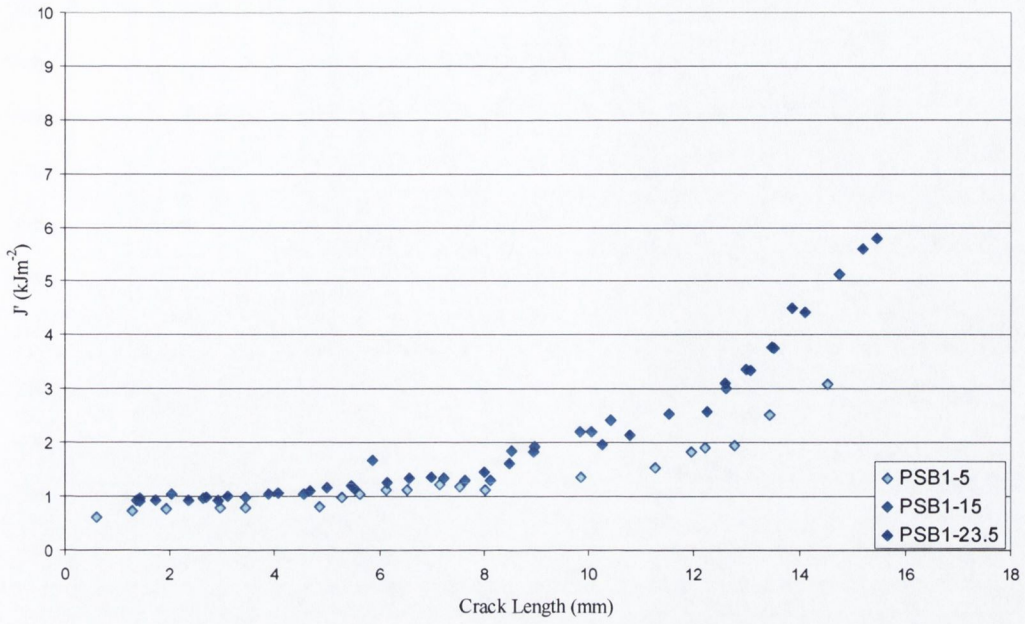


Figure 4.18. Strain energy releases J' vs. a for PSB1-5, 15, 25.

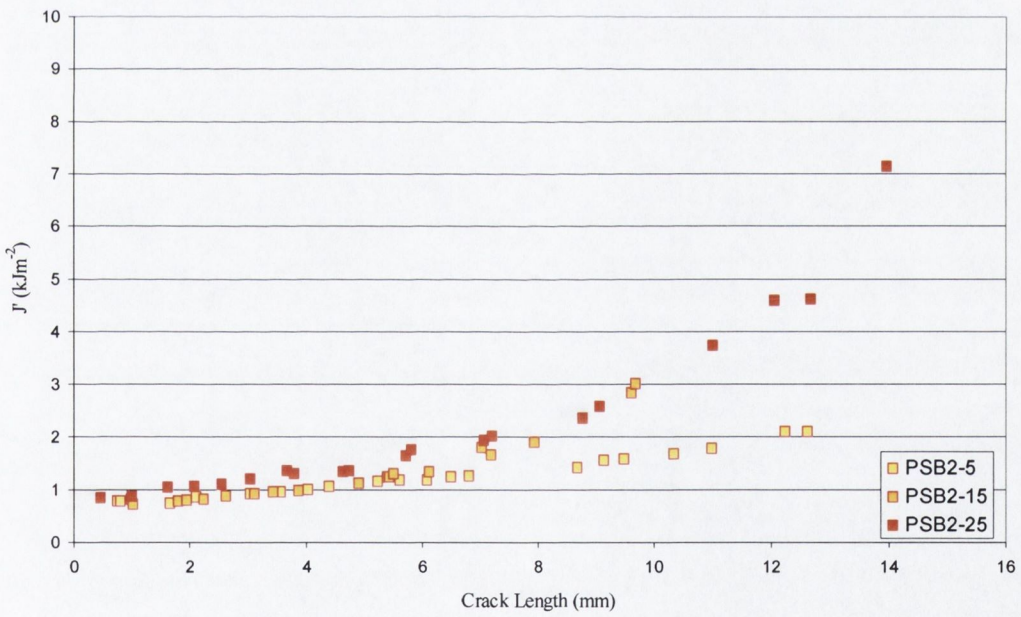


Figure 4.19. Strain energy released J' vs. a for PSB2-5, 15, 25.

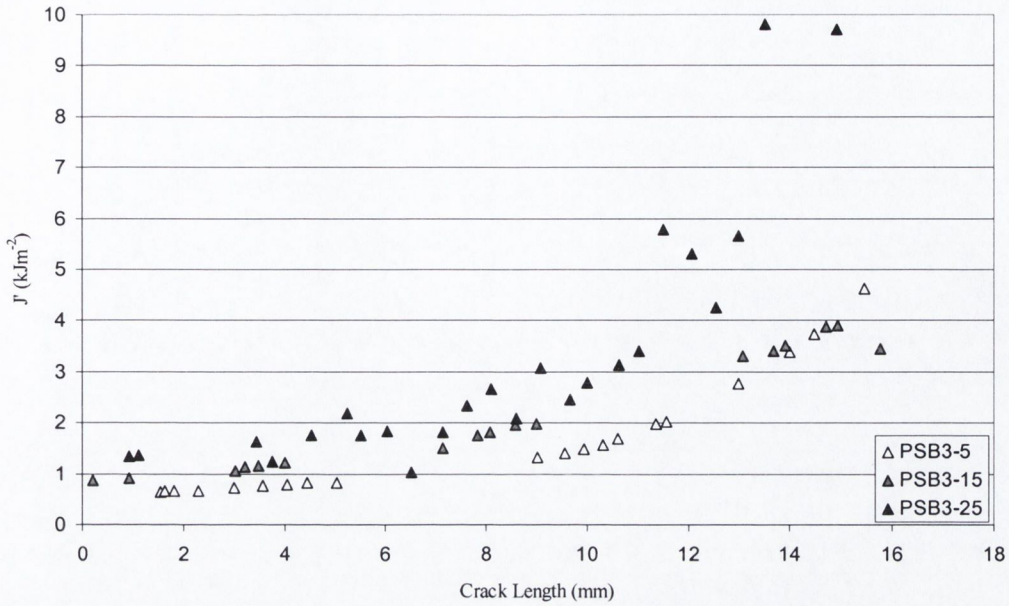


Figure 4.20. Strain energy released J' vs. a for PSB3-5, 15, 25.

4.4.7 Results of J_c from Fatigue

J Integral	J' (kJm ⁻²) (n = 3)		
	PSB#1	PSB#2	PSB#3
PSB#-5	0.57	0.6	0.57
PSB#-10	0.59	0.6	0.71
PSB#-15	0.697	0.628	0.79
PSB#-20	0.72	0.76	0.804
PSB1-23.5	0.809		
PSB#-25		0.72	0.96
PSB2-32.5		0.963	
PSB3-45.4			0.82

Table 4.3. Results of J Integral analysis (J') of fatigue tests for PSB#1, 2 and 3 resin series

4.5 Discussion of HIPS Fracture Toughness

While it is possible to determine HIPS intrinsic toughness from large specimens, ($t > 20\text{mm}$), they are difficult to prepare free of faults, e.g., voids, using conventional processing techniques and atypical of practical applications. The techniques employed in the present work employed specimens of standard thickness of the order of 5 mm; 1) LEFM analysis was applied to the results of impact tests; 2) The J integral was determined from monotonic SENT tests; 3) An attempt was made to determine the essential work; 4) The J' integral was evaluated from cyclic tensile tests (fatigue tests). The appropriateness of each of the methods used in characterising HIPS intrinsic toughness and micro-structure.

4.5.1 Comment on results for G_c determined from LEFM analysis of Impact test data.

The method used to determine the LEFM strain energy release rate G_c from impact tests, by modelling behaviour in terms of $BD\Phi$ is widely used in determining the intrinsic toughness of plastics [1]. As standard impact test specimens can be used, the test method is considered to be especially convenient for HIPS resins.

The technique worked extremely well with the brittle matrix resin. The value obtained for the polystyrene, 0.5 kJm^{-2} was in good agreement with the values quoted in the literature [1]. Initial examination of the plots of the data for the HIPS, e.g., Figure 4.7, suggested the technique would also work well with all of the polyblends. The plots of the impact strength vs. $BD\Phi$ that were generated for all of the materials each exhibited a linear relationship over the range of notch depths considered. Their slope representing G_c (Table 4.1), could be readily obtained and its magnitude tended to increase with increasing ERPV in each series.

When the results, G_c , were plotted against the RIPD, in Figure 4.21, they showed that the value of G_c fell uniformly as the interparticle distance increased, up to distances corresponding to the low levels of addition. The three tended to minimum values of G_c below 15 % ERPV. However the PSB#1 series tended towards much lower values of G_c , of the order of the PS matrix resin, 0.5 kJm^{-2} , while the PSB#2 and PSB#3 series 'levelled-out' at higher limiting values in the region of $2.25 \pm 0.25 \text{ kJm}^{-2}$. The linear variation of G_c with RPD for high volume loadings suggested the parameter modelled the materials reasonably well. The behaviour at lower levels of addition was believed to be somewhat more complicated and the differences observed were considered to reflect upon the efficiency of the particle size populations to craze and impede crack propagation.

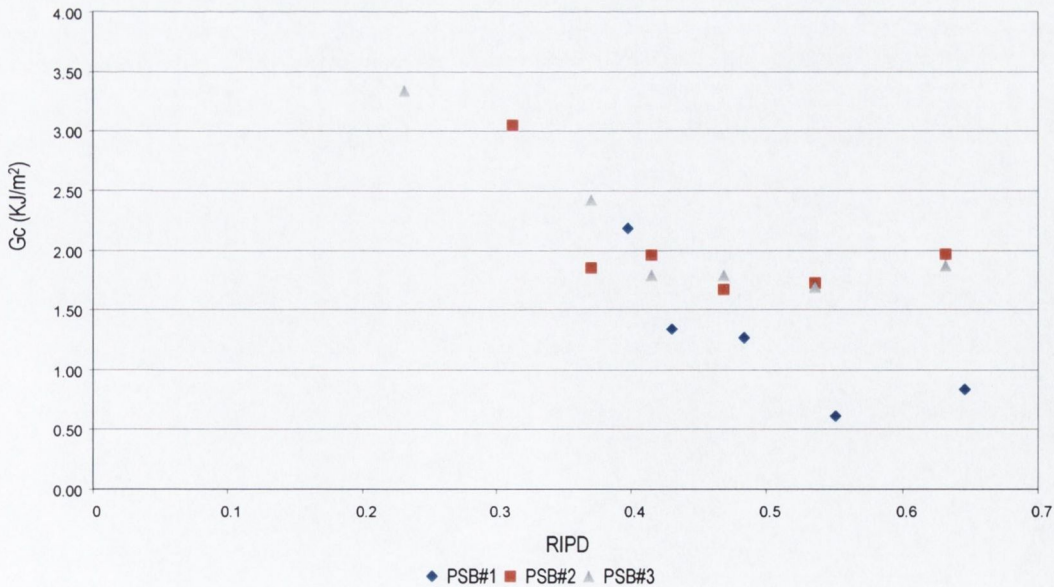


Figure 4.21. Plot of G_c vs. RIPD, PSB#1- \diamond , PSB#2 - \square , PSB#3 - \triangle .

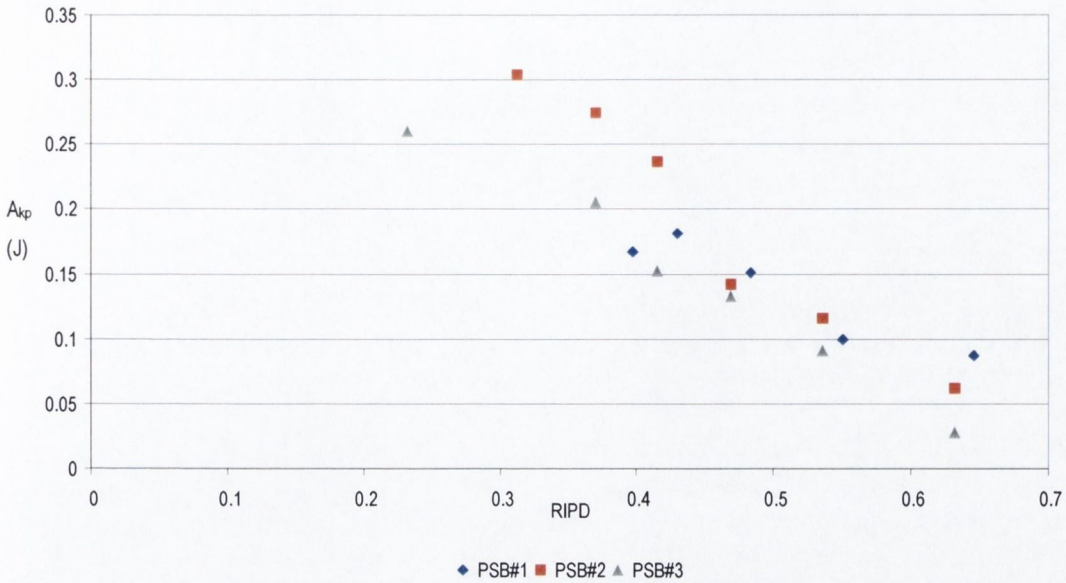


Figure 4.22. Plot of A_{kp} vs. RIPD, PSB#1 - \diamond , PSB#2 - \square , PSB#3 - Δ .

It was noted that the higher strain energy release rate values, obtained from resins containing secondary phase volumes found in conventional HIPS at low values of secondary phase addition, were similar to the values obtained for J_{Ic} from monotonic tests. They were also similar to the values determined by Lee et al for their HIPS [34].

It had been anticipated that the intrinsic toughness of the materials should tend to that of the matrix resin as the ERPV reduced to very low concentrations. This speculation was what had motivated plotting the impact toughness of the polyblends and the matrix PS impact strength as a quotient. The correlation obtained between it and the RIPD in Chapter 3 appeared to corroborate the supposition in respect of impact strength. The same correlation had been anticipated for the case of the strain energy release rate. Though the values obtained for the PSB#1 series did tend to that of the PS matrix, and so lend some credit to the speculation, the values obtained for the other series, PSB#2 and #3, were much greater and ranged between 3.5 and 4 kJm^{-2} . One explanation for this which doesn't offend the hypothesis, nor reject the veracity of the results, is offered in considering the sources of energy associated with G .

In the case of an ideal elastic system the intersection of $BD\Phi$ versus Impact strength, A_{kp} , is associated with the kinetic energy lost in the impact of the test devices 'tup' on the test specimen [1]. In a sense the parameter reflects the initial energy losses associated with applying the loading to fracture the specimen. When the values obtained for A_{kp} (kp-kinetic process) were plotted against the RIPD linear curves were obtained for each series of materials, Figure 4.22. These plots revealed that the parameter exhibited a greater correlation in RIPD than did the values obtained for G_c .

Instead of falling to a plateau value, as the values for G_c had, the fall of A_{kp} with RIPD appeared uniform over the entire range of polyblends considered, just as the impact values had. Consequently it was thought

that the measurement reflected in A_{kp} , must have provided some contribution to the impact strength. Its value should only relate to the initial dynamic elastic and plastic kinetic energy losses to the 'tup'. However the analysis of the data suggests it also included an additional contribution from the initial losses in establishing a fracture process zone (blunting) in the case of the larger particles. Figure 4.22 then reflects the sensitivity of the impact toughness to the energy contribution from the initial deformation and blunting dictated by changes in the secondary phase morphology.

As a result the plateau, and the slight recovery observed in strength below 15 % ERPV, in the results of the PSB#2 and PSB#3 series, in Figure 4.21, was considered to be an artefact introduced by 1) harmonic instabilities associated with the apparatus, 2) the non-linear responses of the materials and 3) remote deformation and crazing that was amplified by blunting or notch opening before crack initiation. Thus it reflected the effectiveness of the PSB#2 and #3 series particle size populations at diffusing stress away from the crack/notch tip throughout the specimen, even at low concentrations and not necessarily their intrinsic toughness. The values that were obtained for G_c then were not purely associated with fracture but incorporated other dynamic energy contributions, associated with specimen fixturing and remote deformation as well as blunting in the region of the notch.

Ultimately it was concluded that the test method did not yield comparable measures of G_c . In fact the differences observed suggested that it didn't provide valid measurements of G_c because conditions for LEFM did not exist. Consequently the method and the values obtained for G_c using this method were found to be unsuitable for comparing the influence of microstructure on HIPS intrinsic toughness.

4.5.2 Comment on the Results obtained for J from Monotonic Tests.

The J integral is more forgiving as a method of characterising intrinsic toughness. As described above the parameter is, in effect, a non-linear strain energy release rate. The non-linear component accommodates limited levels of plastic deformation associated with (quasi-stable) crack advance. In the experimental technique that was employed, the energy determined for crack extension, from the interpolated curves for constant crack length, effectively decoupled energy associated with fracture from energy associated with remote yield/flow.

It was noted that the general shape of the loading curves obtained for the materials were similar for each notch depth. However, in the case of the larger ligament sizes it can be seen in Figures 4.9–4.10, a PSB#1-5 test series, the 'shape' of curves did differ slightly. The difference reflects differences in the way in which the material deformed and yielded in the specimen in advance of and during crack extension. It influenced the shape of interpolated curves for constant crack length, the slope of the strain energy versus constant crack length curve, the variation of J with displacement and ultimately the values used in generating the J-R curve from the load displacement record. However the linearity of plots of J vs. displacement, e.g., Figure 4.12, showed the errors were not significant and though they affected energy measurements in the J-R curve, tending to overstate them slightly, the integrity of the technique was not undermined. The least squares fit for the slope of J also served to minimise the adverse influence of larger ligament sizes.

In Figures 4.13, 4.14, 4.15, it can be seen that the J-R curves obtained for longer ligament lengths were greater and offset from those of the shorter ligament lengths. The curvature of the plots is also more expressed as the ERPV rose in the longer ligaments than in specimens with longer notches. The curvature of the J-R curve reflects the dissipation of energy by crazing, or yielding in the ligament, which decreased as the ligament length was reduced. The energy dissipated during extensive deformation associated with the monotonic loading of specimens with large ligaments eclipsed the energy contribution associated with crack extension. In shorter ligaments < 12 mm, i.e., notch depths > 10 mm, crack growth dominated and so the energy recorded reflects that required to propagate the cracks. In the case of the latter the values of J tended to converge to a single curve. This showed that the extent or influence of remote yielding was uniform in these specimens and that the energy associated with crack extension was approaching a characteristic value for a uniform state of stress.

Thus care was taken to extrapolate the values for J_c from the lower, linear portions of the curves associated with initial crack growth in the shorter ligament lengths. The process of stable ductile tearing that accompanied crack growth allowed measurement of the J integral in rubber modified resins. It contrasted sharply with the unstable (brittle) crack growth that accompanied tests on unmodified PS. These fast-fractures made determining J_c for PS, using the experimental protocol impossible. Indeed from the practical perspective of comparison, that fracture appeared to have occurred in a plane strain stress state negated the purpose of determining the materials toughness. This was because the tests on the HIPS resins had yielded a measurement of J_c that reflected the material's plane stress toughness.

Although the values obtained for J_c in plane stress are valid and relevant for many applications they do not necessarily reflect the ranking of the materials critical intrinsic toughness, J_{Ic} , associated with plane strain. The values of J_c obtained could be used in designing parts of similar wall thickness likely to experience the loading regime. However their magnitude may fall as the volume associated with crack extension would reduce if the section thickness of parts were increased. In effect a value obtained for J_c can be considered as lying along curves that will intersect with J_{Ic} at a maximum constraint. The value doesn't facilitate a direct comparison of the intrinsic toughness of the materials as they need not necessarily experience the same level of constraint and so it may not represent equivalent measurements and so correlate with J_{Ic} .

Table 4.2 presents the values determined for the J_c of the materials. The relationship between the RIPD and the J_c obtained at the intersection of the J-R (fracture resistance curves) curves at $a = 0$ for the materials at a notch depths > 12 mm, considered to offer the most comparable data is presented in Figure 4.23. The plots were constructed from the average value of the intersection of the interpolated J-R curves with J at 0 crack length. The plots revealed there to be a strong correlation between J_c and the RIPD, as there had been with the impact data, though the relationship was not as linear and there appeared to be less difference between the toughness of the materials at equivalent RIPD. The relationship also contrasted with that observed with G_c , obtained from the $BD\Phi$ analysis of the impact data, in that the values for all three series tended to a similar value of J_c at high RIPD, or low ERPV. The value of J_c they tended to was approximately 1kJm^{-2} , interesting as it is the value regularly quoted in the literature for the plane stress toughness of the matrix resin [1,18].

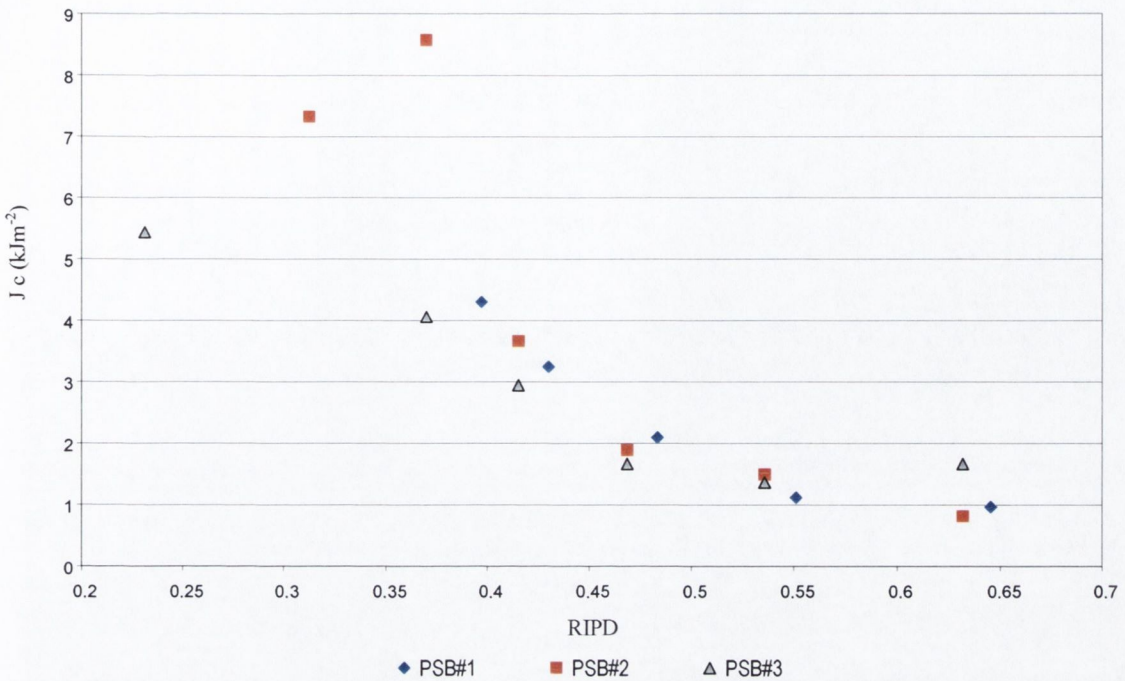


Figure 4.23. Plot of RIPD vs. J_c determined under plane stress.

The plane stress toughness of the PSB#3 series were noted to be slightly lower than those for the PSB#2, which in turn tended to be lower than those obtained for the PSB#1 series, over the range of secondary phase additions that were considered. The values did not vary greatly between the three and the ranking was consistent. This it's thought reflects the influence and efficiency of the secondary phase particles in effecting larger, and or denser, process zones in advance of the crack tip. The implication of the results is that the accumulated damage in the process zones reduced the crack growth resistance of the materials. Thus the resistance of the PSB#3 series possessing larger particles and process zones but lower density of crazing presented less resistance to crack extension than that the densely crazed PSB#2 series or the PSB#1 series who presented greater resistance due to their small process zone. The process zone extending less distance ahead of the crack conserved matrix integrity and raised the level of toughness.

However at similar levels of addition, the J_c obtained for the three series of materials were similar, indicating that the ability of the secondary phase to dissipate energy in the process zone was similar for equivalent particle distances illustrating the dominance of the ERPV in dictating material response. The effect of particle size, though less significant in determining the magnitude of J_c , did order ranking, and so, as in tensile and impact behaviour, it exhibited itself as the fundamental determining influence on behaviour. The fall in toughness levelled off for ERPV <10 %, indicating that the stress state was approaching plane stress/strain transition. That the three series tended to the same limiting toughness lended integrity to the use of the parameter in comparing material toughness.

The results also highlight the superiority of the RIPD in modelling the behaviour of the materials over parameters such as the ERPV, emphasising the importance of considering both particle size and ERPV.

4.5.3 Comment on the Results of the Essential Work tests.

The conflict experienced in determining valid and comparable measures of toughness observed in the previous two sections can be overcome in many respects through the use of the essential work approach. The physical limitations of LEFM and the conflict between material behaviour with the assumptions required for applying the J integral are overcome. The essential work theory was outlined above, Section 4.3.2.2, and its essence summarised in Figure 4.6.

The approach allows for the characterisation of the toughness over the entire range of deformation of a material. However at an experimental level there are difficulties in determining the essential work. These were encountered in this study and it is considered useful to discuss the findings as it contributes to understandings of the intrinsic strength and the results that were obtained from the other tests. The results of the essential work tests are presented in Figures 4.24-4.26 below.

The results that had been obtained by Mai et al on specimens of two HIPS resins, one a commercial resin, the second a SBR/PS polyblend, using DENT (double edge notched tests) samples, vindicated the attempt to apply the method [42]. The results obtained, according to Mai et al, were excellent for both the materials, and they agreed closely with measurements that had been made, in plane strain, by Yap and Mai et al, on 22mm HIPS samples [18]. Also the agreement obtained in DSEN and DENT tests on nylon and polyethylene demonstrated that valid comparable measurements could be obtained using either loading configuration.

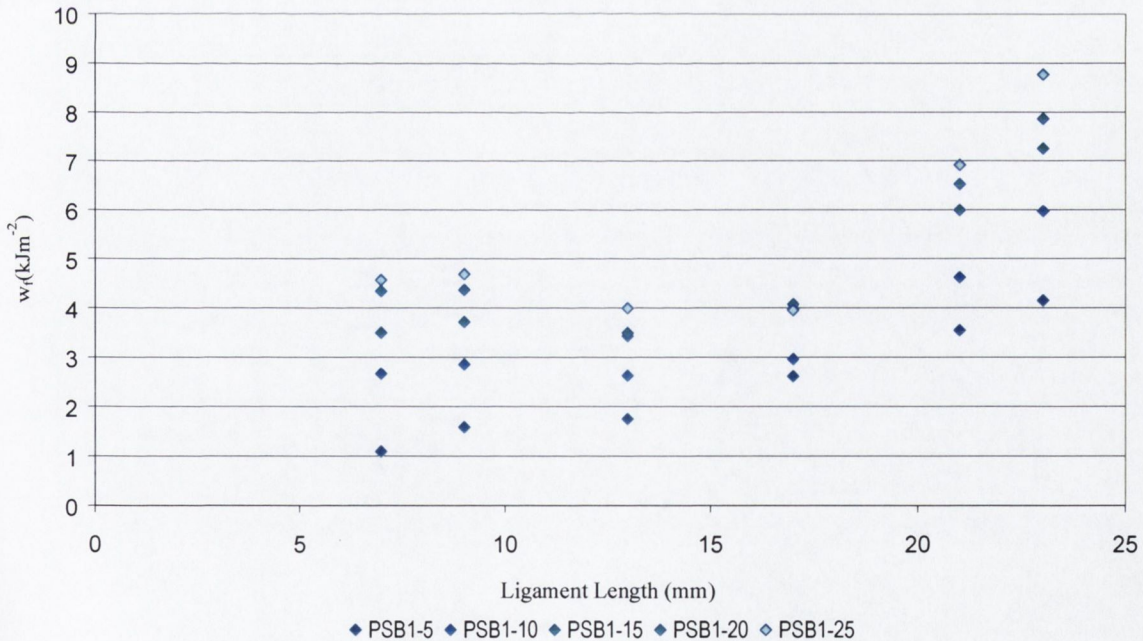


Figure 4.24. Plot of Work of fracture vs. Ligament length for PSB#1.

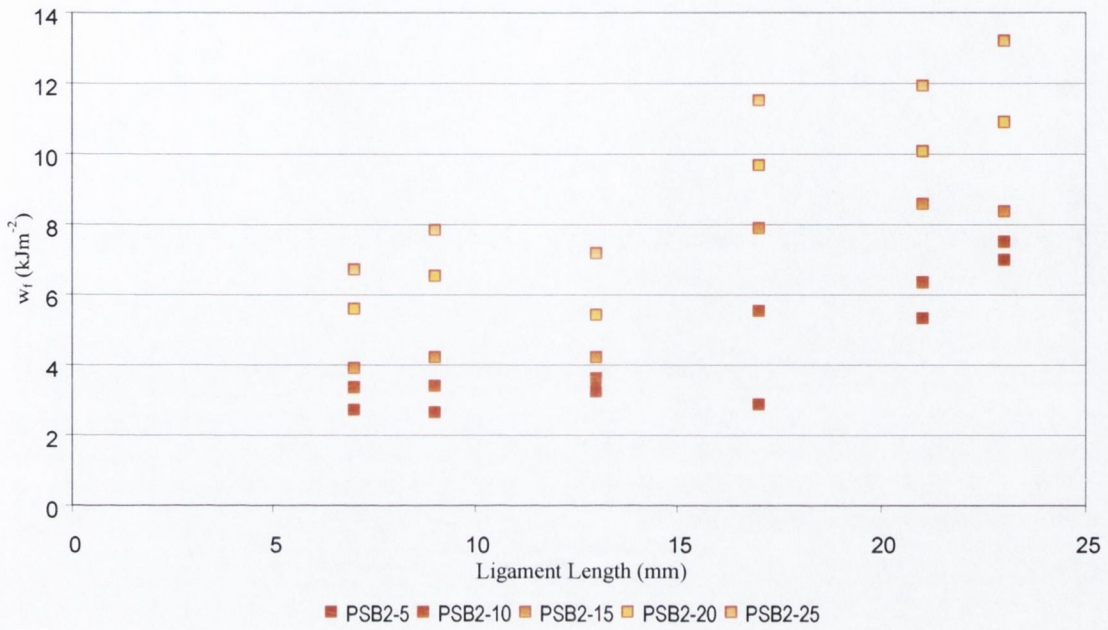


Figure 4.25. Plot of Work of fracture vs. Ligament length for PSB#2.

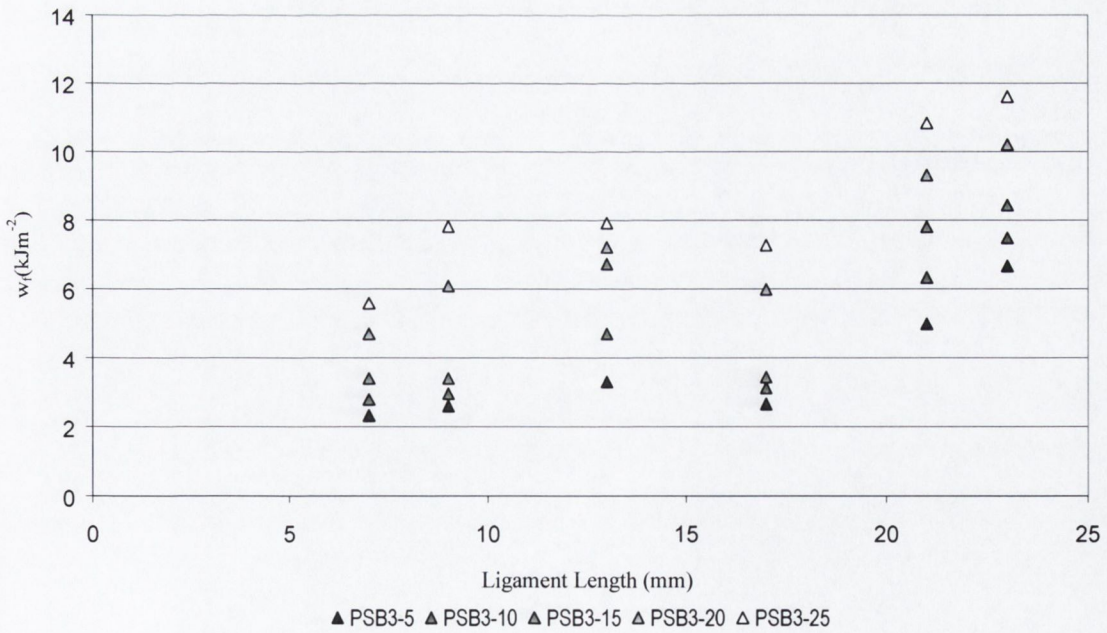


Figure 4.26. Plot of Work of fracture vs. Ligament length for PSB#3.

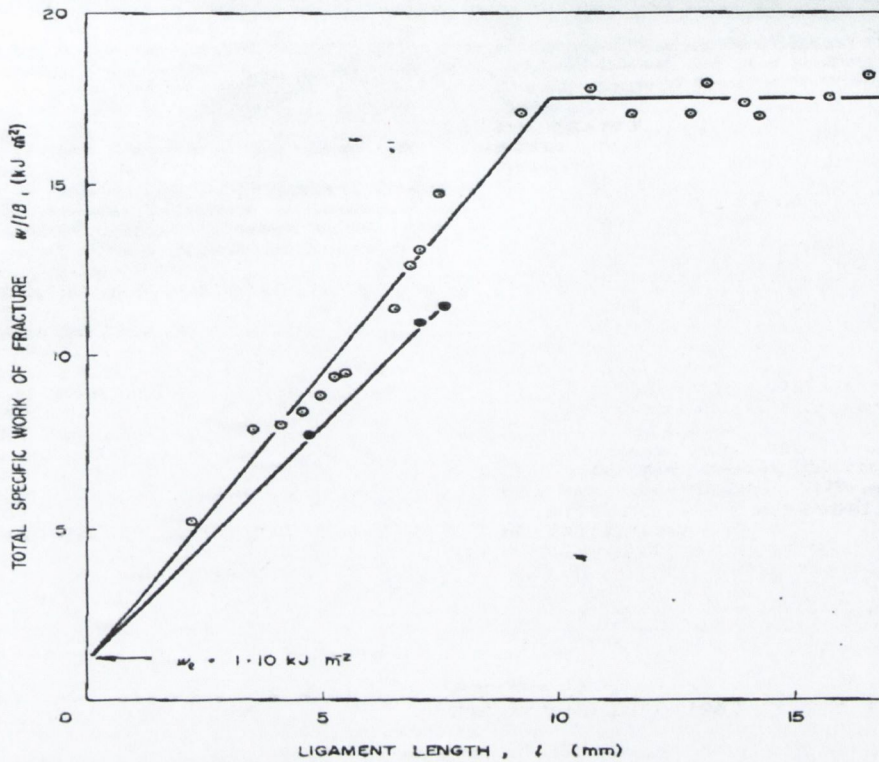


Figure 4.27. Plot of w_f versus $L(1)$ for HIPS as per Mai and Cotterell [42]

The presumption of the essential work method, and the J integral, is that the outer plastic zone, the fracture process zone, which propagates in advance of the crack front, is proportional to crack advance/ligament length [24,36]. Thus, ideally, in the plane stress essential work approach, the energy associated with fracture should be additive, proportional, and for consistent damage zone size and density, linear [42]. In the transition between plane stress and plane strain it should be non-linear. While in plane strain it should be linear and independent of thickness.

In all instances then extrapolating the energy associated with fracture to zero ligament length provides a measure of the critical work essential for crack propagation. The expectation of the essential work analysis was that a linear variation in the essential work with ligament length would produce a curve that could be extrapolated to zero ligament length to yield w_e . The slope of the curve, representing the plastic component should, ideally, have been linear. Its slope representing the shape factor, B , and a plastic energy constant, w_p , and its value proportional to ligament length. Variations in value should have been with respect to thickness and reflect the influence of constraint. As Figures 4.24 -4.26 show, this was far from what was obtained.

In the experiments characteristic stress whitened zones were observed for each series of materials. The shape of these process zones, associated with each parent resin, was consistent in every test, including fatigue tests. Their characteristic shapes are sketched in Figure 4.28. In the case of the materials studied, as was the case in Mai and Cotterell's studies (Figure 4.27), the behaviour observed was not the ideal. Instead the material in advance of the crack front crazed, lowering the in plane resistance to the advance of the crack. This increased the total energy dissipated, by involving a greater volume of material in the process of fracture.

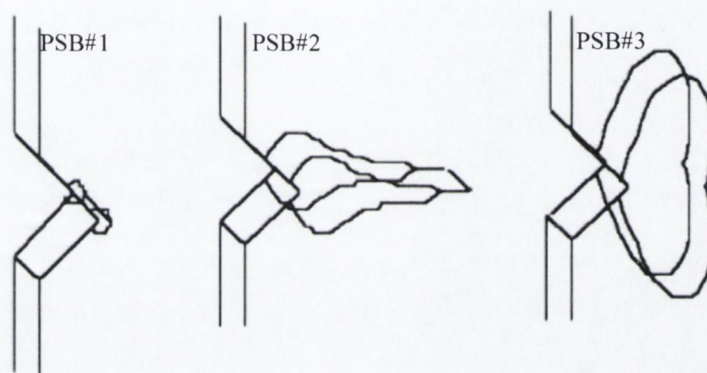


Figure 4.28. Sketches of the characteristic damage zone shapes for the three resin series.

In the tests instead of a linear response, a curvilinear response was observed. The values for the essential work fell initially, with decreasing ligament width. Then at approximately 12-13mm, they appeared to increase slightly in value before they fell again at shorter lengths. In longer ligaments variable, partial, or incomplete, yielding preceded crack propagation and resulted in relatively higher levels of energy being absorbed in crack propagation. As ligaments grew shorter the amount of yielding reduced, more complete yielding prior to crack initiation was considered responsible for the slight increase in shorter ligaments.

The results presented, combined with the observations made from the results of the J integral analysis and during tests, show that crack growth through the material was stable. The volume of material involved in fracture can be considered to have been in a (relatively) uniform state of (pseudo) plane stress though the extent to which yielding could occur was limited by the volume of material that could yield in the short ligament. Consequently the energy absorbed in crack advance could be considered to have been additive and crack tip specific (in breaking down and coalescing the pre-crazed material). In the case of longer ligaments the energy, associated with crack growth, was eclipsed by the magnitude of remote yielding.

If it is concluded that the specimens were in self-similar states of stress and the energy measurement was crack tip specific the method used to determine J may be seen as having provided for the separation of specific and non-specific contributions to crack advance. In this sense the results corroborate the findings made in the previous section. Thus the measures of J determined for each of the materials provide a valid measure of toughness. In this instance then we may conclude that the J_c measured in the previous section was in fact equivalent to w_e , even though w_e could not be determined directly from the essential work (w_f) analysis of the data.

4.5.4 Comment on the results of J integral measurement of J' from Fatigue tests

Low level cyclic loading facilitates the consistent imposition of conditions approaching plane strain and may do so for any geometry or wall thickness, i.e., under low levels of applied cyclic loads, with $R=0$, conditions approaching plane strain exist near the tip of propagating cracks. The fatigue based method for characterising toughness employed in this study was first employed to characterise the intrinsic toughness of toughness (J_{1c}) of polyethylene by Strebel and Moet [42].

There are theoretical reservations in applying the term 'J integral' to describe the energy release rate associated with a fatigue crack propagation. However as Strebel, Moet and others have pointed out, there are instances where many defining assumptions of the J integral are neglected in testing plastics, even when the standard protocols are applied. It could be argued that, for many materials determining J_{1c} from fatigue test data, or hysteresis curve analysis, is less offensive to the practical interpretation of the J integral than the conventional methods. In some respects determining J_{1c} from fatigue could be considered as superior, e.g., it effects measurement of material toughness in a state of quasi-stable crack growth in plane strain, it extrapolates J_{1c} from direct measurements of J and it does not involve interrupting crack growth.

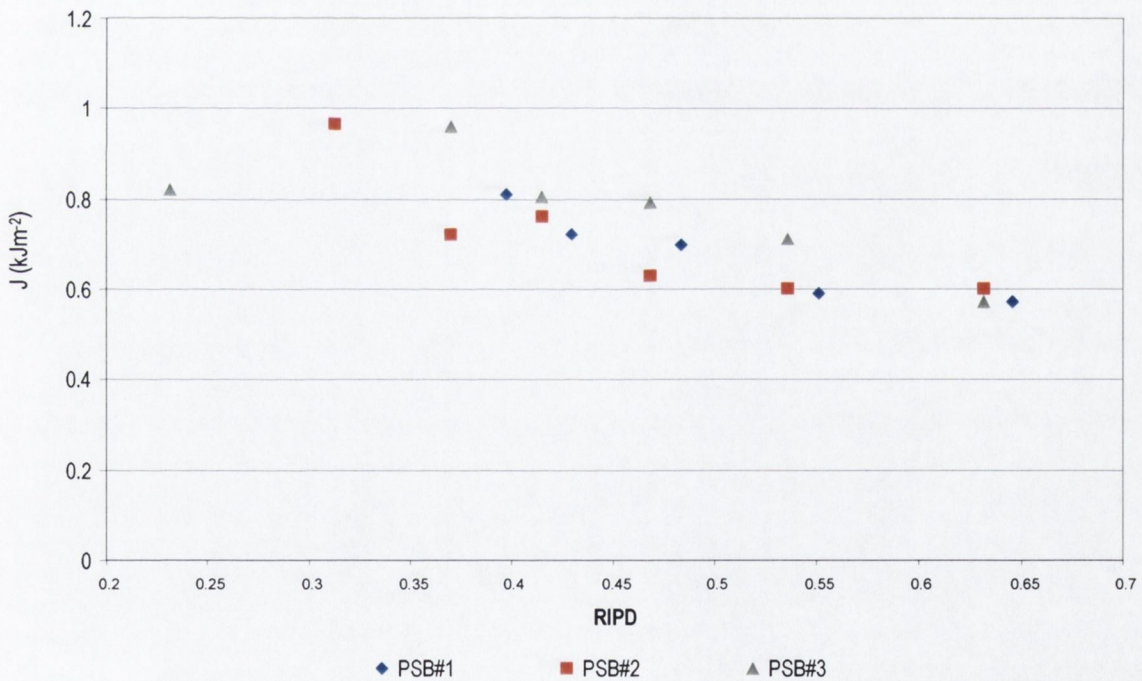


Figure 4.29. Plot of J'_{1c} determined from fatigue vs. RIPD.

In Figures 4.18-20 the variation of J'_{1c} , with 'a' is presented for each of the three parent resin series at 5, 15 and 25 %ERPV. The values obtained for J'_{1c} for all of the polyblends from the fatigue tests are presented in Table 4.3. These values are averaged from the results of three tests. The variation of J'_{1c} with RIPD is presented in Figure 4.29. In all of the polyblends, despite the maximum load about the notch being less

than half the yield stress of even the weakest resin, crazing did occur, eventually. However, initially it was very limited. At the time incipient cracks formed (cracks were considered to have initiated when they reached a length of 1 mm) it was considered that the level of crazing represented the minimum associated with crack growth, i.e., under the specific geometry and loading regime applied. How closely this minimum level of crazing reflected the conditions of plane strain in early stage crack growth can only be surmised by comparing the results obtained for all of the materials. The range of values over which their toughness varies suggests that it was very close.

The amount of crazing increased with continued cycling, crack extension occurred under a falling level of constraint, in the presence of more profuse crazing. Throughout the test the change in energy associated with crack extension measured reflected that required to propagate a crack of unit length through the crazed matrix polystyrene. Its value was equivalent to the cumulative energy lost to the system (-PE) in establishing the damage but independent of the total energy 'cycled' into the system ($\Sigma F \cdot \delta \epsilon \delta \tau$, where F is force, ϵ is strain and τ is time) over time to create this damage. As crack lengths exceeded ≈ 5 mm the energy associated with crack growth through material that had already yielded facilitated a larger pseudo plastic response, and eclipsed the energy associated with driving the crack through 'uncrazed' material. The different J_c 's, obtained from fatigue and monotonic fracture toughness tests, reflect the difference between, energy required purely to drive a crack forward through constrained and unconstrained, or pseudo-plastically yielded material, i.e., between conditions approaching plane strain and conditions akin to plane stress. That the data from each series appeared to converge to single values of toughness, of $\approx 0.5 \text{kJm}^{-2}$ and $\approx 1.0 \text{kJm}^{-2}$ respectively, as RIPD increased, indicated consistent levels of constraint were achieved in both tests.

In both J integral tests the two energy contributions, i.e., that associated with crack tip specific and that associated with remote deformation, are embodied in the energy loss measurements. In the load controlled fatigue tests, the energy contribution associated with small scale plastic yielding, local to the crack tip (characteristic of the intrinsic toughness), is separated from the contribution of remote flow by only considering growth associated with small zone size in extrapolating J_c .

The difference between the values of toughness measured from the fatigue tests for the three series was not great. However the ranking of material toughness determined from fatigue, under conditions that were considered to approach maximum constraint, was the opposite to that obtained from the monotonic tests. In the case of the latter the PSB#3 series tended to exhibit the lowest toughness. However when toughness was determined under fatigue testing they exhibited the highest toughness. The PSB#2 series exhibited the lowest level of intrinsic toughness in fatigue, yet they appeared to be tougher than the PSB#3 series under monotonic tests indicating their propensity to form crazes at lower stress levels served to facilitate crack extension.

The results thus illustrate the competitive process of failure and how subtle changes in morphology effect significant differences in response and the complexity this introduces to the design of HIPS materials. The ease with which the PSB#2 particle size population craze and craze in greater density, allows them facilitate a more extensive pseudo-plastic plastic response that resists crack growth in pseudo-plane stress

state. Yet their efficiency at crazing is also responsible for their lower intrinsic toughness under conditions of elevated constraint.

The agreement between the three series and the energy associated with the brittle matrices toughness suggested implied that the incorporation of the secondary phase in HIPS only marginally, alters the intrinsic toughness of the materials, an observation supported by the findings of Mai and Cottrell [18]. Determining comparative values of toughness is an important element in understanding the relationship between the influence of the secondary phase morphology on toughness and fatigue strength. Differences ranging from 1.0kJm^{-2} – 4.0kJm^{-2} have been obtained for HIPS intrinsic toughness over the years. This is the first study to have been conducted to consider the influence of the secondary phase on intrinsic toughness.

4.6 Conclusions

4.6.1 Strain Energy Release Rate determined from analysis of impact test data

- The findings of the strain energy release rate (G_c) analysis, based on impact specimen test data found the value of G_c tended to a limiting value of $1.7 - 3.3 \text{kJm}^{-2}$ for the case of the PSB#2 and PSB#3 series of resins. In the case of the PSB#1 series the value of G_c tended to the value for PS (0.9kJm^{-2}).
- It was concluded from the results that the technique used to determine G_c yielded valid measurements of G_{1c} for polystyrene. However, variable levels of constraint prevented obtaining comparable measurements of G_c for the HIPS polyblends.
- It was concluded that applying LEFM analysis to standard ASTM and ISO impact test specimens is not an appropriate way in which to determine comparable measures of intrinsic toughness for HIPS materials.
- The different levels of correlation between G_c and A_{kp} with RIPD, suggests that a significant component of the impact toughness measurement is comprised of energy lost in the initial deformation of specimens and not the actual process of fracture. This it's thought undermine the veracity of the impact test as a means of comparing the intrinsic toughness of HIPS resins.

4.6.2 J Integral determined from analysis of Monotonic Tensile Fracture Tests.

- Monotonic tensile fracture tests, employing SENT specimens, provide a practical means of determining comparative measurements of the J integral of HIPS in conventional wall thickness. In the case of such section thickness the method realises practical measurements of J_c .
- The results show that the J_c for the three series of resins decreases with increasing RIPD. The PSB#2 series, whose particle size population is most efficient in promoting crazing exhibited the greatest plane stress toughness, whilst the PSB#3 whose particle population is least effective at promoting crazing exhibited the lowest values of J_c . But it is noted that these differences were small.

- While the J_c determined in the tests is considered to be valid, and comparable for the thickness considered the pseudo-plastic process of deformation and variable levels of constraint suggest that it is not a suitable parameter for considering the intrinsic toughness of the materials.

4.6.3 Essential work analysis

- The finding of the essential work analysis was that it is not possible to determine the plane stress or plane strain essential work of fracture of HIPS using SENT specimens (in the thickness considered).
- The observations made during the essential work studies support the findings of the J integral results in that the separation crack tip specific and non specific energy in the J integral tests yielded values that are equivalent to w_e .
- The observations made during the tests and the monotonic J integral tests suggest employing DENT (double edge notched tensile) specimens, of appropriate ligament lengths and thickness', will yield a valid w_e for plane stress and strain.

4.6.4 J Integral determined from analysis of Fatigue Crack Propagation.

- It was concluded that fatigue tests provide a means to determine comparable intrinsic fracture toughness parameters, approaching the plane strain toughness J_{1c} , from specimens possessing through thickness dimensions similar to those used in conventional parts.
- The results show that the J_{1c} for the three series of resins falls with increasing RIPD tending to the intrinsic toughness of polystyrene at very low concentrations of secondary phase volume.
- The PSB#2 series, whose particle size population is most efficient in promoting crazing consistently exhibited lower values of J_{1c} , whilst the PSB#3 series exhibited the highest values. But these differences were small.

4.6.5 General Conclusions on the Characterisation of Fracture Toughness in HIPS.

- The particle size and/or particle size distribution effects a primary influence on the elevation of toughness with increasing secondary phase volume. The finding of this work is that these variations are best expressed in terms of RIPD.
- The effective rubber phase volume effects greatest control over the magnitude of the toughness of HIPS materials
- The more efficient a secondary phase particle size population is at promoting crazing while increasing its impact and plane stress toughness will serve to lower the intrinsic plane strain toughness of a material.

- The ranking of HIPS resins varying in ERPV and RPS by impact toughness does not correlate with plane stress or plane strain toughness.
- The plane stress toughness of HIPS resins may be characterised for the purposes of comparison and design using conventional wall thickness by the J integral.
- The plane strain intrinsic toughness of HIPS resins may be characterised by the direct interpretation of J from fatigue tests.
- Impact tests do not provide for an appropriate basis for the characterisation or comparison of the intrinsic toughness of HIPS resins

4.7 References

- 1 WILLIAMS, J.G., *Fracture Mechanics of Polymers*, Ellis Horwood, 1987.
- 2 GRIFFITH, A.A., *Phil. Trans. Roy. Soc.*, A221, 163, 1921.
- 3 GRIFFITH, A.A., *Proc. 1st Int. Conf. Appl. Mech.*, 55, 1924.
- 4 INGLIS, C.E., *Trans. Inst. Naval. Arch.*, LV, 219, 1913.
- 5 OROWAN, E., *Rept. Prog. Phys.*, 12, 214, 1949.
- 6 IRWIN, G.R., *J. Appl. Mech.*, 24, 361, 1957.
- 7 WESTERGAARD, H.M., *J. Appl. Mech. Trans. ASME*, 6,A49-A53,1939.
- 8 TADA, H., PARIS, P.C., IRWIN, G.R., *The Stress Analysis of Cracks Handbook*, Del research Corp. St. Louis, Missouri, USA, 1985.
- 9 SURESH, S., *Fatigue of Materials*, Cambridge University Press, 1998.
- 10 IRWIN, G.R., *Proc. 7th Sagamore Conf.*, IV, 36, 1960.
- 11 DUGDALE, D.S., *J. Mech. Phys. Solids*, 8, 100, 1960.
- 12 DOLL, W., Ch. 10, *'Fractography & Failure Mech.'s of Polym.'s and Comp.'s'*, Elsevier, 1989.
- 13 MUSHELISHVILI, N.J., *'Some Basic Problems in the Mathematical Theory of Elasticity*, Groningen, Noordhff, 340, 1953.
- 14 GOODIER, J.N., FIELD, F.A., *Fracture of Solids*, J. Wiley, N.Y., 1963.
- 15 MORGAN, G.P., WARD, I.M., *Polymer*, 18, 87, 1977.
- 16 DOLL, W., KONCZOL, SCHINKER, M.G., *Coll. Polym. Sci.*, 259, 171, 1981.
- 17 KRAMER, E.J., HART, E.W., *Polymer*, 25, p.p. 1667, 1984.
- 18 YAP, O. F. , Y. W. MAI, & B. COTTERELL, *J. Mater Sci* 18, 657-668: 1983.
- 19 LU, M-L, CHIOU, K-C, CHANG, F-C, *Polymer*, 37, 19, 4289, 1996.
- 20 ESHELBY, J.D., *Solid State Phys.*, 3, 79, 1956.
- 21 SANDERS, J.L., *J. Appl. Mech.*, 27, 289, 1960.
- 22 RICE, J.R., *J. Appl. Mech.*, 35, 379, 1968.
- 23 CHEREPANOV, G.P., *Int. J. Solids and Structures*, 5, 863, 1969.
- 24 BEGLEY, J.A., LANDES, J.D., *Fracture Toughness*, ASTM STP 514, ASTM, p.p.1, 1972.
- 25 *Standard Test Method for J_{1C}, A measure of Fracture Toughness*. ASTM, Designation: E 813 - 81.
- 26 ZHOU, Z., LANDES, J.D., *Polym. Eng. & Sci*, 34, 2, 129, 1994.
- 27 JIANG, Z., YIN, J., LIU, W., et al. *Polym. Comm.*, 32, 14, 423, 1991.
- 28 CHANG-BING, L., LU, M-L., CHANG, F-C., *J. Appl. Polym. Sci* , 47, 1867, 1993.
- 29 NARISAWA, I., TAKEMORI, M.T., *J. Polym. Eng & Sci*, 28, 22, 1462, 1988.
- 30 HASHEMI, S., WILLIAMS, J.G., *J. Polym. Eng. & Sci.*, 26, 11, 760, 1986.
- 31 HA,C-S., KIM,Y., CHO, W-J. *J. Appl. Polym. Sci*, 51, 1381, 1994.
- 32 CROUCH, B. A., HUANG, D.D., *J. Mat. Sci*. 29, 861, 1994.
- 33 NARISAWA, I., TAKEMORE, M.T., *J. Polym Eng & Sci*, 29, 10, 671-677, 1989.
- 34 LEE, C-B, LU, M-L, CHANG, F-C, *J. Appl. Polym. Sci* , 47, 1867, 1993.
- 35 LEE, C-B., LU, M-L., CHANG, F-C., *J. Appl. Polym. Sci* , 47, 1867, 1993.
- 36 BROBERG, K. B, *Int. J. of Fracture*, 4, 11, 1968.

-
- 37 MAI, Y-M., COTTERELL, B., HORLYCK, R., et al, Polym. Eng. & Sci., 27, 11, 1987.
 - 38 COTTERELL, B., SIM, M.C, AMRUTHARAJ, G., et al, J. Mat. Sci., 31, 291, 1996.
 - 39 HASHEMI, S., O' BRIEN, D., J. Mat. Sci., 28, 3977, 1993.
 - 40 MAI, Y. M., COTTERELL, B., HORLYCK, R., VIGNA, G., Polym. Eng & Sci., 27, 11, 1987.
 - 41 MOUZAKIS, D.E., STRICKER, F., MULHAUPT, R., J. Mat. Sci., 33, 2551, 1998.
 - 42 MAI, Y.W., COTTERELL, B., Int. J. of Fracture, 32, 105, 1986.
 - 43 STREBEL, J.J., MOET, A., J. Appl. Polym. Sci, 52, 1815, 1994.
 - 44 CHAN, M.K.V., WILLIAMS, J.G., Int. J. of Fracture , 145, 1983.

Chapter 5

Fatigue Crack Growth in HIPS

The Influence of the Secondary Phase on Fatigue Crack Resistance

5.1 Preface

Fatigue as a design criterion only came of age in the last century. Although the fatigue behaviour of HIPS has been considered generically, the influence of the secondary phase morphology on fatigue behaviour has not been investigated. This is unsurprising as the knowledge has only found purpose in recent years, when, increasingly, HIPS has become employed in more demanding applications. The latter trend has advanced expectations of the material and motivated manufacturers to develop materials optimised for this aspect of performance. With fatigue becoming a design consideration, if not a critical criterion, in selecting a polymer for many applications and with manufacturers attempting to customise materials for optimum performance the importance of understanding the influence of microstructure is clear. The following chapter introduces fatigue, previous studies of fatigue in HIPS and the findings of the research conducted concerning the influence of the secondary phase morphology on fatigue in HIPS.

5.2 Contents

Fatigue Crack Growth in HIPS	146
5.1 Preface	146
5.2 Contents	146
5.3 Introduction	147
5.3.1 A Brief History of Fatigue.	147
5.3.2 Fatigue as a Design Criterion in HIPS applications; The Need for Research.	148
5.3.3 The Mechanical Response of HIPS to Cyclic Loading.	149
5.3.4 Comparison of the Fatigue lives of Un-notched HIPS and PS.	151
5.3.5 Thermal effects in un-notched testing of HIPS.	152
5.3.6 The influence of mean stress on fatigue life of HIPS.	153
5.3.7 The Influence of Surface Topography on Fatigue Life in HIPS.	154
5.3.8 Influence of test frequency on the Fatigue Life of HIPS.	155
5.3.9 Characterising Fatigue Crack Growth using Fracture Mechanics.	156
5.3.10 Comparison of Fatigue Crack Propagation in Polystyrene and HIPS.	162
5.3.11 The Influence of Mean Stress on FCP in HIPS.	163
5.3.12 The Influence of Test Frequency on FCP rates in HIPS.	163
5.3.13 FCP rates in Toughened Thermoplastics.	164
5.3.14 Applications of HIPS involving Fatigue	166
5.4 Experimental	166
5.4.1 Introduction.	166
5.4.2 Experiment Materials and Equipment.	167
5.4.3 Equipment	168
5.4.4 Experimental Procedure	169
5.5 Results and discussion	170
5.5.1 Micro-Mechanism of FCP in HIPS.	170
5.5.2 Micro-deformation Processes Involved in the Micro-mechanism of FCG in HIPS.	173
5.5.3 Influence of Morphology on Fatigue Damage Accumulation in HIPS	175
5.5.4 Influence of the Secondary Phase Morphology on Fatigue Life	180
5.5.5 Evaluating the kinetics of fatigue crack growth using the Paris Law.	183
5.5.6 Modelling Fatigue Crack Propagation in terms of ΔI .	191
5.6 Conclusions	197
5.6.1 Concerning Fatigue Crack initiation and propagation from Microscopy.	197
5.6.2 Concerning Fatigue Life.	197
5.6.3 Concerning Fatigue Crack Propagation.	198
5.7 Appendix 5.1: Data Acquisition and Signal Conditioning System	199
5.8 Appendix 5.2: Data Acquisition program 'CAPTURE' source code C++	200
5.9 References	211

5.3 Introduction

5.3.1 A Brief History of Fatigue.

Fatigue, from Latin, '*fatigare*' has, since 1839 been accepted as the term for the damage and fracture of materials under repeated or cyclic loading [1]. The majority of failures in machinery and structural components can be attributed to fatigue processes. These 'fatigue failures' may take many forms, mechanical fatigue, creep fatigue, thermo-mechanical fatigue, corrosion fatigue, rolling contact and fretting fatigue. Each of them can be linked to distinct mechanisms, distinguished by the manner in which force is applied and the nature of the ambient environment.

Research on metal fatigue dates back to the early part of the 19th century, a German engineer, W. A. J. Albert, often being accredited as the first researcher in the field [2]. The advent of the railways and the industrial revolution fuelled further research by Braithwaite and Woehler [3,4]. Woehler introduced the concept of a fatigue endurance limit and characterised fatigue behaviour in terms of S-N curves [4]. By 1874, Gerber was developing methods for fatigue design, including methods for fatigue life calculations [5]. Bausinger confirmed much of Woehler's work and popularised the notion that the elastic limit under repeated loading was different to that observed under monotonic deformation [6]. Basquin proposed empirical laws to characterise fatigue endurance of metals [7]. Bairstow contributed much to the early understanding of cyclic hardening and softening in metals [8]. Investigations by Palmgren led to the development of damage accumulation models [9]. By the end of the 1920's fatigue had evolved into a major field of scientific research.

Early theories regarding the mechanisms of fatigue failure in metals postulated that their weakening and eventual failure, under repeated loading, was a consequence of a crystallisation process within their microstructures. The work of Ewing and Humphrey ended such speculation and showed that fatigue failure occurred through the slow growth of microscopic flaws [10]. Micrographs they took of the fracture surfaces of a high purity polycrystalline Swedish iron showed evidence of slip bands. The work of Inglis and Griffith laid the foundations for quantitative treatments of fracture [11,12]. Irwin showed the amplitude of the stress singularity at a crack tip could be expressed in terms of a scalar quantity, the stress intensity factor, K [13]. Paris, Gomez and Anderson, related the advance of the fatigue crack per cycle to the range of the stress intensity factor ΔK [14]. Forsyth and Ryder correlated the distance between fatigue striations with crack growth [15]. With the assistance of new technologies and a revived interest, spurred by the developments in linear-elastic and elasto-plastic mechanics, research in fatigue flourished throughout the 1960's.

The major appeal of LEFM is the concept of similitude, i.e., that the stress intensity factor range, calculated from the geometry and loading conditions in a cracked component can uniquely characterise fatigue crack propagation, such that for an increase in the stress intensity factor range there is a commensurate increase in the fatigue crack growth rate. Its virtue as a method is that while it describes the process of fatigue crack growth it does not require a detailed knowledge of the mechanisms of

fatigue fracture. However, Elber showed that fatigue cracks could remain closed, even under cyclic tension loading [16]. Extending from the subsequent research into crack closure has been the realisation that the concept of similitude, so implicit in LEFM, is invalid. What researchers found was that the rate of fatigue crack growth is not only affected by the imposed ΔK , but also, by prior loading history and crack size. Consequently a significant fraction of research has since concentrated on the study of the crack closure phenomenon and crack size effects in fatigue failure [17].

Research of the fatigue behaviour of polymeric materials is more recent. The earliest review on the matter was published by Dillon in 1950 [18]. However in the past forty years a large quantity of work has been published. The function of the present discourse is to present a brief overview of the current understandings of fatigue in HIPS. As would be appreciated, in view of the vast amount of information published on the subject, a complete survey of fatigue in plastics would be impractical and beyond the scope of this work. Therefore, the subject will be broached by developing brief discourses on specific topics, which could be perceived as being, the elements of fatigue research relevant to the experimental work of this project. In so doing, reference to the literature is necessarily selective and perhaps as a consequence biased. However, a balanced and representative presentation is hopefully achieved. For a greater appreciation of the subject of fatigue in plastics the reader may consult a number of reviews that have been published over the past two decades by Hertzberg (1980), Sauer and Richardson (1980), Sauer and Chen (1983), Kausch (1987), and Takimori (1990) detailing the experimental, phenomenological and theoretical aspects of the research in more depth [19, 20,21,22,23].

5.3.2 Fatigue as a Design Criterion in HIPS applications; The Need for Research.

How the compliant secondary phase morphology in rubber toughened polystyrene effects and affects tensile and impact toughness has been considered, see Chapter 3. The research, despite some shortcomings, has been of practical significance to HIPS manufacturers in enabling them to prepare resins whose structures are tailored, or optimised, to realise specified material properties for customers.

The attention by researchers to the influence of the rubber phase morphology on fatigue in HIPS has not been as extensive as that applied to the tensile and impact behaviour. The oversight is unusual in view of the type of markets and applications the material increasingly finds use in, e.g. vacuum cleaner casings, refrigerator linings, various small appliances and automotive components. This is because in these and indeed most other applications, failure is most likely to be the outcome of multiple loadings rather than a single impact or monotonic loading event.

The published work that has considered fatigue in HIPS has done so in a generic fashion comparing the behaviour of the toughened resin with that of polystyrene or other rubber reinforced thermoplastics. Some researchers have considered the effects of modifying the rubber phase in other toughened materials, e.g., the effect of rubber content in rubber modified PVC and ABS [24,25]. However no articles have been published that consider the influence of these morphological characteristics on the fatigue lifetime or crack growth phenomena in HIPS.

With fatigue's increasing relevance as a design criterion for product designers aspiring to use HIPS and so to HIPS manufacturers wishing to broaden their materials market share, it's easy to appreciate the growing importance of understanding how changes in rubber phase morphology influence fatigue behaviour and how it may be optimised for fatigue performance. The findings of the following work then while most relevant to HIPS also contribute to understanding how other similarly modified thermoplastic and thermoset polymer resins can be characterised and constructed for fatigue.

5.3.3 The Mechanical Response of HIPS to Cyclic Loading.

Under monotonic tensile and impact loading at room temperature crazing is seen as being the dominant micro-mechanism of deformation, controlling monotonic deformation and fracture in HIPS [26,27]. This appears to be the case under conditions of cyclic loading at room temperature also.

Studies by Bucknall showed that when the material was subject to repeated tensile loadings it exhibited significant hysteretic losses, with each successive loading event [28].

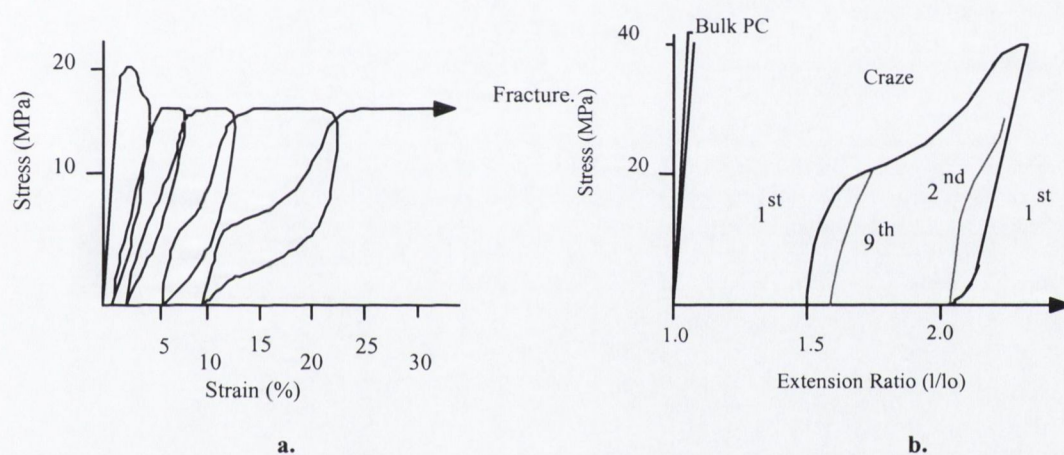


Figure 5.1. a. The cyclic Stress-Strain behaviour of a HIPS resin @21 °C illustrating the increasing hysteresis loss with successive loading due to crazing [28].
b. The stress-strain response of bulk polycarbonate and that of an individual craze and the stress strain response of the craze upon the 2nd and 9th reapplication of load [29].

The shape of the hysteresis loops obtained by Bucknall (Figure 5.1.a.) resemble those observed for a single polycarbonate craze by Kambour and Kopp (Figure 5.1.b.) [28,29]. The stress strain response is typical of crazing, initially the material exhibits a high secant modulus typical of the matrix, which, on further extension, initially falls as the material crazes and yields. It then rises again as molecular orientation causes macromolecules in the craze fibrils to align and 'strain harden' [26]. Upon unloading the materials exhibit considerable viscoelastic recovery mapping out a large hysteresis curve. These observations, and the fact that very little change was observed in the specimen's cross-sectional area, inferred crazing dominated damage accumulation in the material under cyclic loading (See Chapter 3).

Further work by Bucknall and Stevens, comparing the mechanisms of fatigue damage accumulation in ABS and HIPS corroborated Bucknall's earlier interpretation (see **Figure 5.2.**)[30]. The work showed that the response of HIPS contrasted sharply with that of ABS resin in which strain softening was mainly effected through the process of shear yielding (see Chapter 3.).

The hysteresis loops obtained at intervals, from fully reversed loading cycles, throughout the low cycle fatigue life of HIPS showed that hysteresis losses were higher and values of secant moduli were lower in the tension half of the loading cycle than in compression. The shape of the loop in tension they considered as typical for a 'crazed' material. The material's response under compression loading was explained by the modulus of the material approaching that of the unmodified polymer as crazes closed.

However as closure could not restore the material to its original condition, on reapplication of a tensile load existing crazes enlarged and new crazes were formed which resulted in a fall in the secant moduli and an increase the hysteresis loss in the tension half of the loading cycle. Thus, the increase in the hysteretic loss accompanying each successive loading was observed to be cumulative.

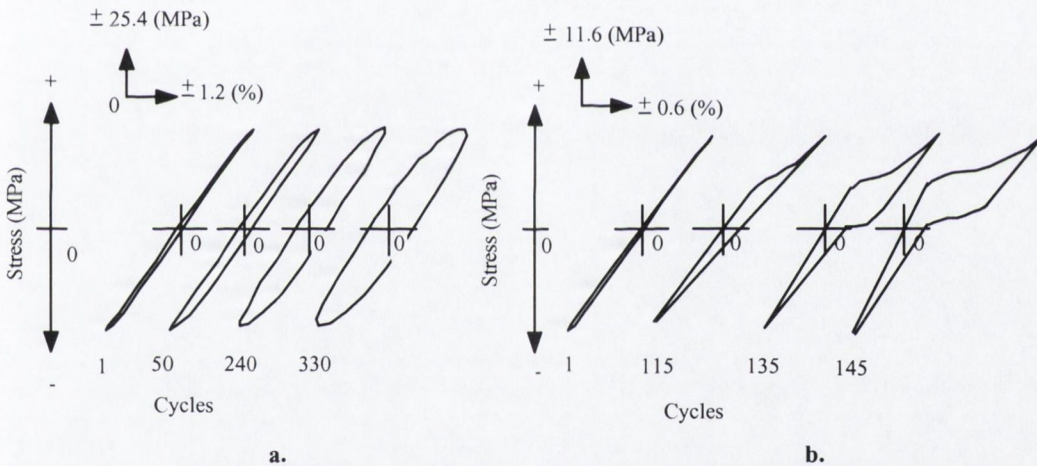


Figure 5.2. Diagrams illustrating the different responses of **a.** ABS and **b.** HIPS materials observed by Bucknall and Stevens at various test intervals [30].

In contrast the hysteretic losses in the tensile and compressive halves of the alternating loading cycle in ABS were similar as were the magnitudes of their secant moduli, this being what would normally be anticipated in a material where shear yielding dominates (**Figure 5.2.**).

The volume of specimens of both materials, was also monitored during testing. The changes in volume that accompanied the increase in hysteretic loss, confirmed the deduction drawn from the hysteresis curves. In HIPS, where dilatational crazing dominated, large increases in volume accompanied the increase in hysteresis loop area. In ABS, where some crazing did occur, the deviatoric process of shear

yielding was dominant, and increases in volume were moderate. The results illustrated crazing as the solitary process of plastic deformation in HIPS.

Sauer and Chen conducted similar tests comparing the hysteresis loss of a rubber modified and homogeneous polystyrene [31]. Though crazing also dominated the process of damage accumulation in polystyrene little apparent difference in the hysteresis loop shape was observed between specimens tested using an alternating stress amplitude of 24.1 MPa at a frequency of 0.2 Hz. Tests conducted at a frequency of 0.02 Hz and a $\Delta\sigma$ of 17.2 MPa also showed no detectable hysteresis loss up to the final catastrophic cycle, though a reduced number of cycles to failure were recorded. In the case of HIPS tested at a $\Delta\sigma$ of 17.2 MPa and a frequency of 0.2 Hz changes in hysteresis loss similar to that observed by Bucknall and Stevens were observed. The localised nature of crazing in the homogeneous polystyrene, compared to the extensive crazing experienced in HIPS, was thought to account for the lack of change observed in the PS hysteresis curves. Thus the differences observed between the hysteresis loops of the PS and the HIPS were seen as further evidence of the critical role played by the rubber phase in effecting crazing in greater volume and density which allowed more energy absorption to occur in HIPS. In tests conducted on HIPS under the same $\Delta\sigma$ but at a different test frequency, i.e. 0.02 Hz, an increase in the hysteresis loss accumulated under each loading excursion was noted as well as a reduction in the number of cycles to failure (N). The suggestion being that the reduction in the number of cycles to failure at the lower frequency was the consequence of an increased creep component affected through a greater integrated time under load.

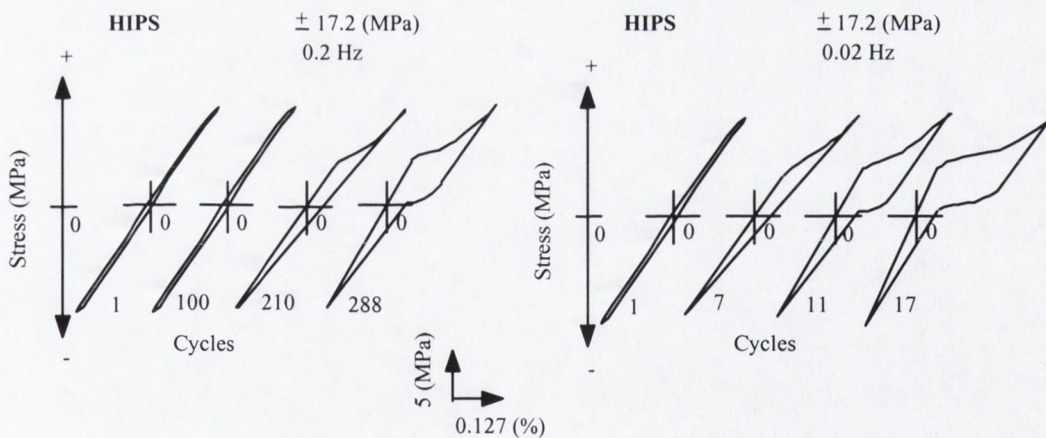


Figure 5.3. Diagram illustrating the different hysteresis losses observed in HIPS materials cycled under the same cyclic stress amplitude at frequencies of **a.** 0.2 and **b.** 0.02 HZ [31].

5.3.4 Comparison of the Fatigue lives of Un-notched HIPS and PS.

The relative stress ratio (σ_a/σ_f), i.e., that ratio of the endurance strength (σ_a) to the ultimate tensile strength (σ_f) of a material is a parameter often used in fatigue design calculations. When the fatigue

lifetimes of HIPS and polystyrene are compared on a relative stress basis it is found that the fatigue performance of HIPS is significantly better, by 1 to 2 decades of N , than that of polystyrene, (**Figure 5.4.**); their relative stress ratios being ≈ 0.44 for HIPS and ≈ 0.22 for polystyrene [32].

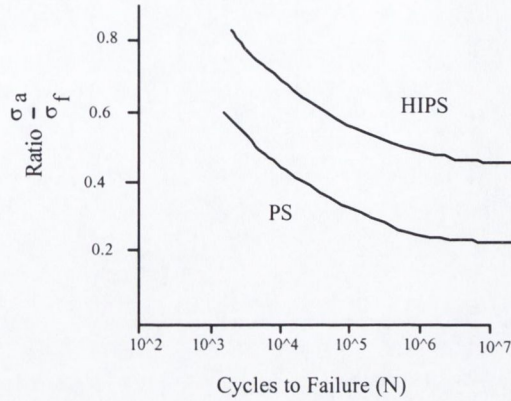


Figure 5.4. Plot of σ_a/σ_{ut} vs. N comparing of the fatigue lifetimes of HIPS and PS on a relative stress basis [32].

However, when the performance of the two materials are compared on an absolute stress basis, as done by Der Jin Woan et al, the fatigue lifetime to fracture at any given stress amplitude is appreciably greater (≈ 3 times greater) in polystyrene than in HIPS [33]. Thus it could be concluded that the effect of incorporating a compliant rubber phase is to reduce the fatigue endurance limit of polystyrene (see **Figure 5.5.**)

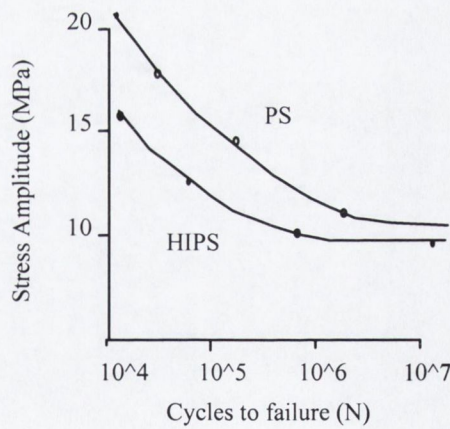


Figure 5.5. Comparison of the SN curves for PS and HIPS on an absolute stress basis [33].

5.3.5 Thermal effects in un-notched testing of HIPS.

Der-Jin Woan et al (1981) in a series of tests, conducted at 31 Hz, monitored the rise in the temperature (ΔT) of HIPS specimens under various amplitudes of alternating load (**Figure 5.6**). In all tests

mechanical failure was observed and the maximum increase in specimen temperature recorded, under an alternating stress amplitude of 18.6 MPa, was only a modest 8°C. The rate at which temperature increased (dT/dN) during testing was noted to diminish with reduced alternating stress amplitudes. At a $\Delta\sigma$ of 12.4 MPa the temperature was noted to have stabilised at $\approx 3^\circ\text{C}$ above ambient temperature prior to failure. At a lower stress amplitude of 10.3 MPa the temperature stabilised after only an increase of $\approx 2^\circ\text{C}$ prior to failure. Thus, it was concluded that while thermal effects may have contributed to the lower fatigue lifetimes in the HIPS that their contribution was modest and insufficient to wholly be responsible for the disparity in performance.

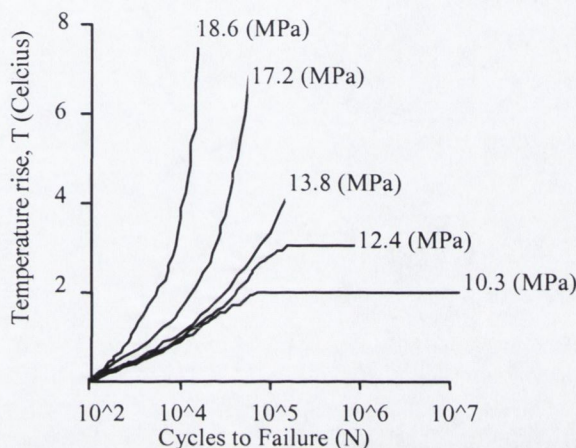


Figure 5.6. Specimen temperature rise in HIPS ($^\circ\text{C}$) vs. the number of cycles to failure (N) at various $\Delta\sigma$. [33]

5.3.6 The influence of mean stress on fatigue life of HIPS.

The possibility that the magnitude of loading could account for the disparity between the performance of HIPS with that of PS was also considered by Der Jin Woan and Sauer [33]. The apparent contradiction between the observations of Skibo et al [34] and Hertzberg et al [35], i.e., that the FCG resistance of HIPS was greater than that of PS, with earlier work of Sauer et al [32], showing HIPS exhibiting fewer cycles to failure, led Der Jin Woan to speculate that the fully reversed alternating loading in the latter's case might have been more deleterious to the fatigue performance of HIPS than polystyrene than the fluctuating tensile load used in the FCG analysis of Hertzberg and Skibo [35].

However, Sauer et al's tests using a fluctuating tensile load, $\Delta\sigma = 17.2$ MPa and $R = 0.2$, showed the fatigue life of HIPS was still less than half that of PS. The N_f recorded for HIPS was 36300 while that for polystyrene was 78,900 [31]. Their results showed that while varying sensitivities to loading may contribute to a poorer performance by HIPS it was insufficient to account for the entire difference.

Consequently Sauer and co-workers concluded that the lower fatigue life observed in HIPS was a consequence of the material's propensity to form extensive crazing at lower levels of applied stress.

The hypothesis that extends from this is that the damage allowed for the earlier incipience of fatigue cracks which, in spite of the greater FCP resistance of HIPS, resulted in earlier failure. Sauer and Chen tested the hypothesis by considering the effect of stress amplitude on the number of cycles to craze initiation and catastrophic failure.

A reflected light technique was used to determine the onset of crazing in polystyrene while a 'significant' change in hysteresis loss was used to indicate its onset in HIPS. The results of their work are presented in **Table 5.1**.

Material	Stress Amplitude (MPa)	Cycles to Initiation N_{ci}	Cycles to Failure N_f	N_{ci}/N_f (%)
PS	13.8	42,200	62,800	67.2
	17.2	9,230	20,500	45.0
	20.7	2,050	9,120	22.5
HIPS	10.3	9,050	9,390	96.4
	13.8	1,150	2,030	56.7
	17.2	10	183	5.4
	20.7	1	23	4.3

Table 5.1. Effects of Stress Amplitude on the Cycles to Craze Initiation and specimen Fracture [31]

The poorer sensitivity of the method used to determine craze initiation in HIPS compared to that used in PS mean the results are not directly (i.e. quantitatively) comparable. However, they do provide a valid comparison within each material type as to the time to initiation of crazing; from which catastrophic cracks may grow. They also offer a comparison of the portion of fatigue lifetime spent in each material in effecting the precursors to failure with the total fatigue life. At any given stress level then the number of cycles for the first observation of crazing as well as for fracture are significantly lower in HIPS than in polystyrene also noted was that in both materials the portion of fatigue lifetime spent in craze initiation falls with increasing $\Delta\sigma$ (see section 3.5.1.1). However the shorter propagation life they observed in HIPS undermined their hypothesis.

5.3.7 The Influence of Surface Topography on Fatigue Life in HIPS.

In view of the fact that in the majority of tests conducted by Sauer and Co-workers, fatigue cracks were initiated from a surface craze, Sauer, Habilullah and Chen investigated the influence of the condition (roughness) of the surface on fatigue life in HIPS[32]. In this work Sauer and his co-workers considered the effects of hand and vapour polishing as well as the effect of surface coating specimens

with silicone oils of various Mw as well as a nitrile rubber latex coating on the fatigue life of HIPS and polystyrene.

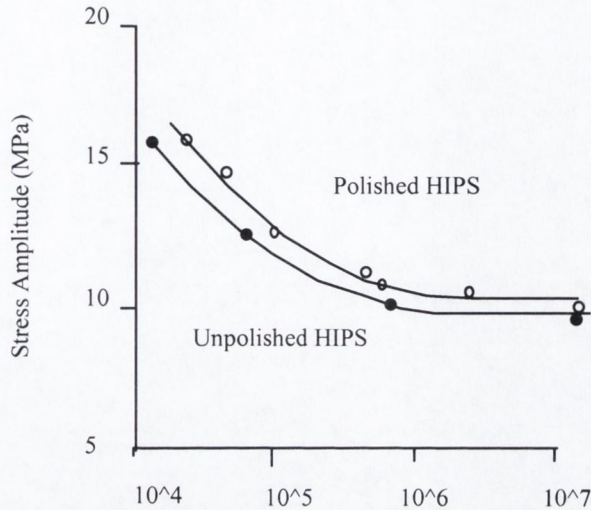


Figure 5.7. Figure comparing the SN curves of polished and unpolished HIPS specimens.

They found that hand polishing shifted the S-N curve of HIPS to the right (**Figure 5.7.**) while vapour polishing (using chloroform vapour) proved deleterious to fatigue lifetime. The consequence of vapour polishing polystyrene led to an increase in the fatigue life of specimens, but had the opposite effect on HIPS.

The contrast in the response was considered to have been the result of differential etching by the chloroform vapour. The chloroform while etching away the surface polystyrene was being selectively absorbed by the rubber phase swelling it and creating a mismatch in local stress. Coating specimens with silicone oil reduced fatigue lifetimes in both materials yet the extent to which it did so was seen to reduce with increasing Mw of the oil. The permeation of the silicone oil was considered most likely the cause of this while, the migration of only low molecular weight oligomers pre-empted average macromolecular size from exerting any influence.

Coating with a rubber latex increased the fatigue lifetimes of HIPS by 2.5, for the case of unpolished samples, and by a factor of four in polished samples. This enhancement of fatigue life was seen as being a consequence of the rubber coating reducing the intensity of any local stress concentrations set up at surface defects or voids along the specimen's gauge length and so delaying the onset of substantial crazing.

5.3.8 Influence of test frequency on the Fatigue Life of HIPS.

Sauer et al also compared the influence of the loading frequency on fatigue life in PS and HIPS. In tests conducted over a three decade frequency range, i.e., 0.02 to 20 Hz at alternating stress amplitudes of

17.2 and 20.7 MPa, for polystyrene, and 13.8 and 17.2 MPa, for HIPS, they noted that fatigue life increased with increasing loading frequency.

In both materials Sauer and Chen noted a log-linear relationship between the fatigue lifetime and test frequency. The slope of these $\log(\text{fatigue life})$ vs. test frequency (Hz) curves also appeared to be independent of the alternating stress amplitude, i.e., it appeared that for both materials the rate of increase in the number of cycles to fracture with frequency was the same at each $\Delta\sigma$ considered. **Figure 5.8.a.** illustrates these findings over the frequency range under a $\Delta\sigma$ of 17.2 MPa. These plots also discredit the notion that thermal effects are any way significant in dictating fatigue life, indeed, the SN curve appears to extend to longer lifetimes with changes in frequency (**Figure 5.8.b.**).

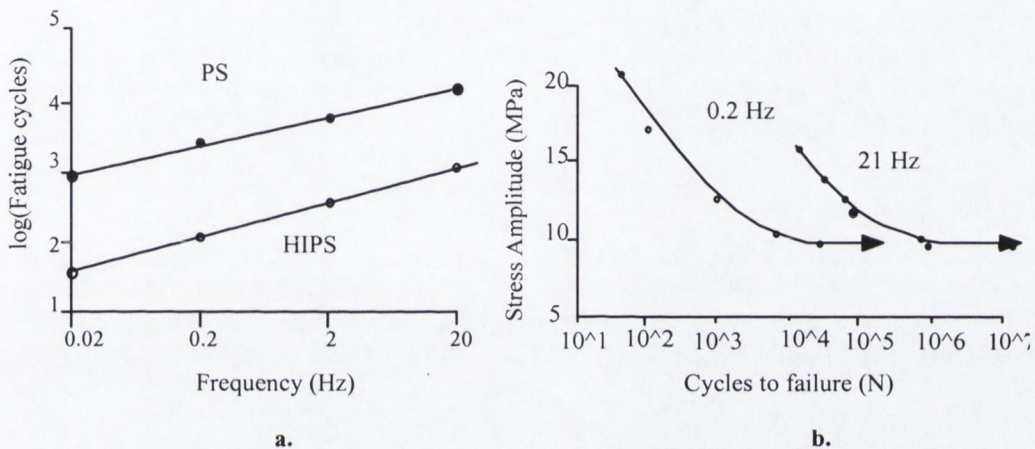


Figure 5.8. Plots showing **a.** The cycles to failure vs. frequency for samples of PS and HIPS at a stress amplitude of 17.2 MPa and **b.** The Stress amplitude vs. the cycles to failure of HIPS specimens tested at 0.2 Hz and 21 Hz [31].

5.3.9 Characterising Fatigue Crack Growth using Fracture Mechanics.

Fatigue crack growth in solids may be analysed most simply by measuring the change in crack length, a , as a function of the number of cycles, N . Such measurements are most commonly made using a travelling microscope. Other methods based on acoustics and optical interferometry have also been used to make direct measurements by some workers, e.g., Doll [36]. Indirect implicit measurements of crack length have also been employed, e.g., based on COD (crack opening displacement) using clip gauges, which can be very effective in instances where small plastic zones are experienced. A typical plot of crack length versus number of cycles is presented in **Figure 5.9.**

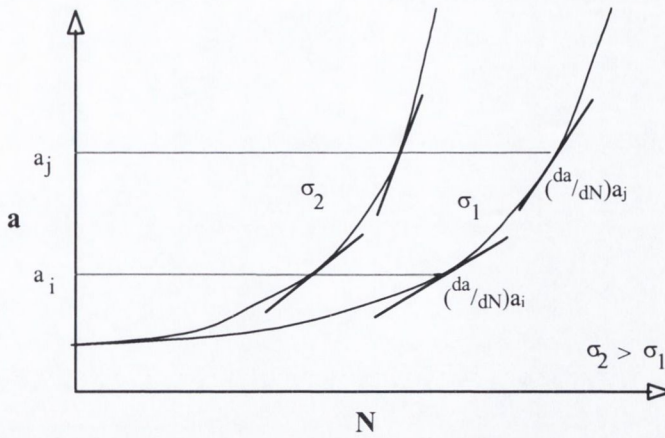


Figure 5.9. Diagram illustrating a typical plot of crack length (a) against the number of cycles (N).

The plot in Figure 5.9 reveals that the crack growth rate accelerates with increasing crack length. Also the crack growth rate at any given time or number of cycles varies with the magnitude of the applied stress:- da/dN increasing with increased stress level. Therefore, da/dN is proportional to some function of a and σ .

Until the mid 1950's many attempts were made to characterise the crack growth rate in terms of arrangements and combinations of the applied stress range ($\Delta\sigma$) and the crack growth rate with expressions of the form,

$$\frac{da}{dN} \propto \sigma^p a^q$$

Equation 5.1.

where p and q are constant empirical exponents [37]. However, with the emergence of fracture mechanics more effective and reliable means of characterising fracture processes emerged. The earliest application of fracture mechanics to fatigue crack growth (FCG) in polymers was the precocious energy approach by Rivlin and Thomas who modified the Griffith equation (*Equation 4.16.*) to describe crack instability in a more general sense which did not require the material to conform to the classical theory of elasticity [38].

They contrived a surface work parameter J , related to $(\gamma_s + \gamma_p)$, which for the case of SEN specimen geometry could be expressed by the relationship,

$$J = k_1 2a U$$

Equation 5.2.

with k_1 , being a constant which varies slowly with the material; a is the crack length and U is the uniform strain energy density [39]. Thus for the case of a uniformly elastic material $k_1 = \pi$ and $U = \sigma^2/2E$, so J was equivalent to G . The similarity in meaning to Rice's J integral is interesting.

Thomas (1958) showed that fatigue crack growth in natural rubber could be expressed in terms of the energy parameter J by,

$$\frac{da}{dN} = AJ^n$$

Equation 5.3.

where A and n were constants. The expression could describe behaviour over a sizeable portion of the fatigue crack growth range [40]. The expression itself (Equation 5.3.) bears strong resemblance to that of Paris, Gomez and Anderson (1961) Equation.5.4) [14].

Paris et al postulated that the stress intensity factor was a major controlling factor in FCG [14]. They argued that when fatigue stresses were applied to a component that resulted in a small plastic zone ahead of the propagating crack tip in what was an otherwise elastic field, then linear elastic fracture mechanics would provide appropriate continuum descriptions for fracture. They so postulated that the growth of a crack under cyclic loading should be governed by the expression[♦],

$$\frac{da}{dN} = C^i \Delta K^{m^i}$$

Equation 5.4.

where C^i and m^i constants, $\Delta K = K_{\max} - K_{\min}$ and

$$\Delta K = Y \sigma \sqrt{\pi a}$$

Equation 5.5.

with Y the correction factor for finite dimensions of a specimens geometry and loading configuration.

Despite some initial controversy further experiments by Paris and Erdogan on aluminium alloys established the validity of the method of characterising fatigue crack propagation [41].

The work echoed that of Thomas on tyres, which was perhaps ahead of its time, and never achieved the same notoriety [40]. Despite the fact that the mechanical behaviour of almost all polymers is time dependent and the majority would be considered as being highly viscoelastic many have been successfully modelled using the Paris relationship. Though Paris, reliant upon LEFM, strictly applies

[♦] **Note.** In this section C is used to denote the constant in the Paris, and modified Paris, expressions, while m denotes the exponent. Roman superscripts are employed to distinguish between the different models.

only to elastic materials the fatigue crack propagation rates of the many polymers considered have correlated with the stress intensity factor range at the crack tip, i.e., ΔK (see **Figure 5.10**).

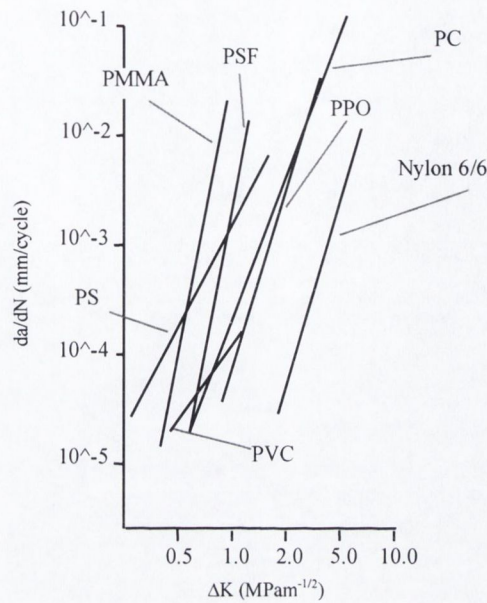


Figure 5.10. Paris plots for some of the more common 'commodity' thermoplastics [19].

However, this logarithmically linear relationship does not extend over the entire range of stress intensity values instead it exhibits a sigmoidal variation at high and low ΔK values exhibiting three distinct regions of behaviour (see **Figure 5.11**).

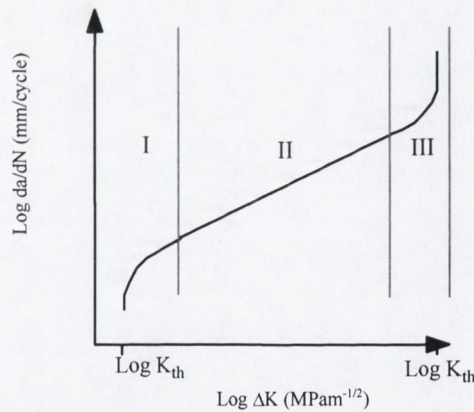


Figure 5.11. Diagram illustrating the sigmoidal variation of fatigue crack growth rates ($\log da/dN$) at high and low values of ΔK .

Region I is associated with a threshold value of stress intensity factor range ΔK_{th} , below this threshold value cracks either remain dormant or grow at undetectable levels, above it, the rate of crack propagation increases rapidly with respect to ΔK . Region II is associated with stable crack propagation, in this region the rate of crack propagation is, generally, observed to increase in a logarithmically linear manner with increasing ΔK , in accordance with the Paris law. In Region III,

associated with rapid crack propagation, the rate of crack propagation increases rapidly as K_{\max} approaches K_c at which point unstable catastrophic fracture occurs.

In polymers a lack of linearity over wide ranges of ΔK is the norm. Nevertheless, Paris plots continue to be used to evaluate the relative resistance of materials to crack propagation and are referred to in the overwhelming majority of papers considering fatigue crack growth. Even where Paris has failed, modified Paris expressions have been developed, e.g., to model FCG rates at high and low levels of ΔK . Foremans' equation, a modified Paris equation that models high crack propagation rates takes the form,

$$\frac{da}{dN} = \frac{C^{ii} \Delta K^{m^{ii}}}{K_c(1-R) - \Delta K}$$

Equation 5.6.

where C^{ii} and m^{ii} are constants and R is the stress ratio ($\sigma_{\min} / \sigma_{\max}$) [42]. For simplicity and clarity, superscripts are introduced to differentiate between the constants and power law exponents of the some of the models used in exemplifying the variety of models proposed.

Pearson modified Foreman's expression to model plane strain fracture toughness, replacing K_c with K_{Ic} [43]. Thus,

$$\frac{da}{dN} = \frac{C^{iii} \Delta K^{m^{iii}}}{\sqrt{K_c(1-R) - \Delta K}}$$

Equation 5.7.

Other factors influencing behaviour have also been introduced e.g., Mukherjee and Burns expressed the rate of fatigue crack propagation for the case of PMMA in terms of the frequency (f) and mean stress intensity (K_m),

$$\frac{da}{dN} = C^{iv} K \beta_m^{iv} \Delta K^{m^{iv}} f^{\alpha^{iv}}$$

Equation 5.8.

where c^{iv} , β^{iv} , m^{iv} , and α^{iv} are material constants and K_m is the mean average stress intensity [44].

While Arad et al modelled the effects of the mean stress intensity,

$$\frac{da}{dN} = C^v \lambda^{m^v}$$

Equation 5.9.

where $\lambda = K_{\max}^2 - K_{\min}^2$ and c^v and m^v are material constants [45,46].

Wnuk superimposing the elastic and viscoelastic components to model FCP rates in polymers;

$$\frac{da}{dN} = C_1^{vi} \left(\frac{\Delta K}{K_{Ic}} \right)^{n_1^{vi}} + C_2^{vi} \left(\frac{\Delta K}{K_{Ic}} \right)^{n_2^{vi}}$$

Equation 5.10.

where C_1^{vi} and n_1^{vi} are rate independent constants and C_2^{vi} and n_2^{vi} are rate dependent constants with f the frequency. C_2^{vi} represents the normalised creep compliance ($I(t)/I(0)$), which for the case of an ideal material is 1 [47].

Branco et al modified Arad's equation, Equation 5.9, in an attempt to model FCP over the entire range of ΔK from ΔK_{th} to K_c [48] Their expression took the form,

$$\frac{da}{dN} = C^{vii} \Phi^{m^{vii}}$$

Equation 5.11..

where ϕ is defined as,

$$\Phi = \frac{2K_m(\Delta K - \Delta K_{th})}{K_c^2 - K_{max}^2}$$

Equation 5.12.

Radon et al extended Arad's expression to incorporate both the shear modulus (G^{viii}) and Poisson's ratio ν such that,

$$\frac{da}{dN} = C_1^{viii} \left(\frac{((1-\nu)^2 \lambda)^{m^{viii}}}{2G^{viii}(1-\lambda)} \right)$$

Equation 5.13.

with C^{viii} and m^{viii} constants which are functions of the material and test conditions [49].

Williams proposed a two stage line plastic zone model using the critical crack tip opening displacement (COD) fracture criterion [50]. Using continuum mechanics of the crack tip based on Dugdale's line plastic zone analysis (Chapter 3) he assumed the cyclic effect was to reduce the craze stress. Continued cycling then would lead to the growth of the craze ahead of the crack and an increase in the corresponding COD and when it reached a critical size, crack growth occurred. Thus he proposed,

$$\frac{da}{dN} = \frac{\pi}{8(1-\alpha^{ix})^2} \frac{1}{\sigma_c^2} [K_{max}^2 - \alpha^{ix} K_c^2]$$

Equation 5.14.

where $\alpha^{ix} = (1-f^x) + f^x R^2$ and f^x is a damage factor.

Chudnovsky and Moet developed a damage accumulation model that described fatigue crack propagation in polystyrene in terms of a crack layer [51]. They proposed a law of fatigue crack layer propagation (FCLP) that may be described in the following dimensionless form,

$$\frac{da}{dN} = \frac{(\beta^X \lambda^{X^2} - Q^X)}{(\omega^X - \lambda^X)}$$

Equation 5.15.

where $\lambda^X \cong l^{xi} (N)/l^{xcrit}$, l^X is the crack layer length, l^{xcrit} is the critical crack layer length, ω^X -the crack layer width, β^X and Q^X are energy dissipation and heat evolution functions respectively.

5.3.10 Comparison of Fatigue Crack Propagation in Polystyrene and HIPS.

The incorporation of a rubber phase enhanced the fatigue crack resistance of polystyrene, evidence of this being the lower values of crack growth rates exhibited by HIPS under equivalent loading conditions, see Figure 5.12 [52].

The lower crack propagation speed in HIPS is understood to be a consequence of the extensive crazing in the material. The hypothesis being, that in effecting a diffuse damage zone about the crack tip the local crack tip stress intensity is lowered which in turn reduces the rate of crack propagation. The behaviour observed in HIPS is similar to that reported for other ‘rubber-toughened’ polymers [19].

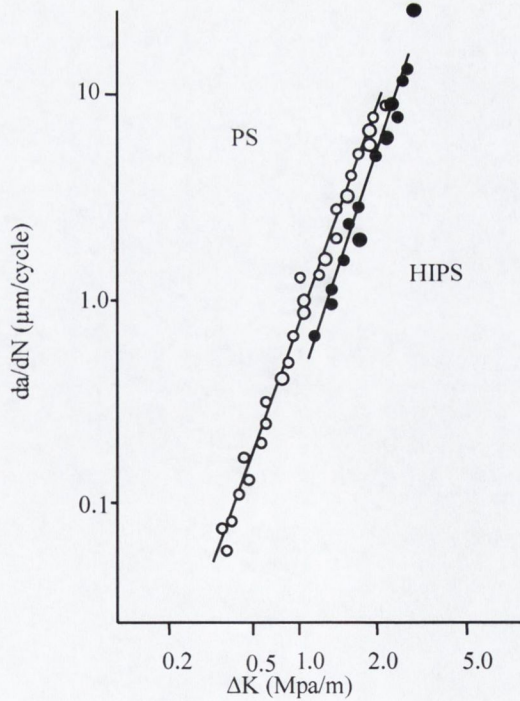


Figure 5.12. Comparison of fatigue crack propagation in HIPS and PS, [52].

5.3.11 The Influence of Mean Stress on FCP in HIPS.

The influence of mean stress on fatigue crack propagation behaviour in HIPS was investigated by Yap, Mai and Cotterell [53]. Their tests were conducted on extruded HIPS at R ratios of 0 to 0.5. They found, as Mai and Williams had for polystyrene, that the rate of crack propagation was insensitive to changes in R. This, they suggested, was a consequence of HIPS not displaying crack closure, which implied, that both effective ΔK_{eff} (incorporating crack closure effects) and applied (nominal) ΔK values were equal, **Figure 5.13**.

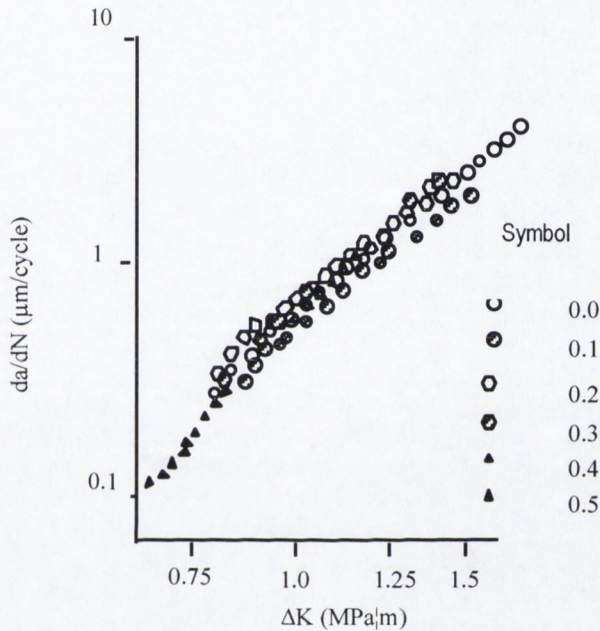


Figure 5.13. Plot illustrating the Influence of R ratio on Fatigue Crack Propagation rates in HIPS[53].

5.3.12 The Influence of Test Frequency on FCP rates in HIPS.

Yap et al also considered the influence of cyclic loading frequency on FCP [53]. Tests they conducted over a frequency range of 0.1 to 25 Hz revealed that crack growth rates decreased moderately as frequency increased.

These results concurred with the observations made by Hertzberg et al in PPO/HIPS blends [35]. The authors speculated that local thermal effects may have contributed to the increased crack growth resistance at higher frequencies. This is in line with the effect of increased frequency on the magnitude of hysteretic heating referred to above that possibly also assisted crack blunting processes. However the similarity between the curves at the different frequencies suggests that the contribution of the thermal effects was not large, concurring with the conclusions offered by Der Jin Woan et al [33].

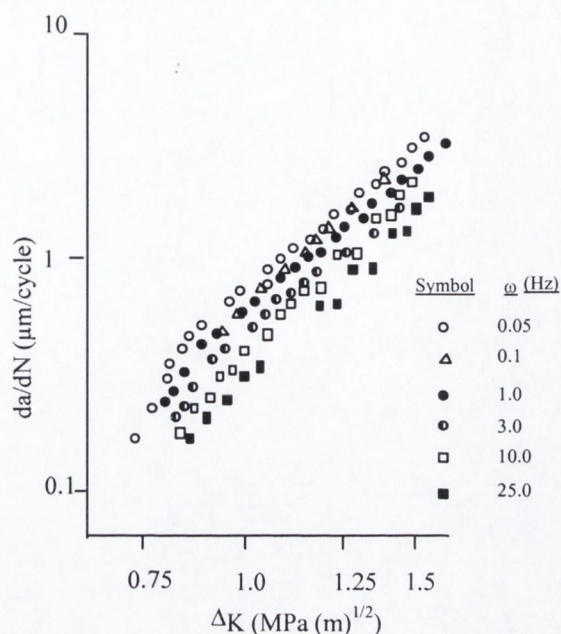


Figure 5.14. Plot of da/dN ($\mu\text{m}/\text{cycle}$) vs. ΔK ($\text{MPa}\sqrt{\text{m}}$), illustrating frequency effects on the FCP behaviour of HIPS [53].

5.3.13 FCP rates in Toughened Thermoplastics.

A number of searches of the literature have revealed no published work that considers the influence of changes to the secondary rubber phase morphology on the fatigue crack growth resistance in HIPS.

However, the work conducted by Skibo et al, on rubber toughened PVC, and by Bucknall and Faitrouni on ABS do cover some of the same ground, in respect of the influence of the rubber phase volume on fatigue behaviour [25,54].

The work of Bucknall and Faitrouni is perhaps the most relevant [25]. It considered the influence of changing the rubber phase volume in matrices varying in molecular SAN molecular weight and though not directly comparable to HIPS, they do provide some indication of what would be expected in HIPS. The significant difference the two materials is the transformation of the micro-deformational process in ABS above a certain ERPV, that does not occur in HIPS.

Bucknall and Faitrouni conducted their study by mechanically melt blending ABS in unmodified PSAN materials of equivalent AN content and varying Mw. They found that the fatigue crack resistance of the materials increased with increasing rubber content, especially in the low molecular weight matrix. However additions greater than 7.5% rubber content, conferred little additional resistance to crack propagation, see **Figure 5.15 a.**

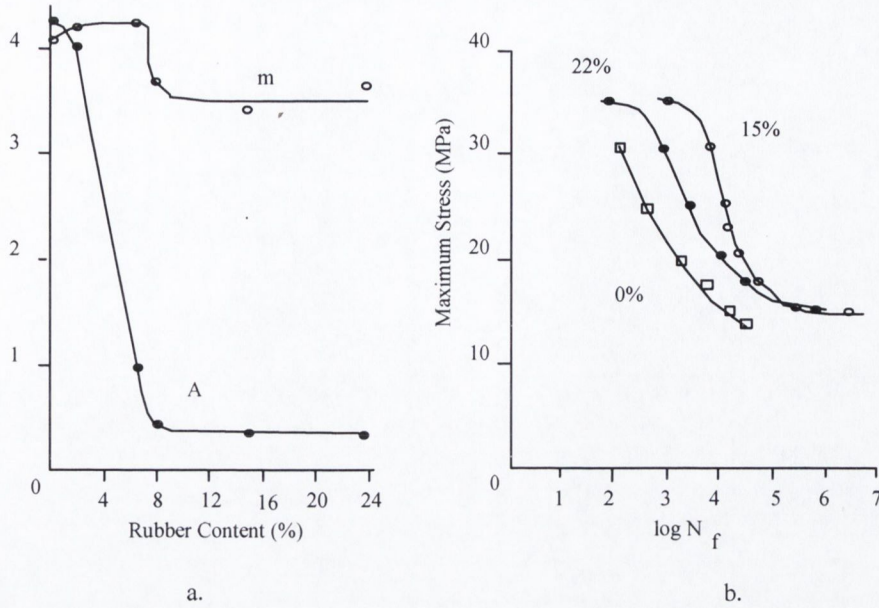


Figure 5.15. a. The influence of rubber content on Paris law fatigue crack propagation rate constants in toughened PSAN (ostensibly ABS materials). b. SN curves for PSAN matrix containing different concentrations of rubber phase [25.]

Their observations were similar to those made by Skibo et al who studied FCG in melt blends of MBS in PVC matrices varying in molecular weight. They observed considerable improvement in crack growth resistance with increasing MBS up to 6 phr, but no improvement at higher concentration, see **Figure 5.16**. They also noted the greatest improvement in rubber phase addition occurred in lower Mw matrices although the greatest fatigue resistance observed in high molecular weight blends.

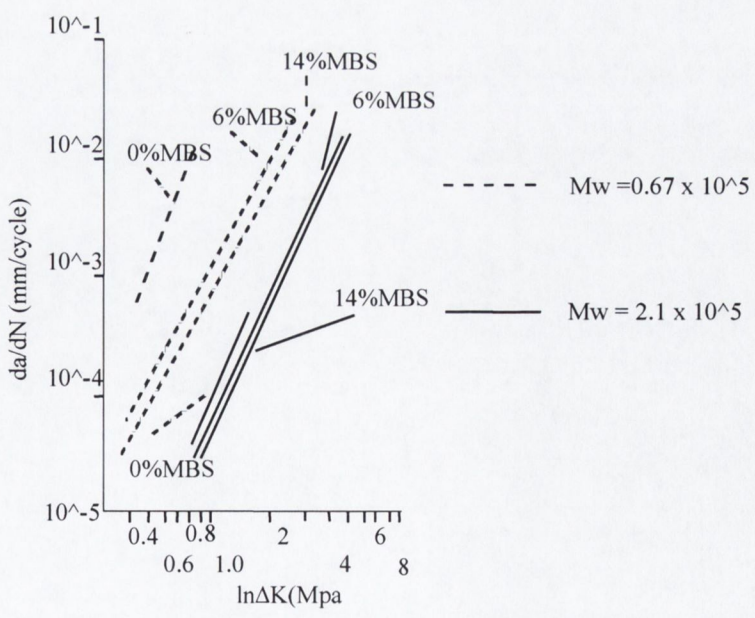


Figure 5.16. Plot showing the effect of Mw and rubber content on FCP [54].

In both systems the introduction of the secondary phase led to a transmutation in the process of deformation from cavitation to shear that accounted for the shift in the behaviour. No studies however have considered the properties or size of the secondary phase particles on fatigue behaviour.

5.3.14 Applications of HIPS involving Fatigue

Notable everyday examples of applications where HIPS is used and likely to experience repeated cyclic loading are; vacuum cleaner, shower, TV, radio and computer monitor casings and hand held equipment casings e.g., phones, hair driers, hand drills, etc. In most of these instances the material is exposed to repeated loading events. In many instances the repetitive impact events involve significant levels of force and deformation. Awareness that such events are likely to occur is often what motivates the selection of the material.

Additionally in most of these applications the material is an integral part of the structure, e.g., a casing bearing the load of its contents. Consequently, in a number of instances, the material may also be exposed to low and perhaps high cyclic loads that might arise, as a result of unbalanced motor bushings, force transmission mechanisms, or reverberated loads, etc. The mass of contents can be significant and consequently the cyclic forces, resultant from whatever cause, are often catastrophically destructive. Especially vulnerable are joints, tethering points, e.g., screw and spring bosses, i.e., where changes in geometry or material continuity are disrupted. These factors conspire to raise local levels of strain and so promote cracking.

However HIPS strength:weight:cost ratios combined with its ease of processing, continue to make it appealing to high volume appliance manufacturers. So much so that innovative design solutions and custom modification to the materials microstructure are preferable to selecting other materials, i.e., engineering thermoplastics. Its popularity fuels HIPS manufacturer's desire to broaden the indications for its use, and consequently a desire to understand the means through which improved performance may be affected.

5.4 *Experimental*

5.4.1 Introduction.

In addition to considering the fatigue crack propagation behaviour of the materials the fatigue tests were also used to determine their intrinsic fracture toughness. The latter results were reported in Chapter 4. The protocol of testing adopted for fatigue tests reflected the primary focus on understanding the relationship between micro-structural morphology and fracture and fatigue crack initiation and growth.

Chapter 3 had illustrated how manipulating the secondary phase morphology modified the micro-process of crazing and how this affected impact toughness. The findings in Chapter 4 concluded that incorporating a secondary phase, and changing its micro-morphology, altered the intrinsic toughness of HIPS. The relationship between the two was sensitive to constraint. The results illustrated the

effectiveness of the incorporated phase at lowering constraint and promoting the dissipation of energy through diffuse crazing. Chapter 4 also showed how the nature of the micro-mechanism and the sensitivity to constraint translated into inconsistencies within the experimental approaches used in characterising intrinsic toughness that how this prevented direct comparison of the material's intrinsic toughness. The results in both chapters showed that the influence of morphology was related to the size, polydispersity and concentration of secondary phase particles.

For many years the reasonable assumption, suggested in the experimental findings of Hertzberg, was that a HIPS resin optimised for fracture toughness, would provide the optimum performance in fatigue [52]. The fracture toughness of HIPS has usually been adjudicated from impact toughness tests.

For equally many years this, in practise, has not proven to be the case. The rationale upon which the premise is founded appears to be true for most materials, it being that the fatigue crack growth resistance of a material should be greater at any given level of load, and concomitantly at any given stress amplitude, or ΔK , the higher the apparent toughness, viz., J_c , G_c or K_{Ic} .

In the specimens considered the critical values measured for these parameters rose consistently, if not constantly, with the magnitude of the secondary phase features considered. However the discussions in Chapters 3 and 4 inevitably turned to focus on the inconsistencies and aberrations between what is implied by the parametric measurements and the physical events that occur in the material. Ultimately these inconsistencies centred on the distortion, by crazing, of the classical mechanistic interpretation of fracture toughness and the engineering appreciation of the paradoxical relationship between material strength (resistance to deformation) and toughness (crack resistance). They suggest that the basis for the speculation could be unfounded, as the intrinsic toughness of the materials is not greatly affected by the secondary phase. The experiments reported below, focus on the dilemma posed by crazing on characterising fatigue fracture to explaining the inconsistent correlation between fracture toughness and fatigue crack growth.

5.4.2 Experiment Materials and Equipment.

The fatigue tests were conducted on flat 8x25x100mm single edge notched tensile (SENT) specimens of each material, notched to a depth of 2mm using a 0.5mm notch root radius. They were then cycled under a fluctuating load of 500 N with $R=0$. A load controlled, fatigue test regime was adopted in the experiments for a number of reasons.

1. It reflects in-service loading associated with many applications where fatigue occurs, i.e., its typically load controlled.
2. Low forces were chosen to promote conditions approaching plane strain and so offer the most efficient means of comparing the relative influence of morphology on FCG as well as facilitate intrinsic toughness measurements.
3. Notched samples confined failure to a specific plane, allowing crack propagation to be monitored.

5.4.3 Equipment

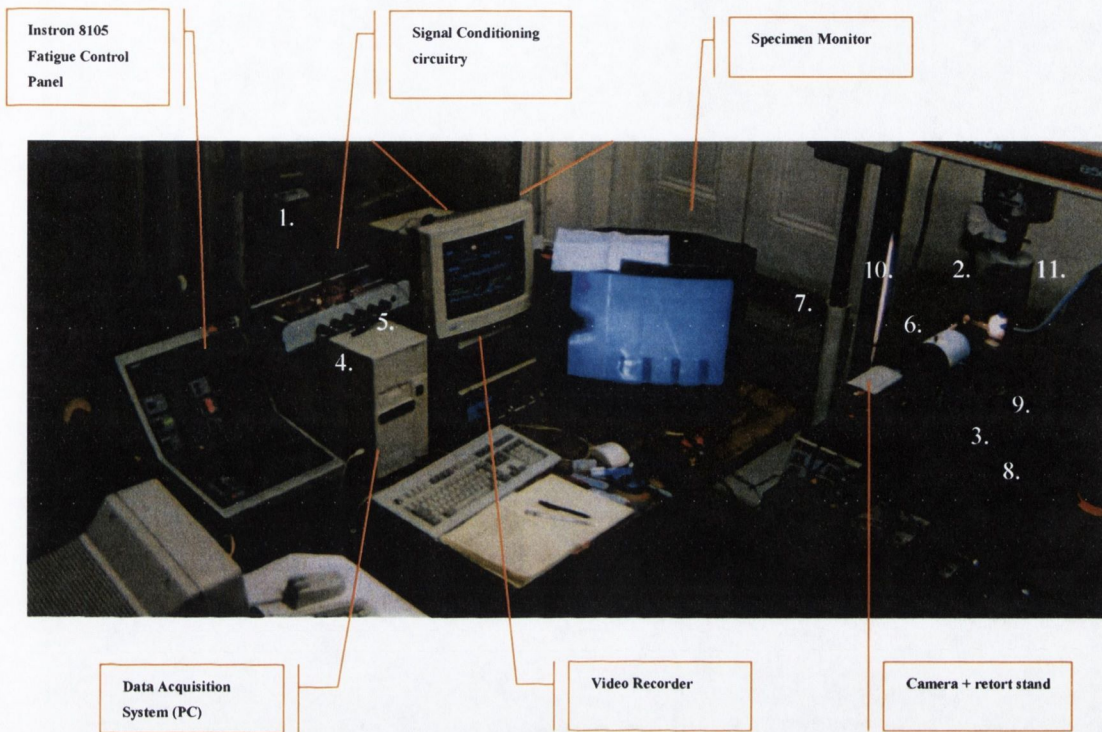


Figure 5.17. The apparatus used for conducting the fatigue tests. The centerpiece of the system was an Instron 8501 servo-hydraulic testing frame. In order to conduct the desired testing it was necessary to develop a series of customised ancillary devices.

As Instron were unable to provide details of the digital encoding of the digital output signals from the machine it was necessary to develop (1.) customised signal amplification and conditioning circuitry for both (2.) the displacement transducers and (3.) the load cell.

A (4.) double buffered data acquisition card was sourced to interface between the analog signal output from the DASC circuitry and (5.) the dedicated data acquisition PC. The card selected was a LAB-PC which provided a continuous signal (A-D) through 12 channels and also provided digital input channels with interrupts.

A (6.) stereo-microscope was mounted on a (7.) microscope stage, which had been fitted with a (8.) digital linear voltage displacement vernier gauge in order to measure crack advance.

The stereo microscope and stage were fixed in place using (9.) fixturing joists that firmly attached it to the testing frame. In order to detect crack initiation a (10.) standard small travel microscope was used. Swan neck fibre-optic lamps (11.) provided illumination of samples.

Finally as, at the time of the work, it was not possible to determine fracture properties using Inston's (or any other manufacturer's) software a dedicated application was written to do so and interface with the hardware. The source code for the system's data acquisition and control is presented in the Appendix 5.2.

Displacement Transducer #1

Full travel over the entire gauge

Displacement Transducer #2

Measuring travel over crack opening.

Travelling light Microscope

Crack Initiation establishment of the crack front

Microscope

Crack extension measure.

Microscope over LVDT travel.

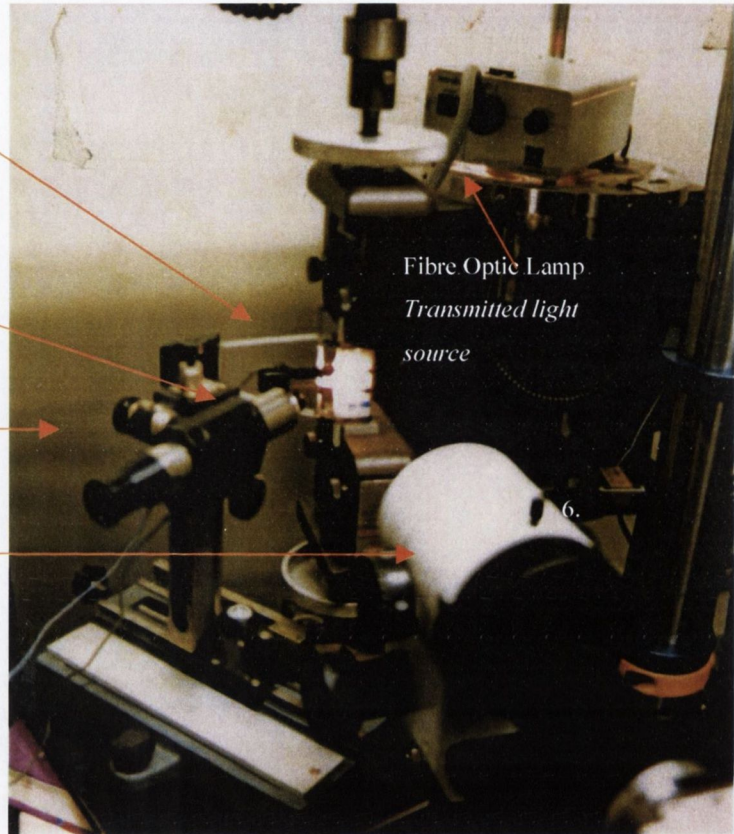


Figure 5.18. Close-up of the arrangement of apparatus during fatigue testing.

5.4.4 Experimental Procedure

Standard techniques were employed in characterising HIPS behaviour and associated micro-mechanical processes.

1. 100 x 100mm plaques 8mm thick were injection moulded from each of the materials, see Chapter 2, under standard moulding conditions (see Chapter 2).
2. The plaques were then annealed in a compression press at 250°C for 10 minutes.
3. 100 x 25 mm specimens were machined from the plaques using a high speed saw
4. 2 mm notches were introduced on the same 'moulded' edge of the specimens
5. The edges of the specimens were sanded with 200 and 50µm grade sand paper.
6. They were numbered and 0.5mm adhesive transfer stripes affixed to them.
7. The samples were clamped and displacement transducers attached.
8. After offset load and amplitude were entered samples were ramped to the mean load.
9. Samples were then fatigued at nominal cyclic stress 2.5 MPa at 1 Hz (sine wave:R=0).
10. Load, displacement, hysteresis loss, crack extension were recorded in tests.
11. 3 replica tests were conducted for each material.

.4.4.1 Fractographic techniques.

Fracture surface analysis, was conducted using 1) light microscopy and 2) scanning (SEM) and 3) transmission (TEM) electron microscopy.

1. Light microscopy was conducted using a stereo microscope during fatigue tests.
2. SEM was used to study the topography of fractured surfaces
 - Specimens were prepared by sputtering fractured sample surfaces with gold and precautions were taken to minimise charging under high magnification.
 - Its high magnification allowed examination of particles and fibrils.

3. TEM used to examine crazing beneath the surface of fractured samples

TEM samples were prepared by sectioning of fractured specimens perpendicular to the plane of fracture.

Care was taken to remove samples from the same region of each sample (7mm along specimen centre).

The sections were then stained with OsO₄ and cryogenically microtomed into thin (0.5 μm) coupes,.

The methods and techniques employed are in line with those set out for characterising the morphology in Chapter 2.

It allowed the extent of craze damage beneath the fracture plane to be studied.

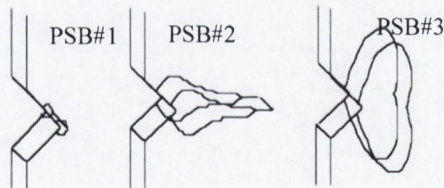
5.5 Results and discussion

5.5.1 Micro-Mechanism of FCP in HIPS.

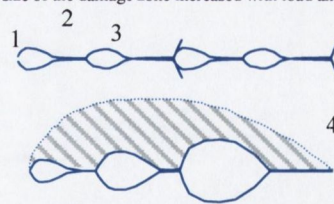
Transmitted light microscopy used in monitoring FCG also allowed the development, extent and the density of crazing in the materials to be observed as cracks advanced. The appearance of the process zone darkened as cycling continued and damage accumulated. In the wake of the propagating crack the damage zone 'lightened' in its contrast.

.5.1.1 The Process of Fatigue Crack Propagation in HIPS.

The slip stick process of crack propagation involved the steps outlined below. The shaded area represented by '4' indicates how the size of the damage zone increased with load and ERPV.



a. The size and shape of the damage zone were noted to be the same as those observed in monotonic fracture, cf, Figure 4.28.



b. Sketches illustrating: 1. Crazing prior to 2. rapid crack advance through pre-crazed material, 3. retardation damage accumulation and slow stable crack growth. 4. crack advance that increased with load and ERPV

Figure 5.19. a. sketches of characteristic damage or craze zones and b. illustrating the process of interrupted crack growth.

The process zones associated with the three parent resins were found to have precisely the same shapes as those observed during the monotonic fracture tests **Figure 5.19.a**. Although the size of the process zones increased with continued cycling, because of the lower forces and strains applied, they were much smaller than those observed in the monotonic fracture tests and were confined within the 'body' of the test pieces for most of their fatigue lives.

Light microscopy revealed that the process of crack advance in all of the materials, especially in the early stages of crack advance, was episodic. **Figure 5.19 b**. illustrates how this presented itself during the tests. The mechanism is termed 'discontinuous fatigue crack' growth and was first described by Elinck, working with PVC, in 1971[55].

The polyblends that contained low ERPVs exhibited 'classical' interrupted crack propagation, Figure 5.19.b. In these polyblends, containing, 5 and 10 % ERPV, only a limited amount of damage accrued up to the 'maturity' of the damage zone. When mature the crack fronts quickly jumped through the damage zone, and often a small distance beyond it, where the process of damage accumulation then restarted. In some instances it was possible to hear the material crack, and 'pop' forward. Polyblends containing higher volume loadings tended to exhibit less defined discontinuous growth. However when their fracture surfaces were examined they exhibited fatigue crack striations indicating that a discontinuous process of crack growth had occurred.

As the size of the process zones increased with cycling, especially in the polyblends with high ERPV's it became more difficult to identify interrupted discontinuous crack advance. Instead of jumping from one 'damage zone' to the next, the propagating crack fronts slowly traversed the damage zone, speeding up then slowing down, depending upon the facility of the process zone to dissipate energy away from the crack front.

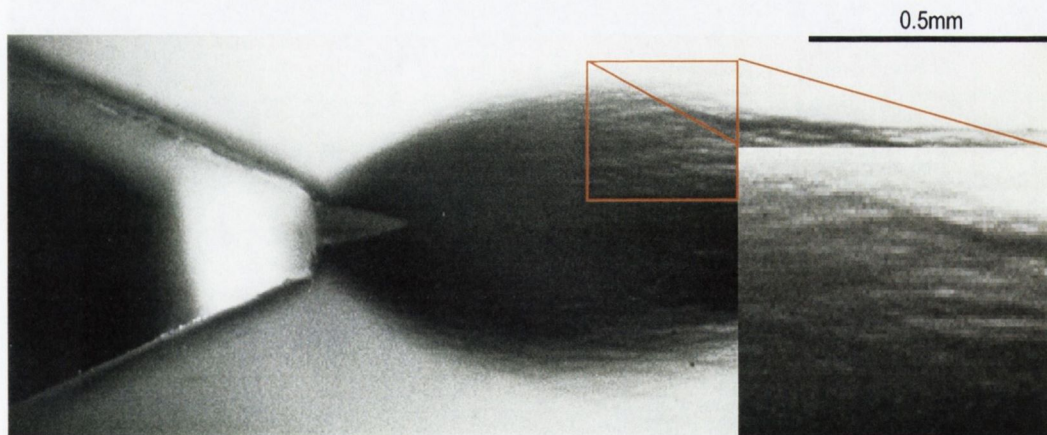


Figure 5.20. 4.a. Close-up of crack initiation (edge crack initiation) and the damage zone in the region about the crack/notch for a PSB#2 series resin. 4.b. Zoom into crazed region showing orientation of individual craze bands.

Thus the process of damage accumulation, involved in setting down DCG striations, could be observed in the course of tests, Figure 5.21. The process zones initially served to retard crack initiation and slow growth. During their early development damage zones were observed to deepen in contrast and grow in size. When 'mature', a point where the material was unable to initiate more crazes, or extend its existing complement, it coalesced with, or was traversed by, the main crack front and the process zone lightened in contrast.

Subsequent to fracture DCG bands confirmed that an interrupted process of crack growth had occurred and the surfaces of all specimens tested exhibited striations. In the case of the low volume loading materials they appeared as the thin 'beach marks'. As cracks grew the striations became less defined, and much wider. The entire surface of the specimen betrayed evidence of extensive surface crazing, however it was particularly evident in the case of the higher volume loaded materials. For many years these striations, were considered to represent 'per cycle' growth. However it was clear from the tests that they represented the cumulative result of repeated loading in effecting damage at the crack front, up to and during, crack advance.

Their appearance, size and number was dependent upon, and representative of, the different material's intrinsic secondary phase morphology. Their size was determined by its response to the pattern, magnitude and rate of loading, i.e., the energy absorbed in creating sufficient damage to promote the advance of a catastrophic crack.

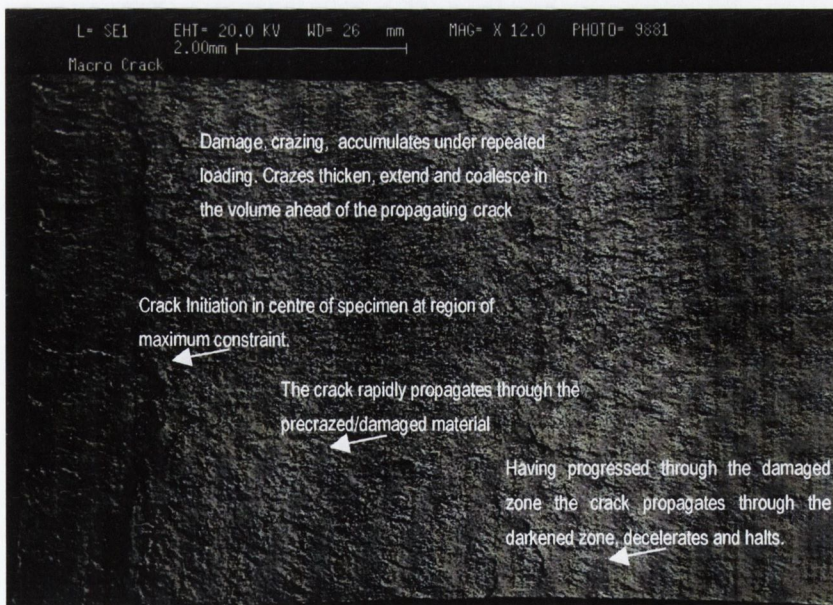


Figure 5.21. Fracture surface of 8mm PSB#3-45.4 (3.2 μ m) material fatigued under alternating 500 N load (R=0).

Crack advance can be studied in terms of fatigue crack growth striations, and their number, size and spacing may be correlated with the number of cycles associated with their development. Though some informal effort was made at establishing such a correlation, at the time of microscopy, it had to be abandoned as the information it offered could not justify the costs of EM and IA (image analysis) time required to complete it. DCG striations are a phenomenon of fatigue crack growth (FCG) and though they contribute to understanding behaviour, and it was thought to be better explored in the 'energy' analysis of the damage accumulation associated with crack propagation which was directly available from the test telemetry.

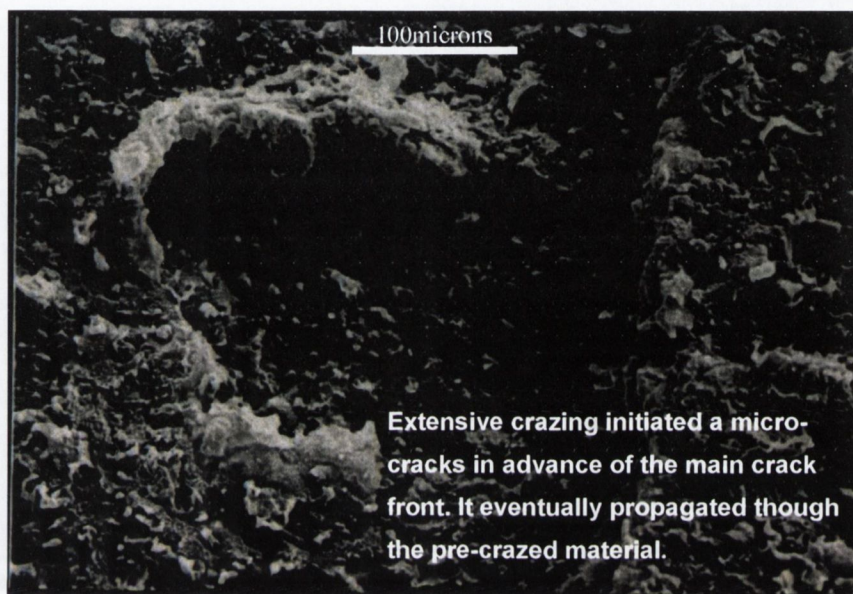


Figure 5.22. SEM plate of the fracture topography in PSB3-45.4 indicating the extent of damage in advance of crack front, precipitated by profuse crazing.

5.5.2 Micro-deformation Processes Involved in the Micro-mechanism of FCG in HIPS.

The process of energy dissipation was considered to be competitive, between (i) the dissipation of energy through the formation of new crazes and (ii) the cavitation and coalescence of existing crazes to form cracks and promote catastrophic failure. Balancing the ability of materials to craze or to crack, was determined and driven by the level of constraint they experienced. Chapter 4 illustrated how, when it was low, the materials expressed their relative abilities to dissipate stress freely, and where it was high they tended toward to the intrinsic properties of the matrix resin.

Study of the fractured surfaces of fatigued specimens suggested that the competitive nature of the process of energy dissipation was even more pronounced under cyclic loading, because of the recurrent low level loading and the duration of the tests. To illustrate SEM images from the surface topography of two PSB#3 resins are presented in Figures 5.22, 5.24 and 5.25.

Figures 5.22 and 5.24 are images of surface detail on a PSB3-45.4 specimen. Figure 5.25 is an image from the fracture surface of a PSB3-5 specimen. The surface artefacts presented in the images provide a great deal of information about the micro-deformation processes involved in the incipience, growth

and coalescence of crazes under fatigue loading and the role that micro-structural morphology played in mitigating the competitive process of failure.

The highly disrupted fracture surface in Figure 5.22 shows that extensive crazing occurred in the process of crack development and propagation. The density of crazing slowed the growth of individual crazes, although their proximity led many to coalesce and form micro-cracks that grew to form incipient fracture planes within the matrix. The image also illustrates how, in resins containing high ERPVs, crazes were permitted to thicken significantly before coalescing. This illustrates how large microcracks could grow before being surpassed by the main crack front. These micro-cracks present in the damage zone preceding the crack front, suggest that plasticity induced crack closure accompanies fatigue crack growth, contrary to Yap et al's conclusions from mean stress analysis [53].

Indeed evidence of plasticity induced crack closure was visible during the tests. In Figure 5.23 bridging ligaments, artefacts of mature micro-cracks that had developed from crazes, were observed to remain attached to opposed faces of the crack, intact, after the crack front had passed. The extensive crazing of the material about these ligaments allowed them articulate during loading while during closure they became trapped between the apposing crack faces, effecting zero load at greater strain.

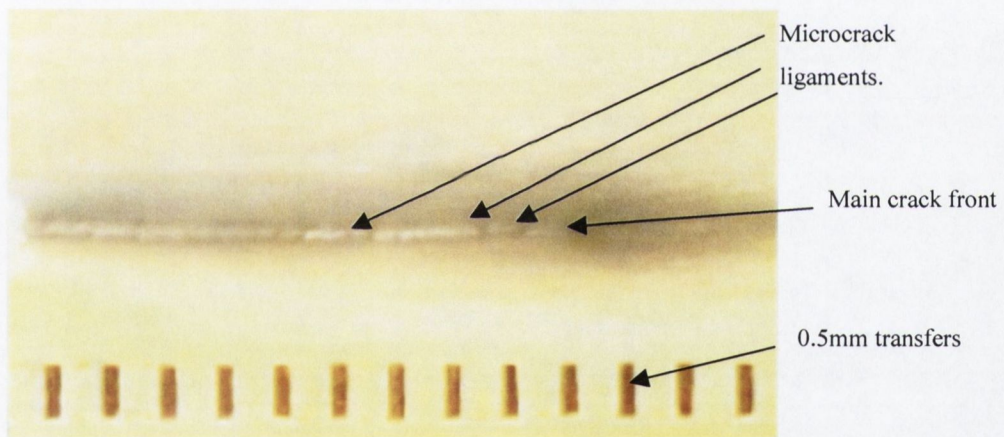


Figure 5.23. Photo image of fatigue crack growth in PSB2-15 taken from TV screen. The image was scanned in from one produced on a video printer.

This, it is considered, had a significant effect on the fatigue lives and fatigue crack behaviour of the materials. The differences observed between the artefacts of crazing on the fracture surfaces of resins containing high and low ERPV indicated it expressed a significant influence on behaviour, especially in the case of the higher ERPV loaded resins.

5.5.3 Influence of Morphology on Fatigue Damage Accumulation in HIPS

5.5.3.1 *The role of the matrix in the process of FCG*

Higher magnification, in Figure 5.24, of the PSB#3-45.4 specimens revealed that individual rubber particles were surrounded by large ‘drawn-out’ fibrils of polystyrene that were the result of significant macromolecular/plastic deformation. The number, length and diameter of the fibrils was much greater than that observed in resins containing low ERPV and showed that matrix deformation, at a micro-scale, was extensive.

For this to have occurred within brittle polystyrene required constant strain to have been applied for a significant period of time during the test, i.e., sufficient to enable the randomly arranged, entangled and sterically hindered polystyrene molecules to ‘slip’ past each other and so form the large fibrils. The observation confirmed that under the fluctuating load, within the process zone, plasticity induced crack closure not only occurred but exercised a significant influence on the material’s response. The observation of extensive matrix drawing associated with the craze fibrils in materials containing high volume loadings of secondary phase indicated that more time, and consequently energy, was exhausted in their development and growth. Thus while secondary phase particles facilitated crazing, plasticity induced closure maintained a residual strain on fibrils during unloading that provided sufficient time to allow the polystyrene molecules viscoelastically/viscoplastically draw more material from the matrix resin and resist the growth and failure of the crazes.

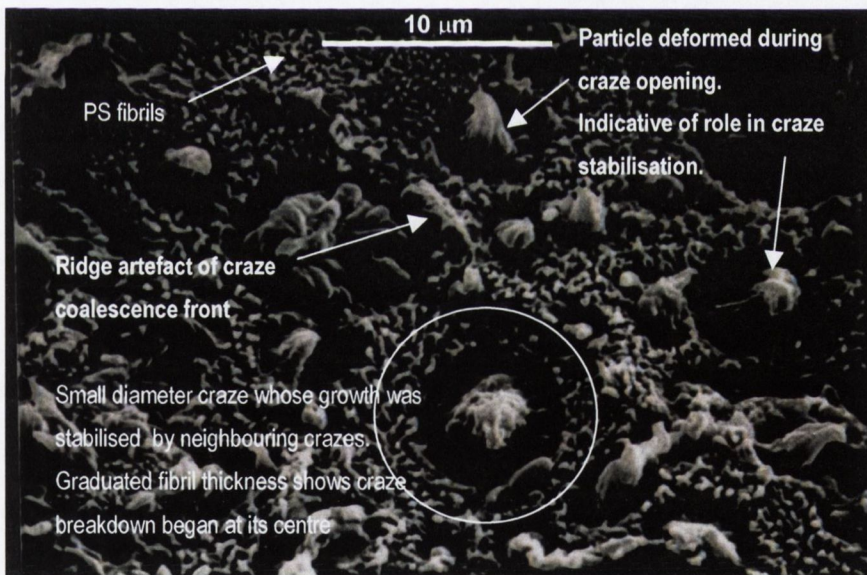


Figure 5.24. High magnification image of fatigue fracture surface topology of PSB#3 45.4. .

In plastics plasticity induced crack closure can amplify the viscoelastic response of the matrix, increasing the material made available to fibrils to resist craze, and so, crack growth. Thus a process that would have been anticipated to accelerate the extension, breakdown and coalescence of crazes, in a polymer also possesses the potential to retard this growth by involving a greater amount of matrix, through the nano-mechanical process of fibril drawing. However, in effecting this mechanism, a greater

volume of matrix is cavitated which exhausts the materials potential to resist further crack propagation, a factor contributing to increasing crack growth rates. These arguments illustrate the primacy of matrix involvement in determining the energy associated with and absorbed, during fracture. They also highlight the competitive process of damage accumulation and crack growth and HIPS and its sensitivity to micro-structural changes.

.5.3.2 *The role of the Rubber Particle on the process of FCG.*

It has been established that the primary role of the particulate phase in HIPS under cyclic loads is to instigate crazing at lower levels of stress [28]. Whether particles themselves contribute significantly to toughness is a matter of some debate (Chapter 3, [28,56]). The micrographs provide some indication of the role played by the rubber particles. Their 'drawn-out' appearance indicates that they underwent extensive plastic deformation. Their 'expectant' appearance post fracture betrays the presence of polystyrene sub-inclusions within them. One particle, in Figure 5.24, is so deformed it appears to have been almost 'scooped out' of its cavity (centre right).

The particles undoubtedly failed at greater levels of strain, than the matrix. The 'whispy' appearance of dissected particles shows that the cross-linked rubber failed by ductile tearing. Their appearance contrasts with the 'rounded' aspect of the polystyrene fibrils. These may have strained as much as the rubber particles during craze opening. However viscoelastic recovery of the amorphous PS molecules, post failure ruined the fidelity of their fibrils reflection of strains experienced at failure. The presence of the included polystyrene and crosslinking prevented the rubber particles recovering their original shape. FTIR (Fourier Transform Infra Red) conducted on one fractured surface identified the presence of increased trans crystallised butadiene content, (the original rubber was almost exclusively the cis isomer). This reformation of molecules is a time dependent process and would only have occurred in a crosslinked material at very high levels of relative strain under load for significant periods of time. The effect of the crystallisation is akin to strain hardening which indicates that the rubber phase would have contributed to the contribution made by the particles to resisting craze growth and failure [57].

These observations confirm that the rubber particles bore load and therefore must have contributed to the 'strength' and/or the stability of the crazes. That the same response was observed on the fatigued surfaces of all of the resins suggests that only modest energies were required to promote deformation and plastic tearing. This implies that its contribution to strength was only slight. So while it's impossible to determine the scale of the contribution made by the particles to resisting crack growth it is concluded from studying the images that their contribution is finite but limited.

.5.3.3 *The effect of ERPV and RPS on the process of FCG.*

The greatest contrast observed between the surfaces of high and low ERPV blends then was the level of matrix involvement in deformation. Though polystyrene fibrils were present on all fractured surfaces, those observed on low ERPV surfaces were smaller and not drawn from as much polystyrene as those on the fracture surfaces of resins containing higher ERPV. The contrast between high and low levels of addition, with respect to the levels of matrix deformation associated with damage accumulation, is visible around particles. Despite the difference in image quality, the contrast between topographies in Figure 5.24 and Figure 5.25 is very clear. Greater strains, associated with greater levels of crazing, experienced in the high ERPV materials is considered to have contributed to the stability of crazes. Their thicker fibrils involved more matrix resin, took longer to draw apart and/or required greater strains and energy to fail. Consequently they accommodated greater craze opening displacements

during loading, and resisted craze growth and failure under higher loads. Craze diameter was also smaller in the case of the higher volume loaded resins. This and the proximity and size of the polystyrene fibrils to rubber particle edges indicate that these crazes were stable. The features contrast sharply with those observed on the fracture surfaces of the low volume loaded materials, e.g., PSB3-5 in Figure 5.25. It is important to note that the area considered is roughly the same distance from the notch root as the previous image, in a beach mark, and the specimen had been loaded according to the same loading regime.

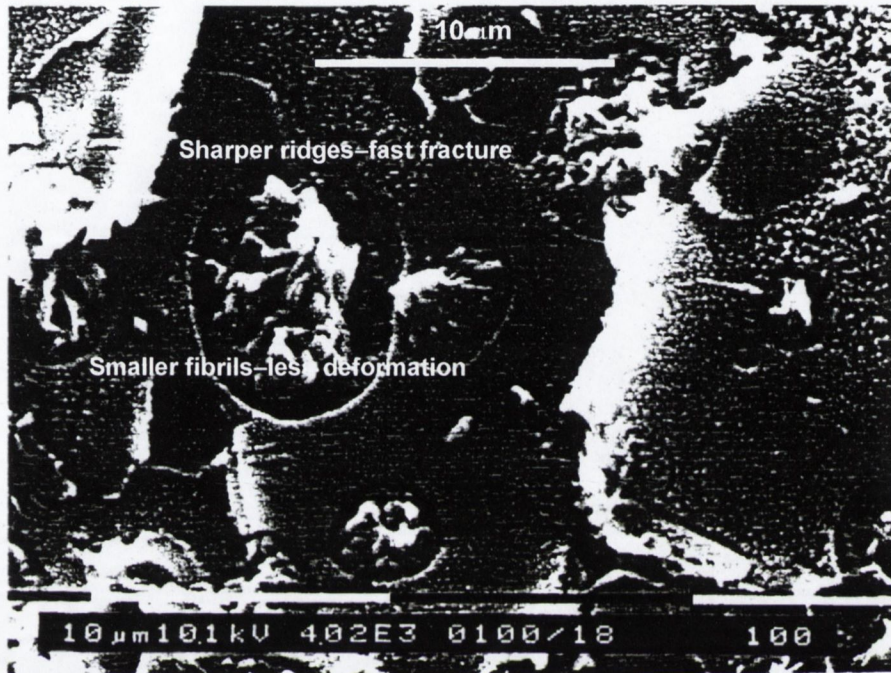


Figure 5.25. Fatigue fracture surface of PSB3-5, illustrating the difference between its effectiveness in involving the matrix resin in the crazing process with PSB3-45.4

In contrast to Figure 5.24, where the fibrils appear larger, more closely spaced and lie close to the particle edge. In figure 5.25 they are smaller and far less evident in the area surrounding particles. The stunted appearance of fibrils suggested that once the crazes had formed they quickly failed at lower strains. The sharp 'ridges' observed in Figure 5.25, aren't present in Figure 5.24. The fibrils appear as 'dimples', on the surface of the ridges, which confirms them to be part of the fracture plane. In contrast the ridges observed on the surfaces of higher volume loaded specimens are deformed matrix material that form a boundary between competing craze fronts.

The coarser, larger and sharper ridges in Figure 5.25, indicate that crazes opened less and involved far less plastic deformation of the matrix. Their size indicates that failure through their plane occurred more rapidly. Consequently it would be considered that the propagating crack fronts in lower volume loaded resins were more brittle and the process zone accompanying their growth was smaller and/or more diffuse. The differences observed between the ridges and fibrils underline the importance of the efficiency of the secondary phase in 'diffusing' load by crazing. Their efficiency determines the extent

to which energy is slowly diffused by craze initiation and growth, micro-crack formation or quickly released from the system by cracking and fracture.

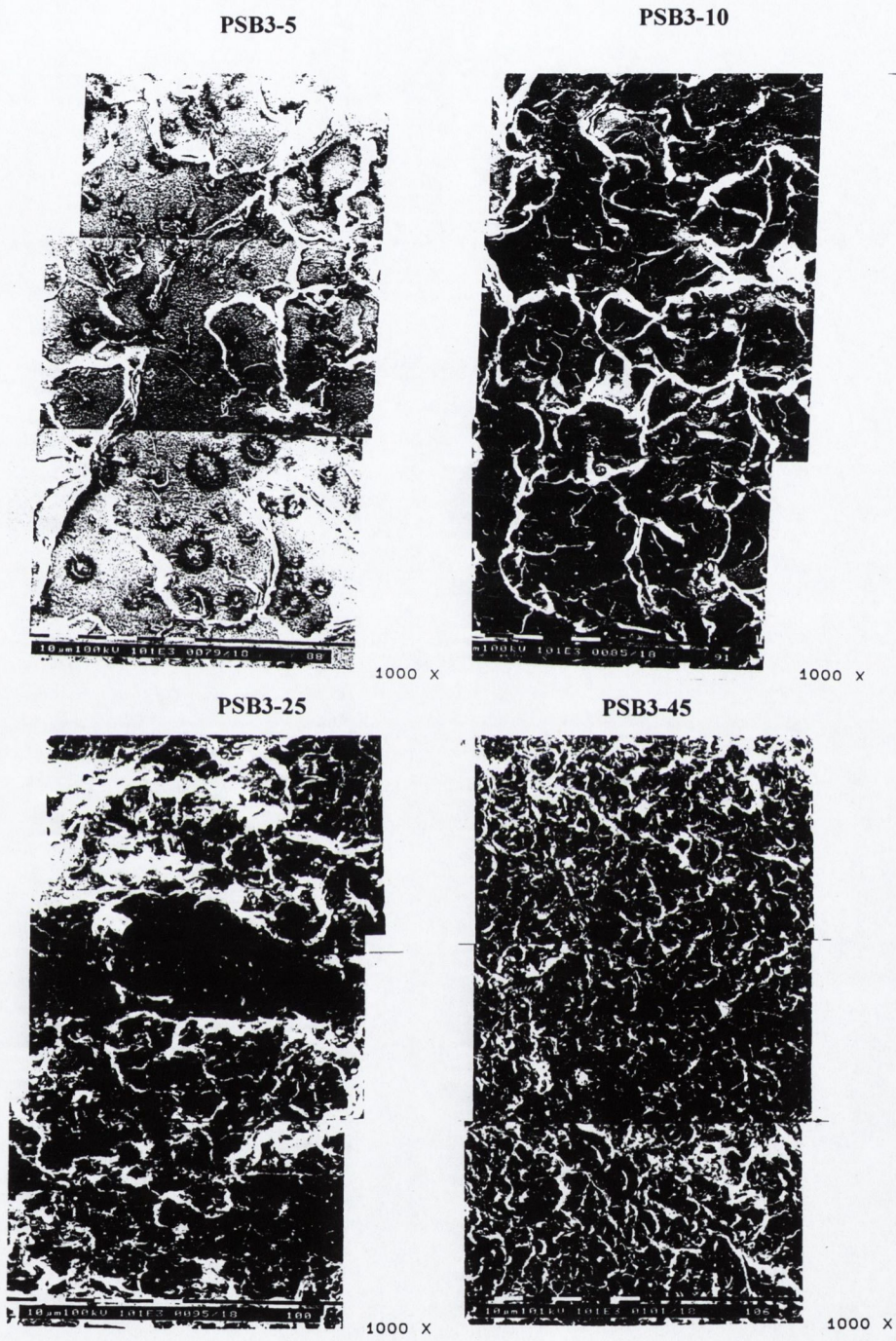


Figure 5.26. SEM images of PSB3 series resins illustrating the increased disruption of the fracture surface with increased rubber phase content indicating increased levels of crazing.

As the ERPV was increased in the resins, the difference between these micro-structural features became less dramatic. However the different facility of each of the resins to initiate and then restrain the growth was evidenced in the topographies of fractured specimens. The series of topographies presented in Figure 5.36 are of PSB3-5, 10, 20 and 45.4 specimens and show how the density of crazing increased with increased rubber content.

The difference between the surfaces over the range of ERPVs is dramatic and indicative of the difference in the potential energies released from the matrix resins on crack extension associated with increasing the ERPV. Though some differences could be observed between the topographies of the three series at equivalent ERPV it was not as clear as that between surfaces of materials with different ERPV.

Surface crazing alone does not provide a complete picture of the artefacts of material disruption resulting from the dissipation of energy associated with resisting crack growth. Indeed it is difficult to appreciate the magnitude of difference in crazing between the surfaces. Crazing though occurs throughout the volume of the process zone.

Figure 5.19.a illustrated how each particle size population affected distinctive fracture process zone shapes. Each pattern mapped out a different craze zone volume that increased with ERPV reflecting the efficiency of the secondary phase in crazing. Populations of particles instigating the process of crazing throughout a greater volume could potentially realise a greater amount of potential energy than others exhibiting higher densities of crazing in smaller volumes and visa versa.

In Figure 5.27 the level of sub-surface crazing associated with each of the PSB3 series of resins is presented. The extent of sub-surface damage is reflected in the disruption of the surfaces. The images also corroborated the notion of crazing being directly influenced by interparticle distance. The images are easier to study in terms of craze density and provide a potential route for validating predictive models of crazing. A quantitative appraisal of the correlation between superficial and sub-surface craze density and the interparticle distance was not conducted but it is clear from 5.27 that the size and proximity of particles increases the number and density of crazes formed. The differences in the volume of material crazed clearly would have determined the energy absorbed in propagating fatigue cracks.

The observations made using the different microscopy techniques illustrated how the process of fatigue crack propagation occurred in the materials. They show how crazes grew and coalesced to form cracks and how the secondary phase influenced this process of damage accumulation. These processes dictated the resistance of the resins to fatigue cracking and while qualitative they indicate how differences in micro-morphology influenced behaviour they cannot address the differences observed in terms of fatigue life and crack growth rates.

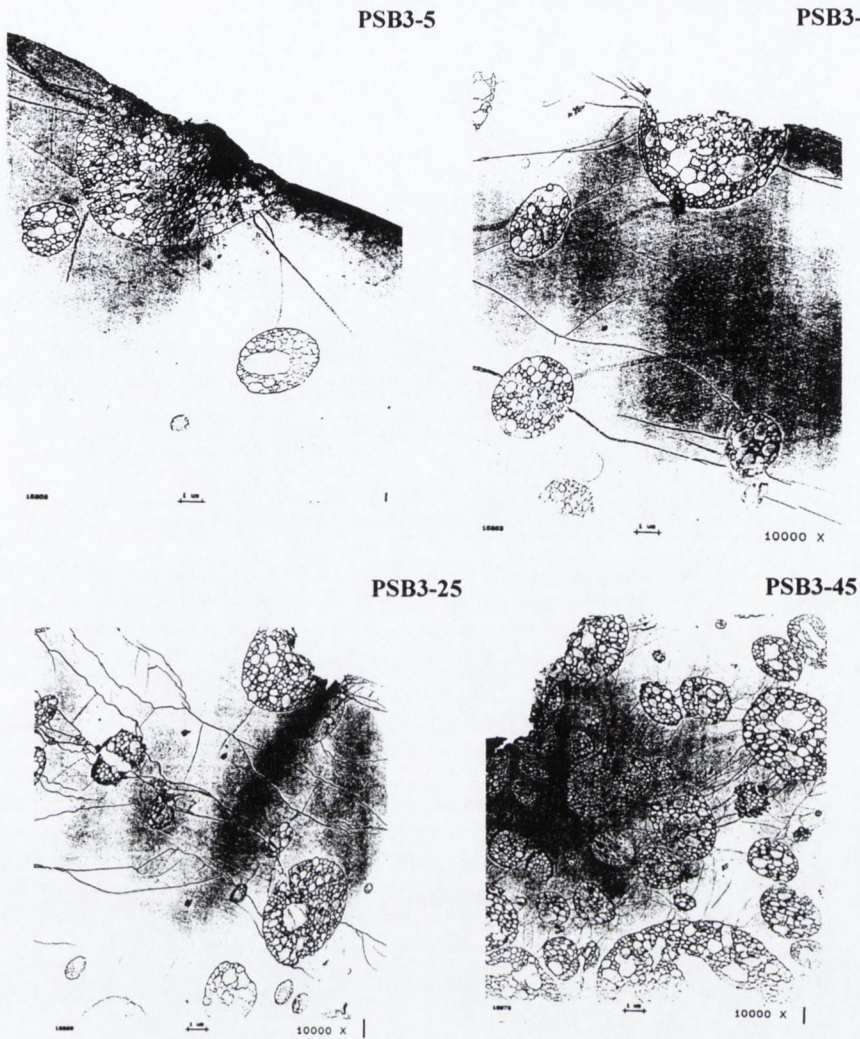


Figure 5.27. TEM images of PSB3 series resins sectioned beneath the plane of fracture indicating the extent of damage beneath the propagating crack front.

5.5.4 Influence of the Secondary Phase Morphology on Fatigue Life

Figure 5.28, plotted from Table 5.2, p. 182, illustrates the influence of the secondary phase volume on the fatigue life of the materials. It shows that in general the influence of increasing ERPV was to extend the fatigue life of the materials. However, its influence was inconsistent and differed significantly between the three resins. These differences are to be accounted for as having arisen as a result of the differences between the particle size and/or particle size distributions of the three parent resins.

In the PSB#1 series fatigue life rose with successive ERPV additions, while in the case of the PSB#2 and PSB#3 series, maximum fatigue life was achieved between 15-25% ERPV and fell thereafter. Figure 5.29 considers fatigue life in more detail, comparing the portions of the fatigue life expended in initiating and propagating cracks to failure. The plot shows that the pattern of the proportions of fatigue

life expended on initiation and propagation of the three series to increasing additions of the secondary phase to be reasonably consistent over the range of ERPV's considered.

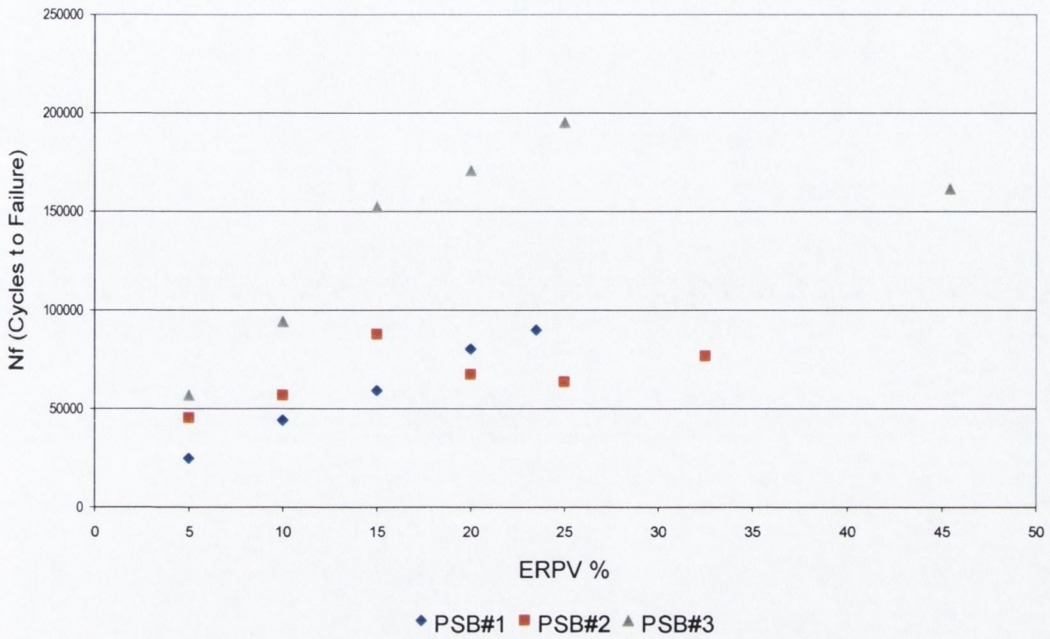


Figure 5.28. Total fatigue life (n=4) vs. ERPV for the three series.

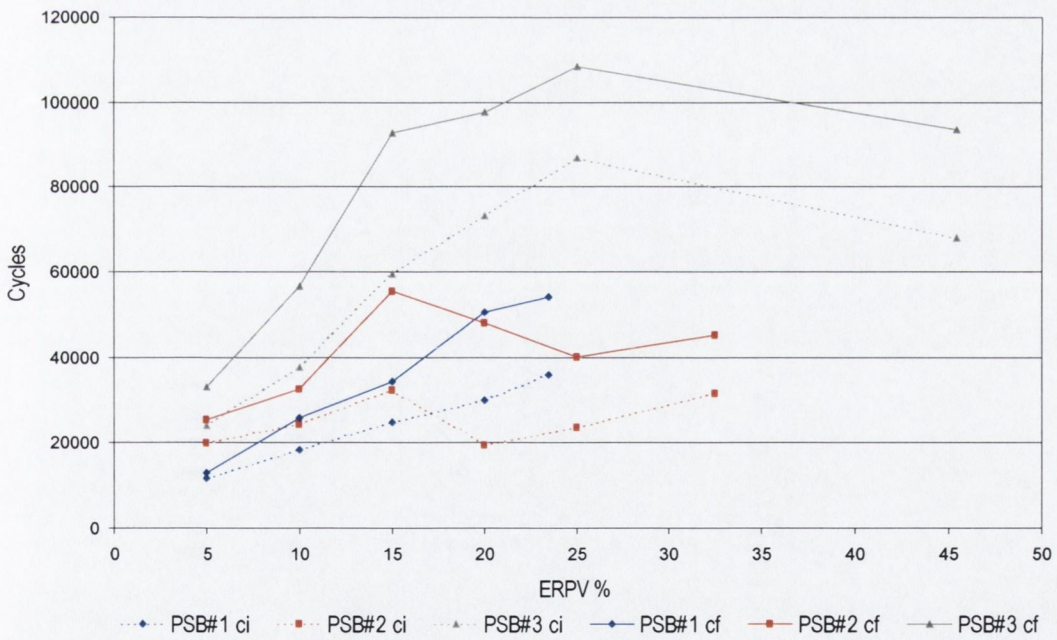


Figure 5.29. Comparison of the fatigue life consumed in crack initiation and propagation to failure vs. ERPV for the three series.

In the case of the PSB#1 series, increasing the ERPV increased the number of cycles associated with initiation and propagation over the range of secondary phase additions considered. The number of cycles required to initiate and propagate cracks to failure also increased with ERPV in the PSB#3

series. However at its highest volume loading, 45.4%, the resistance of the particles size population to crack initiation and fatigue crack growth fell. Up to 15 % ERPV the response of the PSB#2 series was consistent with PSB#1 and PSB#3 series. However with additions over 15% ERPV the number of cycles associated with initiation and propagation declined.

The results were contrary to the expectations inspired by the impact test data. Up to 15 % ERPV, the PSB#2 series, which possessed the highest impact strengths, and had been expected to perform best under fatigue, ranked only second in terms of fatigue life and resistance to crack growth. With ERPV > 15%, their resistance to crack initiation and growth was less than that of the PSB#1 series who, from the impact data set, it was thought should have performed worse. The PSB#3 series exhibited the largest fatigue life and greatest resistance to crack initiation and growth.

Figure 5.30 considered the relationship between the ERPV and fatigue life in terms of the ratio of the number of cycles expended in crack initiation (N_{ci}) to that expended in propagation (N_{cf}). Initial inspection suggested there was little or no change. However closer examination suggested there was a consistent pattern of response to increasing ERPV.

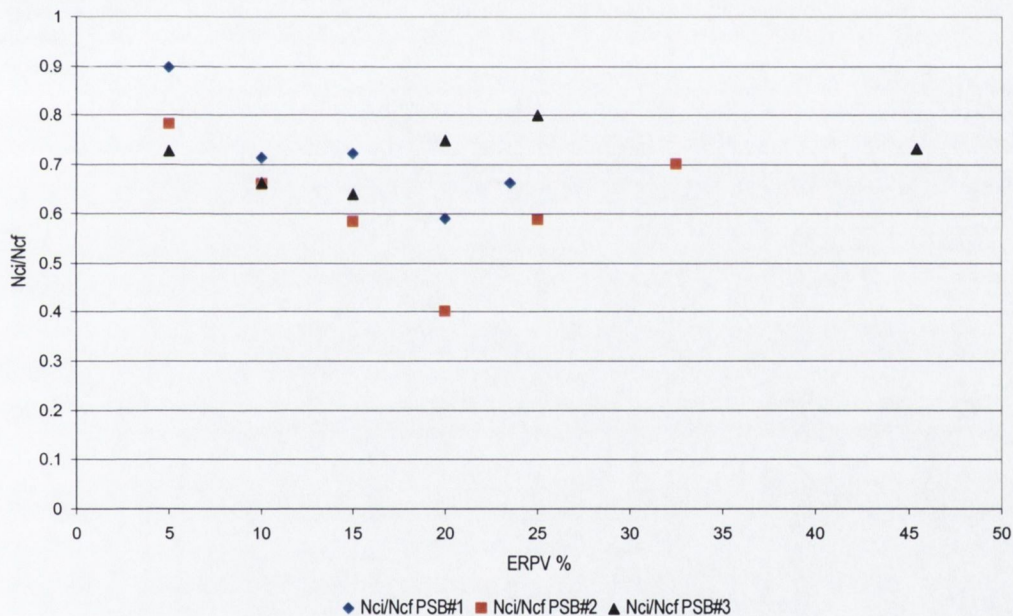


Figure 5.30. Plot of ERPV vs. N_{ci}/N_{cf} for the three series. [◆-PSB1 , □ – PSB2 and ▲ – PSB3].

In all tests N_{cf} exceeded N_{ci} , and initial additions of secondary phase volumes increased the N_{cf} in all of the materials. However additions over 15 and 25%, led to a fall in this trend and an increase in the relative contribution of N_{ci} in PSB#2 & 3 series. This was particularly noticeable in the PSB#2 series which had been most sensitive to changes in ERPV.

Fatigue Materials	PSB#1 (n = 4)			
	Nf	Nci	Ncf	Nci/Ncf
PSB1-5	24640	11654	12986	0.90
PSB1-10	44016	18315	25701	0.71
PSB1-15	59089	24755	34334	0.72
PSB1-20	80213	29754	50459	0.59
PSB1	89873	35770	54103	0.66
PSB#2 (n = 3)				
	Nf	Nci	Ncf	Nci/Ncf
PSB2-5	45110	19788	25322	0.78
PSB2-10	56619	24162	32457	0.74
PSB2-15	87516	32208	55308	0.58
PSB2-20	67191	19197	47994	0.40
PSB2-25	63536	23518	40018	0.59
PSB2	76500	31500	45000	0.70
PSB#3 (n = 3)				
	Nf	Nci	Ncf	Nci/Ncf
PSB3-5	56908	23996	32912	0.73
PSB3-10	94189	37581	56608	0.66
PSB3-15	152249	59464	92785	0.64
PSB3-20	170667	73143	97524	0.75
PSB3-25	195171	86766	108405	0.80
PSB3	161500	68100	93400	0.73

Table 5.2. Results of 8mm (500N) series Fatigue Tests.

Figures 5.29 and 5.30 suggested that small additions of secondary phase volume contribute more to resisting fatigue crack growth (FCG) than they do to inhibiting crack initiation. At higher levels of addition, in the PSB#2 and PSB#3 series, the slight decline in fatigue life observed at ERPV >15% was accompanied by a recovery in the proportion of fatigue life spent initiating cracks. The observation appeared to suggest that the energy expended in resisting crack initiation somehow exhausted the materials ability to resist future fatigue crack growth.

The differences between the three series of resins suggested that the influence of the particle size/distribution was fundamental in dictating how increasing the secondary phase volume influenced the process of crazing, or damage accumulation, and consequently fatigue life and resistance to failure.

5.5.5 Evaluating the kinetics of fatigue crack growth using the Paris Law.

The interpretation outlined above was supported, in somewhat conflicting ways, by a number of observations made of the kinetics of crack growth using the Paris analysis. These suggested that significant differences existed between the manner in which the different particle size populations influenced fatigue crack initiation and growth resistance as their ERPV was increased.

A first point of note is that the behaviour of all of the resins conformed to the Paris law; i.e., in so far as a linear relationship between the rate of crack growth and ΔK was exhibited. A second consistent point was that the rate of crack growth in each series of materials fell as ERPV increased. This is presented in Figures 5.31 – 5.33.

Compliance with the Paris law was expected, as reported in the introduction, it is widely employed in modelling the fatigue crack propagation behaviour of many polymers, and was successfully applied to both PS and HIPS previously [19, 54]. The fall in crack propagation rates, da/dN , with ΔK , as ERPV was increased, was also anticipated from Hertzbergs' comparison of FCG in PS and HIPS [52].

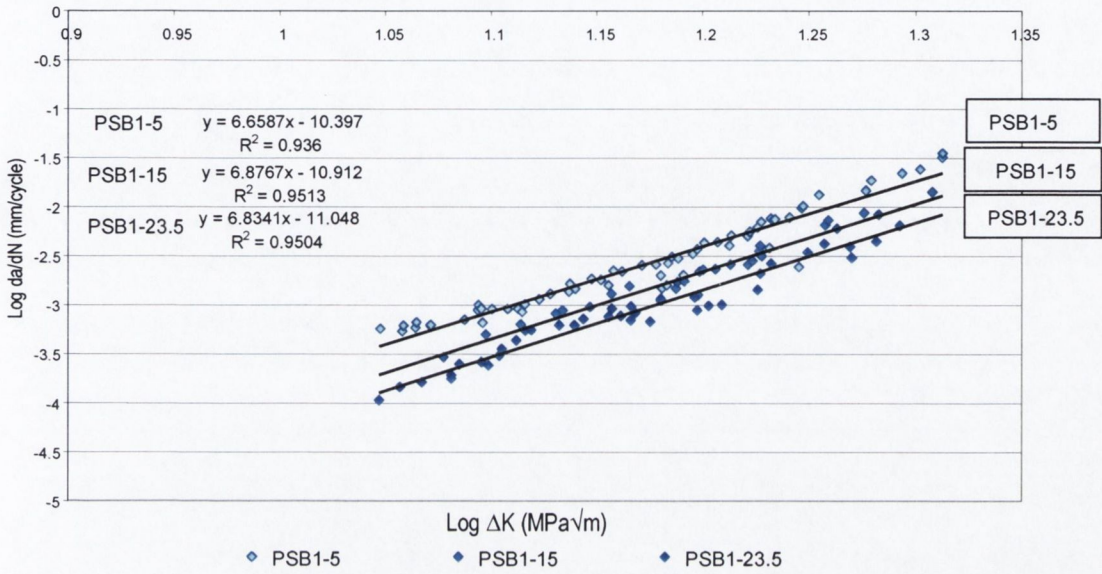


Figure 5.31. Paris plot and linear regression curves for 5, 15 and 25 % blends of PSB#1 resin.

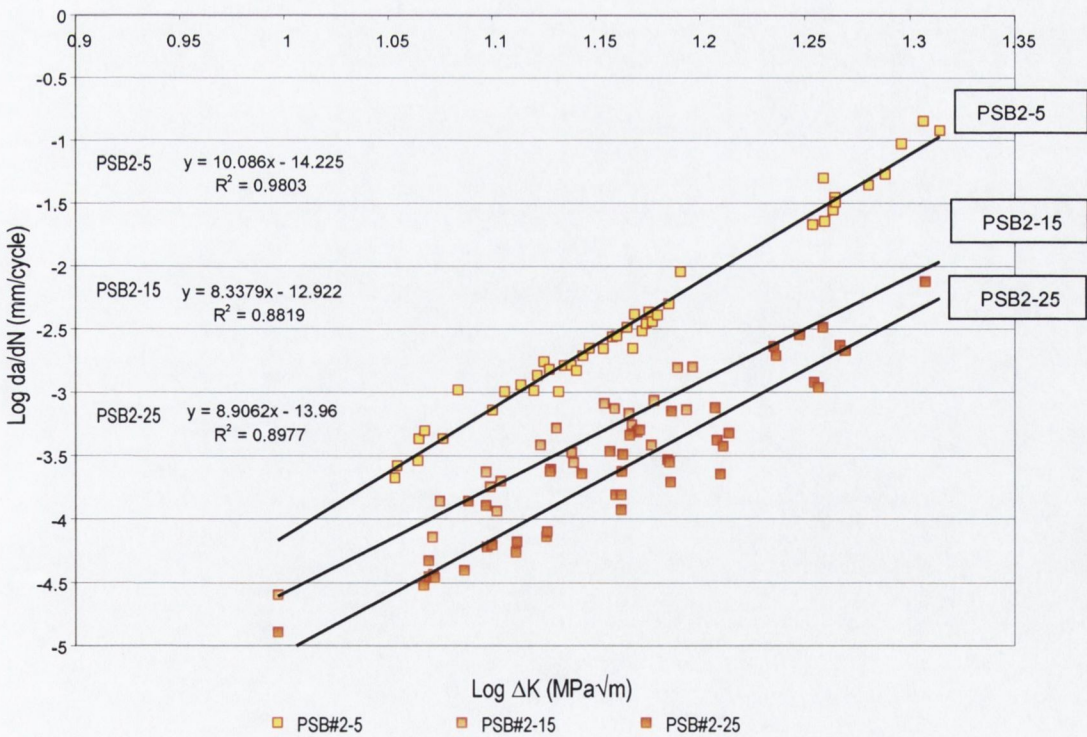


Figure 5.32. Paris plot and linear regression curves for 5, 15 and 25 % blends of PSB#2 resin.

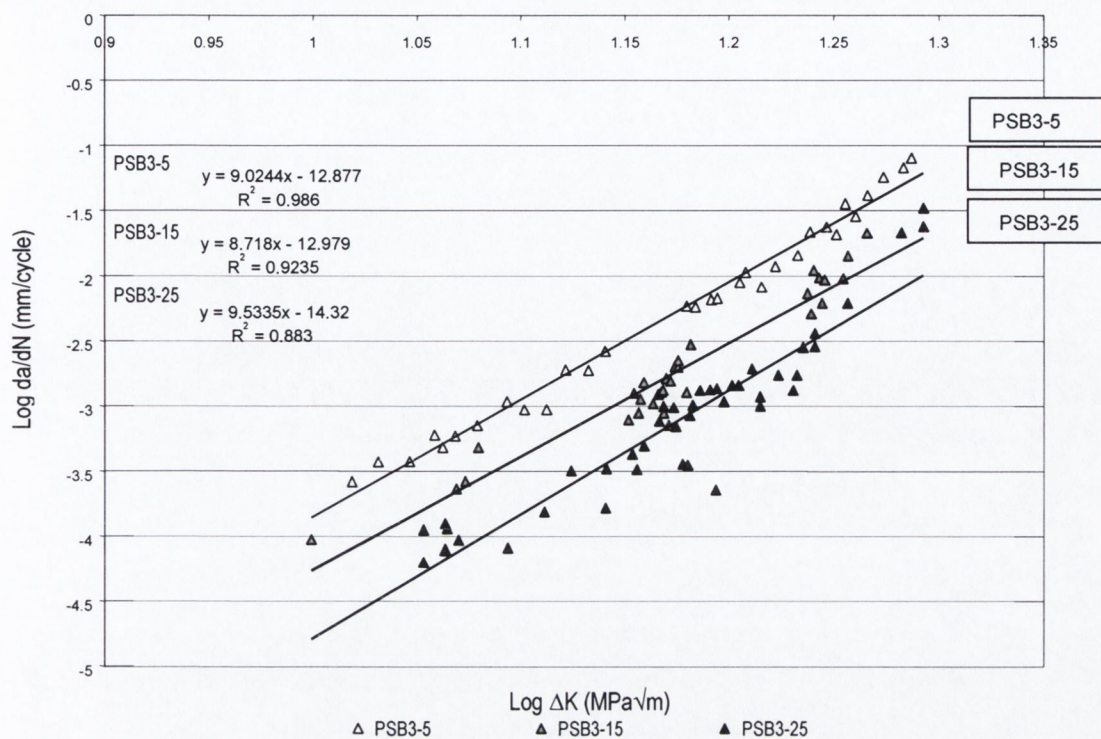


Figure 5.33. Paris plot and linear regression curves for 5, 15 and 25 % blends of PSB#3 resin.

However when Paris plots were prepared to compare the behaviour of the three series at equivalent ERPV, it became apparent from the graphs and the slopes of each curve that the three series exhibited distinct and unexpected trends in relation to the influence of increasing the ERPV on FCP. Figures 5.34 – 5.36 illustrate this, with examples of Paris curves from tests on 5, 15 and 25 % ERPV polyblends from each series. The curves are observed to cross each other as ΔK increases. In doing so they reveal the distinct sensitivity expressed by the three particle size populations to increasing ERPV.

Differences were expected. However the sensitivities, implied in the slopes of the curves, did not concur with the expectations raised in previous tests, i.e., tensile, impact, and fracture toughness tests. These suggested that the variation of the crack growth resistance with ERPV would be consistent and rise with increasing ERPV. It was thought that the PSB#2 series, the series that possessed the greatest impact toughness, would exhibit the greatest resistance to crack growth whilst the PSB#1, the weakest, series, the poorest.

Instead conflicting relationships and trends in crack growth rates were observed, within and between, the three series of particle size distributions as ERPV was increased. These differences lay bare the origin of the inconsistencies in material performance and misconceptions that motivated the research, i.e., of a correlation between fracture toughness and fatigue life. They also expose the frailties of the assumptions concerning such a correlation in the case of HIPS. Paris constants (A) and exponents (m), indicating the sensitivity of the rate of each materials crack growth rate to ΔK, are presented in Table 5.3 and Figure 5.37, for each of the materials.

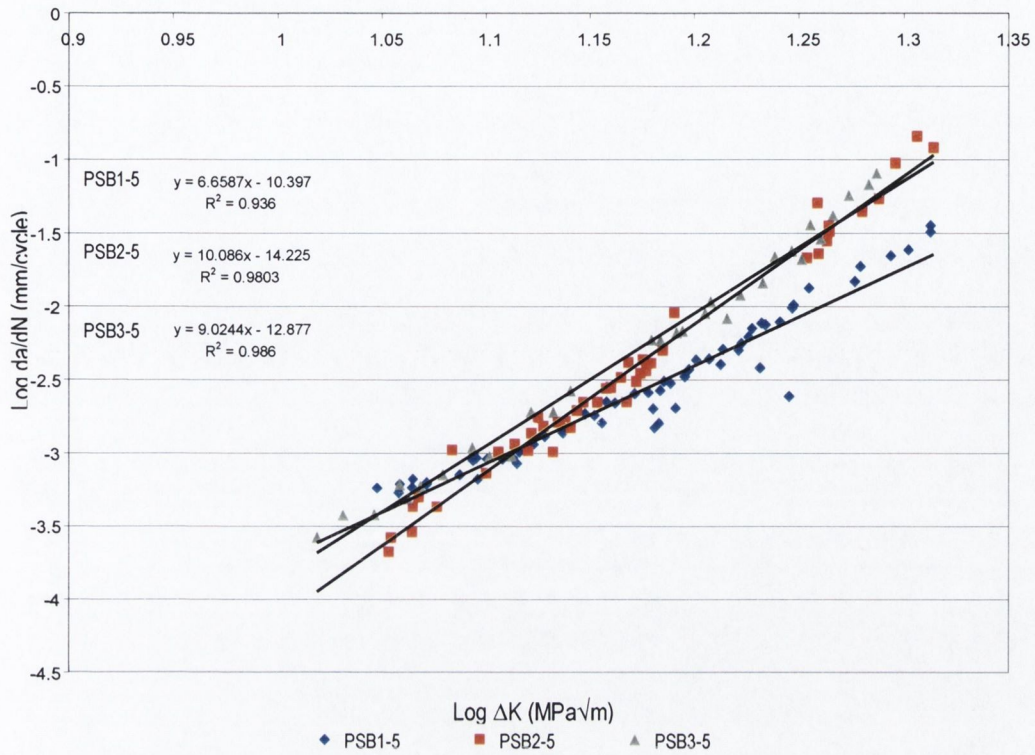


Figure 5.34. Paris plot comparing the FCG of PSB#1- #3 with 5 % ERPV [\diamond -PSB1, \square - PSB2 and \triangle - PSB3]

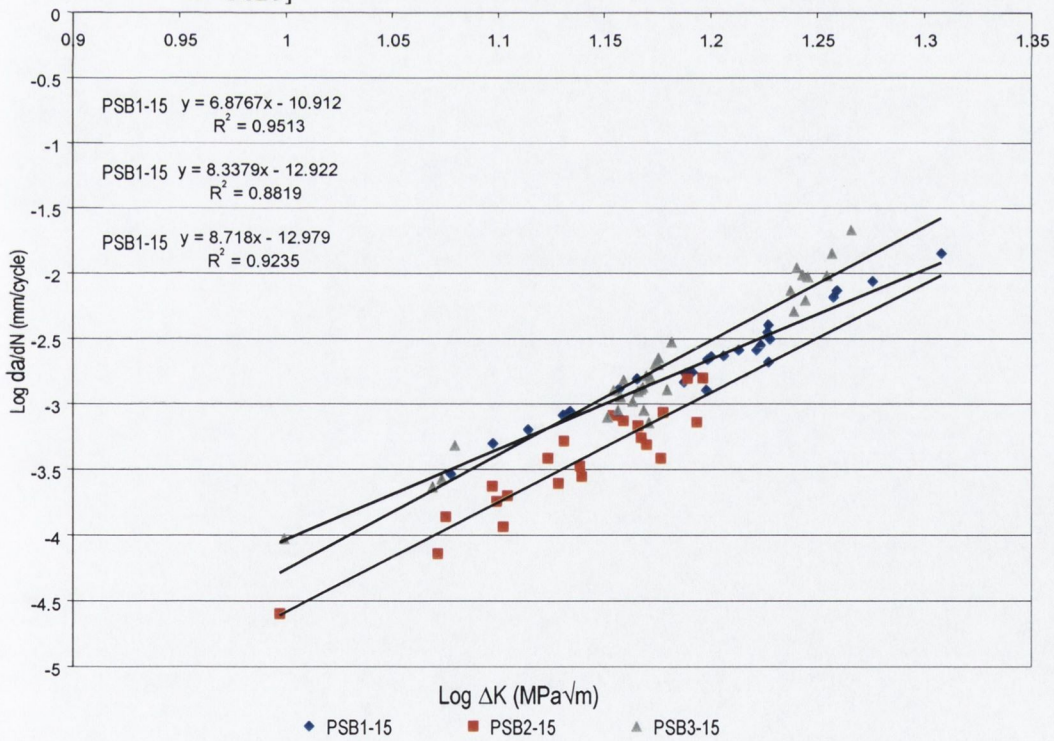


Figure 5.35. Paris plot comparing the FCG of PSB#1- #3 with 15 % ERPV [\diamond -PSB1, \square - PSB2 and \triangle - PSB3]

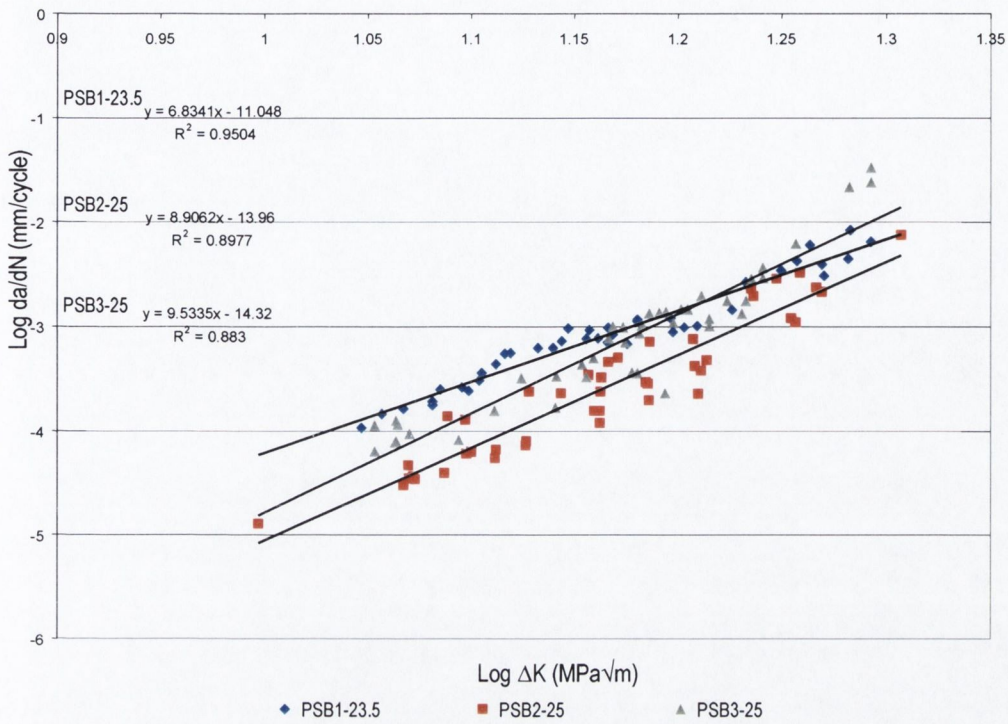


Figure 5.36. Paris plot comparing the FCG of PSB#1- #3 with 23.5 and 25 % ERPV[◇-PSB1 , □ – PSB2 and △ – PSB3]

Paris Materials	PSB#1		PSB#2		PSB#3	
	A	m	A	m	A	m
PSB# -5	10.397	6.6587	14.225	10.086	12.877	9.0244
PSB# -10	10.537	6.798	13.225	9.456	13.581	9.425
PSB# -15	10.912	6.8767	12.922	8.3379	14.283	9.8828
PSB# -20	11.01	6.84	13.567	8.547	14.34	9.79
PSB# - 25	11.048	6.8341	13.96	8.9062	14.32	9.5335

Table 5.3. Paris constants A and m obtained for PSB#1, 2 and 3 at 1Hz 500N R=0.

The difference in the magnitudes of crack growth rates associated with the three particle size populations is clear, even from Table 5.3. The magnitude of m is greater than what is associated with fatigue in metals, but consistent with that observed for many polymers [21,23]. Figure 5.37 illustrates the differences between crack growth sensitivity and ERPV more clearly.

The plot (figure 5.37) shows that m increases, very slightly, with ERPV in the case of the PSB#1 series, over the entire range of ERPV considered. Though m fell at the highest volume loading of the PSB#3 series, its value had increased as the PSB#1 series had, with ERPV up to 25%. These observations contrast sharply with the changes in crack growth rates with ΔK associated with increasing ERPV in the PSB#2 series. In these it initially slowed as ERPV was increased up to 15% but at higher volume loadings (>15%) it then increased.

The contrast with expectations could not have been greater. Instead of reducing crack propagation rates with increasing ΔK , increasing ERPV tended to accelerate crack growth rates (PSB#1 and PSB#3). While in the case of PSB#3 and PSB#2 the variation in FCG rate with ERPV was found to be inconsistent over the range of ERPVs considered.

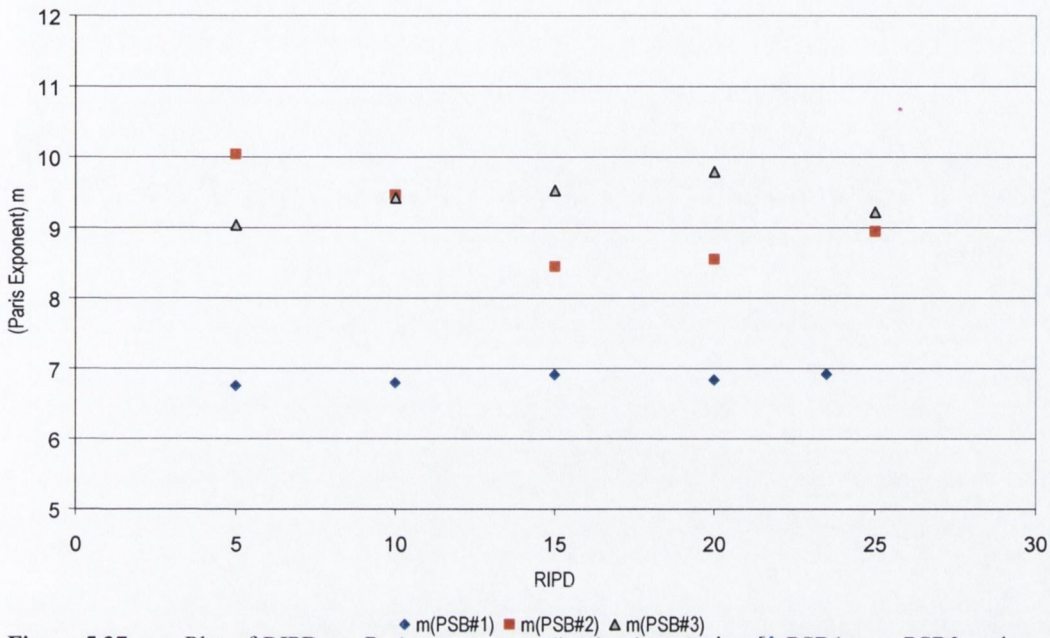


Figure 5.37. Plot of RIPD vs. Paris exponent m for the three series. [\diamond -PSB1, \square - PSB2 and \triangle - PSB3]

.5.5.1 The sensitivities of fatigue lifetimes and Paris exponents to changes in microstructure.

It was remarked, in respect of Figure 5.30, that the three series of materials had exhibited some consistency in relation to the way the pattern of the portions of their fatigue lives, expended in crack initiation and propagation, had varied with increasing secondary phase volume.

The relatively consistent pattern of variation in the relative contribution of the N_{ci} and N_{cf} to N_f , with RIPD (and so ERPV) in the three series, conflicted with the notion that increased secondary phase volume should lead to a consistent influence on fatigue crack growth resistance. This confounded expectations. The results of tensile, impact and fracture toughness tests had each varied in a consistent fashion with ERPV, and so the same was expected of FCG. Though it was surprising to find it didn't, the conflicting trends that were noted in regard to the influence of the secondary phase on the kinetics of crack growth were even more unexpected. The results of the Paris analysis were compared with the fatigue life studies (number of cycles to initiation and propagation to failure). This provided an understanding of the influence of the secondary phase morphology on FCG resistance, m , in the context of the S-N curve for each material. In the case of the latter it is recognised that each individual polyblend possesses a distinct S-N curve, consequently the initial effect of incorporating ever-increasing volumes of secondary phase then is to alter the S-N curve.

The tensile yield (T_y) and rupture (T_r) strength of the materials had fallen as ERPV increased, (chapter 3). Consequently the cyclic stress that was initially applied to each series of polyblends represented an increasing proportion of the T_y and T_r . It might have been anticipated as the ERPV increased that the S-N curves should then shift to the left – to lower N_{ci} , and lower σ_e . However the presence of the notch notch already had offset the initial S-N curve toward lower N_f . Indeed the extreme notch sensitivity of Polystyrene had resulted in most PS samples failing as their notches were being sharpened.

The addition of the secondary phase reduced the materials notch sensitivity, even at very low additions, resulting in a shift in the S-N curves to the right, toward higher numbers of cycles to initiation and failure. The stress amplifying effect of the notch was reduced with increasing ERPV, as the modulus of the materials fell, shifting failure further to the right and higher values of N_f . The effect of the notch on crack propagation rates was minimal.

Comparing Figures 5.30 and 5.37, it appears that the response of the three series at low levels of ERPV differs with their response at high. The differences are small but consistent over the three series and consequently significant, though only 3 replica tests were conducted. Increasing ERPV from low levels of secondary phase increased the number of cycles to initiation and extended the proportion of fatigue life expended in propagating cracks. This suggested that the S-N curve for the materials had indeed been offset to the higher N_f , and the σ_e for the notched part had been raised.

At higher levels of addition the response of the materials is not as easily surmised. The rate of increase in N_f with ERPV began to level off and/or decline. The PSB#2 series were most sensitive to the change and the number of cycles associated with N_{ci} and N_{cf} began falling at 20 % ERPV. The PSB#3 series were less so, and though values for N_{ci} and N_{cf} began to level off at 20% they were not observed to not fall until the maximum volumetric loading, 45.4% ERPV, was tested. The PSB#1 series were least sensitive, though the trend in the fall in N_{ci} was visible at 20 % ERPV. Thus, in contrast to the effect of low levels of addition, high levels of ERPV tended to start shifting the S-N curve for the materials to the left and lowering the σ_e for the specimen.

Similarly the variation in the Paris exponent, m , differed between low and high levels of addition. In respect of the fatigue lives it was noted that the N_{cf} increased with initial low additions of secondary phase in each family of resins and tended to level off or decline at high ERPV. The crack propagation resistance of the materials differed significantly, especially at low ERPV.

Though they exhibited the shortest fatigue lives, the PSB#1 series proved to be least sensitive to increasing ΔK , exhibiting the lowest level of m . Interestingly however, increasing the secondary phase volume slightly increased their crack growth rate sensitivity to ΔK , despite the increase in N_{cf} that accompanied with low additions of ERPV. Similarly, m increased in the PSB#3 series, again, despite the increased N_{cf} . However its magnitude was significantly greater than observed in PSB#1 resins and fell at high ERPV > 20%. It was also much greater in the PSB#2 series. However in contrast to the two,

in the PSB#2 series the value of m initially fell with low ERPV additions, while at high ERPVs m increased.

.5.5.2 *Explaining relationships between microstructure and fatigue behaviour.*

The increase in m accompanying increasing ERPV was consistent and contradicted the expectation, from the impact tests, that there should have been an increase FCG resistance. The apparent conflict is easily explained though, through the increased level of crazing that increased ERPV facilitates. The mechanism of energy dissipation that promotes increased impact toughness in fatigue hastens damage accumulation and ultimately crack advance. Though more energy can be accommodated by the system with a greater ERPV, under fatigue loading, increased levels of cycling will induce more damage in the fracture process volume and in doing so exhaust the strain energy absorbing mechanism.

Consequently as cracks extend and ΔK increases, more energy is made available through the increased effective stress and more damage is accumulated in the process zone. Precrazed material does not possess as much energy absorbing potential and so, as cracks extend, the level of damage increases, and the resistance to crack propagation declines. So m increases.

The contrast in values obtained for m , between the PSB#1 series and the rate sensitive PSB#2 and PSB#3 series is also explained by this. It had been remarked in chapter 4 and earlier in this discussion, that the damage zones in the PSB#1 resins were smaller than those in the other series. The explanation for this was the limited ability of its particles to be effective in crazing, even when RIPD was small. Process zones were larger in the PSB#2 and PSB#3 series because of the efficiency of the secondary phase in initiating crazes. Their size increased with ERPV and with continued cycling. Thus, although more cycles could be accommodated before initiation and consumed during propagation the rate at which damage accumulated and the amount of it was greater. Consequently as cracks advanced they did with increased rates, as ΔK increased.

The contrasting variation of m with ERPV, between the PSB#2 and PSB#3 series, can also be explained similarly. The superior craze efficiency of the PSB#2 series particle size/size distribution, that effected a greater impact strength was also noted to facilitate a higher density of crazing. The damage zones of the PSB#2 resins were noted to exhibit a darker contrast and to be more confined than those of the PSB#3.

The increase in N_{cr} and the greater craze efficiency of the PSB#2 series contributed to their resisting crack propagation at low volume loadings. When the concentration of particles increased, at high ERPV, crazing was easily facilitated and a larger process zone of exhausted precrazed material accelerated crack growth. Consequently the number of cycles to failure fell as did the proportion of N_{cr} and while m increased, as the level of precrazing exhausted the materials crack growth resistance. In contrast, though the sizes of the process zones of the PSB#3 series were larger, the density of crazing in it was lower, or more diffuse. The rate of sensitivity of the materials had increased with initial loadings as the process zone was shielded by the diffuse crazing throughout a greater volume around the crack.

Higher ERPV was required before sufficient craze density was achieved to lower the resistance to initiation and then propagation.

The Paris law assumes LEFM. The stress intensity, K , is purely a function of geometry and load. In applying Paris one assumes the FCG behaviour of HIPS is accurately described by LEFM. Although the size of the process zones were very small, in the early stages of crack growth, their size did increase with cycling and LEFM conditions were not maintained. Thus K , though deterministically involved in determining stress, was not the sole factor driving crack extension. Extensive damage, diluting the concentration of stress at the crack tip, depreciating the intrinsic strength, or the strain energy potential, of the material was clearly complicit.

The correlations offered in the Paris analysis do capture the effects of the events and reflect the reality of the actual growth of cracks. But they do so by ignoring the process through which the secondary phase controls it. They fail to characterise the process through which further crazing, acting as an energy sink, dissipates the energy otherwise destined for the tip of the propagating crack. In effect the collusion offered by increasing stress concentration and crazing, mask the decay in the integrity of the material and its crack resistance in advance of the crack front by involving a greater volume of matrix in the failure process.

Thus though Paris described and provided a rational context in which to discuss observations made in fatigue tests, it did not provide a theoretical paradigm that could explain the context in which variations arose. It is reasonable to employ it to consider the influence of the secondary phase morphology on fatigue crack propagation in HIPS though conclusions based on it alone are incomplete. In the final analysis, irrespective of its flexibility to model behaviour, the process of FCP in HIPS does not arise as a result of a linear elastic process of fracture. Whilst Paris provides a means of modelling and interpreting behaviour, a method that characterises the decay in the potential energy of the system would seem more apt. The J integral is such a parameter.

5.5.6 Modelling Fatigue Crack Propagation in terms of ΔJ .

From the discussion above it was concluded that an energy based approach would be better suited to describing the process of FCG in HIPS and in accounting for the influence of the secondary phase. In addition to being more appropriate it was hoped that modelling FCP behaviour in terms of the energy based parameter might provide a means of modelling the crack growth kinetics in a manner that accommodated the differences associated with microstructure, in terms of toughness and FCP rates.

To this end the rate of crack advance per cycle and ΔJ , the energy released in propagating crack was plotted in accordance with the Paris like expression proposed by Dowling and Begleys' where

$$\frac{da}{dN} = \bar{C} \Delta J^m$$

Equation 5.16.

where C and m' are material constants representing the rate of change of energy expended in crack advance [58]. Figures 5.38 – 5.40 present plots for the same data sets of PSB#-5, 15 and 25% resins modelled using the Paris law. The results of m for all materials is presented in Table 5.4 and plotted in Figure 5.42.

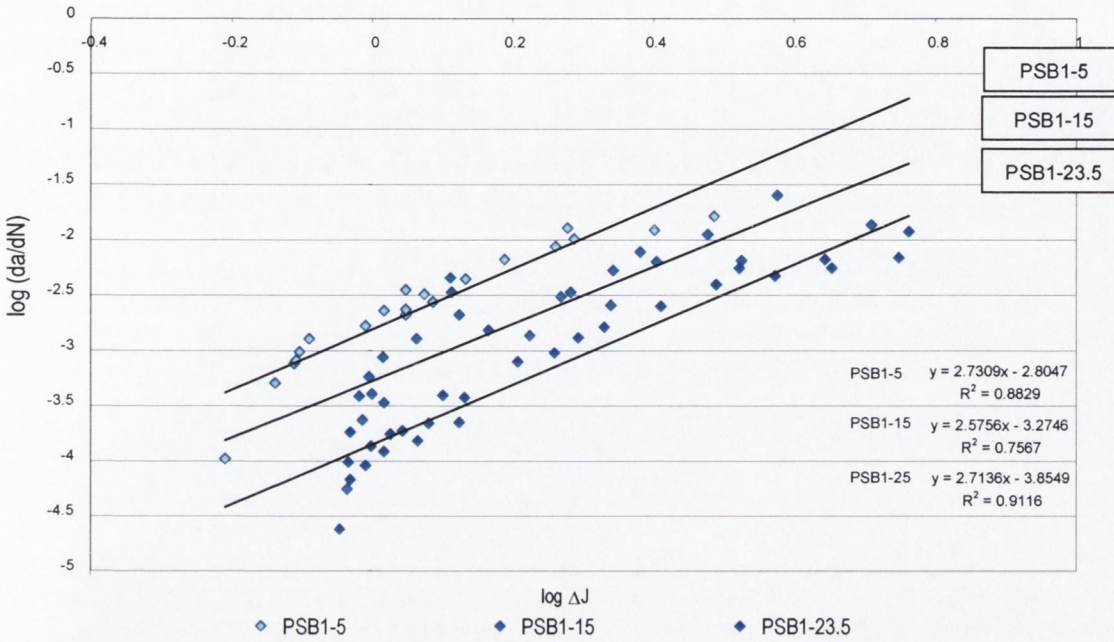


Figure 5.38. Plot of da/dN vs. ΔJ for PSB1-5, 15 & 23.5

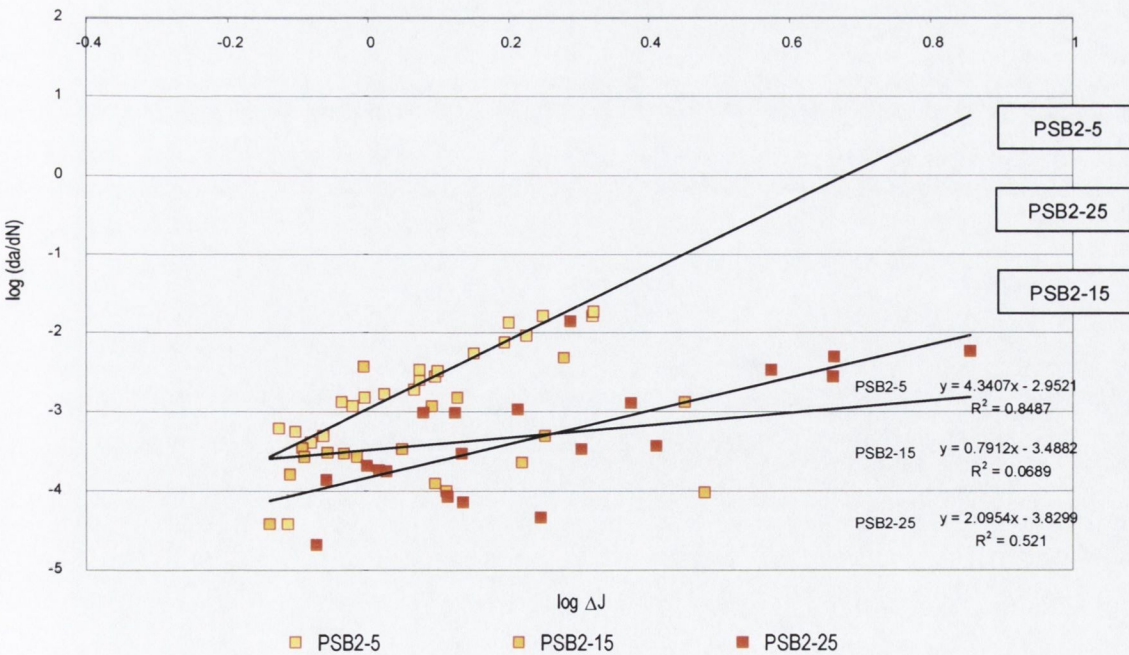


Figure 5.39. Plot of da/dN vs. ΔJ for PSB2-5, 15 & 25

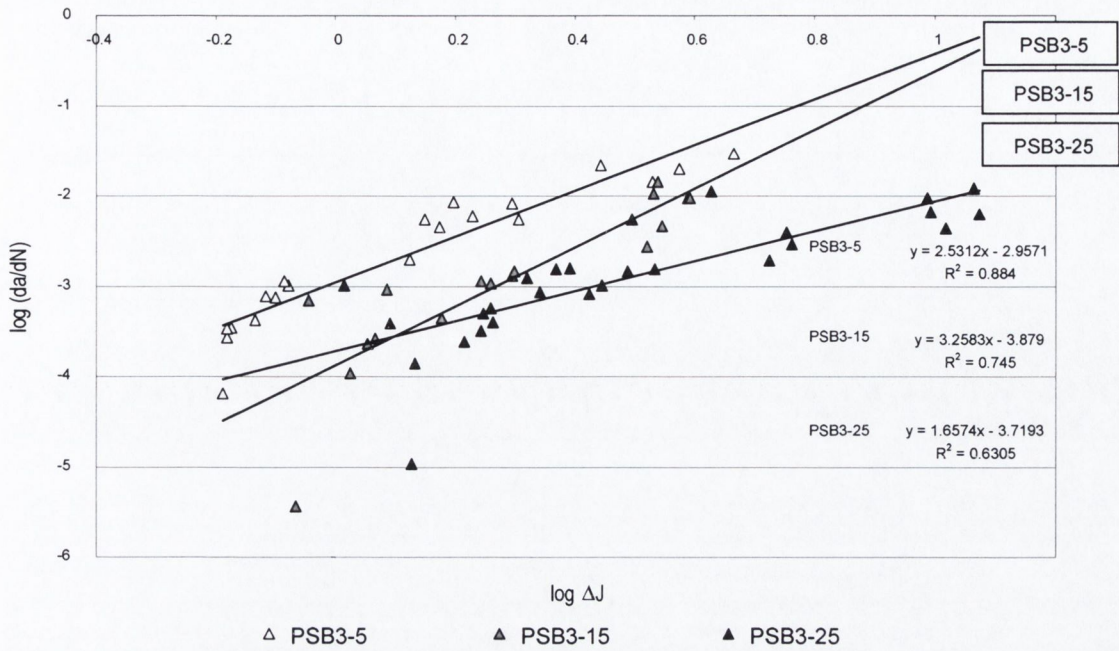


Figure 5.40. Plot of da/dN vs. ΔJ for PSB3-5,15 & 25

ERPv	m'		
	PSB#1	PSB#2	PSB#3
5	2.77	4.31	2.5312
10	2.6	1.6	3.12
15	2.6	0.77	3.2583
20	2.7	1.74	2.546
23.5	2.69		
25		2.15	1.6574
32.5		2.35	
44.5			1.115

Table 5.4. Variation in m' with ERPv

When plotted on logarithmic scales a two-stage fatigue crack propagation curve was obtained, reminiscent of Forsyths' three stage model for LEFM in some cases. The plots for each series revealed, as the Paris plots had, that the rate of crack extension increased with increasing ERPv.

The ΔJ plots contained significantly more scatter than plots of da/dN vs. ΔK. The scatter highlighted the difficulty in obtaining 'clean' measurements at specific crack lengths during crack propagation. Although it was reasonably easy to identify the crack tip, and synchronise data acquisition in the materials containing low volume additions, it became increasingly difficult at higher ERPv. The extent of the difficulty partially explains the contrasting appearance of the plots for high ERPv materials. The difficulty arose because the locus of stress concentration about the crack tip in the process zone continually changed as crack propagated and it was became more difficult to determine when a crack had reached the end of its growth phase and began a new one.

It was possible to distinguish between stages of crack advance, an early Stage I, that tended toward a 'threshold' value of ΔJ_{th} , and a later stage of stable Stage II growth. Identifying a threshold value supported the extrapolation of what was considered to be the J integral from the crack growth resistance curves at zero crack length, presented in Chapter 4.

In many respects the manner in which the fatigue tests were conducted is reminiscent of the load shedding technique commonly used to determine the threshold. In the tests the levels of stress were well below yield. The initial force applied to the materials ($\approx 500\text{N}$) giving rise to an initial maximum nominal stress of only 2.5MPa, and so concentrated stress levels well below the yield strength of the resins considered. Though damage did eventually appear in all of the experiments reported (conducted at 500N on 8mm specimens) it was not apparent upon initial loading in any, many thousands of cycles were required before crazing became evident. This was in contrast to series of tests conducted at under higher loads, (*considered in the course of the experimental work but not included as part of this thesis*). In these tests crazing was occasionally evident during the initial loading of specimens and the values determined for J consequently higher.

The concept of the threshold is not the conventional understanding concerning the flaw size associated with fatigue in metal but a threshold energy associated with initiating a crack. In essence its meaning is the same, i.e., the conclusion of staying below this critical level of energy is that fracture will not occur. However when fracture or failure might occur is not accounted for.

The threshold represents the limiting energy required for crack initiation. The rapid change in ΔJ associated with it reflects the transformation from short fast growth to stable propagation and is indicative of the constrained nature of the initial growth. Although it was possible to identify the J integral by extrapolating the values of J to zero crack length on the plot of J vs. crack length, it was not possible to determine the threshold value for ΔJ from the plots. However the two values are coincident. Thus the increase in J and the number of cycles associated with it increase with ERPV.

The threshold ΔJ was found to correlate reasonably well with fatigue life of the specimens (N_f), see Figure 5.41. The correlation between the threshold ΔJ and the cycles to initiation was good in the case of the PSB#1 and PSB#3 series materials, but very poor for the case of the PSB#2. The agreement between total fatigue life and the latter series indicated the pivotal role played by the secondary phase in resisting crack growth during propagation throughout the fatigue life.

It illustrates the dependence of both the fatigue life and FCP behaviour on the progressive accumulation of damage with successive cycling. The energy paradigm for modelling crack growth thus accommodates the variation in the m and m' with increasing ERPV. However it exposed the limitations of the optimised craze nucleation efficiency of the material in resisting the initiation and subsequent propagation of fatigue cracks.

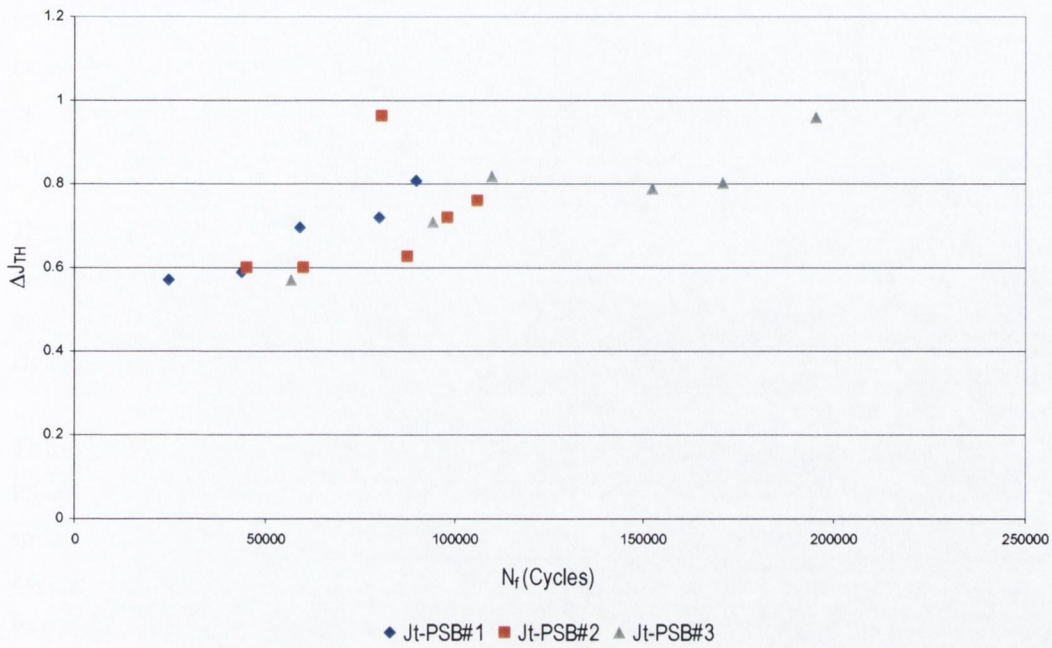


Figure 5.41. The variation of N_f with ΔJ for the three series of resins.

The correlation of fatigue life with the energy associated with crack initiation, or the intrinsic toughness, found the original hypothesis to be true, that fatigue life should increase with intrinsic toughness. The results also vindicate the determination of the intrinsic toughness from low cycle fatigue tests. The findings (Chapter 4) reveal the reasons for materials designers expectations not being realised by simply optimising for impact toughness.

The primacy of the influence of the particle size/particle size distribution was identified in the earlier chapters. The results from fatigue illustrate that its role in the hierarchy of influence is even more predominant in determining how modification of the secondary phase expresses its influence over fatigue.

$$J = G = \frac{K^2}{E}$$

Equation 5.17.

The fulfilment of the expression, equation 5.17., by the measurements made from fatigue tests vindicates the use of the technique in determining intrinsic toughness and also explains the excellent correlation of FCP with ΔK . For this reason it is considered to be more appropriate for characterising FCP in HIPS.

Consequently it is possible to use the data to design against fatigue using ΔJ . Indeed the energy based approach, with use of strain gauges, can allow for the early detection and monitoring of forces likely to promote failure. The technique is much more sensitive for modelling the process of FCP than ΔK .

Of the data sets readily available to designers of HIPS materials and those intending to use the materials the most useful property for considering of fatigue in HIPS then is the tensile modulus, i.e., materials with higher moduli are not worked as much with successive loadings as those with low modulus and thus provide greater fatigue lives.

That crazing eventually occurred at stresses below that required to instigate it under conditions of monotonic loading suggests lower activation energies are actually necessary to allow macromolecular movement in the material. This is unsurprising, polymers are viscoelastic/viscoplastic materials and crazing is associated with all forms of failure in HIPS, including creep.

The trends in the variation in the values of m' mirrored those observed with the Paris exponent m' . The PSB#1 series showed no apparent increase or decrease in the rate of change in ΔJ with crack extension speed. The mirrored trends in response observed between the PSB#2 and PSB#3 series was more exaggerated than it had been in the case of the Paris exponent, highlighting the sensitivity of the energy based approach to the changes in crack growth rates, Figure 5.42.

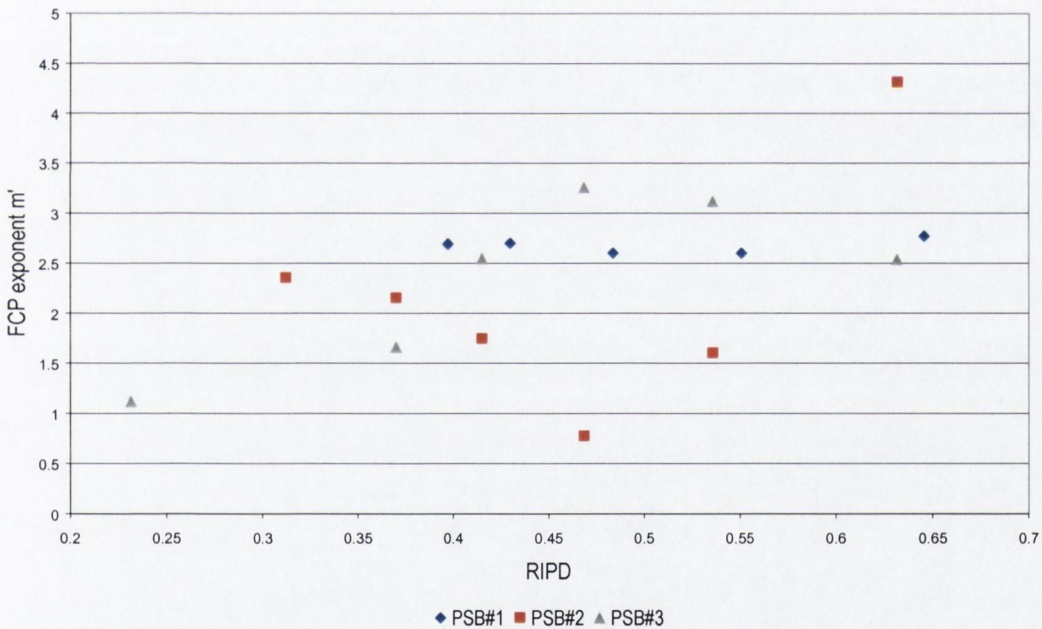


Figure 5.42. The variation of m' with ERPV for the three series of resins.

Some similarity with the trends observed with Paris was anticipated. Thus for the case of the PSB#2 and #3 the effects of increasing ERPV appeared to have opposite effects on the rate of crack extension. In the case of the PSB#3 it appeared to initially speed up but beyond 15 % slowed. The opposite was observed in the PSB#2. This echoed what had been observed in modelling with Paris.

The explanation for this behaviour was considered above in discussing the Paris analysis and fatigue life, section 5.5.5.2..

5.6 Conclusions

5.6.1 Concerning Fatigue Crack initiation and propagation from Microscopy.

- At low levels of addition and high levels of constraint the mechanism of fatigue crack propagation was an interrupted, or discontinuous process of fatigue crack growth.
- The mechanism crack extension changed in character from being, "slip-stick" in nature to "slow- fast", as the level of crazing and the size of the fracture process zone increased.
- The propensity of materials to craze and the stability of their crazes, determined the extent of damage accumulation and the mechanism associated with crack growth.
- Artefacts on fracture surfaces indicated that plasticity induced crack closure became intimately involved in FCP as levels of damage accumulation increased.
- These features of behaviour were determined by the perturbation of stress fields within the matrix by the secondary phase morphology.

It was concluded that crazing dominates fatigue failure and that the onset and extent of crazing is intimately associated with the initiation and propagation of fatigue cracks. From Chapter 3 and 4 this is determined by the micro-morphology of the secondary phase.

5.6.2 Concerning Fatigue Life.

- The fatigue lives of the HIPS increased with ERPV though at high levels of addition the lives associated with high ERPV declined and eventually fell at even greater ERPV.
- Similarly the number of cycles to crack initiation increased with low additions but declined and eventually fell as ERPV increased.
- Low levels of addition (<15-20% ERPV) were associated with increasing the proportion of fatigue life spent propagating cracks, higher additions tended to reduce it.
- The influence of increasing ERPV on fatigue behaviour in notched samples, for low levels of secondary phase addition (<15-20%), differed with that for high (>15-20%).
- The sensitivity of each series to this transition in response to increasing ERPV, or range of ERPVs, differed.
- The materials with most potential to craze exhibited the greatest fatigue lives, i.e., PSB#2 and PSB#3 series. However those that possessed the secondary phase most efficient at crazing, the PSB#2 series, exhibited the greatest sensitivity to increasing ERPV.
- The trends in the fatigue lives of the materials to initiation were influenced, in part, by the materials notch sensitivity. Increasing the secondary phase volume in HIPS reduces notch sensitivity.

It was concluded that particle size population and/or particle size polydispersity exerts a primary influence on the fatigue behaviour of HIPS. That the incorporation of the secondary phase tended to shift the S-N curve for notched materials, or PS and HIPS containing flaws, to the right. However it is

concluded that, because of the increasing propensity of the secondary phase to instigate crazing at lower levels of stress, that incorporation of increasing volumes of secondary rubber phase in HIPS tends to reduce the stress associated with the endurance limit in 'flawless' specimens.

5.6.3 Concerning Fatigue Crack Propagation.

- Fatigue crack propagation rates at any given ΔK , or ΔJ , increased with increasing ERPV in each series.
- The resistance to fatigue crack propagation with increasing ΔK or ΔJ did not correlate with the apparent (impact) toughness of the materials.
- The resistance of the materials to fatigue crack initiation correlated with the intrinsic toughness, i.e., in respect to the ΔJ analysis.
- The sensitivity of crack propagation rates to increasing ΔK or ΔJ , i.e., m or m' , increased with ERPV, except in the case of low additions in the PSB#2 series and the 45.4% PSB#3 resin.
- The number of cycles associated with initiation varied in accordance with the intrinsic toughness of the PSB#1 and PSB#3 series of materials however failed to do so for the PSB#2 series due to its propensity to craze and allow for the earlier initiation of cracks.
- It is unwise to construe the ranking of fatigue properties on the findings of impact tests. In the absence of intrinsic test data it is best to correlate fatigue life with modulus, i.e., materials with higher moduli are not worked as much with successive loadings as those with low modulus.
- Differences in fatigue crack propagation and life of HIPS resins are primarily determined by the particle population size and polydispersity.
- FCP resistance and fatigue life will increase with increasing particle size and secondary phase volume to a maximum life at an optimum ERPV dependent upon the particle size population.

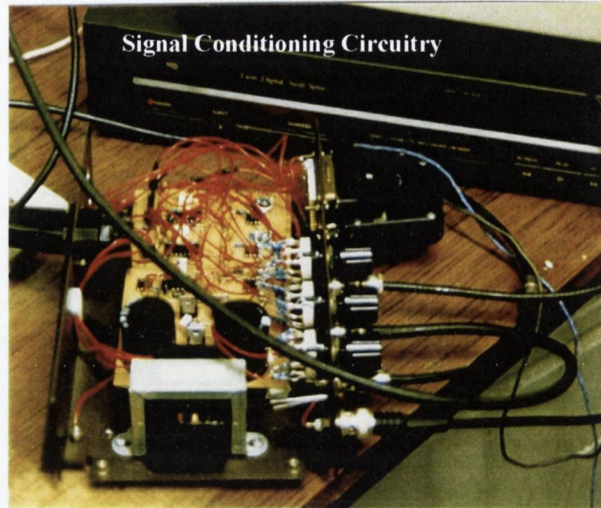
It was concluded that the resistance of HIPS to fatigue crack propagation increased with increasing particle size and falling RIPD. As the fatigue life and FCP resistance of HIPS is controlled by the secondary phase morphology it follows that the fatigue strength of HIPS resins can be optimised for Fatigue crack initiation and propagation for any given geometry and set of loading conditions.

Finally it is concluded from the results obtained that the optimum fatigue crack resistance would be obtained at a given ERPV in a bi-modal distribution of large and small particles. However, further research is required to define the optimum distribution in sizes and ERPV.

5.7 Appendix 5.1: Data Acquisition and Signal Conditioning System

Customised hardware and software were developed to acquire data from the test rig during tests.

As the encoding for the Instron 8501 could not be sourced from Instron signal conditioning circuitry had to be constructed to amplify milli-volt signals from before their acquisition by the data acquisition card. Noise on the signals meant many design iterations were tested before a final circuit was selected.



The ambition to determine the resistance to fracture during fatigue testing required the development of customised software. At the time Instron had not developed Fracture mechanics software and a dedicated program was developed in C++ code. Crack displacement was monitored using a stereo microscope and displacement recorded using an optically encoded displacement transducer mounted on a customised microscope stage attached to the Instron test frame. The tests were recorded on video. An issue with the SYLVAC optical transducer was not detected until all testing had been completed. This had corrupted the file saved to data. The entire series of tests had to be reviewed on video and data regenerated. 600 hrs of Videotape were reviewed to determine the crack displacement and also the gain on the crosshead displacement transducer.

The software code running to 1500 lines is presented below with its construction and operation commented within. The GUI is presented below.

Graphic user interface for CAPTURE

	Extensometer #1	Extensometer #2
	Load Cell	Hysteresis Curve
	Time Date	
	Errors	
Test Status (software) Valid Cycle Count Calculated Cycles Full Cycles Saves	Crack Length Delta K Delta J Video Status (on/off)	
Tests Status Hardware		

5.8 Appendix 5.2: Data Acquisition program 'CAPTURE' source code C++

The image taken of the GUI illustrates the way data was plotted asynchronously as it was acquired from the three analog input channels. The scaling of the plots were modified to reflect increases in Gain on each of the channels and then replotted for maximum resolution. The digital input of crack length was presented in bottom right hand corner. Saving to file was achieved by the automatic cycle save and key input set as an interrupt. All data (2Gb) was saved to file and for future processing.

```
#include <stdio.h>
#include <stdlib.h>
#include <graphics.h>
#include <string.h>
#include <malloc.h>
#include <time.h>
#include <ctype.h>
#include <conio.h>
#include <fcntl.h>
#include <math.h>
#include <dos.h>
#include <dir.h>
#include <time.h>
#include <sys/types.h>
#include <sys/stat.h>
#include "nidaq.h"
#include "nidaqerr.h"

#define CH0 3
#define CH1 2
#define CH2 1
#define CH3 0
#define TRUE 1
#define FALSE 0
#define LABPCPLUS 1

#define LoadOffset Defaults[25]
#define Ext1Offset Defaults[26]
#define Ext2Offset Defaults[27]
#define ScalingLoad Defaults[19]
#define ScalingExt1 Defaults[20]
#define ScalingExt2 Defaults[21]

int huge *circularBuffer=NULL; /*
buffer used to store data cyclically */
int huge *halfBuffer=NULL; /* buffer used to get data
from circularBuffer */

int huge *channel0=NULL; /* Temporary arrays to
ease access */
int huge *channel1=NULL; /* to the data contained
in each */
int huge *channel2=NULL; /* channel read into the */
int huge *channel3=NULL; /* computer */

FILE *outfile; /* file pointer to data */
FILE *logfile; /* file pointer to log file */

struct tm *ourtime; /* structure to access time of */
time_t bintime; /* day & things like that */

char message[300]=" Press ESC key to Exit
";
char Test1[]=" Test in progress....
";
char Error1[]=" Warning: Didn't get a correct sequence of
data....
";
```

```
char Error3[]=" WARNING: You are pressing keys too
fast....
";
char Error5[]=" WARNING: Can't continue until machine
speed is changed
";
char string[200]; /* General use & abuse */
char testName[80]; /* Holds name of test */
char timeNow[50]; /* Holds time */
char buffer[300]; /* General use & abuse */
char startTime[40]; /* Holds start time */

/* Function Prototypes follow... */

void Print(int x,int y,int color,char text[80]);
void Prints(int x,int y,int color,char *text);
float Input(int max_length,int type, char message[80]);
void MakeLog(int closefile);
void get_out(int);
void ErrClean(void);
void ErrPrint(char *proc_name,int err_num);
void setup(void);
void qMessage(char *message);
float GetCrackMeasurement(void);

/* Global variables follow... */
int position=0;
int logFileMade=FALSE;
int errNum; /* error returned from driver function calls */
float Defaults[28]={ /* Stores all Constants for test */
1,10,50,100,100,100,200,500,500,500,1000,10000,20000,5000,
20,3,1,5,12,12,50,50,50,0,0,1,1,1,0,0,0};
long zeroPts[100];

void main(void)
{
int boardCode; /* board code */
timebase; /* selects the interval clock rate for timing */
status; /* flag indicating completion of data acquisition */
halfReady; /* flag indicating a half buffer of data is ready */
ptsTr; /* number of points transferred to halfBuffer */
SampleRate; /* Sampling rate */
MessageColor=14; /* colour of scrollly messages */

unsigned int sampleInt; /* Interval between acquisitions in timebase units*/
unsigned long circularBufferSize; /* Size of the circular buffer in samples */
halfBufferSize; /* Size of the half buffer in number of samples */
offset=0; /* Used to hold starting address of halfBuffer */

/*-----
Constants and Variables used in Calculations
-----*/
int driver=VGA,gmode=VGAHI;
unsigned long s,y,cycleNum=0,savedCycles=0,CycleData=0,positionOfMax,positionOfMin;
unsigned long scanback,newtp,x,xx,min;
unsigned int stepx,stepy,copys,dum,step,save,savecy,cr,skip;
unsigned int zero,one,two,three,currentCycle,cycle,count=0;
float W;
```

```

B,
GE1,
GE2,
max0, /* Max point on CH0 */
max1,oldmax1=0, /* Max value of Load Stress */
min1, /* Min value of Load Stress */
max2, /* Max point on CH2 */

min0, /* Min ext 1 */
min2, /* Min ext 2 */

double ch1mean,

Sam_Thickness,
Sam_Width,
Sam_NotchDepth,
Strain1max,
Strain1min,
dsp1c1max,
dsp1c1min,
Strain2max,
Strain2min,
dsp1c2max,
dsp1c2min,
Stressmax,
Stressmin,
Loadmax,
Loadmin,
J1,
J2,
J3,
A,
Aprevious=0,Aprevious=0,
J=0,
Y,
K=0,
TotalHystLoss1=0,
TotalHystLoss2=0,
HystLoss1=0,
HystLoss2=0,
HystLossDiff,
HystLoss1up,
HystLoss1dw,
HystLoss2up,
HystLoss2dw,
modsec1,
modsec2,
sw,
lw,
Jastm1,
Jastm2,

char ch, /* used to check keypresses */

clock_t start_end, /* Time the keypresses for crack measurements */
float TimeKeysPressed[100], /* Array of time difference of keypresses */
TimeKeys[100],
TimeKeys1[100],
crackMeasurements[100], /* Array holding actual measurement

taken */
int KeyPress=0,
KeyPress1=0,
KeyPress2=0,
video=FALSE,
vidflag=0,
vidscrm=2,
recorderNum=0,

long CycleCount=0,
GapBetweenCycleSaves,

/* Variables used in Simpsons */
float s1,s0,integral,

/* Variables used to find crack length */
int lwdtFound,manual,

.....
Setup of Serial Port for SYLVAC instrument

```

```

.....
system("mode com2: 4800 n 7 1");

.....
Setup of Graphics Mode
.....

initgraph(&gdriver,&gmode,"c:\bcd\bg");
settextjustify(LEFT_TEXT, TOP_TEXT);
settextstyle(SMALL_FONT, HORIZ_DIR, 1);

/* the requested directory name */
setusercharsize(5,3,7,5);

.....
Load Defaults for test and allow editing if required
.....
qMessage("Getting Defaults...");
if(outfile=fopen("defaults.dat","b"))=NULL
{
fread((void *)Defaults,sizeof(float),28,outfile);
fclose(outfile);
}

do{
sound(3000),delay(300),nosound(); /* Beep */
if(input(8,2,"Test Name...")=-1) exit(0);

/* Make up directory
/* Note: Won't continue unless MKDIR returns
while(mkdir(string)); /* the fact that it has actually created

.....
Log start time of test
.....
time(&binime);
curtime=localtime(&binime);
sprintf(startTime,"%s",asctime(curtime));

.....
SCREEN SETUP
.....
directvideo = 0;
cleardevice();setcolor(7);
setfillstyle(SOLID_FILL,0);
settextstyle(DEFAULT_FONT, HORIZ_DIR, 1);
rectangle(100,10,300,110);
rectangle(100,120,300,220);
rectangle(310,10,510,110);
rectangle(310,120,510,220);
//setcolor(9);
//rectangle(50,420,575,395);
setcolor(7);
rectangle(0,290,300,385);
rectangle(310,290,639,385);
Prints(20,2,15,"Load Cell");
Prints(5,2,15,"Ext #1");
Prints(5,6,15,"Ext #2");
Prints(20,6,10,"Hysteresis");
Prints(21,6,10,"Loss");
Prints(31,1,4,"Program Written & Developed by: Donie Kelly & Barry Dolen.");
//Prints(33,11,4,"Phone: (0509) 51397");
setcolor(1);moveto(0,230);lineto(639,230);
moveto(0,233);lineto(639,233);
setcolor(1);moveto(0,275);lineto(639,275);
moveto(0,278);lineto(639,278);

chdir(string); /* Go into the new directory */
Prints(40,51,14,string);
Prints(40,41,14,"Test Name:");
strcpy(testName,string); /* Copy test name into its own string */

Sam_Thickness=Defaults[14];
Sam_Width=Defaults[15];
Sam_NotchDepth=Defaults[16];
GE1=Defaults[17];
GE2=Defaults[18];

outfile=fopen("testfile.txt","a+"); /* Build Test File for storing cycle results */
fprintf(outfile,"%s",testName);

```

```

fprintf(outfile, "CycleNo, HystLoss #1, HystLoss 1up, HystLoss 1dw, HystLoss #2, HystLoss
2up, HystLoss 2dw, HystLossDiff, Strain #1(max), Strain #1(min), Dspic #1(max), Dspic #1(min), Strain
#2(max), Strain #2(min), Modsec 2, Modsec 1, Dspic #2(max), Dspic #2(min), Stress (max), Stress
(min), Load (max), Load (min), A, J, I, J2, J3, K, TotalHystLoss #1, TotalHystLoss #2, Video, V");
fclose(outfile);

.....
CONFIGURATION
.....

errNum = Get_DA_Brds_Info (LABPCPLUS, &boardCode, &dum, &dum, &dum, &dum, &dum, &dum,
&dum);
if(errNum!=noErr) ErrPrint ("Get_DA_Brds_Info", errNum);
/* Returns the board code, base address, interrupt level, interrupt trigger mode
DMA channels and data acquisition mode settings of a board and an indication of
potential configuration conflicts with other data acquisition boards in the
system.
NOTE: The variable "dum" is used as some of the returned values are not required by
this program.
See NI-DAQ function reference manual p.3-79 for more details...
*/

errNum = AI_Configure (LABPCPLUS, 1, 1, 10, 1, 0);
if(errNum!=noErr) ErrPrint ("AI_Configure", errNum);
/* Informs NIDAQ of the input mode (single-ended or differential), input range & input
polarity. Must use this function if jumpers on the card have been changed from their
factory settings.
NOTE: See NI-DAQ function reference manual p.3-5 for more details...
*/

errNum = DAQ_Config (LABPCPLUS, 0, 0);
if(errNum!=noErr) ErrPrint ("DAQ_Config", errNum);
/* Stores configuration information for subsequent data acquisition operations
NOTE: See NI-DAQ function reference manual p.3-38 for more details...
*/

errNum = DAQ_Trigger_Config (LABPCPLUS, 0, 0);
if(errNum!=noErr) ErrPrint ("DAQ_Trigger_Config", errNum);
/* Enables the pre-trigger mode of data acquisition and indicates the number of data
points to acquire after the stop trigger pulse is applied at EXTTRIG input of the
LAB-PC.
NOTE: Pre-trigger mode is disabled here as it is not required or desired
See NI-DAQ function reference manual p.3-
51 for more details...
*/

errNum = DAQ_DB_Config (LABPCPLUS, 1);
if(errNum!=noErr) ErrPrint ("DAQ_DB_Config", errNum);
/* Enables or disables double buffered data acquisition operations.
NOTE: See NI-DAQ function reference manual p.3-40 for more details...
For an overview on Double Buffering see Chapter 7 of the NI-DAQ software
reference manual.
*/

if(Defaults[23]<=0.2) {SampleRate=400,circularBufferSize=20000;}
if(Defaults[23]==1) {SampleRate=4000,circularBufferSize=40000;}
if(Defaults[23]==10) {SampleRate=20000,circularBufferSize=60000;}

errNum = DAQ_Rate (SampleRate, 0, &timebase, &sampleInt);
if(errNum!=noErr) ErrPrint ("DAQ_Rate", errNum);
/* Converts a data acquisition rate into the time base and sample-interval
values needed to produce the desired rate.
Note: See NI-DAQ function reference manual p.3-47 for more details...
*/

SampleRate=SampleRate/4;
halfBufferSize = circularBufferSize/2;
sprintf(buffer, "Sampling rate per channel %uHz", SampleRate);
Prints(55, 1, 14, buffer);

.....
Allocate memory for all the arrays
.....

if (zeroPts == NULL)
    get_out(1);
circularBuffer = (int huge *) malloc ((unsigned long)circularBufferSize, sizeof(int));
if (circularBuffer == NULL)
    get_out(1);
halfBuffer=(int huge *)malloc((unsigned long)65000, sizeof(int));

```

```

if (halfBuffer == NULL)
    get_out(1);
channel0=(int huge *)malloc((unsigned long)11000, sizeof(int));
if (channel0 == NULL)
    get_out(1);
channel1=(int huge *)malloc((unsigned long)11000, sizeof(int));
if (channel1 == NULL)
    get_out(1);
channel2=(int huge *)malloc((unsigned long)11000, sizeof(int));
if (channel2 == NULL)
    get_out(1);
channel3=(int huge *)malloc((unsigned long)11000, sizeof(int));
if (channel3 == NULL)
    get_out(1);

/* make log file to show defaults */

MakeLog(0);
logfile=fopen("message.log", "a+");
fprintf(logfile, "Width % 3f\n\r",
        Defaults[14]);
fprintf(logfile, "Thickness % 3f\n\r",
        Defaults[15]);
fprintf(logfile, "Notch Depth % 3f\n\r",
        Defaults[16]);
fprintf(logfile, "Gauge Length 1 % 3f\n\r",
        Defaults[17]);
fprintf(logfile, "Gauge Length 2 % 3f\n\r",
        Defaults[18]);
fprintf(logfile, "Scaling Factor (Load) % 6f\n\r",
        Defaults[19]);
fprintf(logfile, "Scaling Factor (EXT1) % 6f\n\r",
        Defaults[20]);
fprintf(logfile, "Scaling Factor (EXT2) % 6f\n\r",
        Defaults[21]);
fprintf(logfile, "Percentage change % 1f\n\r",
        Defaults[22]*100);
fprintf(logfile, "Test Speed % 1f\n\r",
        Defaults[23]);
fprintf(logfile, "Mean Load % 1f\n\r",
        Defaults[25]);
fprintf(logfile, "Mean Ext1 % 1f\n\r",
        Defaults[26]);
fprintf(logfile, "Mean Ext2 % 1f\n\r",
        Defaults[27]);

fclose(logfile);

.....
SAMPLING ROUTINE
.....

errNum = Lab_ISCAN_Start (LABPCPLUS, 4, 1, circularBuffer, circularBufferSize, timebase, sampleInt,
0);
if (errNum!=noErr) ErrPrint ("Lab_ISCAN_Start", errNum);
/* Initiates a multiple-channel scanned data acquisition operation and stores
its input in an array.
NOTE: See NI-DAQ function reference manual p.3-93 for more details...
This is a new function and is not fully documented in the function
reference manual. An extra parameter is added that is not mentioned in the
reference manual and a description(?) of the new
parameter can be found in the readme.txt
file in the NIDAQ directory. The extra parameter is "scanInterval"
and is the last parameter in the above call.
This function is only called once in a program. It starts the card
acquiring data and this will continue in the background. It's now up to the
programmer (me) to keep an eye on this background task and collect the
acquired data every now and again. The function "Daq_Db_HalfReady()" is
used to do this...
*/
Prints(40, 2, 14, "Getting Data...");
start=clock(); /* Begin Timing for crack measurements */
do{
while ( !kbhit())
{

```

```

errNum = DAQ_DB_HalfReady(LABPCPLUS, &halfReady, &status);
if(errNum!=noErr) ErrPrint("DAQ_DB_HalfReady", errNum);

/* Checks whether the next half buffer of data is available during a double-buffered
data acquisition. When halfready is 0 the data is no yet available. When its value
is 1 then the data is available... hopefully!
NOTE: See NI-DAQ function reference manual p.3-40 for more details...
*/

/* The routine that follows extracts the time from the internals of this
confounded machine and prints it in a corner of the screen where it
looks quite pretty
*/

time(&binTime);
curTime=localtime(&binTime);
sprintf(buffer, "%s",asctime(curTime));
y=0;
for(x=11,x<19,x++)
{
    timenow[y]=buffer[x];
    y++;
}
timenow[9]='0';

/* Well, maybe it was't that bad after all !
*/

/* This next routine is quite silly really. Its only function in life is
to scroll any silly messages I tell it to across the bottom of the
screen in glorious color.
*/
cr=0;
for (x=position,x<=position+59,x++)
{
    string[cr]=message[x];
    cr++;
}
string[cr]='0';
window(1, 1, 80, 25);
gotoxy(10,17);
textcolor(MessageColor);
//settextstyle(DEFAULT_FONT, HORIZ_DIR, 1);
cprint("%s",string);

count++;
if(count==20){position++;count=0;}
if(position==120)
{
    position=0;
    strcpy(message,Test1);
    MessageColor=7;
    Prints(55,1,0,"");
    Prints(56,1,0,"");
}
// and that ends the silly routines ... Phew!

*/

if (halfReady)
{
    if(cycleNum<=10 ) {GapBetweenCycleSaves=Defaults[0]; goto QuickExit;}
    if(cycleNum<=100 ) {GapBetweenCycleSaves=Defaults[1]; goto QuickExit;}
    if(cycleNum<=500 ) {GapBetweenCycleSaves=Defaults[2]; goto QuickExit;}
    if(cycleNum<=1000 ) {GapBetweenCycleSaves=Defaults[3]; goto QuickExit;}
    if(cycleNum<=1500 ) {GapBetweenCycleSaves=Defaults[4]; goto QuickExit;}
    if(cycleNum<=3000 ) {GapBetweenCycleSaves=Defaults[5]; goto QuickExit;}
    if(cycleNum<=5000 ) {GapBetweenCycleSaves=Defaults[6]; goto QuickExit;}
    if(cycleNum<=10000 ) {GapBetweenCycleSaves=Defaults[7]; goto QuickExit;}
    if(cycleNum<=15000 ) {GapBetweenCycleSaves=Defaults[8]; goto QuickExit;}
    if(cycleNum<=20000 ) {GapBetweenCycleSaves=Defaults[9]; goto QuickExit;}
    if(cycleNum<=50000 ) {GapBetweenCycleSaves=Defaults[10]; goto QuickExit;}
    if(cycleNum<=100000 ) {GapBetweenCycleSaves=Defaults[11]; goto QuickExit;}
    if(cycleNum<=200000 ) {GapBetweenCycleSaves=Defaults[12]; goto QuickExit;}
    if(cycleNum> 200000 ) {GapBetweenCycleSaves=Defaults[13]; goto QuickExit;}

QuickExit:

    setpalette(0,4); /* Turn Screen Red */
}
    
```

```

errNum=DAQ_DB_Transfer(LABPCPLUS,(halfBuffer+offsetof(&ptsTr,&status));
if(errNum!=noErr) ErrPrint ("DAQ_DB_Transfer ", errNum);

/* Transfers half of the data from the buffer being used for
double-buffered
data acquisition to another buffer, which is passed to the function, and
waits until the data to be transferred is available before returning
NOTE: See NI-DAQ function reference manual p.3-42 for more details...
*/

Prints(40,2,5,"Calculating ");

/*****
Put each channel into an array & get mean
*****/

/* Extract Strain#1 (CH0) data from halfbuffer and put it in its own array to
ease access while doing the calculations.
*/
zero=0,skip=1;
for (y=CH0,y<=halfBufferSize+offsetof(y,y+4)
{
    channel0[zero]=halfBuffer[y];
    zero++;
}zero--;

/* Extract Load Stress (CH1) data from halfbuffer and put it in its own array
to ease access while doing the calculations. The second loop gets the mean
of the data in Channel 1
*/
one=0,ch1mean=0,skip=1;
for (y=CH1,y<=halfBufferSize+offsetof(y,y+4)
{
    channel1[one]=halfBuffer[y];
    one++;
}one--;
for (y=0,y<=one,y++)
if(channel1[y]>10)
{
    ch1mean=ch1mean+channel1[y];
    skip++;
}
ch1mean=ch1mean/skip; /* skip is the current number of samples in Channel 1 */

/* Extract Strain#2 (CH2) data from halfbuffer and put it in its own array to
ease access while doing the calculations.
*/
two=0;
for (y=CH2,y<=halfBufferSize+offsetof(y,y+4)
{
    channel2[two]=halfBuffer[y];
    two++;
}two--;

/* Extract Crack Length Measurement (CH3) data from halfbuffer and put it in
its own array to ease access while doing the calculations.
*/
three=0;
for (y=CH3,y<=halfBufferSize+offsetof(y,y+4)
{
    channel3[three]=halfBuffer[y];
    three++;
}three--;

/*****
Find the turning points
*****/

/* The turning points are found by scanning the data in CH0 and looking at where
the data values pass through the mean value. When a possible point is found
it is checked to see if it is a valid one and not just noise or a glitch. This
is done by looking ahead by 50 samples and checking if the
sample here is greater
than the current value by at least 50mV. If it is then we presume
that we have
found a turning point. This is not fool-proof but it should work
adequately
for this application
*/
x=0,currentCycle=0;
for (y=100,y<=one-50,y++)
if(channel1[y]>ch1mean && channel1[y-1] <ch1mean)
    
```

```

{
    if(channel1[y+50]-ch1mean>20) /* Look ahead of Turning
Point and */
    {
        /* see if it is greater than the */
        zeroPts[0]=0; /* current sample */
        zeroPts[x+1]=y; /* Store turning Point. */
        x=x-(x-90); /* Dont store more than 90 points. */
        y=y+50; /* Jump 50 and search for next TP. */
        currentCycle++; /* Count the cycles found. */
    }
}

if(currentCycle<=1 || currentCycle>25)
{
    Prints(55,1,0," ");
    Prints(55,1,14,"WARNING: Test Running at Incorrect Speed !!!");
    stropy(message_Error5);
    MessageColor=14;
    printf("!\n");
    goto JumpOverCalc;
}

/* Modify turning point addresses to point at minimum values
on the signal coming in....
*/

for(y=1;y<currentCycle;y++)
{
    scanback=zeroPts[y];
    x=channel1[scanback];

    do
    {
        if( channel1[scanback] < x )
        {
            x=channel1[scanback];
            min=scanback;
        }
        scanback--;
    }
    while( scanback > zeroPts[y-1]);

    zeroPts[y-1]=(long)min;
}
currentCycle--;

.....
Graph channels
.....

setcolor(0);
bar(101,11,299,109);
bar(101,121,299,219);
bar(311,11,509,109);
bar(311,121,509,219);

y=zeroPts[0];step=(zeroPts[currentCycle]-zeroPts[0])/198+1;
for(x=101;x<300;x++)
{
    putpixel(x+210,105-(channel2[y]/45),14);
    putpixel(x,215-(channel1[y]/45),14);
    putpixel(x,105-(channel0[y]/45),14);
    y=y+step;
}

.....
Do calculations on each cycle
.....

for(cycle=0;cycle<currentCycle;cycle++)
{
    max0=0, max1=0, max2=0, min1=4096;

    for(y=zeroPts[cycle]; y<zeroPts[cycle+1]-1;y++) /* Max Ext#1 */
        max0=max(channel0[y],max0);

    for(y=zeroPts[cycle]; y<zeroPts[cycle+1]-1;y++) /* Max Ext#2 */
        max2=max(channel2[y],max2);
}

```

```

for(y=zeroPts[cycle]; y<zeroPts[cycle+1]-1;y++) /* Min Ext#1 */
    min0=min(channel0[y],min0);

for(y=zeroPts[cycle]; y<zeroPts[cycle+1]-1;y++) /* Min Ext#2 */
    min2=min(channel2[y],min2);

for(y=zeroPts[cycle]; y<zeroPts[cycle+1]-1;y++) /* Min Load */
    min1=min(channel1[y],min1);

for(y=zeroPts[cycle]; y<zeroPts[cycle+1]-1;y++) /* Max Load */
{
    xx=channel1[y];
    if(xx>max1)
    {
        max1=channel1[y];
        positionOfMax=y;
    }
}

/* Calculate Hysteresis Losses using Ext #1 */
HystLoss1=0;x=0;
for(y=zeroPts[cycle]; y<positionOfMax;y++)
{
    sw=(channel0[y+1]-Ext1Offset)-(channel0[y]-Ext1Offset); /* get strain width */
    lw=((channel1[y+1]-LoadOffset)-(channel1[y]-LoadOffset)/2)-(channel1[y]-
LoadOffset); /* load width */
    HystLoss1up=HystLoss1up+(lw*sw);
    x++;
    if(channel0[y]>0)
        modsec1=((channel1[y]-LoadOffset)/(channel0[y]-LoadOffset))/x;
}
for(y=positionOfMax; y<zeroPts[cycle+1]-1;y++)
{
    sw=(channel0[y+1]-Ext1Offset)-(channel0[y]-Ext1Offset);
    lw=((channel1[y]-Ext1Offset)-(channel1[y+1]-Ext1Offset)/2)-(channel1[y+1]-
Ext1Offset);
    HystLoss1dw=HystLoss1dw-(lw*sw);
}
HystLoss1=HystLoss1up-HystLoss1dw;

TotalHystLoss1=TotalHystLoss1+HystLoss1;

/* Calculate Hysteresis Losses using Ext #2 */
HystLoss2=0;x=0;
for(y=zeroPts[cycle]; y<positionOfMax;y++)
{
    sw=(channel2[y+1]-Ext2Offset)-(channel2[y]-Ext2Offset);
/* get strain width */
    lw=((channel1[y+1]-Ext2Offset)-(channel1[y]-Ext2Offset)/2)-(channel1[y]-
Ext2Offset); /* load width */
    HystLoss2up=HystLoss2up+(lw*sw);
    x++;
    if(channel2[y]>0)
        modsec2=((channel1[y]-LoadOffset)/(channel2[y]-
LoadOffset))/x;
}
for(y=positionOfMax; y<zeroPts[cycle+1]-1;y++)
{
    sw=(channel2[y+1]-Ext2Offset)-(channel2[y]-Ext2Offset);
    lw=((channel1[y]-Ext2Offset)-(channel1[y+1]-Ext2Offset)/2)-(channel1[y+1]-
Ext2Offset);
    HystLoss2dw=HystLoss2dw-(lw*sw);
}
HystLoss2=HystLoss2up-HystLoss2dw;

TotalHystLoss2=TotalHystLoss2+HystLoss2;

/* Calculate Total Hysteresis Loss */
HystLossDiff=(HystLoss1+HystLoss2);

```

```

/* Calculate Stress */
Stressmax=((max1-LoadOffset)*ScalingLoad)/(Sam_Width*Sam_Thickness);
Stressmin=((min1-LoadOffset)*ScalingLoad)/(Sam_Width*Sam_Thickness);

/* Calculate Loads */
Loadmax=((max1-LoadOffset)*ScalingLoad);
Loadmin=((min1-LoadOffset)*ScalingLoad);

/* Calculate Displacement */
dspic1max=((max0-Ext1Offset)*ScalingExt1);
dspic1min=((min0-Ext1Offset)*ScalingExt1);

dspic2max=((max2-Ext2Offset)*ScalingExt2);
dspic2min=((min2-Ext2Offset)*ScalingExt2);

/* Calculate Strain */
Strain1max=dspic1max/GE1;
Strain1min=dspic1min/GE1;

Strain2max=dspic2max/GE2;
Strain2min=dspic2min/GE2;

/* find LVDT Position */
Aprevious=Apresent;
lvdtFound=FALSE;
for(y=0;y<KeyPress,y++)
    {
        if( (TimeKeysPressed[y]*SampleRate) >=zeroPts[cycle] &&
            (TimeKeysPressed[y]*SampleRate)<=zeroPts[cycle+1])
            {
                lvdtFound=TRUE; /* Found a match with time of key
press */
                Apresent=crackMeasurements[y]; /* Update Crack
Measurement */
            }
    }

if(lvdtFound==TRUE)
    {
        MakeLog(0);
        position=0;
        sprintf(buffer,"Valid crack length measurement taken at cycle
#%lu",cycleNum<cycle);
        Printz(55,1,5,buffer);
        sprintf(buffer,"Valid crack length measurement taken at cycle
#%lu\n\n",cycleNum<cycle);
        logfile=fopen("message.log","a+");
        Printz(56,1,8,"Log File Generated! (message log)");
        fprintf(logfile,"%s",buffer);
        fclose(logfile);
    }

if(Apresent>=0)
    {
        /* Calculate Delta K */
        A=Apresent*Sam_NotchDepth;
        Loadmax=max1;
        Y=1.99-(0.41*(A/Sam_Width))+(18.70*pow(A/Sam_Width,2)-
(38.48*pow(A/Sam_Width,3))+53.85*pow(A/Sam_Width,4));

        K=((Loadmax-Loadmin)/Sam_Width*Sam_Thickness)*(sqrt(A))*Y;

        /* Calculate Delta J */
        J=(HystLoss1up^2)/(Sam_Width-A)*Sam_Thickness;
    }
else lvdtFound=FALSE;

/* Manual Cycle saves */
manual=FALSE;
for(y=0;y<KeyPress,y++)
    {
        if( (TimeKeys[y]*SampleRate) >=zeroPts[cycle] &&
            (TimeKeys[y]*SampleRate)<=zeroPts[cycle+1])
    }

```

```

manual=TRUE; /* Found a match with time of key press
*/
}

/* Switch video flag ON/OFF */
vidflag=0,save=0,savecy=0;
for(y=0;y<KeyPress,y++)
    {
        if( (TimeKeys1[y]*SampleRate) >=zeroPts[cycle] &&
            (TimeKeys1[y]*SampleRate)<=zeroPts[cycle+1])
            {
                if (video==TRUE)
                    {
                        video=FALSE;
                        vidflag=2;
                    }
                else
                    {
                        video=TRUE;
                        recorderNum++;
                        vidflag=1;
                    }
            }
        }

        vidscrn=2;
        save=1;

        vidscrn=1;
        save=1;
    }

/*-----
Determine whether cycle should be saved
-----*/

CycleCount++;
if(Defaults[24]<=1.5)
    {
        if (CycleCount==GapBetweenCycleSaves) /* If a cycle is due to be saved.
Save */
            {
                save=1;
                CycleCount=0;
                sprintf(buffer," Note : Saving every %d
cycles... ",GapBetweenCycleSaves);
                strcpy(message,buffer); /* Cycle save rate is changing */
                MessageColor=14;
                position=0;
                sound(6000),delay(10),nosound();
            }
        }

if((int)Defaults[24]>1.5 && manual)
    {
        save=1;
        sound(6000),delay(10),nosound();
    }

if(lvdtFound==TRUE)
    {
        save=1;
        savecy=1;
        sound(4000),delay(10),nosound();
    } /* Save if crack
measurement taken */

/*-----
Now save relevant data if conditions met
-----*/

step=(zeroPts[cycle+1] - zeroPts[cycle]) / 100; /* Divide cycle
into 100 for saving */

if(save)
    {
        if(outfile=fopen ("logfile.txt","a")==NULL)
            {
                MakeLog(0);
                logfile=fopen("message.log","a+");
            }
    }

```

```

                                fprintf(logfile,"Fatal: Couldnt open
**TestFile** while saving data!\n");
                                fclose(logfile);
                                get_out(0);
                                }
                                fprintf(outfile,"%4u",cycleNum-cycle); /* cycle No
*/
                                fprintf(outfile,"%3f",HystLoss1*ScalingLoad*ScalingExt1); /*
HystLoss #1
*/
                                fprintf(outfile,"%3f",HystLoss1up*ScalingLoad*ScalingExt1);
                                fprintf(outfile,"%3f",HystLoss1dw*ScalingLoad*ScalingExt1);
                                fprintf(outfile,"%3f",HystLoss2*ScalingLoad*ScalingExt2);
                                fprintf(outfile,"%3f",HystLoss2up*ScalingLoad*ScalingExt2);
                                fprintf(outfile,"%3f",HystLoss2dw*ScalingLoad*ScalingExt2);
                                fprintf(outfile,"%3f",HystLossDiff);
                                fprintf(outfile,"%3f",Strain1max);
                                fprintf(outfile,"%3f",Strain1min);
                                fprintf(outfile,"%3f",dspic1max);
                                fprintf(outfile,"%3f",dspic1min);
                                fprintf(outfile,"%3f",Strain2max);
                                fprintf(outfile,"%3f",Strain2min);
                                fprintf(outfile,"%3f",modsec1*ScalingLoad*ScalingExt1);
                                fprintf(outfile,"%3f",modsec2*ScalingLoad*ScalingExt2);
                                fprintf(outfile,"%3f",dspic2max);
                                fprintf(outfile,"%3f",dspic2min);
                                fprintf(outfile,"%3f",Stressmax);
                                fprintf(outfile,"%3f",Stressmin);
                                fprintf(outfile,"%3f",Loadmax);
                                fprintf(outfile,"%3f",Loadmin);
                                if(!vidFound==TRUE) /* Only save these three if
there was a */
                                {
                                        /* crack measurement taken
                                        /* Valid Crack Length
                                        fprintf(outfile,"%3f",A);
                                        fprintf(outfile,"%3f",J);
                                fprintf(outfile,"%3f",J1);
                                fprintf(outfile,"%3f",J2);
                                fprintf(outfile,"%3f",J3);
                                fprintf(outfile,"%3f",K); /* Delta K
                                }
                                else
                                fprintf(outfile,"....."); /* Otherwise dont put in any of
them */
                                fprintf(outfile,"%3f",TotalHystLoss1); /* Sum of HystLoss #1
*/
                                fprintf(outfile,"%3f",TotalHystLoss2); /* Sum of HystLoss #2
*/
                                if(vidflag==1)
                                        fprintf(outfile,"Rec ON %d",recorderNum);
                                if(vidflag==2)
                                        fprintf(outfile,"Rec OFF %d",recorderNum);
                                if(vidflag==0)
                                        fprintf(outfile,"");
                                fprintf(outfile,""); /* Terminate line
*/
                                fclose(outfile);
                                savedCycles++; /* Update the number of cycles
saved */
                                }
                                if(!saveocy)
                                {
                                        CycleData++;
                                        sprintf(string,"CY%06lu.txt",cycleNum-cycle);
                                        if((outfile=fopen(string,"wb+"))==NULL)
                                        {
                                                MakeLog(0);
                                                logfile=fopen("message log","a+");
                                                fprintf(logfile,"Fatal: Couldnt open file while saving data!\n");
                                                fclose(logfile);
                                                get_out(0);
                                                }
                                        fprintf(outfile,"%s\n",testName); /* Put test name at top of file
*/
                                        fprintf(outfile,"Cycle %4u",cycleNum-cycle);
                                        fprintf(outfile,"LoadCell"); /* Save load cell data
*/
                                        for (y=zeroPts[cycle], y<=zeroPts[cycle+1],y+=step)
                                        fprintf(outfile,"%d",channel0[y]);
                                        fprintf(outfile,"");

```

```

                                fprintf(outfile,"ClipGauge#1"); /* Save clip gauge #1 data
*/
                                for (y=zeroPts[cycle], y<=zeroPts[cycle+1],y+=step)
                                        fprintf(outfile,"%d",channel0[y]);
                                fprintf(outfile,"");
                                fprintf(outfile,"ClipGauge#2"); /* Save clip gauge #2 data
*/
                                for (y=zeroPts[cycle], y<=zeroPts[cycle+1],y+=step)
                                        fprintf(outfile,"%d",channel0[y]);
                                fprintf(outfile,"");
                                fclose(outfile);
                                }
                                cycleNum=cycleNum-currentCycle; /* Update number of cycles to date
*/
                                /* Plot Hysteresis
*/
                                x=0,stepx=zeroPts[1]/200;
                                for (a=311; a<=509; a++)
                                {
                                        putp(a(311-(channel0[x]/219-(channel1[x]/42)/10);
                                        x=x+stepx;
                                }
                                /*-----
Copy leftovers back into halfBuffer
-----*/
                                copya=0;
                                for(y=zeroPts[currentCycle]-1; y<=zero; y++)
                                {
                                        halfBuffer[copya]=channel3[y].copya++;
                                        halfBuffer[copya]=channel2[y].copya++;
                                        halfBuffer[copya]=channel1[y].copya++;
                                        halfBuffer[copya]=channel0[y].copya++;
                                }
                                offset=copya;
                                /* Something wrong if the next statment executes This will correct for
it but will be linked to bad data coming into the computer !!
*/
                                if(offset>18000)
                                {
                                        MakeLog(0);
                                        logfile=fopen("message log","a+");
                                        offset=0,printf("a");
                                        strcpy(message,Error1);
                                        MessageColor=14;
                                        position=0;
                                        Prints(56,1,8,"Log File Generated! [message log]");
                                        fprintf(logfile,"Error handling cycle #%4u\n",cycleNum);
                                        fclose(logfile);
                                }
                                JumpOverCalc:
                                sprintf(string,"Valid Cycles found: %4u",cycleNum);
                                Prints(43,2,10,string);
                                sprintf(string,"Cycle Calculations Saved %4u",savedCycles);
                                Prints(44,2,10,string);
                                sprintf(string,"Cycle Data Saved: %4u",CycleData);
                                Prints(45,2,10,string);
                                sprintf(string,"Crack Length: %3f ",A,Present);
                                Prints(43,41,10,string);
                                sprintf(string,"Delta K : %3f ",K);
                                Prints(44,41,10,string);
                                sprintf(string,"Delta J : %3f ",J);
                                Prints(45,41,10,string);
                                if(vidscrm=1)
                                {
                                        sprintf(string,"Video ON ");
                                        Prints(47,41,12,string);
                                }
                                if(vidscrm=2)
                                {
                                        sprintf(string,"Video OFF");

```

```

        Prints(47,41,12,string);
    }

    setpalette(0,(long)0); /* Turn off screen flash */
    start=clock(); /* Begin timing again for crack length measurements */
    KeyPress=0;
    KeyPress1=0;
    KeyPress2=0;
    while(kbhit())
        getch(); /* Flush Keyboard Buffer as any keypresses during calculations */
/* cannot be matched to
data
*/
Prints(40,2,14,"Getting Data...");
Prints(31,72,14,timenow);
}
}
end=clock(); /* Get the time that the Crack Measurement was made */
ch=getch();
if(ch==13) /* If used did make a crack measurement work out when he did */
{
    TimeKeysPressed[KeyPress]=(end-start)/CLK_TCK; /* Work out the gap between crack
/*
/* measurements and store in array */
    crack.Measurements[KeyPress]=GetCrackMeasurement();
    KeyPress++;
    while(kbhit()) /* Flush keyboard buffer */
        getch();
}
if(ch==32)
{
    TimeKeys[KeyPress1]=(end-start)/CLK_TCK; /* Work out the gap between data save
/*
/* keypresses and store in array */
    KeyPress1++;
    while(kbhit()) /* Flush keyboard buffer */
        getch();
}
if(ch=='r')
{
    TimeKeys[KeyPress2]=(end-start)/CLK_TCK; /* Work out the gap between data save
/*
/* keypresses and store in array */
    KeyPress2++;
    while(kbhit()) /* Flush keyboard buffer */
        getch();
}
}while (ch != 27); /* Sampling continues until the ESC key is pressed */

get_out(0);
}

-----
CLEANING UP
-----

void get_out(int mem)
{
    restorectmode(); /* Back to Text Mode */

    errNum = DAQ_Clear (LABPOPLUS);
    /* Clearing the acquisition halts the buffered acquisition, disables interrupts
    and DMA and restores the interrupt vector table (v. important unless you want
    a dead machine when the program terminates!!)
    NOTE: See NI-DAQ function reference manual p.3-38 for more details...
    */

    if (mem) /* This will show that enough memory was
not available */
    {
        /* for allocation for all arrays needed in the prog. */
        printf("Memory allocation Error !!!\n");
        printf("Try running the program with more memory free (about 350kbyte)\n");
    }
    if(logFileMade)

```

```

{
    printf("Log file (message.log) was built. Check it if you had problems ");
    MakeLog(1); /* Calling Log() with this parameter closes the log */
} /* file and puts messages at the end of the log file */
ErrClean(); /* Deallocated memory used to hold all data. */
printf("\nGoodbye!\n");
exit(0);
}

-----
void MakeLog(int closefile)
This function opens a log file for writing errors to if required
-----
void MakeLog (int closefile)
{
    static hereBefore=1;

    if(hereBefore)
    {
        logfile=fopen("message log","a+");
        fprintf(logfile,"Test: %s\n",testName);
        fprintf(logfile,"Test started on: %s\n",startTTime);
        fprintf(logfile,"The following list of messages may highlight a problem if there were
any.\n\n\n");
        fclose(logfile);
        hereBefore=0;
        logFileMade=TRUE;
    }
    if(closefile)
    {
        logfile=fopen("message log","a+");
        fprintf(logfile,"nEnd of message list... \n",testName);
        time(&binTime);
        curTime=localtime(&binTime);
        fprintf(logfile,"Test Finished on: %s\n",asctime(curTime));
        fclose(logfile);
    }
}

-----
void Message(char *message)
This function displays a message in a box on the screen
-----
void qMessage(char *message)
{
    char far *buffer; /* Image buffer to store portion of the screen while entering data */
    double a;

    buffer=(char huge *)malloc (20000L,sizeof(char));
    if (buffer==(char far *)NULL)
    {
        printf("a");
        return;
    }

    getimage(190,110,426,135,buffer); /* Save portion of screen that the routine uses
*/

    setcolor(4);
    setfillstyle(SOLID_FILL,7);
    bar(214,110,426,135);
    setcolor(0);
    settextjustify(CENTER_TEXT,CENTER_TEXT);
    outtextxy(320,123,message);
    setcolor(4);
    rectangle (214,110,426,135);

    delay(1000);

    putimage(190,110,buffer,COPY_PUT);
    hfree (buffer);
    settextjustify(LEFT_TEXT,TOP_TEXT);
}

-----
void Print(int x,int y,int color,char *string)
This function prints contents of string at location x,y in specific color
-----
void Print(int x,int y,int color,char *text)
{
    int width,height,charwidth;

```



```

        height=textheight(text);
        width=textwidth(text);
        charwidth=textwidth("Q");

        moveto((y-1)*charwidth, (x-1)*height);
        bar((y-1)*charwidth, (x-1)*height+3,
            ((y-1)*charwidth)+width-3,((x-1)*height)+height+3);
        setcolor(color);
        outtext(text);
    }

    void Prints(int x,int y,int color,char *text)
    {
        int width,height,charwidth;

        height=textheight(text);
        width=textwidth(text);
        charwidth=textwidth("Q");

        moveto((y-1)*charwidth, (x-1)*height);
        bar((y-1)*charwidth, (x-1)*height,
            ((y-1)*charwidth)+width,((x-1)*height)+height);
        setcolor(color);
        outtext(text);
    }
}
//-----
void Input(int maxLength, int type, char message)
// This function takes in a set number of input characters on screen
// and allows only numbers or characters (specified by "type")
//-----
float Input(int maxLength,int type, char message[80])
{
    int len,x,i;
    char far *buffer; /* Image buffer to store portion of the screen while entering data */
    char ch=0;
    int pr=0,a;

    buffer=(char huge *)halloc(20000L,sizeof(char));
    if (buffer==(char far *)NULL)
        printf("a");

    getimage(230,155,440,195,buffer); /* Save portion of screen that the routine uses */

    setcolor(0);
    setfillstyle(SOLID_FILL,7);
    bar(230,155,440,195);

    setcolor(4);
    rectangle(230,155,440,195);
    sprintf(string,"Input %s ",message); /* Tell user what input is required */
    Print(14,26,0,string);

    i=0;
    string[0]='\0';
    do
    {
        if (ch>32 && ch<123) /* Only valid ascii characters ie: No spaces, etc */
        {
            string[i]=ch;
            i+=1;
            pr=1;
        }
        if (ch==8) /* Allow DELETE Key to be used for corrections */
        {
            i=i-1;
            pr=1;
        }
        if (ch==13) /* When ENTER pressed close the dialogue and */
        {
            /* return a number if required */
        }
    }

    putimage(190,208,buffer,COPY_PUT);
    hfree (buffer);
    if (type==0)
        return (atoi(string));
    else return(0);
}
if (ch==27) /* If ESC key pressed close dialogue and return */
{
    putimage(230,155,buffer,COPY_PUT);
    hfree (buffer);
    return (-1);
}

```

```

    }
    if (pr)
    {
        string[i]='\0';
        string[i+1]='\0';
        Print(15,26,WHITE,string);
        pr=0;
    }
    ch=0;
    if(kbhit()) ch=getch();
    Print(15,26+WHITE," ");
    for(a=0;a<10000;a++); /* Delay a while so that cursor flashes */
}
while(1);
}
//-----
void ErrClean()
// Tides up before program terminates.
//-----
void ErrClean(void)
{
    /* The following lines free the arrays allocated by the program if they exist */
    if (circularBuffer != NULL) hfree(circularBuffer );
    if (halfBuffer != NULL) hfree(halfBuffer );
    if (zeroPts != NULL) hfree(zeroPts );
    if (channel0 != NULL) hfree(channel0 );
    if (channel1 != NULL) hfree(channel1 );
    if (channel2 != NULL) hfree(channel2 );
    if (channel3 != NULL) hfree(channel3 );
}
//-----
float GetCrackMeasurement(void)
{
    int loc;
    char ch,reading[20];

    loc=0;
    outp(0x2fc,0xa);
    delay(80);
    outp(0x2fc,0xb);
    setpalette(0,14); /* Turn Screen yellow */
    do{
        while( (inp(0x2fd) & 1)==0 && kbhit()); /* wait for new char */
        if(kbhit()) break;
        ch=inp(0x2f8);
        reading[loc]=ch;
        loc++;
    }
    while(ch!=13);

    setpalette(0,0); /* Turn Screen black */
    return atof(reading);
}
//-----
void ErrPrint(char *proc_name,int err_num)
// Prints the relevant error which N-Daq calls return
//-----
void ErrPrint(char *proc_name,int err_num)
{
    switch (err_num)
    {
        case notEnoughExtMem:
            sprintf(buffer,"WARNING: BIOS reports insufficient extended memory");
            break;
        case DMAReprogramming:
            sprintf(buffer,"WARNING: The given buffer requires DMA reprogramming at run-
            time");
            break ;
        case pageBreakinDMAbuf:
            sprintf(buffer,"WARNING: In DMA mode, page breaks could cause glitches in
            waveform");
    }
}

```

```

        break;
        case overWriteBeforeCopy:
            sprintf(buffer, "WARNING: Data has been overwritten before the copy operation was
started");
                break;
        case simulOpAcrossChips:
            sprintf(buffer, "WARNING: A CTR_Simul_Op call is make affecting more than one
9513 chip.");
                break;
        case inOnSomeOutLines:
            sprintf(buffer, "WARNING: An In_Port call has been made to some lines set for
output");
                break;
        case outOnSomeInLines:
            sprintf(buffer, "WARNING: An Out_Port call has been made to some lines set for
input.");
                break;
        case readOutputLine:
            sprintf(buffer, "WARNING: A digital line configured for output has been read");
                break;
        case relatedPortBusy:
            sprintf(buffer, "WARNING: Another port on the same chip is busy");
                break;
        case readOutputPort:
            sprintf(buffer, "WARNING: A digital port configured for output has been read");
                break;
        case dupDMALevels:
            sprintf(buffer, "WARNING: Two or more boards have the same DMA level");
                break;
        case dupIntLevels:
            sprintf(buffer, "WARNING: Two or more boards have the same interrupt level");
                break;
        case dupIOAddrRange:
            sprintf(buffer, "WARNING: Two or more boards have overlapping io address
space");
                break;
        case noErr: /* No need to print anything for a case of no error */
            break;
        case notOurBrdErr:
            sprintf(buffer, "Board in slot specified is not an MC, AT or EISA Series board");
                break;
        case badBrdNumErr:
            sprintf(buffer, "Slot number is out of range");
                break;
        case badChanErr:
            sprintf(buffer, "Channel number is out of range");
                break;
        case noSupportErr:
            sprintf(buffer, "Function is not supported on this board");
                break;
        case badPortErr:
            sprintf(buffer, "Port number is out of range");
                break;
        case badOutPortErr:
            sprintf(buffer, "Port specified is not configured for output");
                break;
        case noLatchModeErr:
            sprintf(buffer, "Port has not been configured for latched mode");
                break;
        case noGroupAssign:
            sprintf(buffer, "Port cannot be or is not assigned to a group");
                break;
        case badInputValErr:
            sprintf(buffer, "One or more input parameters are out of range");
                break;
        case timeOutErr:
            sprintf(buffer, "Call timed out");
                break;
        case outOfRangeErr:
            sprintf(buffer, "A voltage is out of range");
                break;
        case daqInProgErr:
            sprintf(buffer, "Data acquisition was in progress. Call not executed");
                break;
        case counterInUseErr:
            sprintf(buffer, "Counter specified (or needed) was in use. Call not executed");
                break;
        case noDAQErr:
            sprintf(buffer, "No data acquisition is in progress. Call had no effect");
                break;
        case overFlowErr:

```

```

            sprintf(buffer, "A/D first-in, first-out (FIFO) has overflowed");
                break;
        case overRunErr:
            sprintf(buffer, "Overrun error : minimum sample interval exceeded");
                break;
        case badCntErr:
            sprintf(buffer, "Scan count must be a multiple of number of channels");
                break;
        case brdTypeErr:
            sprintf(buffer, "Invalid board type for operation");
                break;
        case noCountOpErr:
            sprintf(buffer, "Counter specified is not configured for an event counting operation");
                break;
        case ctrReservedErr:
            sprintf(buffer, "Counter specified is reserved for data acquisition operations only");
                break;
        case noGrpBlockInProg:
            sprintf(buffer, "No block digital transfer is in progress");
                break;
        case grpBlockInProg:
            sprintf(buffer, "A block digital transfer is in progress");
                break;
        case laterIntUpdateNotSet:
            sprintf(buffer, "Analog outputs are not configured for later update mode");
                break;
        case wfnProgErr:
            sprintf(buffer, "There is a waveform generation in progress");
                break;
        case noWLoadErr:
            sprintf(buffer, "No waveform has been loaded");
                break;
        case noWInProgErr:
            sprintf(buffer, "No waveform generation is in progress");
                break;
        case extConvErr:
            sprintf(buffer, "External conversion pulses cannot be used with external triggering");
                break;
        case badSigDirErr:
            sprintf(buffer, "Bad RTSI signal direction");
                break;
        case noDbDaqErr:
            sprintf(buffer, "No double buffered acquisition is in progress");
                break;
        case overWriteErr:
            sprintf(buffer, "Data has been overwritten");
                break;
        case memErr:
            sprintf(buffer, "Not enough memory or disk space available");
                break;
        case noConfigFile:
            sprintf(buffer, "Configuration file not found. It must be in the current or root
directory");
                break;
        case intLevelInUse:
            sprintf(buffer, "The interrupt level assigned is in use by another board");
                break;
        case DMAChanInUse:
            sprintf(buffer, "The DMA channel assigned is in use by another board");
                break;
        case multiSourceInputErr:
            sprintf(buffer, "RTSI: two signals cannot drive a given input");
                break;
        case lowScanIntervalErr:
            sprintf(buffer, "Scan interval must be 2 microseconds greater than the total interval");
                break;
        case noConnectorErr:
            sprintf(buffer, "The RTSI path specified is not connected");
                break;
        case noPGInProg:
            sprintf(buffer, "No pattern generation is in progress");
                break;
        case PGInProg:
            sprintf(buffer, "Pattern generation is currently in progress");
                break;
        case grpRateErr:
            sprintf(buffer, "The hardware cannot accommodate the rates requested");
                break;
        case openFileErr:
            sprintf(buffer, "Could not open the file.");
                break;

```

```

case writeFileErr:
    sprintf(buffer, "Could not write to the file");
        break;
case noDwWfmErr:
    sprintf(buffer, "No double waveform generation in progress");
        break;
case dataNotAvailErr:
    sprintf(buffer, "The requested block of data is not yet available");
        break;
case DMATransferCntNotAvail:
    sprintf(buffer, "Could not get a reliable reading from the DMA controller");
        break;
case noLabScanErr:
    sprintf(buffer, "Cannot call Lab_SCAN_Check after DAQ_Start");
        break;
case dbOpErr:
    sprintf(buffer, "Double buffered mode is not allowed when using DAQ_Op_SCAN_Op
");
        break;
case brdIsAmedErr:
    sprintf(buffer, "Board must be disarmed");
        break;
case noSetupErr:
    sprintf(buffer, "MDAQ_Setup must be called before MDAQ_Start");
        break;
case extConvDrvErr:
    sprintf(buffer, "Can't receive and drive external convert pin simultaneously");
        break;
case triggerSourceErr:
    sprintf(buffer, "Must be in pre-trigger mode to receive TRIGGER over RTSI");
        break;
case noArmErr:
    sprintf(buffer, "MAI_Arm must be called before MAJ_Read when clock source is
external");
        break;
case intDisabledErr:
    sprintf(buffer, "Interrupts are disabled, cannot perform the function.");
        break;
case keyNotFoundErr:
    sprintf(buffer, "The Lab-PC key file (LAB_PC.KEY) is not present");
        break;
case noTrigEnabledErr:
    sprintf(buffer, "A hardware trigger must be enabled when in pre-trigger mode");
        break;
case digPortReserved:
    sprintf(buffer, "Digital port is busy with AMUX-64 or SCXI
communications");
        break;
        case noRTSlineAvailErr:
            sprintf(buffer, "No RTSI line available for dacupdates");
                break;
case scanRateErr:
    sprintf(buffer, "Scan rate is too fast for the number of channels scanned");
        break;
case invalidGetErr:
    sprintf(buffer, "MDAQ_Get parameters are invalid in the context of the acquisition");
        break;
case callInputOutOfRange:
    sprintf(buffer, "External reference out of range");
        break;
case EEPROMAddrErr:
    sprintf(buffer, "Unable to address the EEPROM");
        break;
case EEPROMresponseErr:
    sprintf(buffer, "EEPROM failed to respond");
        break;
case EEPROMreadErr:
    sprintf(buffer, "Unable to read data from EEPROM");
        break;
case EEPROMwriteErr:
    sprintf(buffer, "Unable to write data to EEPROM");
        break;
case calResponseErr:
    sprintf(buffer, "Unable to collect calibration data from the board");
        break;
case calConvergeErr:
    sprintf(buffer, "Calibration unable to converge");
        break;
case calDACerr:
    sprintf(buffer, "Bad DAC value generated during calibration");
        break;
    
```

```

case externalCalRefErr:
    sprintf(buffer, "External reference does not match the software input value");
        break;
case internalCalRefErr:
    sprintf(buffer, "Bad internal calibration reference");
        break;
case badOutLineErr:
    sprintf(buffer, "Output on line configured for input");
        break;
case interlvdDataAlignErr:
    sprintf(buffer, "DMA waveform generation interleaved data must be aligned across
page break");
        break;
case cannotAlignBufErr:
    sprintf(buffer, "Buffer size is not big enough for alignment of data to avoid page
break");
        break;
case configFileErr:
    sprintf(buffer, "Data in the configuration file has been corrupted");
        break;
case dacUpdateRTSINotAvailErr:
    sprintf(buffer, "DACUPDATE RTSI line is currently being driven by a RTSI bus line");
        break;
case chanPauseErr:
    sprintf(buffer, "A waveform channel cannot be paused if it is using interleaved
DMA");
        break;
case portInLatchedModeErr:
    sprintf(buffer, "Illegal to configure port 0 to bidirectional");
        break;
case fifoModeErr:
    sprintf(buffer, "Fifo mode cannot be use in waveform generation");
        break;
case cannotFreeMemErr:
    sprintf(buffer, "Attempted to free memory that is locked. Use
NIDAO_Mem_Unlock");
        break;
case memNotLockedErr:
    sprintf(buffer, "Attempted to unlock memory that is not locked");
        break;
default:
    sprintf(buffer, "Error number is %d. Consult the error codes in the NI-DAQ
manual", err_num);
        break;
    }
Prints(28, 1, 0, " ");
Prints(29, 1, 0, " ");
MakeLog(0);
Prints(55, 1, 5, buffer); /* print error on screen */
logfile=fopen("message log", "a+");
fprintf(logfile, "%s\n", buffer); /* write error message to log */
sprintf(buffer, "Error (%d) occurred in call to ", err_num); /* say where error occurred */
Prints(56, 1, 5, buffer);
fprintf(logfile, "%s", buffer); /* write error message to log */
Prints(56, 33, 4, proc_name);
fprintf(logfile, "%s\n", proc_name); /* write error message to log */
fclose(logfile);
if(err_num < 0) /* Only ask to continue if */
do{ /* there was an error! */
    printf("\a"); /* ie. Just log warnings.... */
}
while(input(1, 2, "Error... Continue Y/N"));
if(string[0] != 'N' || string[0] != '\n') get_out(0);
}
    
```

5.9 References

- 11 PONCELET, J.V., *Introduction a la Mecanique Industrielle, Physique pour Experimentale.*, 317, 2e ed., Imprimerie de Gauthier-Villars, Paris, 1839.
- 2 ALBERT, W.A.J., *Uber Treibseile am Harz* *Archive fur Mineralogie Geognose, Berbau und Huttenkund*, 10, 215, 1838.
- 3 BRAITHWAITE, F., *On the Fatigue and Consequent Fracture of Metals*, *Proc. Inst. Civil Eng.* London, 13, 463, 1854.
- 4 W¹HLER, A., *Zeitschrift fur Bauwesen*, 1860; English Translation; *Engineering*, 4, 160, 1967.
- 5 GERBER, H., *Zeitschrift des bayerischen Architekten und Ingenieur Vereins*, 6, 101, 1874.
- 6 BAUSINGER, J., "Weber die Veränderungen der Elastizitätsgrenze und der Festigkeit des Eisens und Stahls durch oftmals wiederholte Belastung"; *Mitt. Mech-tech Lab, Munchen*. 1886.
- 7 BASQUIN, O.H., *Proc. ATSM*. 10, 625, 1910.
- 8 BAIRSTOW, L., *Phil. Trans. Royal Soc., London*, 210, 35, 1910.
- 9 PALMGREN, A., *Zeitschrift des Vereins Deutscher Ingenieure*, 68, 339, 1924.
- 10 EWING, J.A., *Phil. Trans. Royal Soc., London*, A200, 241, 1903.
- 11 INGLIS, C.E., *Trans., Inst. Naval Archite.*, 55, 219, 1913.
- 12 GRIFFITH, A.A., *Phil. Trans. Royal Soc., London*, A221, 163, 1921.
- 13 IRWIN, G.R., *J. Appl. Mech.*, 24, 361, 1957.
- 14 PARIS, P.C., GOMEZ, M.P., ANDERSON, W.P., *The Trend in Engineering*, 13, 9, 1961.
- 15 FORSYTH, P.J.E., RYDER, D.A., *Aircraft Engineering*, 32, 96, 1960.
- 16 ELBER, W., *ASTM, STP 486*, 230, 1971.
- 17 TAYLOR, D., *Fatigue Thresholds*, Butterworths, London, 1990.
- 18 DILLON, J.H., *Adv. Coll. Sci.*, 3, 219, 1950.
- 19 HERTZBERG, R.W., *Fatigue of Engineering Plastics*, Academic Press, NY, 1980.
- 20 SAUER, J.A., RICHARDSON, G.C., *Int. J. Fract.*, 16(6), 499, 1980.
- 21 SAUER, J.A., CHEN, C.C., *Adv. Polym. Sci.*, 52/53, 170, 1983.
- 22 KAUSCH, H.H., *Polymer Fracture*, 2nd Ed., Springer Verlag, Berlin, 1987.
- 23 TAKEMORI, M.T., *Adv. Polym. Sci.*, 91/92, Ed., Kausch, H.H., 23, 1990.
- 24 SKIBO, M.D., HERTZBERG, R.W., MANSON, J.A., KIM, S.L., *J. Mat. Sci.*, 12, 531, 1977.
- 25 BUCKNALL, C.B., FAITHROUNI, T., *Proc. 8th. Int. Conf. Deformation. Yield & Fracture of Polymers*, Paper 30, 199.
- 26 BUCKNALL, C.B., *Toughened Plastics*, Applied Science Publishers, 1977.
- 27 ARGON, A.S., COHEN, R.E., *Crazing in Polym.*, Vol. 2, *Advances in Polymer Science*, 91/92, ed. Kausch, H.H., Springer Verlag, 1990.
- 28 BUCKNALL, C.B., *Brit. Plas.*, 40(12), 84, 1967.
- 29 KAMBOUR, R.P., KOP, R.W., *J. Polym. Sci.*, 7, 183, 1969.
- 30 BUCKNALL, C.B., STEVENS, W.W., *J. Mat. Sci.*, 15, 2950, 1980.
- 31 SAUER, J.A., CHEN, C.C., *Polym. Eng. Sci.*, 24, 786, 1984.
- 32 SAUER, J.A., HABIBULLAH, M., CHEN, C.C., *J. Appl. Phys.*, 52, 10, 5970, 1981.

- 33 WOAN, D.-J., HABIBULLAH, M., SAUER, J.A., *Polymer*, 22, 699, 1981.
- 34 SKIBO, M.D., HERTZBERG, R.W., MANSON, J.A., *J. Mat. Sci.*, 11, 479, 1976.
- 35 HERTZBERG, R.W., MANSON, J.A., SKIBO, M.D., *Polym. Eng. Sci.*, 26, 74, 1975.
- 36 DOLL, W., *Fractography and Failure Mechanisms of Polymers and Composites*, Ch. 10, ed., Roulin-Moloney, A.C., Elsevier Applied Science, 1989.
- 37 SURESH, S., *Fatigue of Materials*, University Press Cambridge, 1991.
- 38 RIVLON, R.S., THOMAS, A.G., *J. Polym. Sci.*, 15(7), 500, 1953.
- 39 LAKE, G.L., LUNDLEY, P.B., THOMAS, A.G., *Proc. Int. Conf. Fracture*, 2nd, 493, 1969.
- 40 THOMAS, A.G., *J. Polym. Sci.*, 31, 467, 1958.
- 41 PARIS, P.C., ERDOGAN, F., *J. Basic Eng.*, 85, 528, 1963.
- 42 FOREMAN, R.G., KEARNEY, V.E., ENGLE, R.M., *J. Basic Eng.*, 89, 459, 1967.
- 43 PEARSON, S., *Eng. Fract. Mech.*, 4, 9, 1972.
- 44 MUKHERJEE, B., BURNS, D.J., *Exp. Mech.*, 11, 433, 1971.
- 45 ARAD, S., RADON, J.C., CULVER, R.E., *J. Mech. Eng. Sci.*, 13, 75, 1971.
- 46 ARAD, S., RADON, J.C., CULVER, R.E., *Eng. Fract. Mech.*, 4, 511, 1972.
- 47 WNUK, M.P., *J. App. Mech.*, 41, 1, 239, 1974.
- 48 BRANCO, C.A.M., RADON, J.C., CULVER, L.E., *J. Test Eval.*, 3, 195, 1975.
- 49 RADON, J.C., ARAD, S., CULVER, L.E., *Eng. Fract. Mech.*, 6, 195, 1974.
- 50 WILLIAMS, J.G., *J. Mat. Sci.*, 12, 2525, 1977.
- 51 CHUDNOVSKY, A., MOET, A., *Polym. Eng. Sci.*, 22, 15, 923, 1981.
- 52 HERTZBERG, R.W., MANSON, J.A., *ASTM, STP*, 536, 391, 1973.
- 53 YAP, O.F., MAI, Y.-W., COTTERELL, B., *Polym. Eng. Sci.*, 22, 449, 1981.
- 54 SKIBO, M.D., *ACS Symp. Ser.*, 95, ACS, 311, 1979.
- 55 ELINCK, J.P., BAUENS, J.C., HOMES, G., *Int. J. Fract.* 7, 277, 1971.
- 56 GEBIZLIOGLU, O.S., ARGON, A.S., COHEN, R.E., *Polymer*, 26, 519, 1985.
- 57 SPRENKEL, J., DOLAN, F., *Dow Confidential Internal communication*, 1993.
- 58 DOWLING, N.E., BEGLEY, J.A., *Mech. Crack Growth, ASTM, STP* 590, 82, 1976.

Chapter 6

Findings and Suggestions for Future Research

1.1 Preview

The following chapter reviews the findings from the conclusions of the previous chapters and proposes subjects for future research.

1.2 Contents

<i>Findings and Suggestions for Future Research</i>	213
1.1 Preview.....	213
1.2 Contents.....	213
1.3 General Conclusion.....	213
1.3.1 Origin, Composition and Polymerisation.....	214
1.3.2 Experimental Materials Preparation and Characterisation.....	214
1.3.3 Micro-Structure and Mechanical Properties in HIPS.....	215
1.3.4 The Fracture Toughness of HIPS.....	216
1.3.5 Fatigue Fracture Toughness of HIPS.....	217
1.4 Summary of Principal Findings.....	218
1.5 Summary of Future Research Proposals.....	219
1.6 Final Comments.....	219
1.7 References.....	219

1.3 General Conclusion

The principal finding of the research is that the secondary phase morphology does exert a significant influence on the fatigue behaviour of HIPS. It was concluded that it is possible to optimise the secondary phase morphology of HIPS for fatigue performance, in terms of fatigue life and crack growth resistance for intended applications. It was concluded that the efficiency in the interaction between the matrix material and the stress field interactions, i.e., the perturbation and diffusion of stress within the composite system, determines the nature of the mechanical performance.

Consequently, the influence of RPS and ERPV are combined, linked in their interaction with mechanical load and their perturbation of stress fields in effecting cavitation or shear processes. In HIPS the secondary phases promotion of crazing dominates deformation and failure. Effecting competitive processes of energy dissipation that, at once, through damage accumulation, initially delay and then hasten crack advancement.

It was found that the particle size population exercises a greater influence on fatigue life and fatigue crack propagation rates than on fracture toughness or other mechanical properties. However the observations from the other tests, i.e., tensile, impact and other fracture toughness tests, illustrated that

the particle size and the distribution of size, exerted the most fundamental influence on behaviour. Thus it is concluded that the particle size dictates the character of the influence of other features of secondary phase morphology, such as ERPV, on mechanical properties. Consequently it was concluded improper to exclude consideration of particle size in modelling the influence of morphology on mechanical properties.

Analysis of the test data from the impact, tensile, fracture and fatigue tests illustrated that the RIPD model provided an effective means of modelling the combined influence of secondary phase particle size and volume. Also the incorporation of a stress efficiency factor in modelling data in regard to the RIPD provides a means of accommodating differences arising from different particle size distributions and facilitates mesoscale modelling of materials for specific applications parts.

A further conclusion drawn from the results is that a critical size limit does exist, at which the size and distance between particles can affect material properties in a consistent fashion, i.e., with changes to the magnitude of RPS and ERPV. For mono-modal particle size distributions it is considered that there is an optimum mean average particle size, or particle size distribution, and ERPV for secondary phase toughening. For bimodal or multi-modal distributions it is concluded that there are optimum complimentary sets of optimum RPS and ERPV, dictated by the properties of the matrix material.

These and other findings, as well as proposals for future research are explored in at greater length in the following sections.

1.3.1 Origin, Composition and Polymerisation of HIPS

From the literature it was concluded that the morphology of the secondary phase particles may be controlled during polymerisation through both chemical, e.g., grafting, etc., and physical, e.g., shear, etc., methods [Section 1.8]. Recent patents in the area of HIPS points to the continued research on bulk, or industrial, scale manufacture of such polymer systems[1]. The increasing interest in the preparation of functional self assembly polymers, adds to the value of this research, as the basic technology, controlling the organisation of macromolecules, is the same[2]. Thus it is considered that future research should focus on the manipulation and control of polymerisation methods and processes in regard to the control of secondary and tertiary phase morphology.

Thus it is proposed that an integrated programme of research be undertaken to study the effect of the introduction of initiator, chain transfer and chemical grafting agents as well as temperature and agitation (shear) on the on the process of molecular folding and subsequent particle formation, morphology, assembly and organisation.

1.3.2 Experimental Materials Preparation and Characterisation

Image analysis of TEM plates was found to provide the more reliable means of characterising the secondary phase morphology, in terms of particle size and effective rubber phase volume. However the

method is costly in terms of capital, human resources and time. Consequently it is considered that future research should focus on the development of a more efficient means of characterising morphology, for the purposes of quality control and research and development.

It is proposed that techniques be considered; 1) coulter counter method and 2) acoustic tomography. A technical solution should be developed that overcomes the issue of accuracy in measuring the dilution of suspensions of HIPS and the tiny volumes used in the CC analysis. This would allow the determination of both particle size and ERPV. Research would also be required to determine, and calibrate for, the swelling effect of solvents on the particles themselves and the impact this would have on measurements made. The low cost of the equipment and the rapidity with which the technique could be applied make such research attractive, and though not as explicit a technique as TEM it would be ideal for in line quality control.

The second approach, the development of an acoustic tomography technique, or an opto-acoustic tomography method, could with some research provide a far more comprehensive and accurate measurement system in the medium term. Current commercialised products can resolve down to 2 – 10 μm while developmental high frequency, modulated and interferometric methods could offer the potential to achieve much smaller spatial resolutions, to nano-meters [3]. The current commercialisation of devices by MTS for fracture analysis illustrates the potential and application of the technology in materials science [4]. The technique would also interface with fracture and fatigue experiments.

1.3.3 Micro-Structure and Mechanical Properties in HIPS

It was found that particle size exercises a fundamental, if less profound, influence on mechanical behaviour. It was concluded from results on impact and tensile specimens that particle size determines the sensitivity of the system to increases in effective rubber phase volume. Consequently it followed that modelling behaviour in terms of parameters that ignore this must be less precise than those that do.

Thus it was concluded that the Relative Inter-Particle Distance (RIPD), which provided for the inclusion of both in a simple parameter, and that also lent itself to resolving the continuum mechanics problems, provided more accurate models of behaviour and was thus more appropriate. The parameter facilitated the characterisation of the sensitivity of different HIPS to increases in effective rubber phase volume, in terms of a craze efficiency factor. Both quotients are empirically derived parameters. They are associated through, and based upon the notion of, there being a unique stress field interaction between each distribution of particle sizes in a HIPS. This then heightens stress and promotes crazing about particles in a unique fashion in each population.

However, further research is required to examine and evaluate the effect of particle size and polydispersity on stress field interactions. Further work is also required to determine the impact of

these on the mechanical properties of HIPS and relate them explicitly and coherently to the rules and relationships of continuum mechanics.

The finite element method (FEM) it is thought provides an efficient means of doing so. However the application of finite element analysis to large volumes of materials is impractical, due to the processing time that would be required to solve for millions or particles. However the parameters of RIPD and craze efficiency factor, allied to particle size and matrix molecular weight, could provide useful parameters in defining mesoscale algorithms for modelling the macroscopic behaviour of behaviour of parts manufactured from HIPS.

Thus it is proposed that future research project consider FEM modelling of small volumes of materials populated, e.g., using random routines, e.g., Monte-Carlo routines, with a population of particles characteristic of the entire populations size and polydispersity. These models could easily resolve the RIPD and solve for the level of stress concentration and consequently, at an upper bound associated with crazing (which would also need be defined for a visco-plastic matrix), determine the stress concentrating efficiency factor of the population and the characteristic properties of the materials.

This work would provide for means to prepare for the stochastic and competitive process of craze growth and diffusion (damage accumulation) and also crack growth (that could then be predicted from conventional deterministic theories).

1.3.4 The Fracture Toughness of HIPS

It followed from Chapters 3, 4 and 5, from their literature reviews and the results that were obtained that the mechanical behaviour of HIPS is dominated by crazing. Crazing creates an anomalous state of loading to which it is difficult to apply conventional or classical continuum mechanics rules in characterising toughness.

It was found that the impact strength of HIPS did not correlate with other measures of toughness. This was concluded to result from size effects using standard specimens, e.g., determining G_{1c} , the strain energy release rate, from $BD\Phi$, based on LEFM theory from standard impact specimens in Chapter 3, where fracture process zones varied greatly with morphology.

The J integral was found to be a more appropriate measure of material toughness. However, the variation of toughness with thickness, led to the conclusion that although a valid J_c could be determined for all of the HIPS it did not necessarily reflect the true intrinsic toughness of the materials. Also as many of the assumptions of the path independent line contour J integral are violated in the experiments that it does not provide an ideal means of characterising toughness.

Though it was found that it was not possible to determine the intrinsic toughness of the HIPS from SENT specimens, the method was concluded to be the most attractive means of characterising toughness in HIPS. This as its measure, when successfully made, does not violate its and other principles of fracture or continuum mechanics theory. It may be determined readily from a series of experiment as and for a given thickness provides, depending upon the dimensions employed, the plane stress or plane strain intrinsic toughness. That the measurement made under plane strain conditions is equivalent to, the strain energy release rate, G_{Ic} and also the J_{Ic} in plane strain, adds to its attraction and potential use of measures of the parameter in design applications.

Thus it is considered that future search work should consider the determination of the essential work of fracture for HIPS. Thus it is proposed that a future programme of research determine the essential work of fracture from Double sided Single Edge Notched (DSEN) specimens. Also that it be determined for specimens of different thickness for different materials to examine the variation with thickness and the utility of the parameter in design and development of HIPS.

It was found that the fatigue method, after Strebel and Moet[5], provided the only accurate measure of intrinsic toughness in specimens of conventional part thickness. It was found that the intrinsic toughness of HIPS increased with increasing ERPV. The measurements made were in close agreement with those in the literature. However the sensitivity of the apparatus used in the determination, its thought, affected the ability of the system to resolve and contrast the difference between the toughness of the three materials systems and so expose differences arising from morphology.

Thus it is considered that future efforts to determine the intrinsic toughness of HIPS be done on more sensitive load cell. It is also proposed that the intrinsic toughness measurements be determined for specimens over a range of thickness.

1.3.5 Fatigue Fracture Toughness of HIPS

The principal finding from the fatigue tests was that it is possible to optimise the morphology of HIPS for fatigue. It was also found that the particle size population exercised a more significant influence on fatigue life and fatigue crack propagation than it had on fracture toughness or the other mechanical properties.

It was also found that the fatigue life did not correlate with impact strength. This was concluded, from the analysis of the hysteretic losses associated with FCP, to not be due to a variation in the intrinsic toughness of the materials but because of the nature of the behaviour promoted in impact tests.

Fatigue testing also showed that increasing the secondary phase volume did increase the intrinsic toughness of the materials, but only did so slightly. It was concluded that the principal effect of the secondary phase morphology on fatigue was associated with its influence on damage accumulation.

Larger particles, with greater RIPD and thus higher modulus for equivalent RIPD, were found to exhibit superior fatigue lives and crack growth resistance. This was due to their more efficient means of energy dissipation, at low levels of loading. Contrary to expectations that would have been inspired from the impact tests the series of materials that exhibited the greatest toughness exhibited poor fatigue lives whilst one possessing poorer toughness exhibited the best. Whilst those with the smallest particles with limited propensity to craze tended to be most brittle and exhibit the shortest fatigue life. This it is considered is explicable in terms of the craze nucleation efficiency of the materials and their propensity to promote crazing.

Thus it is proposed that an integrated approach to studying the fatigue life of HIPS be adopted in order to study:

- Fatigue crack propagation and damage accumulation in samples of increasing thickness. The intention of this to examine the sensitivity of FCP and energy dissipation mechanisms to stress state.
- The effect of bi-modal and multi-modal distributions of particle sizes in high molecular weight polystyrene and also in syndiotactic polystyrene. It is suspected that smaller particle sizes will be more effective as craze initiators as it is slightly more brittle.
- It is also proposed that the work consider the fatigue endurance of the materials and determine the energies associated with ΔK_{th} and compare it with that of PS and the energy required for the initiation of cracks in HIPS.

As mentioned in section 6.1.4., though the measurements made by image analysis and from the strain and load gauges provided satisfactory characterisation of the process of damage accumulation and crack propagation it is thought that the nature of the tests signal control and acquisition that a more sensitive hardware be employed (5-10 kN load cell).

If possible it is proposed that the future work employ acoustic tomography and interferometry techniques, in order to provide measure of strain and also the mapping and quantification of damage accumulation and crack propagation. Integration of such a system with load cell signal would provide for a comprehensive and coherent data acquisition system that could be related to secondary phase morphology and provide direct feedback to FEA and materials design programmes.

1.4 Summary of Principal Findings

The main findings of the present work have been that:

- It is possible to manipulate the secondary phase morphology of HIPS.
- Image analysis of TEM plates is the most accurate means of characterising RPS and ERPV.
- RIPD is a more accurate way of modelling the mechanical properties of HIPS than the ERPV.
- The RPS and polydispersity effects a critical influence on the mechanical response of HIPS.

- The RPS and polydispersity determine the nature of the influence of ERPV in HIPS.
- The impact toughness of HIPS do not correlate with their intrinsic toughness.
- LEFM is inapt to characterise the intrinsic toughness of HIPS of conventional wall thickness.
- The J integral provides a valid comparative measure of toughness.
- The fatigue method is the most accurate means of characterising intrinsic toughness in HIPS of conventional wall thickness
- The morphology of HIPS may be optimised for fatigue behaviour.
- The impact strengths of HIPS do not correlate with their fatigue behaviour.

1.5 Summary of Future Research Proposals.

It is proposed that future research consider:

- Methods of manipulating macromolecular morphology in bulk polymerisation processes.
- Development of coulter counter and acoustic tomography methods to characterise RPS and ERPV.
- Finite Element analysis of stress field interactions between different RPS populations in HIPS.
- Employ mesoscale techniques in FE modelling of macro-scale behaviour in parts made of HIPS.
- Characterise Essential work of fracture properties for HIPS of containing different morphologies.
- Investigate the sensitivity to thickness of measures of intrinsic toughness using the fatigue method.
- Evaluate the effectiveness of bi and multi modal particle size populations on fatigue behaviour.
- Compare strain energy and LEFM methods of modelling fatigue in samples of different thickness.

1.6 Final Comments

Whilst the conclusions and findings of this work relate to HIPS it is suggested that these findings are relevant to self-assembled copolymers and polymer composites. It is also thought that the energy based approaches to modelling and continuum mechanics and the experimental techniques and methods used and proposed for future work have applicability across a broad range of materials and fields of research.

1.7 References

-
- 1 US6248807, Method for the preparation of core-shell morphologies from polybutadiene-polystyrene graft copolymers, Fina Technology, Inc., Dallas, TX., June 19, 2001
 - 2 US6261469: Three dimensionally periodic structural assemblies on nanometer and longer scales, Honeywell International Inc., Morristown, NJ., July 17, 2001.
 - 3 Acoustical Imaging, Volume 24 edited by Hua Lee Kluwer Academic, 2000.
 - 4 Acoustic Emission Equipment, MTS Systems Corp., MTS.com 2001.
 - 5 STREBEL, J.J., MOET A., J. Appl. Polym. Sci., Vol. 52, 1815, 1994.